

	NASA Engineering and Safety Center Technical Assessment Report	Document #: NESC-RP- 06-071	Version: 1.0
Title: Flight Force Measurements of the Gamma-Ray Large Area Space Telescope / Delta II Flight		Page #: 1 of 226	

**Flight Force Measurements (FFMs) of the Gamma-Ray Large Area
Space Telescope (GLAST) / Delta II Flight**

September 24, 2009

	NASA Engineering and Safety Center Technical Assessment Report	Document #:	Version:
		NESC-RP-06-071	1.0
Title: Flight Force Measurements of the Gamma-Ray Large Area Space Telescope / Delta II Flight		Page #: 2 of 226	

Report Approval and Revision History

Approval and Document Revision History

NOTE: This document was approved at the September 24, 2009, NRB. This document was submitted to the NESC Director on October 16, 2009, for configuration control.

Approved Version:	<i>Original Signature on File</i>	10/19/09
1.0	NESC Director	Date

Version	Description of Revision	Office of Primary Responsibility	Effective Date
1.0	Initial Release	Daniel Kaufman, NESC Loads and Dynamics Deputy	September 24, 2009

	NASA Engineering and Safety Center Technical Assessment Report	Document #: NESC-RP- 06-071	Version: 1.0
Title: Flight Force Measurements of the Gamma-Ray Large Area Space Telescope / Delta II Flight		Page #: 3 of 226	

Table of Contents

Volume I: Technical Assessment Report

1.0	Notification and Authorization	10
2.0	Signature Page	11
3.0	Team List	12
3.1	Acknowledgements.....	13
4.0	Executive Summary	13
5.0	Assessment Plan	17
6.0	Description of the Problem, Phases of the Assessment and Resolution	18
6.1	Phase 1: Methodology Development.....	18
6.2	Phase 3: Ground Dynamic Test Validation.....	38
6.3	Phase 2: Ground Static Test Validation.....	69
6.4	Phase 4: Procurement of Flight System and Flight Data.....	85
6.5	Phase 5: Flight Data Flight Processing and Flight Reconstruction.....	90
7.0	Data Analysis	99
7.1	Flight Data Acquisition System.....	99
7.2	Flight Data.....	104
7.3	Verification Coupled Loads Analysis (VCLA).....	142
7.4	Liftoff Reconstruction and Reconciliation.....	153
7.5	Airloads Reconstruction and Reconciliation.....	191
7.6	MECO Reconstruction and Reconciliation.....	200
7.7	Summary of Flight Reconstruction and Reconciliation Efforts.....	213
7.8	Closing Arguments.....	215
7.9	Proposed Future Work.....	220
8.0	Findings and Recommendations	221
8.1	Findings.....	221
8.2	NESC Recommendations.....	222
9.0	Alternate Viewpoints	222
10.0	Other Deliverables	222
11.0	Lessons Learned	223
12.0	Definitions of Terms	223
13.0	Acronyms List	224
14.0	References	225



NASA Engineering and Safety Center Technical Assessment Report

Document #:
**NESC-RP-
06-071**

Version:
1.0

Title:

Flight Force Measurements of the Gamma-Ray Large Area Space Telescope / Delta II Flight

Page #:
4 of 226

List of Figures

Figure 6.1-1.	6915 PAF Geometry	19
Figure 6.1-2.	Delta II 6915 PAF FEM.....	20
Figure 6.1-3.	Strut 2 Cut Section Showing the Locations of the 4 Strain Rosettes and Gages at 0 Degree (lateral) and 90 Degree (axial).....	24
Figure 6.1-4.	Vishay Strain Rosette CEA-13-125UR-350	25
Figure 6.1-5.	Looking Down the Axis of Strut 1 to Define the Local Strut Coordinate System.....	28
Figure 6.1-6.	The One-Strut Model Used to Find Matrix [C]	28
Figure 6.1-7.	Impedance from the GLAST Dynamic Model	32
Figure 6.1-8.	GLAST Interface Forces Impedance	33
Figure 6.1-9.	GLAST Interface Moments Impedance.....	33
Figure 6.1-10.	GLAST + PAF Translational Residual Weights.....	33
Figure 6.1-11.	GLAST + PAF Rotational Residual Weights	34
Figure 6.1-12.	Updated PAF FEM	35
Figure 6.1-13.	Delta II Second Stage FEM	36
Figure 6.2-1.	GLAST Spacecraft During Assembly	39
Figure 6.2-2.	GLAST FEM with Test Axes	40
Figure 6.2-3.	Delta II 6915 Test PAF (TPAF) used for GLAST Sine Vibration Test	40
Figure 6.2-4.	PAF Strut Strain Gage Placement.....	42
Figure 6.2-5.	Strain Gage Locations on PAF Strut 1.....	42
Figure 6.2-6.	Strain Gage Alignment	43
Figure 6.2-7.	6915 PAF with Strut and Interface Labels for the Sine Test.....	45
Figure 6.2-8.	GLAST Spacecraft in the GD Vibrations Laboratory	46
Figure 6.2-9.	Simulation of PAF Installed Under the GLAST Spacecraft.....	46
Figure 6.2-10.	GLAST and Test PAF Coordinate Systems for the Sine Test.....	47
Figure 6.2-11.	Sweep Frequency Versus Time – X Axis Run 23	50
Figure 6.2-12.	Sweep Frequency Versus Time – Y Axis Run 28	51
Figure 6.2-13.	Sweep Frequency Versus Time – Z Axis Run 15.....	51
Figure 6.2-14.	Two Strain Channels from Run Z18.....	53
Figure 6.2-15.	Spectral Density of the Strain Measurements.....	54
Figure 6.2-16.	A Sample of the Data – Run X23	55
Figure 6.2-17.	A Sample of the Data – Run Z18.....	56
Figure 6.2-18.	Zoom In on the Data Plotted.....	57
Figure 6.2-19.	Impedance from the X-Axis Sweep.....	59
Figure 6.2-20.	Impedance from the Y-Axis Sweep.....	60
Figure 6.2-21.	Impedance from the Z-Axis Sweep	61
Figure 6.2-22.	Forces from FEM Method – Run X23	63
Figure 6.2-23.	Forces from SFM – Run X23.....	64



**NASA Engineering and Safety Center
Technical Assessment Report**

Document #:
**NESC-RP-
06-071**

Version:
1.0

Title:

**Flight Force Measurements of the Gamma-Ray Large
Area Space Telescope / Delta II Flight**

Page #:
5 of 226

Figure 6.2-24. Forces from the FEM Method – Run Y28 65

Figure 6.2-25. Forces from the SFM – Run Y28..... 66

Figure 6.2-26. Forces from the FEM Method – Run Z15 67

Figure 6.2-27. Forces from the SFM – Run Z15 68

Figure 6.3-1. Test PAF and XTE Mass Simulator..... 71

Figure 6.3-2. XTE Mass Simulator and Trunnion Labels 72

Figure 6.3-3. XTE Trunnion Load Collar..... 73

Figure 6.3-4. Cylindrical Extension..... 74

Figure 6.3-5. Configuration with Cylindrical Extension..... 74

Figure 6.3-6. Test Run 19 with the Cylindrical Extension 75

Figure 6.3-7. LVDT Locations 77

Figure 6.3-8. Force versus Strain – Test Run 1A 82

Figure 6.3-9. Force Error Plot – Fixed Base..... 83

Figure 6.3-10. Moment Error Plot – Fixed Base 83

Figure 6.3-11. Force Error Plot – Flexible Base..... 84

Figure 6.3-12. Moment Error Plot – Flexible Base 84

Figure 6.4-1. Flight PAF with Strain Gages and Accelerometers Installed 88

Figure 6.4-2. Accelerometer Installation 88

Figure 6.4-3. Close-up of Strain Gage Installation..... 89

Figure 6.5-1. GLAST Spacecraft on Delta II Vehicle During Fairing Mate 92

Figure 6.5-2. GLAST/Delta II 7920H-10C Launch 93

Figure 6.5-3. ULA Statistical Description of the GLAST Flight Events 99

Figure 7.1-1. GLAST SFI Block Diagram 99

Figure 7.2-1. Sample Data Dropout..... 105

Figure 7.2-2. Data Dropout Before and After Removal 105

Figure 7.2-3. Accelerometer Channels Showing High Frequency Noise..... 106

Figure 7.2-4. Accelerometer Channels After 120 Hz LP Filter..... 107

Figure 7.2-5. Estimated Flight Temperatures 108

Figure 7.2-6. Liftoff Lateral X Acceleration 109

Figure 7.2-7. Liftoff Lateral Y Acceleration 110

Figure 7.2-8. Liftoff Thrust Axis Acceleration at SC to PAF Interface 110

Figure 7.2-9. Acceleration at Liftoff: Shock Response Spectra (SRS) Q=50 111

Figure 7.2-10. Rotational Accelerations at Liftoff: SRS Q=50 112

Figure 7.2-11. Delta II/GLAST Thrust Axis Steady Acceleration..... 113

Figure 7.2-12. Liftoff Thrust Predicted Force and Steady State..... 114

Figure 7.2-13. Thrust Axis Liftoff Force: Dynamic 115

Figure 7.2-14. Force Z Liftoff: SRS Q=50 116

Figure 7.2-15. Liftoff Lateral Forces..... 117

Figure 7.2-16. Liftoff Lateral Moments 117

Figure 7.2-17. Lateral Forces SRS 118



**NASA Engineering and Safety Center
Technical Assessment Report**

Document #:
**NESC-RP-
06-071**

Version:
1.0

Title:

**Flight Force Measurements of the Gamma-Ray Large
Area Space Telescope / Delta II Flight**

Page #:
6 of 226

Figure 7.2-18. Liftoff Lateral Moments SRS 119

Figure 7.2-19. Liftoff Torsional Moment 120

Figure 7.2-20. Liftoff Torsional Moment SRS 120

Figure 7.2-21. Airloads Net Acceleration – Lateral Axes 122

Figure 7.2-22. Airloads Thrust Axis Acceleration 122

Figure 7.2-23. Airloads Rotational Acceleration about Y- Axis (Ry) 123

Figure 7.2-24. Airloads Translational Acceleration SRS (Q=20) 124

Figure 7.2-25. Airloads Rotational Acceleration SRS (Q=20) 124

Figure 7.2-26. Airloads Lateral Forces Calculated Using SFM 125

Figure 7.2-27. Airloads Thrust Force Calculated Using SFM 126

Figure 7.2-28. Airloads Moments Calculated using SFM 126

Figure 7.2-29. Airloads Force SRS Plots (Q=20) 127

Figure 7.2-30. Airloads SRS Moments (Q=20) 128

Figure 7.2-31. First Pre-MECO Lateral Acceleration 130

Figure 7.2-32. Prior-to-MECO and MECO Transient Thrust Acceleration 131

Figure 7.2-33. Lateral Net Acceleration at MECO 132

Figure 7.2-34. Thrust Axis Net Acceleration at MECO 133

Figure 7.2-35. MECO Translational Acceleration SRS (Q=20) 134

Figure 7.2-36. MECO Rotational Acceleration SRS (Q=20) 134

Figure 7.2-37. MECO Lateral Forces Calculated using SFM 135

Figure 7.2-38. MECO Thrust Forces Calculated using SFM 136

Figure 7.2-39. MECO Moments Calculated Using SFM 137

Figure 7.2-40. Lateral MECO SRS Forces (Q=20) 138

Figure 7.2-41. Thrust MECO SRS Force (Q=20) 138

Figure 7.2-42. Thrust MECO SRS Force (Q=20) Filtered 30 – 150 Hz 139

Figure 7.2-43. MECO SRS Moments (Q=20) 139

Figure 7.2-44. Thrust Axis Forces S1-2 Separation, Stage II Ignition, and Fairing Separation (SFM) 141

Figure 7.2-45. Thrust Axis Force at SECO (SFM) 141

Figure 7.3-1. VCLA Y-Axis Liftoff Acceleration (Load Case = 27) versus SFI Data 145

Figure 7.3-2. VCLA Z-Axis Liftoff Acceleration (Load Case = 18) versus SFI Data 145

Figure 7.3-3. VCLA Z-Axis Liftoff Force (Load Case = 18) versus SFM 146

Figure 7.3-4. VCLA Y-Axis Liftoff Force (Load Case = 23) versus SFM 146

Figure 7.3-5. Tolerance Factor 148

Figure 7.4-1. Reconstructed CLA X axis SRSs 154

Figure 7.4-2. Reconstructed CLA Y axis SRSs 155

Figure 7.4-3. Reconstructed CLA Z axis SRSs 156

Figure 7.4-4. Liftoff Full Reconstruction Forces 157

Figure 7.4-5. Liftoff Full Reconstruction Force SRSs 158

Figure 7.4-6. Liftoff Full Reconstruction Moments 159



**NASA Engineering and Safety Center
Technical Assessment Report**

Document #:
**NESC-RP-
06-071**

Version:
1.0

Title:

**Flight Force Measurements of the Gamma-Ray Large
Area Space Telescope / Delta II Flight**

Page #:
7 of 226

Figure 7.4-7. Liftoff Full Reconstruction Moment SRSs 160

Figure 7.4-8. Liftoff Reconstruction VCLA Model Forces..... 161

Figure 7.4-9. Liftoff Reconstruction VCLA Model Force SRSs..... 162

Figure 7.4-10. Liftoff Reconstruction VCLA Model Moments 162

Figure 7.4-11. Liftoff Reconstruction VCLA Model Moment SRSs 163

Figure 7.4-12. Liftoff Reconstruction Impedance Correlated Model Forces 164

Figure 7.4-13. Liftoff Reconstruction Impedance Correlated Model Force SRSs 165

Figure 7.4-14. Liftoff Reconstruction Impedance Correlated Model Moments..... 165

Figure 7.4-15. Liftoff Reconstruction Impedance Correlated Model Moment SRSs..... 166

Figure 7.4-16. Liftoff Reconstruction Impedance Method Forces 167

Figure 7.4-17. Liftoff Reconstruction Impedance Method Force SRSs..... 168

Figure 7.4-18. Liftoff Reconstruction Impedance Method Moment 169

Figure 7.4-19. Liftoff Reconstruction Impedance Method Moment SRSs 170

Figure 7.4-20. Liftoff Thrust Axis Accelerations 171

Figure 7.4-21. Liftoff Thrust Axis Acceleration SRSs..... 172

Figure 7.4-22. Liftoff Lateral X Axis Accelerations 173

Figure 7.4-23. Liftoff Lateral Y Axis Accelerations 174

Figure 7.4-24. Liftoff lateral X Axis Acceleration SRSs 175

Figure 7.4-25. Liftoff lateral Y Axis Acceleration SRSs 176

Figure 7.4-26. Liftoff Thrust Axis Forces (Steady+Dynamic)..... 177

Figure 7.4-27. Liftoff Thrust Axis Dynamic Forces..... 178

Figure 7.4-28. Liftoff Thrust Axis Force SRSs 179

Figure 7.4-29. Liftoff Lateral X Forces 180

Figure 7.4-30. Liftoff Lateral X Force SRSs..... 181

Figure 7.4-31. Liftoff Lateral Y Forces 182

Figure 7.4-32. Liftoff Lateral Y Force SRSs..... 183

Figure 7.4-33. Liftoff Lateral X Moments..... 184

Figure 7.4-34. Liftoff Lateral X Moment SRSs 185

Figure 7.4-35. Liftoff Lateral Y Moments..... 186

Figure 7.4-36. Liftoff Lateral Y Moment SRSs 187

Figure 7.4-37. Liftoff Torsional Moments 188

Figure 7.4-38. Liftoff Torsional Moment SRSs 189

Figure 7.5-1. Airloads X-Axis Force - SFM Versus Basedrive 192

Figure 7.5-2. Airloads Z-Axis Force - SFM Versus Basedrive..... 193

Figure 7.5-3. Airloads Y Moment - SFM Versus Basedrive..... 193

Figure 7.5-4. Airloads X Axis SRS Force (Q=20), SFM Versus Basedrive 194

Figure 7.5-5. Airloads Force Z SRS (Q=20) SFM Versus Basedrive 195

Figure 7.5-6. Airloads Moment Y SRS (Q=20), SFM Versus Basedrive 196

Figure 7.5-7. Airloads X Force, SFM Versus Basedrive (Filtered)..... 198

Figure 7.5-8. Airloads Moment Y, SFM Versus Basedrive (Filtered) 198



**NASA Engineering and Safety Center
Technical Assessment Report**

Document #:
**NESC-RP-
06-071**

Version:
1.0

Title:

**Flight Force Measurements of the Gamma-Ray Large
Area Space Telescope / Delta II Flight**

Page #:
8 of 226

Figure 7.6-1. MECO X-Axis Force – SFM Versus Basedrive 201
 Figure 7.6-2. MECO Y-Axis Force - SFM Versus Basedrive..... 202
 Figure 7.6-3. MECO Thrust (Z-Axis) - SFM Versus Basedrive 202
 Figure 7.6-4. MECO X-Axis Moment - SFM Versus Basedrive 203
 Figure 7.6-5. MECO Y-Axis Force SRS (Q=20) - SFM Versus Basedrive..... 204
 Figure 7.6-6. MECO Thrust (Z) Axis SRS (Q=20) - SFM Versus Basedrive 204
 Figure 7.6-7. MECO Thrust SRS (Q=50) Filtered 30 to 150 Hz 205
 Figure 7.6-8. MECO X-Axis Moment SRS (Q=20) - SFM Versus Basedrive 206
 Figure 7.6-9. MECO Y-Axis Moment SRS (Q=20) - SFM Versus Basedrive 206
 Figure 7.6-10. MECO Torsional (Mz) Moment SRS (Q=20) - SFM Versus Basedrive..... 207
 Figure 7.6-11. MECO Y-Axis Force (Filtered)..... 209
 Figure 7.6-12. MECO Thrust (Z) Axis (Filtered)..... 209
 Figure 7.6-13. MECO X-Axis Moment (Filtered)..... 210

List of Tables

Table 6.1-1. Payload Interface Points 22
 Table 6.1-2. Upper Stage Flexibility 37
 Table 6.2-1. Additional Accelerometers for the GLAST Spacecraft Sine Test 43
 Table 6.2-2. Force Gages Used During GLAST Spacecraft Sine Test 43
 Table 6.2-3. Expected Strain Maxima..... 43
 Table 6.2-4. Test PAF Mass Propertites..... 44
 Table 6.2-5. Mass Properties of GLAST – Flight Versus Test 45
 Table 6.2-6. TPAF Interface Point Coordinates..... 45
 Table 6.2-7. Instrument Channels 47
 Table 6.2-8. Test Runs Acquired by the NESC 49
 Table 6.2-9. Modified Instrument Channels 52
 Table 6.2-10. Natural Frequencies of the Fundamental Modes 57
 Table 6.2-11. Maxima Measured in the Low Level Sweeps..... 58
 Table 6.2-12. Difference Between Dominant Peaks from Strain and Force Gages (percent) 62
 Table 6.3-1. Coordinates of Trunnion Load Points..... 72
 Table 6.3-2. Instrumentation Channels 76
 Table 6.3-3. PAF Limit Loads..... 77
 Table 6.3-4. Absolute Maximum Strain Limiting Values..... 78
 Table 6.3-5. Static Test Runs: Part 1 - Fixed Base..... 79
 Table 6.3-6. Static Test Runs:Part 2 - Cylindrical Extension 80
 Table 6.3-7. Approximate Prediction Accuracy..... 85
 Table 6.5-1. Sequence of Events Summary 94
 Table 7.1-1. Data Acquisition System Parameters..... 99
 Table 7.1-2. Strain Gage Mapping for the Static Measurements 101



**NASA Engineering and Safety Center
Technical Assessment Report**

**Document #:
NESC-RP-
06-071**

**Version:
1.0**

Title:

**Flight Force Measurements of the Gamma-Ray Large
Area Space Telescope / Delta II Flight**

Page #:
9 of 226

Table 7.1-3. Flight Instrumentation Channels..... 102

Table 7.1-4. ULA and FFM Strain Gage Naming Convention..... 103

Table 7.1-5. Static Pre-Flight Data Results* 104

Table 7.2-1. Datasets Used for Various Events..... 105

Table 7.2-2. Liftoff Maximum Predicted Forces 121

Table 7.2-3. Peak Centerline Accelerations Measured at Airloads..... 123

Table 7.2-4. Airloads Interface Forces Calculated from Measured Strains 125

Table 7.2-5. Peak Centerline Accelerations Measured at MECO..... 133

Table 7.2-6. MECO Interface Forces Calculated from Measured Strains 135

Table 7.2-7. SFM Results for Other Flight Events..... 142

Table 7.2-8. FEM Results for Other Flight Events 142

Table 7.3-1. Comparison of VCLA Predictions versus Measured SFI Data for Liftoff..... 147

Table 7.3-2. VCLA Liftoff Results Compared with SFM Forces Scaled to P99/90..... 149

Table 7.3-3. Comparison of VCLA Predictions Versus Measured SFI Data for Airloads 150

Table 7.3-4. VCLA Airloads Results Compared with SFM Forces Scaled to P99/90..... 151

Table 7.4-1. Liftoff Summary Table 190

Table 7.5-1. Unfiltered Airloads Force Comparison - SFM versus Basedrive 191

Table 7.5-2. Airloads Filtered Absolute Max Values – SFM versus Basedrive 197

Table 7.6-1. MECO Absolute Maximum Forces – SFM versus Basedrive (Unfiltered)..... 200

Table 7.6-2. MECO Absolute Maximum Forces - SFM versus Basedrive (5 to 150 Hz) 208

Table 7.6-3. MECO Absolute Maximum Forces – SFM Versus Basedrive (80 to 150 Hz).. 211

	NASA Engineering and Safety Center Technical Assessment Report	Document #: NESC-RP- 06-071	Version: 1.0
Title: Flight Force Measurements of the Gamma-Ray Large Area Space Telescope / Delta II Flight		Page #: 10 of 226	

Volume I: Technical Assessment Report

1.0 Notification and Authorization

A NASA Engineering and Safety Center (NESC) out-of-board activity was approved October 10, 2006. Dr. Curtis Larsen, NASA Technical Fellow for Loads and Dynamics at Johnson Space Center (JSC) was the sponsor for this assessment and Mr. Daniel Kaufman, NESC Loads and Dynamics Deputy, Structural Dynamics Group at the Goddard Space Flight Center (GSFC), was selected to lead the assessment. An Initial Evaluation was presented to the NESC Review Board (NRB) on November 2, 2006. The Assessment Plan was presented and approved by the NRB on February 15, 2007. The Assessment Report was presented to the NRB for approval on September 24, 2009.

The following Stakeholders will be recipients of the final outbrief and engineering report:

- NESC
- NASA Launch Services Program
- Chief Engineer, Mechanical Division at GSFC
- Chief of the Dynamic Environments Branch at the Jet Propulsion Lab (JPL)

The NESC team was tasked to perform this discipline enhancing project consisting of the following activities:

1. Develop an analytical method to convert the strains measured on a Delta II payload adapter into the interface forces experienced between the launch vehicle and the spacecraft.
2. Procure a flight data system for the Gamma-Ray Large Area Space Telescope (GLAST) Delta II flight. This mission was selected because of the launch schedule and due to the trussed payload adapter fitting (PAF) design used on this flight, which is the most suitable for resolving forces based on strain measurements.
3. Perform post-flight data analysis to document the benefits of force measurements and to make recommendations for further Agency action.

	NASA Engineering and Safety Center Technical Assessment Report	Document #: NESC-RP- 06-071	Version: 1.0
		Title: Flight Force Measurements of the Gamma-Ray Large Area Space Telescope / Delta II Flight	

3.0 Team List

Name	Position/TDT Affiliation	Center/Contractor
Core Team		
Curtis Larsen	NASA Technical Fellow for Loads and Dynamics	JSC
Daniel Kaufman	Assessment Co-Lead/Ground Testing and Analysis	GSFC
Scott Gordon	Assessment Co-Lead/Ground Testing and Analysis	GSFC
Dan Worth	Dynamic Testing	GSFC
Isam Yunis ¹	Flight Implementation and Analysis	KSC
Chris Gerace	Flight Implementation and Analysis	KSC
Teresa Kinney	Flight Implementation and Analysis	KSC
Paul Rapacz	Analysis	JPL
Dennis Kern	Ground Testing and Analysis	JPL
William Haile	Analysis and Test	ATK
Michael Fendya ³	Analysis and Test	ATK
Ayman Abdallah ²	Flight Implementation and Analysis	KSC
Timothy Fogarty	Flight Implementation and Analysis	Analex Corporation
Terry Scharton	Consultant	JPL (Retired)
Administrative Support		
Chris Johansen	Program Analyst	LaRC
Linda Burgess	Planning and Control Analyst	ATK, LaRC
Pam Sparks	Project Coordinator	ATK, LaRC
Tina Dunn ⁴	Project Coordinator	ATK, LaRC
Christina Cooper	Technical Writer	ATK, LaRC

- 1) Isam Yunis (KSC) moved to LaRC in 2007 leaving Chris Gerace as KSC lead for the effort.
- 2) Ayman Abdallah (KSC) was added to the Core Team list in 2008
- 3) Mike Fendya (ATK) was added to the Core team in 2007 to mid 2008 when he left ATK.
- 4) Pam Sparks replaced Tina Marie Dunn as Project Coordinator in 2008

	NASA Engineering and Safety Center Technical Assessment Report	Document #: NESC-RP- 06-071	Version: 1.0
Title: Flight Force Measurements of the Gamma-Ray Large Area Space Telescope / Delta II Flight		Page #: 13 of 226	

3.1 Acknowledgements

In Memoriam: This report is dedicated to the memory of our dear colleague Dr. William (Bill) Haile. Bill supported the GSFC Structural Dynamics Community for almost 30 years and was a key member of the NESC assessment team. Bill passed away on November 1, 2008. The Agency will miss Bill's extraordinary technical skills and human warmth.

4.0 Executive Summary

There has been a long-standing need to obtain in-flight force measurements (FFMs). The standard approach over the last 40 years for predicting spacecraft response to the launch environment has been to measure accelerations on the launch vehicle and derive a coupled loads simulation which matches these acceleration levels. Limited measurements have been collected on the payload side to determine how these simulations do at predicting response of the spacecraft and on-board hardware. While acceleration measurements can be readily obtained, they do not directly indicate the loads and stresses that a structure will experience during launch. In order to calculate these critical quantities, it is necessary to perform dynamic analysis using math models and forcing functions developed to simulate the coupled launch vehicle/spacecraft system and the expected flight environments. Even with the best development and correlation tools, dynamic analysis of a coupled system with many degrees of freedom under complex loading conditions requires assumptions to be made about critical parameters relating to system frequencies, mode shapes, damping, and the form of the forcing functions used to replicate the launch environment. Measurement of interface forces during flight provides a direct metric for assessing how acceleration-based methods do at accurately predicting the loads that are generated during launch, and can provide a means for improving the ability to predict how launch vehicle payloads response to the flight environment. This was the primary focus of this NESC assessment.

In the proposal, the NESC team identified two questions that this assessment would attempt to address by the measurement of forces during the GLAST flight. These questions were:

- 1) Is flight correlation and reconstruction with acceleration methods sufficient?
- 2) How much can the loads and therefore the design and qualification be reduced by having force measurements?

The most straight-forward approach to measuring interface forces during launch would be to insert force transducers at or just below the spacecraft separation plane. However, the development effort and lead time required to introduce additional hardware at a critical interface was beyond the scope of this effort. Therefore, the NESC team proposed an effort to measure forces at the spacecraft interface through the use of strain measurements of the launch vehicle payload adapter fitting (PAF).

	NASA Engineering and Safety Center Technical Assessment Report	Document #: NESC-RP- 06-071	Version: 1.0
Title: Flight Force Measurements of the Gamma-Ray Large Area Space Telescope / Delta II Flight		Page #: 14 of 226	

The NESC team had several critical milestones that had to be achieved in order to successfully achieve the goals of the assessment. The critical milestones and the sections of the report that discuss these milestones are presented below:

- 1) Analytical demonstration that a method of predicting interface forces calculated from measured strain on an instrumented PAF was feasible. This was listed as a critical constraint in the proposal. (Section 6.1)
- 2) Validation of the methodology with ground testing. Static and dynamic tests were performed to check the analysis methodology and determine if the required accuracy set forward in the proposal (goal of 10 percent, maximum of 20 percent) could be met for this effort to be of value. (Sections 6.2 and 6.3)
- 3) Development of the flight data acquisition system and installation on the launch vehicle. (Section 6.4)
- 4) Recovery of the strain and acceleration data during the GLAST/Delta II flight. (Section 6.5)
- 5) Post-processing of the flight data and evaluation of the data as compared with coupled loads and basedrive predictions of interface forces. (Section 7.0)

A significant amount of work was performed to post-process the flight data and compare it with the various acceleration-based methods for predicting flight loads. The initial step was to review the flight data that was acquired by the special flight instrumentation (SFI) package which was flown on the GLAST mission. The SFI instrumentation consisted of 64 strain gages and 12 accelerometer channels. The flight data acquired by the SFI package during the GLAST flight is covered in detail in Section 7.2.

The next step in the process was to compare the measured flight forces with predictions from coupled loads and basedrive analyses performed to simulate the flight environment. The measured flight forces and accelerations were compared with the results from the Verification Coupled Loads Analysis (VCLA) for the GLAST mission. The VCLA is the final load cycle that is performed to verify that the spacecraft has been adequately qualified for the predicted flight environment prior to launch. The comparison of VCLA results with the measured forces and accelerations is discussed in Section 7.3.

For the Delta II launch vehicle, there were three flight events which were the primary drivers for spacecraft design. These flight events are Liftoff, Airloads, and Main-Engine Cutoff (MECO). The forces measured during the GLAST flight were compared with analytical predictions for each of these flight events. Basedrive simulations using the measured flight accelerations were performed for each of the flight events to understand differences between measured flight forces and those derived from an acceleration-based analysis. Two different model configurations were used in the basedrive analysis. One was the same model used for the VCLA with an assumed constant damping for all modes. The other model was an updated version of the VCLA model

	NASA Engineering and Safety Center Technical Assessment Report	Document #: NESC-RP- 06-071	Version: 1.0
Title: Flight Force Measurements of the Gamma-Ray Large Area Space Telescope / Delta II Flight		Page #: 15 of 226	

which had been modified to more accurately reflect the results of the GLAST sine test. This correlated model also used damping values that had been measured during the sine test. In addition to the basedrive analyses performed for each flight event, a full coupled loads analysis (CLA) reconstruction analysis was performed for Liftoff. The comparisons between measured flight loads and analytical predictions for Liftoff, Airloads, and MECO are discussed in Sections 7.4, 7.5, and 7.6, respectively.

Based on the review of the forces measured on the GLAST flight and the comparison with analytical predictions, the following are the more important findings derived from this study:

- The GLAST VCLA grossly under-predicted the maximum torsional moment measured during flight.
- The results from the GLAST VCLA showed a greater than expected over-prediction of lateral forces and bending moments at the interface compared to the measured SFM results.
- The basedrive analysis using measured flight accelerations over-predicted the lateral interface forces for all major flight events (Liftoff, Airloads, and MECO).

The above findings indicate that there are areas in which the accuracy of the coupled loads process could be improved if force measurement data was available from additional flights. It should be noted that it was difficult to draw definitive conclusions from force data from a single flight when comparing with an analytical methodology derived to provide a statistical envelope. Additional FFMs would provide greater insight into the accuracy of coupled loads analysis. In addition, evaluation of the basedrive results as compared with the measured flight forces indicates that the basedrive analysis even using measured accelerations tended to produce conservative predictions of interface loads. Therefore, the NESC team suggests a database of measured flight force data could be used to reduce the conservatism of the basedrive analysis and improve its usefulness as a design tool.

The following recommendations are directed to the NASA Engineering and Safety Center (NESC), the NASA Launch Services Program, the Goddard Space Flight Center (GSFC) Chief of the Mechanical Division, and the Jet Propulsion Laboratory (JPL) Chief of the Dynamics Environments Branch and are identified to address the above findings:

- Evaluate the ability of launch vehicle design limit loads and CLA techniques to adequately simulate the torsional loading during launch. Current methods may not be conservative for structures that are sensitive to torsional loading.
- Obtain additional force measurements over a number of flights for a given launch vehicle in order to:
 - Improve the accuracy of CLA by reconciling against a database of both force and acceleration measurements.

	NASA Engineering and Safety Center Technical Assessment Report	Document #: NESC-RP- 06-071	Version: 1.0
Title: Flight Force Measurements of the Gamma-Ray Large Area Space Telescope / Delta II Flight		Page #: 16 of 226	

- Develop statistically meaningful force spectra that could be used in conjunction with basedrive analysis to provide a more accurate tool for preliminary spacecraft design.

The NESC team was able to successfully develop a methodology for measuring interface forces based on instrumenting the Delta II 6915 PAF with strain gages. This methodology was demonstrated through both static and dynamic ground testing, and was flown successfully on the GLAST mission. Processing of the data from the GLAST flight indicated that making force measurements on additional flights may result in improvements in the accuracy of the CLA methodology and could provide a means for reducing the conservatism in the basedrive analysis as a design tool. While there are only a limited number of Delta II flights remaining, the findings and recommendations related to making FFMs are applicable to current and future launch vehicles.

	NASA Engineering and Safety Center Technical Assessment Report	Document #: NESC-RP- 06-071	Version: 1.0
Title: Flight Force Measurements of the Gamma-Ray Large Area Space Telescope / Delta II Flight			Page #: 17 of 226

5.0 Assessment Plan

The Assessment Plan consisted of the following phases:¹

Phase 1 Methodology Development: Development of the methodology to extract PAF global and/or local interface forces and moments, based on selected set of strain gages. This methodology development was followed by sensitivity analyses under different strain gage configurations and boundary conditions to understand the approach robustness and as a methodology independent check. The successful completion of this phase was the first risk that had been identified in the Assessment Plan. The initial assumption that strain gages could be used to extract forces and moments from a complex adapter structure had not been established prior to the start of this phase. This risk was identified in the original Assessment Plan (Section 11.0) Constraints.

Phase 2 Ground Static Test Validation: A Delta II test PAF (TPAF) was instrumented with strain gages and a series of static tests were performed on a simulated payload to measure strains and forces at the payload interface. Forces calculated from the measured strains using the methodology developed in Phase 1 were compared with the applied forces from the test to validate that the accuracy goals could be met.

Phase 3 Ground Dynamic Test Validation: Once the static test validation was successfully performed, a dynamic test series was completed to further reevaluate the methodology. This testing was performed as part of the GLAST sine vibration testing using strain gages mounted to the TPAF. Forces calculated from the measured strains were compared to the forces measured by forces gages that had been installed as part of the GLAST test fixture.

Phase 4 Flight Data System Procurement: The procurement of the flight data system occurred in parallel with the Phases 2 and 3 due to schedule constraints in acquiring the necessary hardware. Development of the flight data system before the feasibility of calculating interface forces based on measured strain had been demonstrated within the required accuracy was identified in the proposal constraints section as a high risk.

Phase 5 Post Flight Data Acquisition and Flight Data Flight Processing: The strain gage measurements acquired during the GLAST flight were used to resolve forces and moments. In addition, all other standard flight data (accelerations, engine pressures, ground winds, etc.) were used in a reconstruction loads analysis as well as basedrive simulations for comparison with the measured forces during the flight.

¹ The NESC team decided to alter the project flow and performed Phase 3 before Phase 2.

	NASA Engineering and Safety Center Technical Assessment Report	Document #: NESC-RP- 06-071	Version: 1.0
Title: Flight Force Measurements of the Gamma-Ray Large Area Space Telescope / Delta II Flight			Page #: 18 of 226

6.0 Description of the Problem, Phases of the Assessment and Resolution

6.1 Phase 1: Methodology Development

The NESC team set the initial guidelines and tasked Swales and Associates (now ATK Space Division) with identifying the mathematical formulation of a strain-based matrix methodology for calculating interface forces. The task given to ATK Space Division was to derive a method for calculating the forces and moments produced at the spacecraft interface using measurements from strain gages bonded to the PAF during liftoff and flight. The techniques developed for calculating interface forces based on measured strain were derived for the Delta II 6915 PAF used for the GLAST spacecraft. The first analytical formulation was derived based on the PAF finite element model (FEM), but in the course of the development several difficulties were encountered including issues with matrix inversion and sensitivities to flexibility at the booster interface. A second methodology called the Summed Force Method (SFM) was formulated in parallel to address these issues.

The SFM was formulated due to initial problems with the FEM based approach. These problems were overcome and the NESC team identified two strain based methodologies to be evaluated during the ground test campaign. Both the FEM based methodology and the SFM approach is documented in the report entitled “Methodology for PAF Flight Force Measurement”, SAI-TM-3150, Revision A [ref. 1].

During this time other alternatives were considered:

- a) An acceleration based methodology called the “Impedance” approach was developed. The goal was not to evaluate this technique for accuracy, but to use this approach as a complementary method to calculate interface forces during ground testing and flight. The Impedance Method is documented in Reference 1.
- b) Langley Research Center (LaRC) and Old Dominion University (ODU) were tasked with a proposal for a proof of concept force prediction method based on strains. However, this methodology was not used in this assessment.

The following sections present a summary of the strain methods for calculating interface forces and in most cases are extracted with minor modifications [ref. 1].

Details of analytical checks of the FEM Method, SFM, and Impedance Method can be found in Reference 1. In addition, a brief sensitivity study was performed whereby each strain method was evaluated for the possibility that a subset of channels may be lost in flight or data drops to occur.



Title:

**Flight Force Measurements of the Gamma-Ray Large
Area Space Telescope / Delta II Flight**

Page #:
19 of 226

6.1.1 The PAF FEM

The Delta II 6915 PAF is a truss type adapter with 8 diagonal struts. The payload attaches at 4 mounting pads to the PAF top through a set of explosive bolts which are fired to separate the spacecraft from the launch vehicle. The 6915 designation is based on the 4 mounting locations at the separation plane are on a 69-inch bolt circle and the PAF is 15 inches tall. The PAF attaches to the Second Stage Guidance Section (SSGS) of the Delta II vehicle through a mounting flange at the PAF base by means of 68 bolts on a 64-inch bolt circle. The loads from each of the mounting pads at the payload interface are carried by a pair of struts, referred to as legs, to the PAF base. The geometry of the 6915 PAF is shown in Figure 6.1-1. The dotted lines labeled I, II, III, and IV denote the quadrants of the launch vehicle and show the vehicle orientation relative to the payload interface mounting pads.

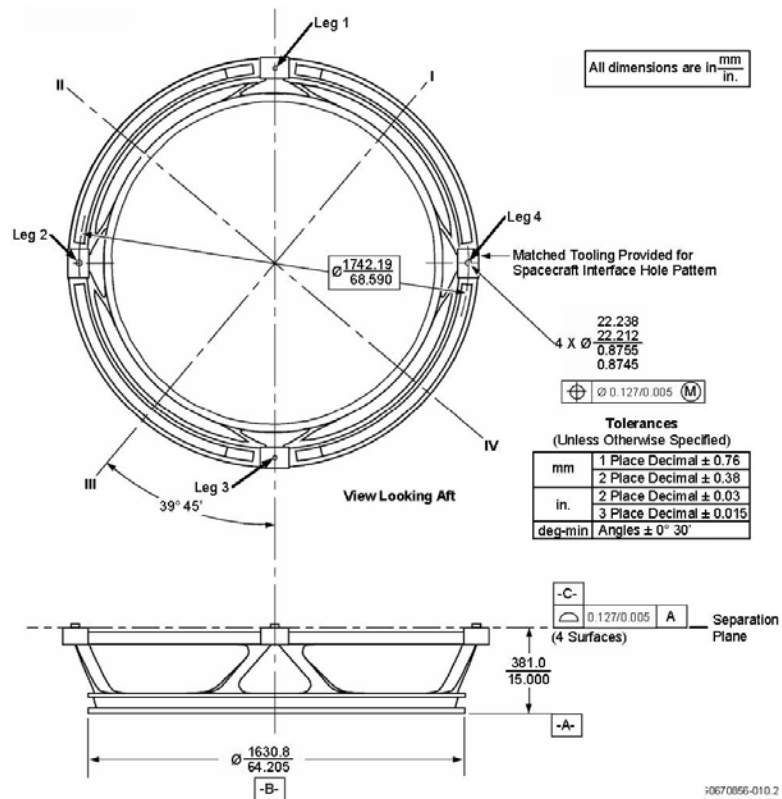


Figure 6.1-1. 6915 PAF Geometry

The PAF FEM developed for the FFM activity is shown in Figure 6.1-2. The figure defines the coordinate axes, the strut numbering scheme, and shows the payload interface points for the PAF FEM. The locations of the payload interface points are defined in Table 6.1-1.



Title:

**Flight Force Measurements of the Gamma-Ray Large
Area Space Telescope / Delta II Flight**

Page #:
20 of 226

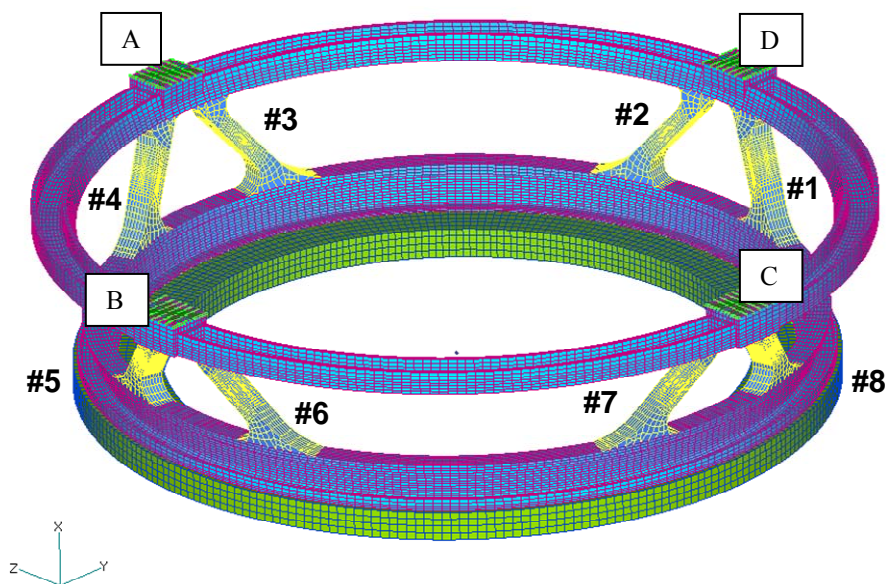


Figure 6.1-2. Delta II 6915 PAF FEM

The Delta II 6915 PAF has 68 booster interface points. However, for test purposes, the GLAST Project used only 8 when the spacecraft was tested dynamically so that 8 Kistler force transducers were used to measure the interface loads. To accomplish this, the PAF was bolted to a stiff adaptor ring that interfaces to the force gages.

Initial Assumptions

1. Each interface point produces 3 forces and 3 moments.
2. Delta II 6915 PAF is a linear structure.
3. Delta II 6915 PAF mass is ignored.
 - a. This eliminates the necessity to include acceleration terms when deriving interface forces.
4. Individual point forces on the PAF are not resolved, only the net forces and moments are calculated.
5. No forces are applied to the GLAST spacecraft except at the PAF boundary. Acoustic loads on the spacecraft during flight are ignored in this formulation.

The development of a methodology to relate forces to strain for the GLAST mission begins with the creation of a 6195 PAF FEM. For this assessment, a detailed solid model was supplied by United Launch Alliance (ULA) and converted into a FEM by ATK Space Division. A high

	NASA Engineering and Safety Center Technical Assessment Report	Document #: NESC-RP- 06-071	Version: 1.0
	Title: Flight Force Measurements of the Gamma-Ray Large Area Space Telescope / Delta II Flight		Page #: 21 of 226

fidelity model was necessary to calculate accurate strains at numerous points. It was important to match the FEM grid size to the strain gage size.

From the FEM, the stiffness and mass matrices are reduced to include degrees-of-freedom (d-o-f) at the interface points in its A-set. This was accomplished by reduction to the Craig-Bampton set of boundary d-o-f and modes shapes. The matrices are symmetric and the stiffness is singular. From this matrix, the linear force-deflection relation is partitioned into the 4 payload and the 8 booster boundary points as:

$$\begin{matrix} \begin{bmatrix} F_P(t) \\ F_B(t) \end{bmatrix} \\ \begin{matrix} (72 \times 1) \\ (72 \times 1) \end{matrix} \end{matrix} = \begin{matrix} \begin{bmatrix} K_{PP} & K_{PB} \\ K_{BP} & K_{BB} \end{bmatrix} \\ \begin{matrix} (72 \times 72) \end{matrix} \end{matrix} \begin{matrix} \begin{bmatrix} u_P(t) \\ u_B(t) \end{bmatrix} \\ \begin{matrix} (72 \times 1) \end{matrix} \end{matrix} \quad \text{or, simply} \quad [F(t)] = [K] \begin{bmatrix} u_P(t) \\ u_B(t) \end{bmatrix}$$

where,

- $F_P(t)$ = forces (and moments) at the payload interface points (24 d-o-f),
- $F_B(t)$ = forces (and moments) at the booster interface points (48 d-o-f),
- $u_P(t)$ = displacements (translational and rotational) at the payload interface points ($6 \times 4 = 24$ d-o-f),
- $u_B(t)$ = displacements at the booster interface points ($6 \times 8 = 48$ d-o-f for the GLAST study, $6 \times 68 = 408$ d-o-f),
- K = matrix of stiffness coefficients, and

Variables are shown as functions of time to distinguish them from constant coefficients (e.g., stiffness matrix elements). Along with this model are the 6 unit rigid body vectors for the interface points, $[R]$. For example, for point “i” located at coordinate x_i , y_i and z_i , the 6×6 rigid body sub-matrix has the form:

$$[R_i] = \begin{bmatrix} 1 & 0 & 0 & 0 & z_i & -y_i \\ 0 & 1 & 0 & -z_i & 0 & x_i \\ 0 & 0 & 1 & y_i & -x_i & 0 \\ 0 & 0 & 0 & 1 & 0 & 0 \\ 0 & 0 & 0 & 0 & 1 & 0 \\ 0 & 0 & 0 & 0 & 0 & 1 \end{bmatrix}$$

For reference, when measuring from the center of the booster interface plane, the payload bolt locations are given in Table 6.1-1 and shown in Figure 6.1-2.

	NASA Engineering and Safety Center Technical Assessment Report	Document #:	Version:
		NESC-RP-06-071	1.0
Title:			Page #:
Flight Force Measurements of the Gamma-Ray Large Area Space Telescope / Delta II Flight			22 of 226

Table 6.1-1. Payload Interface Points

		X(in)	Y(in)	Z (in)
A	80000	15.00	0.000	34.295
B	80001	15.00	-34.295	0.000
C	80002	15.00	0.000	-34.295
D	80003	15.00	34.295	0.000

6.1.2 Coupling PAF and Payload

The NESC team examined the PAF coupled to the payload (i.e., the GLAST spacecraft). If the spacecraft FEM is partitioned into two sets, u_1 for the displacements on the boundary, and u_2 for the other internal displacements, the static force-deflection relation is:

$$\begin{bmatrix} F_1 \\ F_2 \end{bmatrix} = \begin{bmatrix} K_{11} & K_{12} \\ K_{21} & K_{22} \end{bmatrix} \begin{bmatrix} u_1 \\ u_2 \end{bmatrix}$$

Adding the PAF by equating $u_1 = u_p$ and $F_1 = F_p$, the coupled force-deflection equation is:

$$\begin{bmatrix} F_p \\ F_B \\ F_2 \end{bmatrix} = \begin{bmatrix} K_{pp} + K_{11} & K_{pB} & K_{12} \\ K_{Bp} & K_{BB} & 0 \\ K_{21} & 0 & K_{22} \end{bmatrix} \begin{bmatrix} u_p \\ u_B \\ u_2 \end{bmatrix}$$

If by constraining the booster interface ($u_B = 0$) and solve for the forces at the payload interface, F_p , then the equation appears as:

$$[F_p] = \left([K_{pp} + K_{11}] - [K_{12}][K_{22}]^{-1} [K_{21}] \right) [u_p] + [K_{12}][K_{22}]^{-1}[F_2]$$

This is appreciably more complex than the simple PAF-only expression. The coupled equation shows detailed knowledge of the spacecraft FEM is necessary, but undesirable. One approach to simplify the equation is to abandon calculating the force at each interface point and, instead calculate the 6 net loads (3 forces and 3 moments) at the centroid of the spacecraft interface (i.e., the sum of the forces and moments). Though there are 24 forces at the GLAST spacecraft boundary, the forces that cause the interface ring to warp and twist will sum to zero as these are local effects and do not result in global displacement at the interface centroid.

Mathematically,

$$[F_{p \text{ SUM}}] = [R_p]^T [F_p]$$

	NASA Engineering and Safety Center Technical Assessment Report	Document #: NESC-RP- 06-071	Version: 1.0
Title: Flight Force Measurements of the Gamma-Ray Large Area Space Telescope / Delta II Flight			Page #: 23 of 226

where,

(6 x t) (6x24) (24 x t)

$[F_{pSum}] =$ The sum of forces and moments at the centroid of the payload interface (6 x time)

$[R_p] =$ The rigid body transform from the 6 d-o-f at the centroid of the payload interface to the 24 d-o-f at the payload boundary (24 x 6)

$[F_p] =$ The 24 forces at the GLAST spacecraft boundary (24 x time)

It can be shown that:

$$\left([K_{11}] - [K_{12}][K_{22}]^{-1}[K_{21}] \right) [R_p] = 0$$

So, if it is required that no external forces be applied to the payload except at the boundary ($F_2 = 0$), then the equation reduces to:

$$\begin{matrix} [F_{pSUM}(t)] & = & [R_p]^T [K_{pp}] [u_p(t)] \\ (6 \times t) & & (6 \times 24) (24 \times 24) (24 \times t) \end{matrix}$$

Initial assumptions 2, 3, 4, and 5 identified in Section 6.1.1 were necessary to produce this equation. The assumptions applied to both the payload and booster interfaces. If the boundary was a single point, then the net and point forces are identical.

This basic static relationship does not use accelerometer data or the PAF mass (i.e., assumption 3). The relationship does not include deformation of the booster boundary. It is assumed that the booster stiffness is not known.

6.1.3 Strain Gages

Two of the force measurement techniques discussed use strain gages. Generally, gages selected for dynamic events have higher gage factors and higher temperature sensitivity than those selected for static activities.

The criterion used for selecting the strain gage locations is that they should be placed where strain is large and gradient is small. Large strains tend to reduce measurement noise, and low strain gradients tend to make the exact gage position less critical. For the PAF, strain gages were placed at the mid-length points on each of the 8 strut faces. Each strain point was covered by a strain rosette that had three gages in a single patch. The gages are oriented so that, when facing the strut the 0 degree gage is lateral (i.e., at the 3:00 o'clock position), the 45 degree gage is for shear (i.e., at the 1:30 o'clock position), and the 90 degree gage is axial (i.e., at the 12:00 o'clock position). Figure 6.1-3 shows the placement and gage labeling scheme.



Title:

Flight Force Measurements of the Gamma-Ray Large Area Space Telescope / Delta II Flight

Page #:
 24 of 226

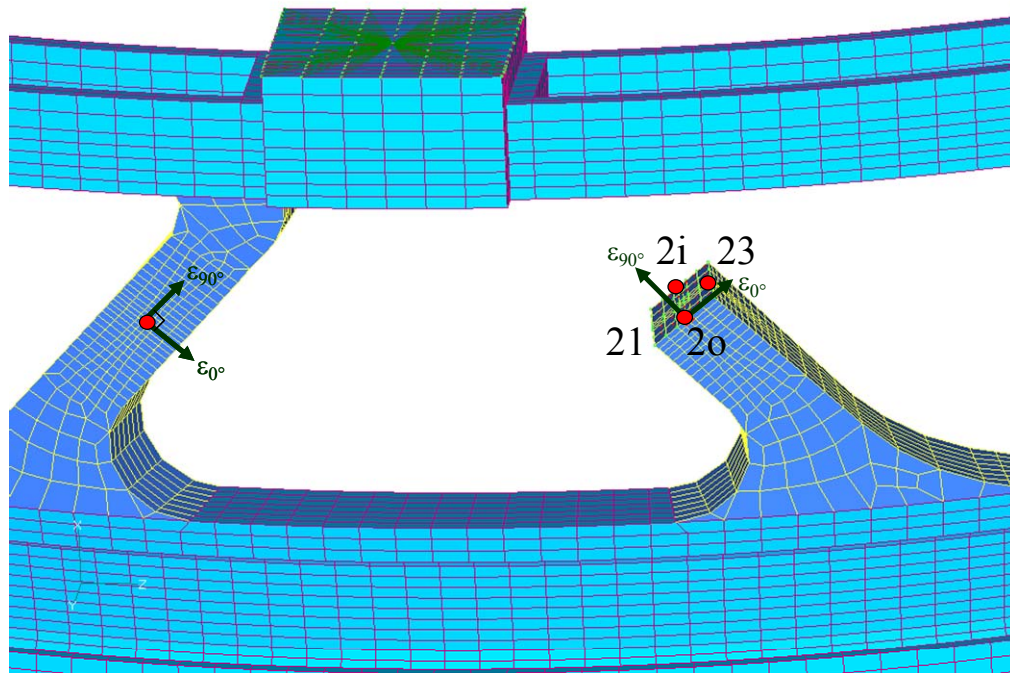


Figure 6.1-3. Strut 2 Cut Section Showing the Locations of the 4 Strain Rosettes and Gages at 0 Degree (lateral) and 90 Degree (axial)

The nomenclature for the gages is a three-character code “i, j, k”, where “i” is the strut number, “j” is the face, and “k” is the orientation. Struts were numbered 1 through 8. Faces were either numbered 1 through 8 to denote the facing strut or labeled “i” (inner) or “o” (outer). Orientation is either 0 degree (lateral), 45 degree (shear), or 90 degree (axial). For 8 struts, 4 faces each and 3 strains per face, a total of 96 strain measurements were possible using the rosettes. For practical reasons, the lateral gages were unnecessary and eliminated, leaving only the axial (A) and shear (S) gages for a total of 64 measurements.

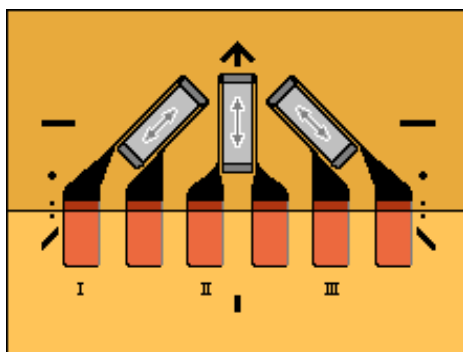
As an example, the 8 gages on strut number 2 are labeled as follows:

21A	21S	on the surface facing strut 1
2oA	2oS	on the inner surface
23A	23S	on the surface facing strut 3
2iA	2iS	on the outer surface.

Figure 6.1-4 shows a typical rosette with three gages. For the configuration used with the PAF, each rosette was oriented such that gage I (at 1:30) was placed across the centerline of the strut at

	NASA Engineering and Safety Center Technical Assessment Report	Document #: NESC-RP- 06-071	Version: 1.0
		Title: Flight Force Measurements of the Gamma-Ray Large Area Space Telescope / Delta II Flight	

the middle point of its length and used to measure shear strain. Gage II (at 12:00) was aligned parallel with the strut axis slightly off-center from the centerline and used to measure axial strain. In this configuration, there is no lateral gage (at 3:00) and gage III (at 10:30) was not used. Tension in the gage was identified positive with compression listed as negative. A detailed description of the gage installation and orientation is provided in Section 6.2.2.



Dimensions:

	<u>Inch</u>	<u>mm</u>
Gage Length	0.125	3.18
Overall Length	0.300	7.62
Grid Width	0.060	1.52
Matrix Length	0.42	10.7
Matrix Width	0.62	15.7

Figure 6.1-4. Vishay Strain Rosette CEA-13-125UR-350

The distance between points was:

From gage "i" to "o"	2.06 in
From gage "23" to "21"	1.60 in

As will be discussed in Sections 6.1.5 (FEM Method) and 6.1.6 (Summed Force Method), 64 strain gages were sufficient to calculate interface loads based on strain measurements and could be accommodated by the SFI system being developed by ULA. While it is possible to calculate interface loads using fewer strain gages, optimizing the number of strain measurements was outside of the scope of this assessment. Therefore, no attempt was made to minimize the number of strain gages that were used once it was determined that the assessment requirements could be met within the constraints of the SFI. Having additional gages above the minimum necessary to resolve interface forces also provided a more robust instrumentation scheme should some gages fail during flight.

6.1.4 Accelerometers

Accelerations were used to support the flight reconstruction and to evaluate alternate acceleration based methods. For this purpose, 4 tri-axial accelerometers were mounted on the bottom PAF flange directly under each payload interface point for a total of 12 acceleration channels. Using

	NASA Engineering and Safety Center Technical Assessment Report	Document #: NESC-RP- 06-071	Version: 1.0
		Title: Flight Force Measurements of the Gamma-Ray Large Area Space Telescope / Delta II Flight	

the 12 accelerometer channels, it was possible to accurately measure both the translational and rotational accelerations at the payload interface.

6.1.5 FEM Method of Solution

The FEM Method relies directly on the PAF FEM. Therefore, the precision of this method is dependent on the FEM accuracy. To produce the matrix of linear coefficients which relate strain to displacement, the PAF FEM is constrained at all interface points. Each interface points is then released 1 d-o-f at a time holding the others fixed and the corresponding unit translation and/or rotation for the release d-o-f is applied in the positive direction. All 64 strains corresponding to the enforced deflection are calculated and placed in a matrix, G_p . This process is then repeated for each payload boundary d-o-f. For the payload boundary, there are $6 \times 4 = 24$ cases.

$$[\varepsilon(t)] = [G_p] [u_p(t)]$$

(64,1) (64,24) (24,1)

where, $\varepsilon(t)$ = strain as a function of time

The process of releasing d-o-f and calculating the corresponding strain field continues for the booster boundary one at a time, for $6 \times 8 = 48$ cases. The complete strain set is calculated and put into a matrix G_B according to the formula:

$$[\varepsilon(t)] = [G_B] [u_B(t)]$$

(64,1) (64,48) (48,1)

Then, for all possible boundary displacements, the strain gage readings were calculated by:

$$[\varepsilon] = [G_p, G_B] \begin{bmatrix} u_p \\ u_B \end{bmatrix} \quad \text{or, simply} \quad [\varepsilon] = [G] \begin{bmatrix} u_p \\ u_B \end{bmatrix}$$

$[G]$ is a poorly conditioned matrix. If part of the booster boundary is fixed, then the inverse is exact. If the booster boundary is flexible, as is the case with the Delta II 6915 PAF, then errors may be introduced.

Other routines provide an inverse where $[G] [G]^{-1} = [I]$ as required, but $[G]^{-1} [G] \neq [I]$. The reason for this is not clear, but noted in the appendix of Reference 1 is that a clean G-matrix for a simple case is singular. The appendix of this reference expands this discussion for a simple, axial bar. However, a subset of G identified as G_1 can always be inverted using the pseudo-inverse technique. Consisting essentially of a least squares fit from the strain measurements to the remaining boundary displacements. For this assessment, 12 d-o-f (2 points) on the booster

	NASA Engineering and Safety Center Technical Assessment Report	Document #: NESC-RP- 06-071	Version: 1.0
Title: Flight Force Measurements of the Gamma-Ray Large Area Space Telescope / Delta II Flight			Page #: 27 of 226

interface ring were constrained to enable the inverse and produce the strain-force relation for the PAF payload side:

$$[F_{PSum}(t)] = [E_F] [\epsilon(t)] \quad \text{where,} \quad [E_F] = [R]^T [K_{PP} \ K_{PB}] [G_1^T \ G_1]^{-1} [G_1]^T$$

As a method accuracy check, the following matrix product should equal the identity matrix:

$$[E_F] [G_P] [K_{PP} \ K_{PB}]^{-1} \text{ should} = [I]$$

During the FEM Method studies it was determined that:

- a) The matrix $[G_P, G_B]$ is sensitive to the strain formulation. Either it cannot be inverted, or if inverted produces a complex result.
- b) The method depends on the FEM accuracy and, in particular, its stiffness matrix. This matrix is not verified by test.
- c) The FEM Method is more sensitive to boundary conditions as channels are lost.

6.1.6 Summed Force Method (SFM) of Solution

For the SFM method, the PAF FEM was not used (except to identify the PAF geometry). However, for study purposes, matrix $[G]$ was used to produce the strains that are representative of the test or flight values. These strain readings on the strut's cross-section were used directly to compute forces and moments at the section by use of simple beam stress equations. For example, the axial strain under an axial force for strut 1 was approximated as:

$$\epsilon_{12,90} = \epsilon_{1i,90} = \epsilon_{18,90} = \epsilon_{1o,90} = \frac{F_{Axial}}{EA}$$

However, developing this relationship between strain and forces based on strut geometry proved to be difficult as the strut is not rectangular and has slight twists and bends. At the strain gage station, the strut cross-section and local coordinate system is shown on Figure 6.1-5. This image was generated before the grid size was reduced to match the strain gage size. For each strut section, local coordinates are defined with Z along the centerline axis, Y almost parallel to the short side, and X almost parallel to the long side. The even numbered struts are slightly different from the odd numbered struts.



Title:

**Flight Force Measurements of the Gamma-Ray Large
Area Space Telescope / Delta II Flight**

Page #:
28 of 226

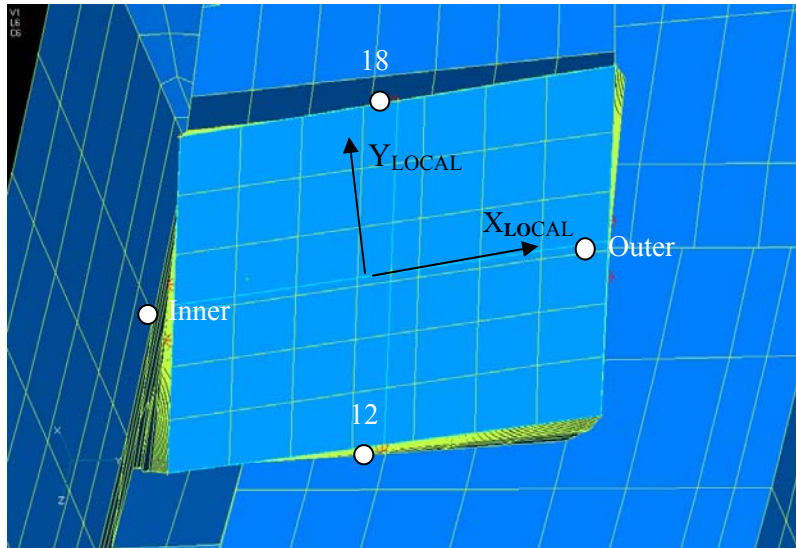


Figure 6.1-5. Looking Down the Axis of Strut 1 to Define the Local Strut Coordinate System

The initial plan was to develop a matrix of coefficients for each strut by applying unit forces at a distance away from the strain station and calculating the resulting strains. Computing the geometry from the local coordinate set to the global set proved to be difficult. To simplify the process, a 1-strut PAF model was constructed and the forces were applied at the payload ring center, Figure 6.1-6.

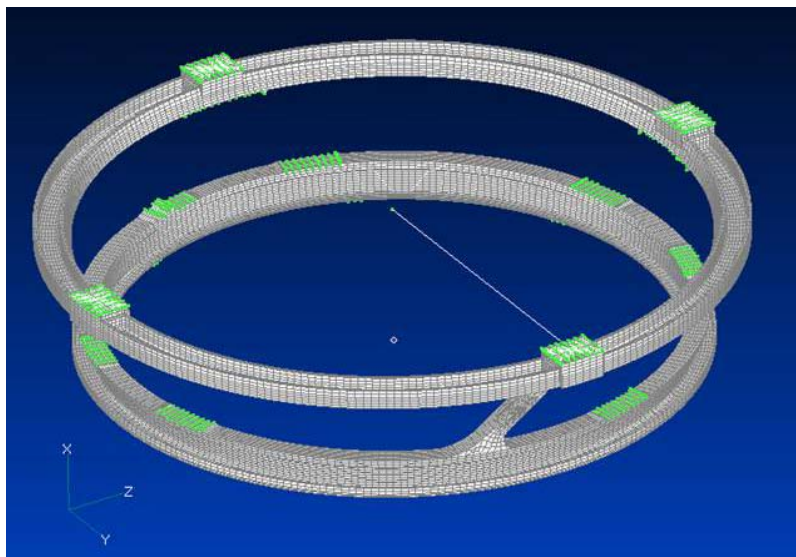


Figure 6.1-6. The One-Strut Model Used to Find Matrix [C]

	NASA Engineering and Safety Center Technical Assessment Report	Document #: NESC-RP- 06-071	Version: 1.0
Title: Flight Force Measurements of the Gamma-Ray Large Area Space Telescope / Delta II Flight		Page #: 29 of 226	

This technique automatically summed the forces. A model was made for an odd-numbered strut and for an even-numbered strut, and rotated around the center point to complete all 8 struts. The equation from the loading of 1 strut is:

$$\begin{bmatrix} \varepsilon_{18,90} \\ \varepsilon_{10,90} \\ \varepsilon_{12,90} \\ \varepsilon_{1i,90} \\ \varepsilon_{18,45} \\ \varepsilon_{10,45} \\ \varepsilon_{12,45} \\ \varepsilon_{1i,45} \end{bmatrix} = [C_1] \begin{bmatrix} Fx \\ Fy \\ Fz \\ Mx \\ My \\ Mz \end{bmatrix}_0$$

or, in a compact notation:

$$[\varepsilon(t)] = [C_1][F(t)]_0$$

The strains are specified at the strut section and the forces and moments are defined in the global axes at the payload center. Though the PAF model was used, the strain coefficients do not depend on the FEM stiffness, only on the strut material properties and dimensions. By inverting the C-matrix, the set of forces at the cut are determined from the 8 strain values. This is a simple, stable matrix inversion that requires at least 6 strain gages. The SFM is then viable if 6 gages are available on a strut (from the set of 8).

The strut forces were summed at the payload interface center using a simple matrix of direction cosines, [S]. Mathematically:

$$\begin{matrix} [F_{P\SUM}(t)] = [S] & [C]^{-1} & [\varepsilon(t)] = [E_S] & [\varepsilon(t)]. \\ (6,t) & (6,48) & (48,64) & (64,t) & (6,64) & (64,t) \end{matrix}$$

The subscripts on E_F and E_S are intended to denote either the FEM Method or the SFM.

6.1.7 Impedance Method of Solution

The term “impedance” is the ratio of a dynamic force-like quantity to an acceleration-like quantity and has English Units of Lb/g or SI Units of N-S²/m. It is a complex function of frequency. The Impedance Method omits the strain gages and uses the spacecraft impedance

	NASA Engineering and Safety Center Technical Assessment Report	Document #: NESC-RP- 06-071	Version: 1.0
Title: Flight Force Measurements of the Gamma-Ray Large Area Space Telescope / Delta II Flight			Page #: 30 of 226

with accelerometer measurements to calculate the interface forces and moments. To help understand this method, the FEM's equation of motion for the payload is written as:

$$[M][\ddot{u}(t)] + [C][\dot{u}(t)] + [K][u(t)] = [F(t)]$$

For basedrive analysis, this equation is transformed into the Craig-Bampton form by use of the transformation:

$$[u(t)] = [B, \phi] \begin{bmatrix} u_p(t) \\ q(t) \end{bmatrix}$$

where,

B = the boundary node functions (constraint modes),
 ϕ = the fixed base normal mode shapes (constrained modes),
 u_p = the base displacements at the payload-PAF boundary,
q = the generalized displacements,
 ω_n = the natural frequencies (rad/s),
 ζ_n = the modal damping ratios.

The FEM equation of motion transforms to:

$$[I][\ddot{q}(t)] + [2\zeta_n \omega_n][\dot{q}(t)] + [\omega_n^2][q(t)] = -[\phi^T MB][\ddot{u}_p(t)]$$

From which can be solved for the generalized accelerations in terms of the base accelerations (i.e., $[\ddot{q}(t)] = [\dots][\ddot{u}_p(t)]$). Then, from the other half of the transformed equation of motion, and evoking assumption 5 from Section 6.1.1, the boundary forces are found from:

$$[F_p(t)] = [B^T MB, B^T M \phi] \begin{bmatrix} \ddot{u}_p(t) \\ \ddot{q}(t) \end{bmatrix} + [B^T CB][\dot{u}_p(t)] + [B^T KB][u_p(t)]$$

In this equation all of the displacements, velocities, and accelerations are known (i.e., the boundary forces can be found as functions of the basedrive accelerations). If the forces are summed at the boundary instead of calculating the individual ones point by point, the velocity and displacement terms shown will vanish.

For the basedrive sine sweep, switch from the time domain to the frequency domain. With a change in notation:

$$[F_{PSUM}(\omega)] = [W(\omega)] [A_{p0}(\omega)]$$



**NASA Engineering and Safety Center
Technical Assessment Report**

Document #:
**NESC-RP-
06-071**

Version:
1.0

Title:

**Flight Force Measurements of the Gamma-Ray Large
Area Space Telescope / Delta II Flight**

Page #:
31 of 226

where, F_{PSUM} = the force and moment resultants summed at the payload interface center,
 W = the matrix of complex impedance coefficients,
 A_{p0} = the average acceleration of the payload interface center, and
 ω = frequency (rad/s or Hz)

In expanded form:

$$\begin{bmatrix} F_{P0X} \\ F_{P0Y} \\ F_{P0Z} \\ M_{P0X} \\ M_{P0Y} \\ M_{P0Z} \end{bmatrix} = \begin{bmatrix} W_{11} & W_{12} & W_{13} & W_{14} & W_{15} & W_{16} \\ W_{21} & W_{22} & W_{23} & W_{24} & W_{25} & W_{26} \\ W_{31} & W_{32} & W_{33} & W_{34} & W_{35} & W_{36} \\ W_{41} & W_{42} & W_{43} & W_{44} & W_{45} & W_{46} \\ W_{51} & W_{52} & W_{53} & W_{54} & W_{55} & W_{56} \\ W_{61} & W_{62} & W_{63} & W_{64} & W_{65} & W_{66} \end{bmatrix} \begin{bmatrix} A_{P0X} \\ A_{P0Y} \\ A_{P0Z} \\ \alpha_{P0X} \\ \alpha_{P0Y} \\ \alpha_{P0Z} \end{bmatrix}$$

where, A_{p0} = the average translational acceleration
 α_{p0} = the average rotational acceleration.

Defining all 36 impedance terms is not necessary because the matrix is symmetric. For most spacecraft there is minimal cross-talk between axes, so many terms are either zero or small enough to be ignored. For this case, only 8 impedance terms survive and the matrix equation simplifies to:

$$\begin{bmatrix} F_{P0X} \\ F_{P0Y} \\ F_{P0Z} \\ M_{P0X} \\ M_{P0Y} \\ M_{P0Z} \end{bmatrix} = \begin{bmatrix} W_{11} & 0 & 0 & 0 & 0 & 0 \\ 0 & W_{22} & 0 & 0 & 0 & W_{26} \\ 0 & 0 & W_{33} & 0 & W_{35} & 0 \\ 0 & 0 & 0 & W_{44} & 0 & 0 \\ 0 & 0 & W_{35} & 0 & W_{55} & 0 \\ 0 & W_{26} & 0 & 0 & 0 & W_{66} \end{bmatrix} \begin{bmatrix} A_{P0X} \\ A_{P0Y} \\ A_{P0Z} \\ \alpha_{P0X} \\ \alpha_{P0Y} \\ \alpha_{P0Z} \end{bmatrix}$$

The impedance terms can be developed from the spacecraft dynamic math model or from a vibration test. The math model has problems with proper damping, model shape fidelity, and errors in natural frequency, even if it has been calibrated. Test data is preferred and is usually obtained with the item on a slip table that cannot impose rotational accelerations (i.e., leaving the M- α terms undefined). The data is collected during a payload vibration test where forces and accelerations can be measured as functions of frequency so that the first three columns (and



NASA Engineering and Safety Center Technical Assessment Report

Document #:
**NESC-RP-
06-071**

Version:
1.0

Title:

Flight Force Measurements of the Gamma-Ray Large Area Space Telescope / Delta II Flight

Page #:
32 of 226

rows) of $[W]$ can be defined. Thus, the method is acceptable to measure forces, but not moments on the spacecraft.

Figure 6.1-7 is a plot of the complex impedance element $W_{33}(\omega)$ that was computed from the GLAST spacecraft dynamic model.

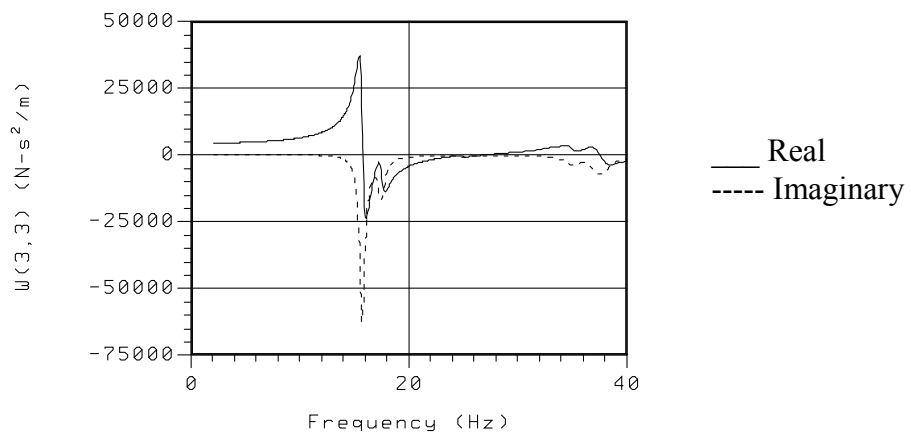
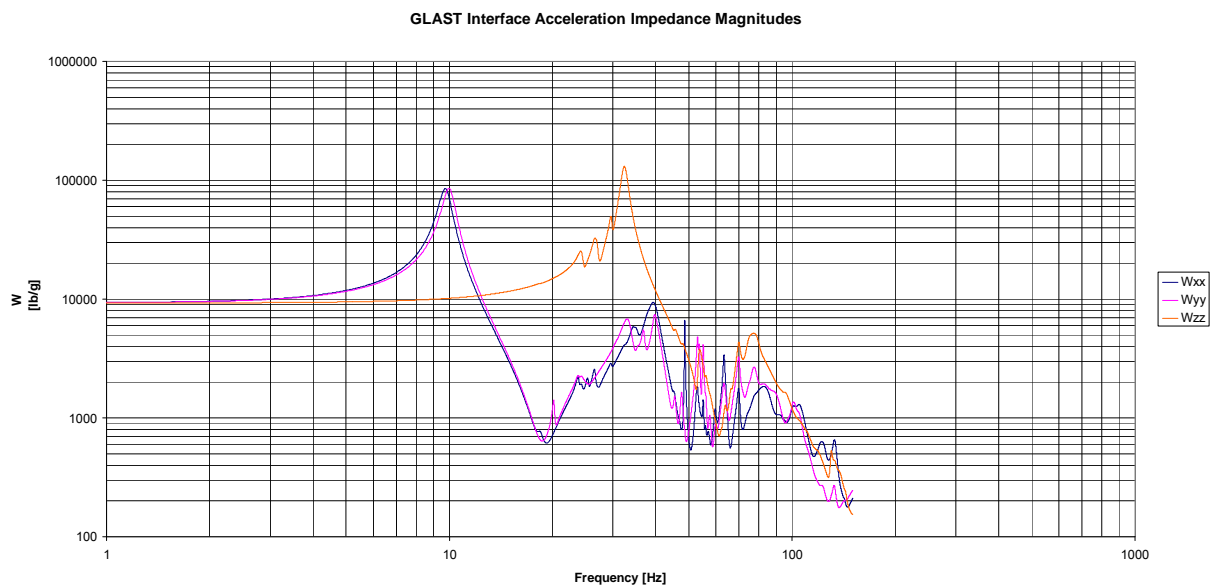


Figure 6.1-7. Impedance from the GLAST Dynamic Model

Figures 6.1-8 and 6.1-9 show some of the main magnitude terms of the GLAST spacecraft plus PAF test correlated model.





Title:

**Flight Force Measurements of the Gamma-Ray Large
Area Space Telescope / Delta II Flight**

Page #:
33 of 226

Figure 6.1-8. GLAST Interface Forces Impedance

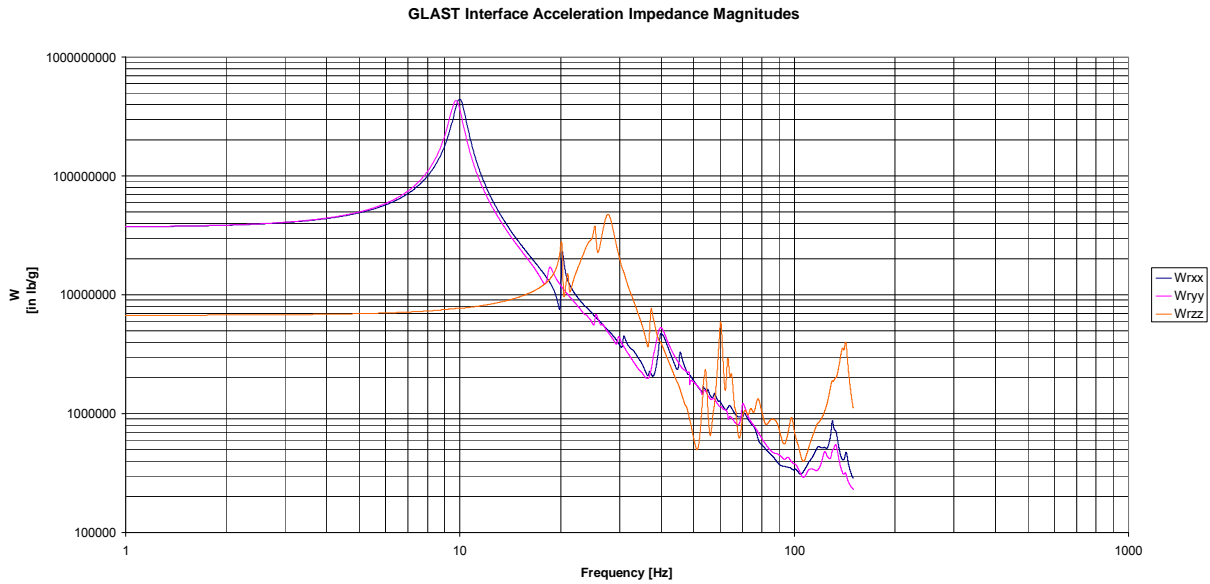


Figure 6.1-9. GLAST Interface Moments Impedance

Figures 6.1-10 and 6.1-11 show plots of the correlated model residual weights.

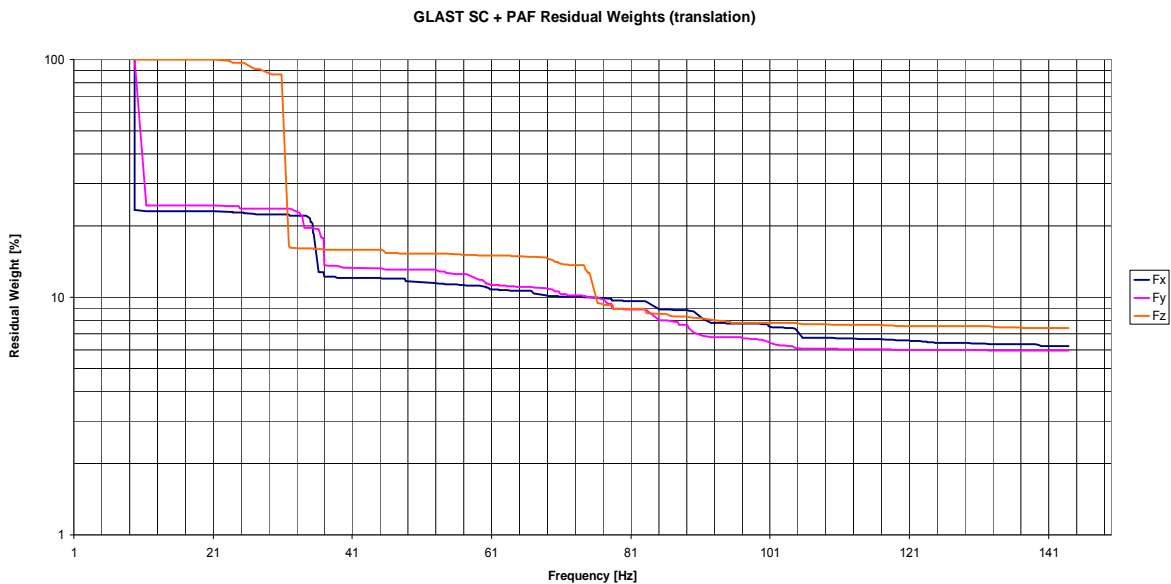


Figure 6.1-10. GLAST + PAF Translational Residual Weights



Title:

**Flight Force Measurements of the Gamma-Ray Large
Area Space Telescope / Delta II Flight**

Page #:
34 of 226

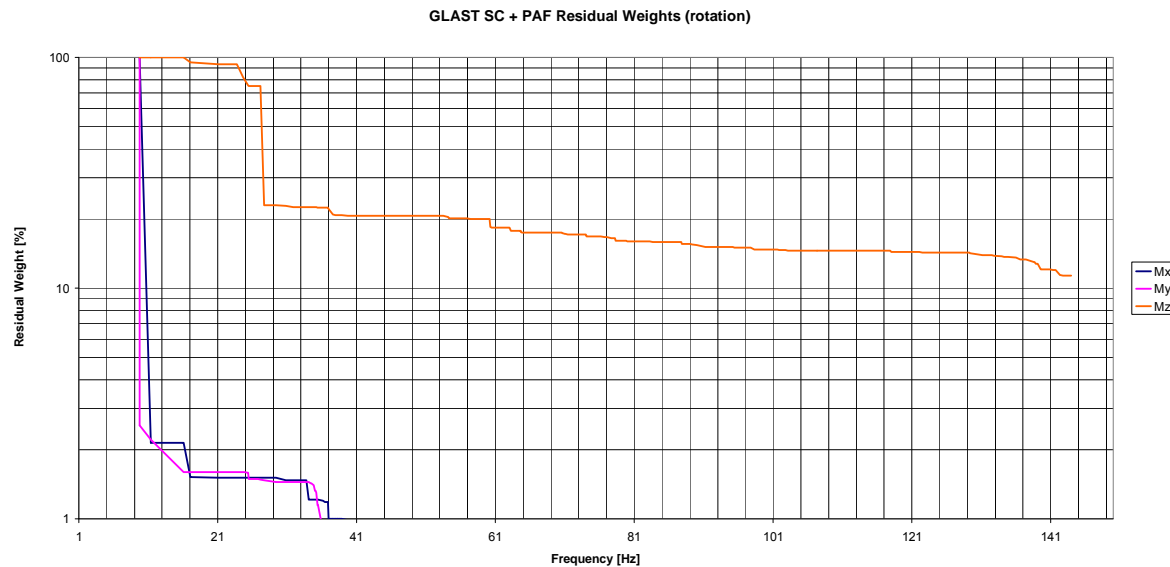


Figure 6.1-11. GLAST + PAF Rotational Residual Weights

Figures 6.1-10 and 6.1-11 suggest the GLAST spacecraft plus PAF stack has their lateral dominant modes around 10 and 35 Hz with the dominant axial modes around 32 and 75 Hz. Both lateral 10 Hz bending modes carry about 97 percent of the rotational inertia. The dominant torsional mode is around 27 Hz.

The Impedance Method was used to calculate interface forces during flight based on the transient signals from the 12 accelerometers placed at the PAF-booster interface. The following is an outline of the process used to calculate flight forces based on the Impedance Method is as follows:

1. Average the signals to obtain the 6 net accelerations time histories.
2. Select a portion of the flight (e.g., Liftoff) and compute the Fourier transforms.
3. Multiply by the complex, frequency dependent impedance matrix to calculate the force spectra.
4. Back-transform to derive the force transients.

Based on step #2 the Impedance Method requires a time record of length 2^N points in order to perform the FFM calculations. In addition, for step #3 to be accomplished, the impedance matrix has to be sized (interpolation) accordingly in order to perform the multiplication.

	NASA Engineering and Safety Center Technical Assessment Report	Document #: NESC-RP- 06-071	Version: 1.0
Title: Flight Force Measurements of the Gamma-Ray Large Area Space Telescope / Delta II Flight			Page #: 35 of 226

6.1.8 Flexibility Sensitivity Studies

During the methodology development, it was found that the accuracy of the FEM Method was sensitive to assumptions of booster interface flexibility. Based on this concern, the NESC team briefed the NESC in May 2007 to consider additional studies to evaluate both the FEM and SFM methods for sensitivity to booster interface flexibility. In addition, it was requested that an independent verification of the proposed methods be performed by Boeing/ULA.

In order to perform the sensitivity studies, the PAF FEM was re-meshed with reduced grid size to match the strain gage size. In addition a detailed Delta II Upper Stage FEM was received from Boeing/ULA. The updated PAF FEM is presented in Figure 6.1-12.

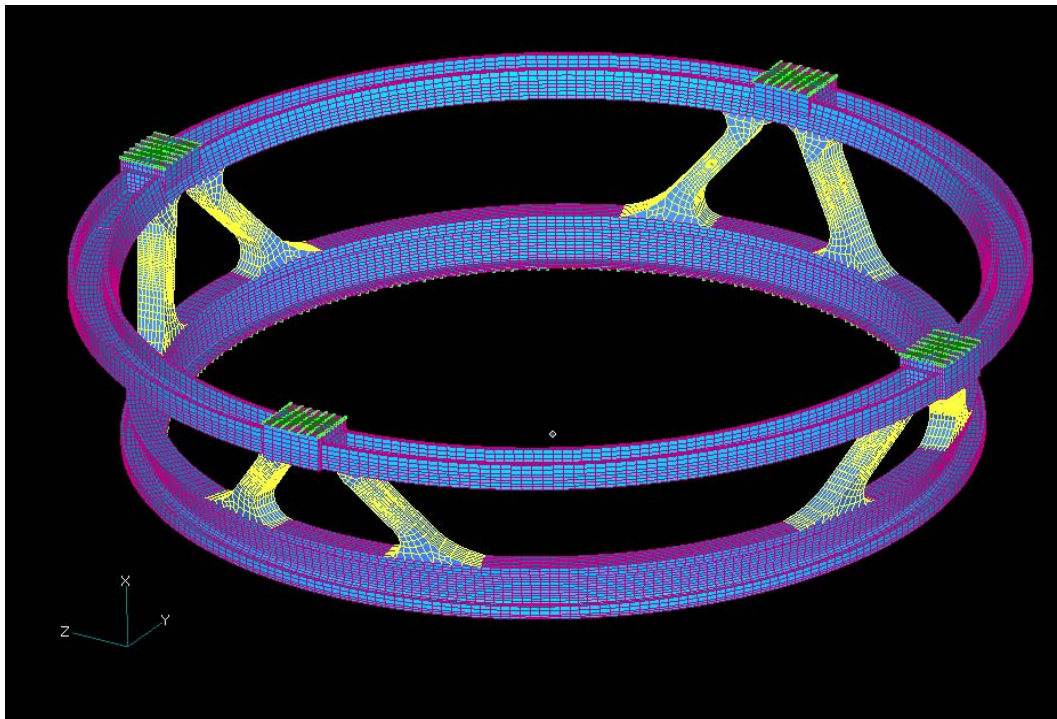


Figure 6.1-12. Updated PAF FEM



**NASA Engineering and Safety Center
Technical Assessment Report**

Document #:
**NESC-RP-
06-071**

Version:
1.0

Title:

**Flight Force Measurements of the Gamma-Ray Large
Area Space Telescope / Delta II Flight**

Page #:
36 of 226

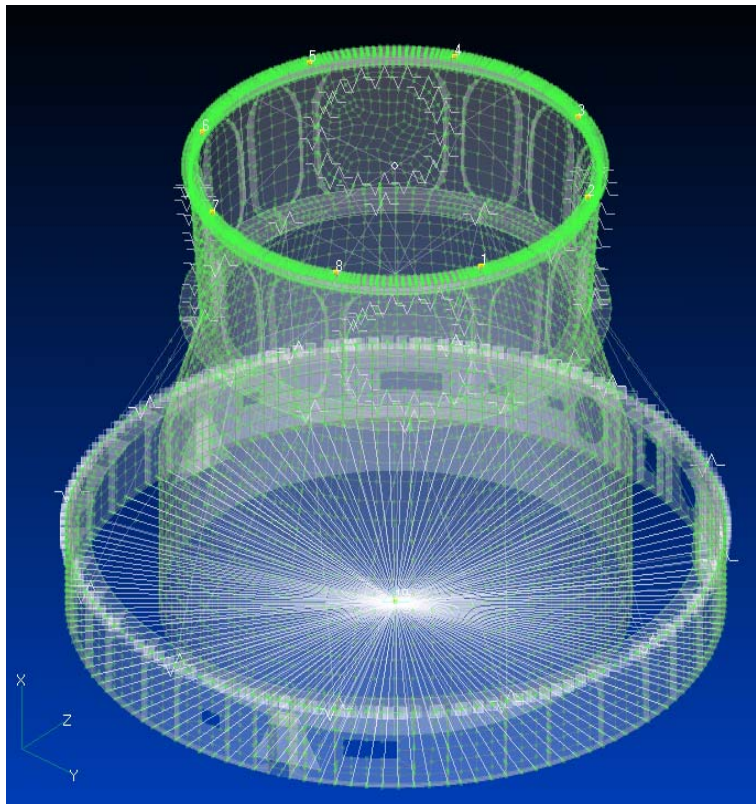


Figure 6.1-13. Delta II Second Stage FEM

The Second Stage upper ring model was reduced to eight points in order to match the PAF FEM and the lower ring constrained at the 6 d-o-f center point, see Figure 6.1-13. The results are documented in a presentation called “Upper Stage Flexibility”, revision A of August 8, 2008 [ref. 13] and summarized in Table 6.1-2.

	NASA Engineering and Safety Center Technical Assessment Report	Document #:	Version:
		NESC-RP-06-071	1.0
Title:			Page #:
Flight Force Measurements of the Gamma-Ray Large Area Space Telescope / Delta II Flight			37 of 226

Table 6.1-2. Upper Stage Flexibility

FEM Method	Errors in Recreating Forces and Moments			
	Axial Force Fx (%)	Lateral Force Fy,Fz (%)	Axial Moment Mx (%)	Lateral Moment My Mz (%)
Nominal Delta II U.S.	1.2	1.1	0.1	3.4
Stiffness / 10	2.1	4.8	0.2	5.4
Stiffness / 100	6.8	15.1	2.0	10.9
Summed Force Method				
Nominal Delta II U.S.	0.8	0.9	0.8	4.7
Stiffness / 10	0.8	1.3	1.0	5.2
Stiffness / 100	0.8	1.8	1.0	5.2

These studies concluded that the SFM is insensitive to boundary conditions while the FEM Method presents sensitivity. However, with the updated PAF FEM, the errors were below the 20 percent goal. These conclusions were independently verified by Boeing/ULA and presented to the NESC team in August 2007. In their evaluation Boeing/ULA was asked to:

- Evaluate the proposed strain-to-load method.
- Independently develop a strain-to-load transformation matrix to investigate the:
 - a. Robustness of the strain-to-load method for static analysis.
 - b. Effects of Second Stage booster flexibility on interface load recovery.
 - c. Numerical sensitivity of strain-to-load matrix.

The Boeing/ULA evaluation concluded:

- a) Results indicate that strain-to-load recovery is viable for static analysis.
- b) Results indicate that strain-to-load method is not sensitive to the Second Stage booster flexibility.
- c) Strain-to-load matrix calculation is sensitive to numerical pseudo-inverse of ‘G’ matrix.

Relevant material corresponding to the Boeing/ULA evaluation is presented “Independent Verification Analysis of Flight Force Measurement Methodology” dated August 8, 2007 [ref. 2].

	NASA Engineering and Safety Center Technical Assessment Report	Document #: NESC-RP- 06-071	Version: 1.0
Title: Flight Force Measurements of the Gamma-Ray Large Area Space Telescope / Delta II Flight		Page #: 38 of 226	

6.2 Phase 3: Ground Dynamic Test Validation

The original plan for ground test activities had static testing preceding dynamic testing. The dynamic testing was to be performed with a mass simulator for the GLAST spacecraft. However, in mid 2007 the GLAST Project was undergoing vibration testing. The NESC team decided to take the opportunity to evaluate the methodologies in advance of the static testing with the GLAST spacecraft. During the GLAST spacecraft tests force gages were planned to measure interface forces and moments, which are a critical parameter for model validation and test implementation. The NESC team contacted the GLAST Project and proposed instrumenting the Delta II TPAF with strain gages during their tests. This was to be done in a non-interference basis with the GLAST test flow.

The NESC team asserted that if the results from the GLAST vibration tests were successful, then the dynamic tests with a spacecraft mass simulator could be eliminated. In addition, part of the risk identified under constraint #2 of the assessment plan would also be eliminated. The original schedule assumed that procurement of the flight data system (4.0 Procurement of Flight System and Flight Data) would start before completion of dynamic testing to meet the GLAST Project launch schedule. This introduced a risk that if PAF dynamic testing (3.0 Vibration Testing) was not successful, funds already committed to development of the flight data system will be at risk. By instrumenting the TPAF and taking strain measurements during the GLAST vibration test, the NESC team was able to get an earlier verification of the ability to successfully measure dynamic loads based on strain measurement and reduce the risk associated with developing the flight data system. As a result of the modified ground test flow, the results from the GLAST dynamic testing (Phase 3) will be presented before the results from the static testing (Phase 2).

A test plan entitled “Test Plan for the NESC Measurements during the GLAST Vibration Test” [ref. 5] was written in July 2007. Relevant portions of this test plan are presented in this report. The objective of the measurements taken during the GLAST spacecraft testing as defined in the test plan was: “to gather strain gage test data to validate the analytical techniques, and to acquire accelerometer and force data to be used to calculate the spacecraft impedance coefficients.” The GLAST spacecraft is shown in Figure 6.2-1 during its assembly process. In this image the PAF and solar arrays have not been installed. The GLAST spacecraft FEM is shown in Figure 6.2-2 along with the spacecraft coordinate axes. During vibration testing a TPAF was used. The TPAF is flight-like in most respects with the same interfaces, dimensions, and materials as the flight PAF. The Delta II 6915 TPAF used for the GLAST sine vibration test is shown in Figure 6.2-3.



**NASA Engineering and Safety Center
Technical Assessment Report**

Document #:
**NESC-RP-
06-071**

Version:
1.0

Title:

**Flight Force Measurements of the Gamma-Ray Large
Area Space Telescope / Delta II Flight**

Page #:
39 of 226

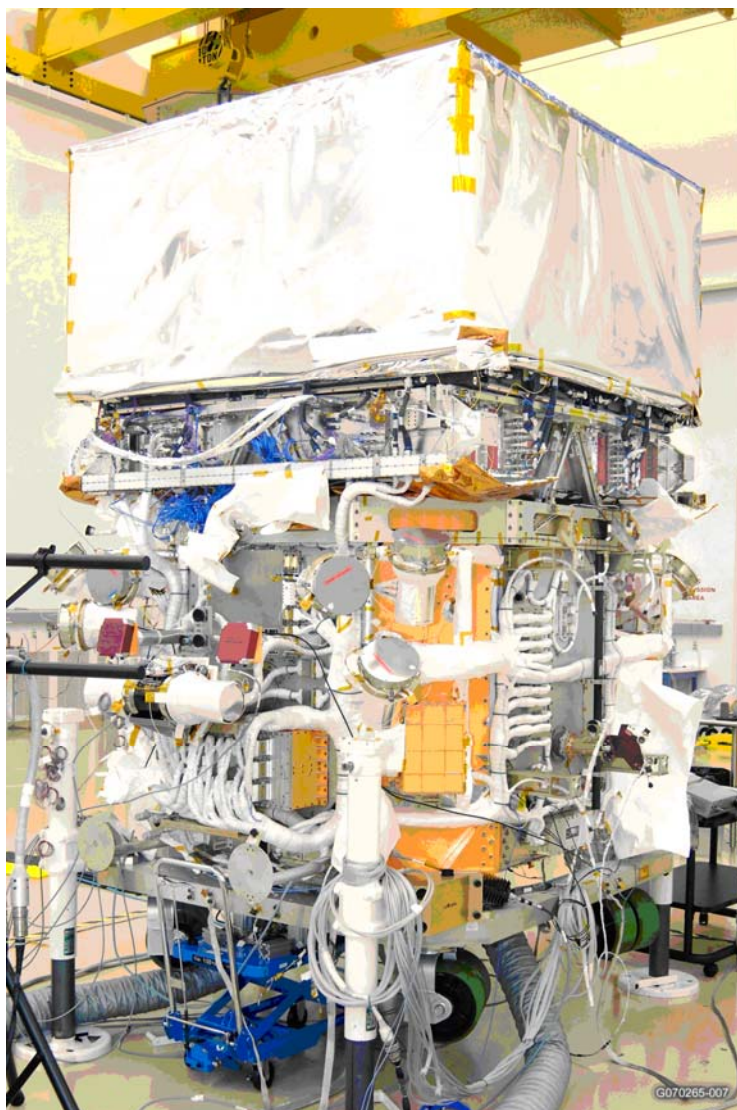


Figure 6.2-1. GLAST Spacecraft During Assembly



**NASA Engineering and Safety Center
Technical Assessment Report**

Document #:
**NESC-RP-
06-071**

Version:
1.0

Title:

**Flight Force Measurements of the Gamma-Ray Large
Area Space Telescope / Delta II Flight**

Page #:
40 of 226

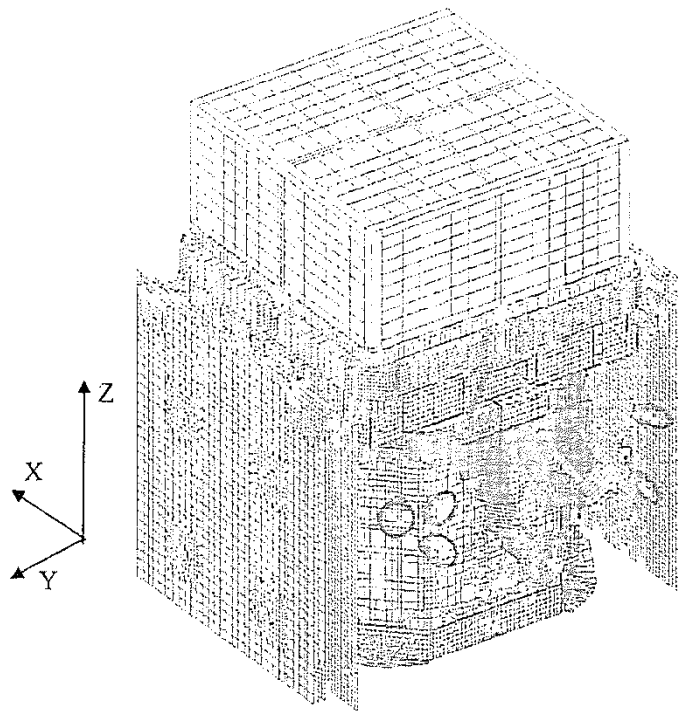


Figure 6.2-2. GLAST FEM with Test Axes



Figure 6.2-3. Delta II 6915 TPAF used for GLAST Sine Vibration Test



Title:

**Flight Force Measurements of the Gamma-Ray Large
Area Space Telescope / Delta II Flight**

Page #:
41 of 226

6.2.1 Instrumentation/Strain Gages

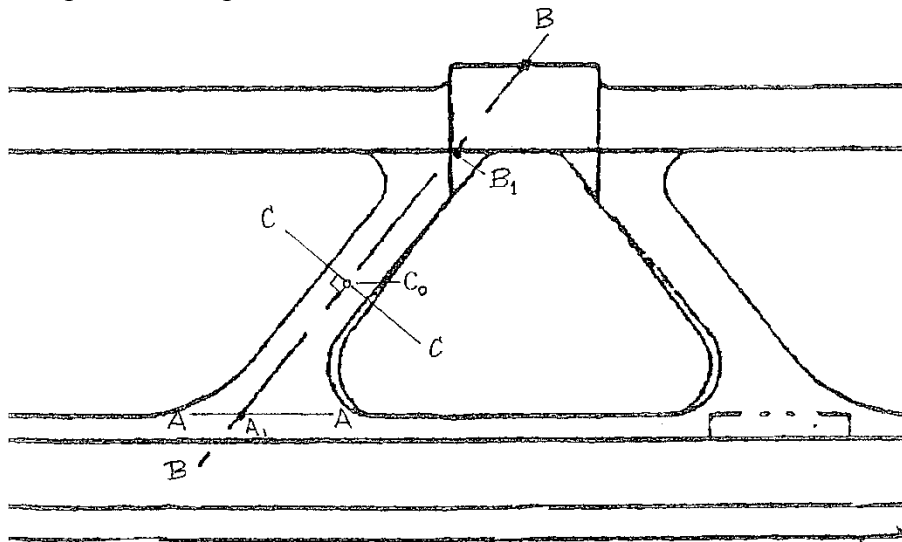
The strain gages used for the GLAST dynamics test were supplied by the NESC and installed on the TPAF by General Dynamics (GD). Vishay CEA-13-125UR-350 strain gages were used during vibration testing. These gages were recommended by Vishay for use on aluminum structures.

It was desired to have 64 strain gages. However, due to conflicts and limitations of the GSFC signal conditioning equipment, only 62 gages could be monitored. This is shown in Table 6.2-1 that omits the two gages (4i, 45 and 8i, 45) with the lowest signals.

6.2.2 Strain Gage Locations

It is important that the strain gages be installed correctly and carefully located. The following method was used to define the location of the strain gages installed on the TPAF by GD. Refer to Figure 6.2-4.

First, mark line A-A on the strut lower limit. Then mark line B-B along the strut center axis. Note that this may be difficult because the strut is slightly bent and twists along its length. Mark point A_1 where the center line intersects A-A and point B_1 at the upper edge. Measure the line mid-point and label it C_0 , marking the station where strain gages are to be installed. Mark line C-C that is perpendicular to B-B. Then, wrap C-C around the strut and marking the center points on each face. These four points are the locations of the central strain gage. For strut "n" they are identified $C_{n,0}$ on the outer face, $C_{n,n+1}$ for the "n+1" face, $C_{n,i}$ for the inner face, and $C_{n,n-1}$ for the "n-1" face. This process is repeated for all 8 struts.





Title:

Flight Force Measurements of the Gamma-Ray Large Area Space Telescope / Delta II Flight

Page #:
42 of 226

Figure 6.2-4. PAF Strut Strain Gage Placement

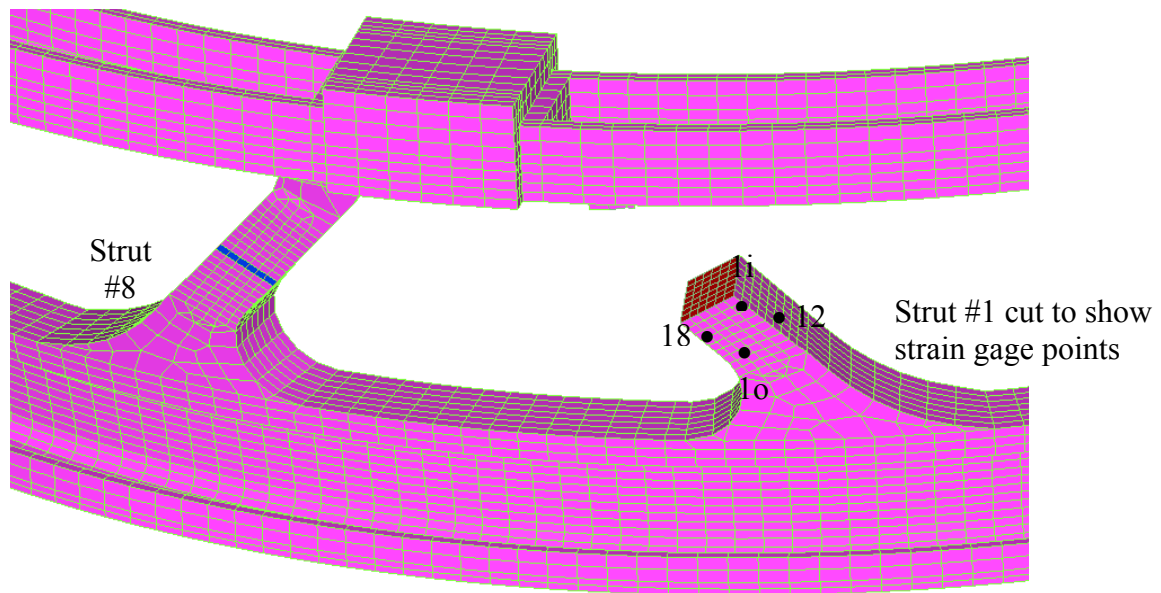
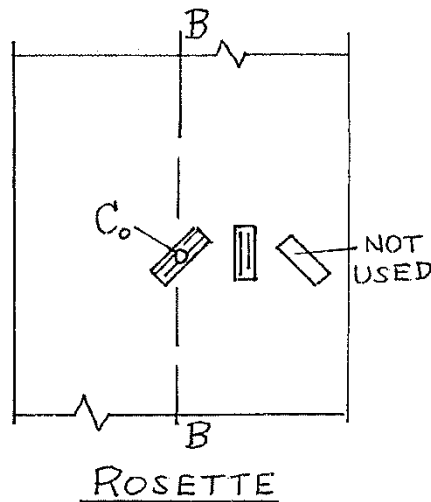


Figure 6.2-5. Strain Gage Locations on PAF Strut 1

Two gages are placed at each point; one axial aligned with B-B, and one shear placed at a 45-degree angle. When viewing the strut's face, the axial gage is in the 12:00 o'clock position parallel to B-B, and the shear gage is at the 1:30 o'clock position along line B-B centered on the C_0 point. The third gage at the 10:30 position is not used in this application. Figure 6.2-6 shows the gage orientation relative to the strut centerline. The strain gages were installed using procedures developed by Vishay.



	NASA Engineering and Safety Center Technical Assessment Report	Document #: NESC-RP- 06-071	Version: 1.0
	Title: Flight Force Measurements of the Gamma-Ray Large Area Space Telescope / Delta II Flight		Page #: 43 of 226

Figure 6.2-6. Strain Gage Alignment

6.2.3 Accelerometers

The GLAST spacecraft test already had a number of accelerometers installed. In addition to the existing accelerometers, 4 additional biaxial accelerometers were located on the PAF lower ring equally spaced every 90 degrees between base points. These additional channels were used for impedance measurements. The specifications for the additional biaxial accelerometers used in the GLAST vibration test are shown in Table 6.2-1. The biaxial accelerometers were aligned with the GLAST Z (vertical) axis and the tangential direction relative to the base of the PAF.

Table 6.2-1. Additional Accelerometers for the GLAST Spacecraft Sine Test

Type	Endevco 2221
Number	4 biaxial
Expected limits	2 g max, 5-200 Hz

6.2.4 Force Gages

The GD installed force gages as a standard part of their test are shown in Table 6.2-2.

Table 6.2-2. Force Gages Used During GLAST Spacecraft Sine Test

Type	Kistler 9077 high impedance triaxial
Number	8
Expected limits	1b, max 5-200 Hz

The gages were identified and labeled according their locations in Table 6.2-6.

6.2.5 Pre-Test Analysis and Test Description

Pre test analysis was performed to set the strain ranges; these are presented in Table 6.2-3.

Table 6.2-3. Expected Strain Maxima

Sweep Axis	Axial Strain		Shear Strain	
	(μ)	At Gage	(μ)	At Gage

	NASA Engineering and Safety Center Technical Assessment Report	Document #:	Version:
		NESC-RP-06-071	1.0
Title: Flight Force Measurements of the Gamma-Ray Large Area Space Telescope / Delta II Flight			Page #: 44 of 226

X – Lateral	580	3i	462	3i
Y – Lateral	704	1i	554	1i
Z – Axial	204	2i	164	1i

The data acquisition was performed at a sample frequency of 1000 Hz and an anti-aliasing filter of 200 Hz. The tests consisted of 3 axis 5 to 50 Hz sine qualification levels plus a 5 to 150 Hz low level sine sweep of 100 mg as signature and to evaluate the Delta II MECO event. The GLAST spacecraft tests were successfully completed without interruption to the GLAST Project hardware flow. A test report entitled “Test Report for the NESC Measurements during the GLAST Vibration Test” was written in November 2007 and summarizes the data gathered during the GLAST sine test [ref. 6]. Relevant portions of this test report are presented in Section 6.2.

The NESC team’s measurements were acquired during the high level sine vibration part of the procedure during September 18 through 22 on a non-interference basis with the consent of the GLAST Project personnel. The GLAST spacecraft is shown in Figure 6.2-8 ready for the Z-axis test. Unfortunately, the TPAF is below the scaffolding platform and is not visible. Before testing, the cooling ducts were removed.

A computer aided design (CAD) model of the TPAF with strut and interface labels is shown in Figure 6.2-7. It should be noted that the coordinate system and strut numbering for the TPAF shown in the figure were unique to the GLAST sine test, and are different from the PAF FEM shown in Figure 6.1-2. The TPAF is non-flight, but is flight-like in most respects with realistic interfaces, dimensions, and materials. The TPAF-booster interface is a solid 68-bolt connection to an aluminum base ring adaptor of approximate dimensions 65 inch outer diameter (OD), 50 inch inner diameter (ID), and 2.5 inch height which mounts to the shaker table by 8 force gages. The PAF-payload interface is a 4-bolt connection and is located at the separation plane. Realistic separation bolts were used and torqued to flight-like levels. Differences between the test and flight PAF were that the release mechanisms were omitted in the test configuration. The lack of the release mechanisms and associated stiffness is considered inconsequential compared to the TPAF stiffness and mass. The mass properties of the TPAF are shown in Table 6.2-4. A CAD simulation of the flight PAF installed under the GLAST spacecraft is shown in Figure 6.2-9.

Table 6.2-4. TPAF Mass Properties

Mass	184.5 pounds		
C.M. Ixx	181110.11 lb in ²	Radius of the booster both circle	29.315 in
Iyy=Izz	95339.09 lb in ²	Radius of the P/L bolt circle	34.292 in

	NASA Engineering and Safety Center Technical Assessment Report	Document #: NESC-RP- 06-071	Version: 1.0
	Title: Flight Force Measurements of the Gamma-Ray Large Area Space Telescope / Delta II Flight		Page #: 45 of 226

The sine vibration test was performed using the GLAST spacecraft axes and all data was gathered in these coordinates using units of pounds, inches, gs, and micro-strain. A sketch of these coordinate systems is shown in Figure 6.2-10 along with points A-L from Table 6.2-6. The mass properties and dimensions of the test items are shown in Table 6.2-5.

Table 6.2-5. Mass Properties of GLAST – Flight Versus Test

Flight GLAST:	Mass 9487.81 lb	$I_{xx} = 36274646.56 \text{ lb in}^2$	at the PAF i/f
		$I_{yy} = 36246967.47 \text{ lb in}^2$	
		$I_{zz} = 7137446.94 \text{ lb in}^2$	
Tested GLAST:	Mass 7808.77 lb	(approx. without 782.86 lb of propellant)	
TPAF:	Mass 190.26 lb	Radius of the booster bolt circle, 29.3 in	
		Radius of the P/L bolt circle, 34.29 In	
Base Ring:	Mass 332.02 lb		

Table 6.2-6. TPAF Interface Point Coordinates

GLAST Interface Points				Base Force Gage Interface Points			
Pt.	X (in)	Y (in)	Z (in)	Pt.	X (in)	Y (in)	Z (in)
A	24.2504	24.2504	0.4750	E	-24.5436	16.8130	-17.000
B	-24.2504	24.2504	“	F	-9.4509	28.2081	”
C	-24.2504	-24.2504	“	G	16.8130	24.5436	”
D	24.2504	-24.2504	“	H	28.2081	9.4508	”
				I	24.5436	-16.8130	”
				J	9.4509	-28.2081	”
				K	-16.8130	-24.5436	”
				L	-28.2081	-9.4509	”

↑
Note Figure 6.2-7

Figure 6.2-7. 6915 PAF with Strut and Interface Labels for the Sine Test



**NASA Engineering and Safety Center
Technical Assessment Report**

Document #:
**NESC-RP-
06-071**

Version:
1.0

Title:

**Flight Force Measurements of the Gamma-Ray Large
Area Space Telescope / Delta II Flight**

Page #:
46 of 226



Figure 6.2-8. GLAST Spacecraft in the GD Vibrations Laboratory

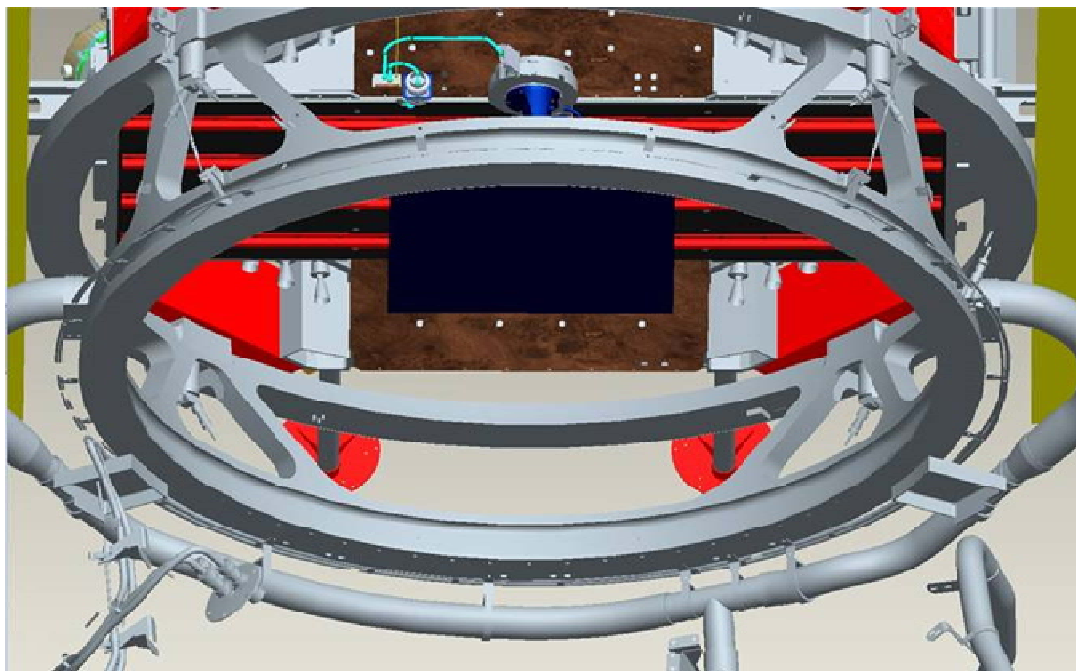


Figure 6.2-9. Simulation of PAF Installed Under the GLAST Spacecraft



**NASA Engineering and Safety Center
Technical Assessment Report**

Document #:
**NESC-RP-
06-071**

Version:
1.0

Title:

**Flight Force Measurements of the Gamma-Ray Large
Area Space Telescope / Delta II Flight**

Page #:
47 of 226

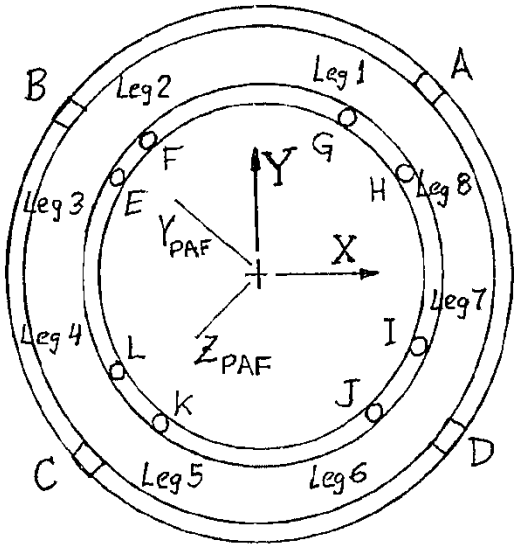


Figure 6.2-10. GLAST and TPAF Coordinate Systems for the Sine Test

It was desired to have 64 strain gages, 8 per strut. However, because of conflicts and limitations of the GSFC signal conditioning equipment, only 62 gages were monitored. These gages are shown in the Instrumentation Log, Table 6.2-7.

Table 6.2-7. Instrument Channels

Test Channel	Label	Dir.	Description	Comments
1	COLA	-	COLA signal	Note Table 1
2-3	C1,C2	Shaker	Shaker control accel	
4-6	Force	-X -Y +Z	Force gage E	
7-9	"	"	Force gage F	
10-12	"	"	Force gage G	
13-15	"	"	Force gage H	
16-18	"	"	Force gage I	
19-21	"	"	Force gage J	
22-24	"	"	Force gage K	
25-27	"	"	Force gage L	
28-31	12,1i,1o,18	Axial	Strut 1 strain gages	
32-35	21,2i,2o,23	"	Strut 2 " "	
36-39	32,3i,3o,34	"	Strut 3 " "	
40-43	43,4i,4o,45	"	Strut 4 " "	
44-47	54,5i,5o,56	"	Strut 5 " "	



**NASA Engineering and Safety Center
Technical Assessment Report**

Document #:
**NESC-RP-
06-071**

Version:
1.0

Title:

**Flight Force Measurements of the Gamma-Ray Large
Area Space Telescope / Delta II Flight**

Page #:
48 of 226

48-51	65,6i,6o,67	“	Strut 6	“	“	
52-55	76,7i,7o,78	"	Strut 7	“	“	
56-59	87,8i,8o,81	"	Strut 8	“	“	
60-63	12,1i,1o,18	Shear	Strut 1 strain gages			
64-66	21,2i, 23	“	Strut 2	“	“	
67-70	32,3i,3o,34	“	Strut 3	“	“	
71-73	43,4i, 45	“	Strut 4	“	“	
74-77	54,5i,5o,56	“	Strut 5	“	“	
78-81	65,6i,6o,67	“	Strut 6	“	“	
82-85	76,7i,7o,78	“	Strut 7	“	“	
86-88	87,8i, 81	“	Strut 8	“	“	
89-90	Accel.	Z, R	Accel. biax A			Radial is positive outward
91-92	"	“	Accel. biax B			
93-94	"	“	Accel. biax C			
95-96	"	“	Accel. biax D			

	NASA Engineering and Safety Center Technical Assessment Report	Document #:	Version:
		NESC-RP-06-071	1.0
Title: Flight Force Measurements of the Gamma-Ray Large Area Space Telescope / Delta II Flight			Page #: 49 of 226

The list of test runs, with relevant comments, is presented in Table 6.2-8.

Table 6.2-8. Test Runs Acquired by the NESC

Run	Date	Time	Axis	Description	Run Name	Notes
15	18 Sep	17:20	Z -	Low level, 0.1g, 5 to 150 Hz, 4 o/m	zswp15	(1)
15b	"	17:25	Axial	Background noise, 30 s	bkgrnd15	
16	"	20:35		Half level, 5 to 50 Hz	zswp16	(2)
17	"	21:45		Full level, 5 to 50 Hz	zswp17	
18	"	22:17		Low level, 0.1g, 5 to 150 Hz, 4 o/m	zswp18	(3)
23	21 Sep	-	X -	Low level, 0.1g, 5 to 150 Hz, 4 o/m	xswp23	
24	"	-	Lateral	Half level, 5 to 10 Hz, 4 o/m	xswp24	(4)
25	"	-		Half level, 15 to 50 Hz	xswp25	(5)
26	"	-		Full level, 15 to 50 Hz	xswp26	(5)
27	"	-		Low level, 0.1g, 5 to 150 Hz, 4 o/m	xswp27	
28	22 Sep	-	Y -	Low level, 0.1g, 5 to 150 Hz, 4 o/m	yswp28	(6,7)
29	"	-	Lateral	Half level, 15 to 50 Hz	yswp29	(5)
30	"	-		Full level, 15 to 50 Hz	yswp30	(5)
31	"	-		Low level, 0.1g, 5 to 150 Hz, 4 o/m	yswp31	(7)

Notes: (1) First indication that 30 strain channels were filled with noise, channels 58-88. This occurred only when the shaker coils were activated and did not occur during the background measurement.

(2) Relocate the strain gage leads away from the shaker with little effect in the noise level.

(3) Run shut down and was re-started at mid-sweep.

(4) Run aborted due to lack of shaker control at ~10 Hz.

(5) The 5 to 10 Hz segment was performed previously in the low level run and not repeated.

(6) Configuration was altered for the Y-axis sweeps. The TPAF was unbolted from its base plate and rotated 90 degrees and re-attached while the force gages remained undisturbed. Resulting in the force directions X and Y reversed.

	NASA Engineering and Safety Center Technical Assessment Report	Document #: NESC-RP- 06-071	Version: 1.0
Title: Flight Force Measurements of the Gamma-Ray Large Area Space Telescope / Delta II Flight			Page #: 50 of 226

(7) Low level runs for the Y-axis swept at 1.5 oct/min to 15 Hz when the fundamental Y-mode had been passed. Performed for shaker control.

6.2.6 Raw Data Manipulation

The raw data was closely examined and four changes were performed. The individual force gage channels were summed to give the net forces and moments at the force gage interface. Similarly, the 8 accelerometers were averaged to produce the net accelerations at the lower TPAF interface for the X and Y sweeps, and at the upper TPAF interface for the Z-sweep. Then, the data was truncated by omitting most of the lead in time before the shaker was activated and after the sweep was completed. Finally, the Constant Output Level Amplitude (COLA) signal was converted into frequency. These changes created a new data set whose map is different from Table 6.2-9.

The COLA signal was converted into frequency versus time by noting the period between zero crossings. The results are plotted in Figures 6.2-11 through 6.2-13. In the subsequent study, the plotted ordinate may be in units of time or frequency, whichever is most appropriate.

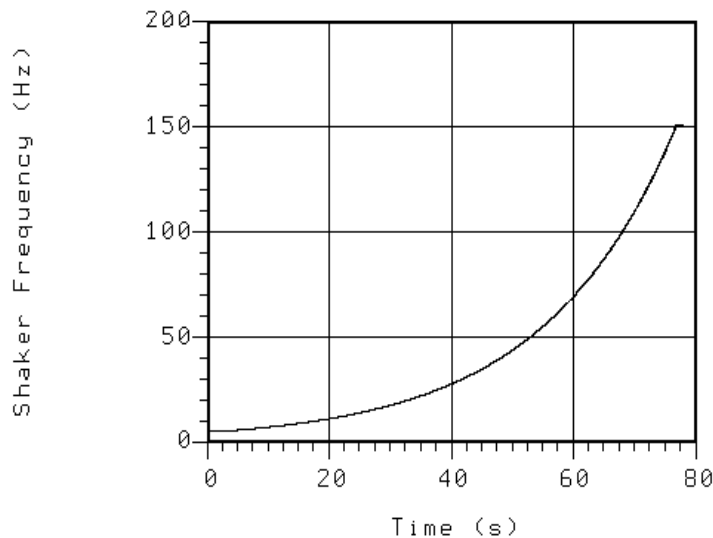


Figure 6.2-11. Sweep Frequency Versus Time – X Axis Run 23



**NASA Engineering and Safety Center
Technical Assessment Report**

Document #:
**NESC-RP-
06-071**

Version:
1.0

Title:

**Flight Force Measurements of the Gamma-Ray Large
Area Space Telescope / Delta II Flight**

Page #:
51 of 226

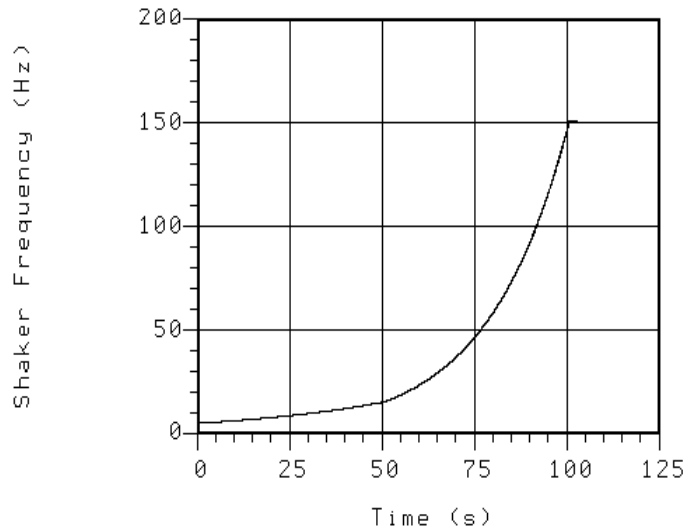


Figure 6.2-12. Sweep Frequency Versus Time – Y Axis Run 28

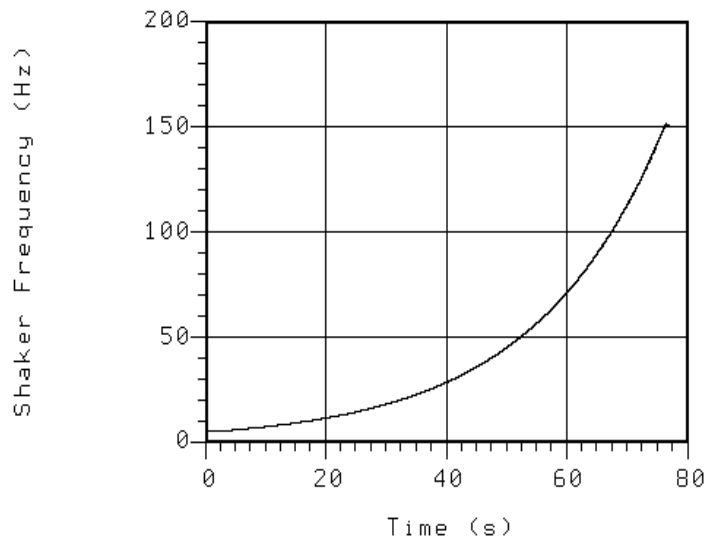


Figure 6.2-13. Sweep Frequency Versus Time – Z Axis Run 15



**NASA Engineering and Safety Center
Technical Assessment Report**

Document #:
**NESC-RP-
06-071**

Version:
1.0

Title:

**Flight Force Measurements of the Gamma-Ray Large
Area Space Telescope / Delta II Flight**

Page #:
52 of 226

Table 6.2-9. Modified Instrument Channels

Test Channel	Label	Direction	Description
1	Frequency	-	Frequency (Hz)
2-3	C1,C2	Shaker	Shaker control accel
4-6	Force	XYZ	Net force at TPAF i/f (lb)
7-9	"	"	Net moment at TPAF i/f (lb-in)
10-27	-	-	Not used
28-31	12,1i,1o,18	Axial	Strut 1 strain gages (μ -strain)
32-35	21,2i,2o,23	"	Strut 2 " "
36-39	32,3i,3o,34	"	Strut 3 " "
40-43	43,4i,4o,45	"	Strut 4 " "
44-47	54,5i,5o,56	"	Strut 5 " "
48-51	65,6i,6o,67	"	Strut 6 " "
52-55	76,7i,7o,78	"	Strut 7 " "
56-59	87,8i,8o,81	"	Strut 8 " "
60-63	12,1i,1o,18	Shear	Strut 1 strain gages (μ -strain)
64-66	21,2i, 23	"	Strut 2 " "
67-70	32,3i,3o,34	"	Strut 3 " "
71-73	43,4i, 45	"	Strut 4 " "
74-77	54,5i,5o,56	"	Strut 5 " "
78-81	65,6i,6o,67	"	Strut 6 " "
82-85	76,7i,7o,78	"	Strut 7 " "
86-88	87,8i, 81	"	Strut 8 " "
89-91	Accel.	XYZ	Net accel at TPAF i/f (g)
92-94	"	"	Net angular accel. at i/f (g/in)
95-96	-	-	Not used

The noisy strain data was problematic. Figure 6.2-14 shows two strain channels from run Z18. The first plot from channel 28 is clean, but shows high harmonics. The second plot from channel 66 shows noise. During the time shown in these plots, the shaker was at 26 Hz. Investigating further, Figure 6.2-15 shows the spectral density of these two strain transients in units of μ -strain/ $\sqrt{\text{Hz}}$. The clean data showed a spike at 33 Hz, the fundamental Z-mode of GLAST



NASA Engineering and Safety Center Technical Assessment Report

Document #:
**NESC-RP-
06-071**

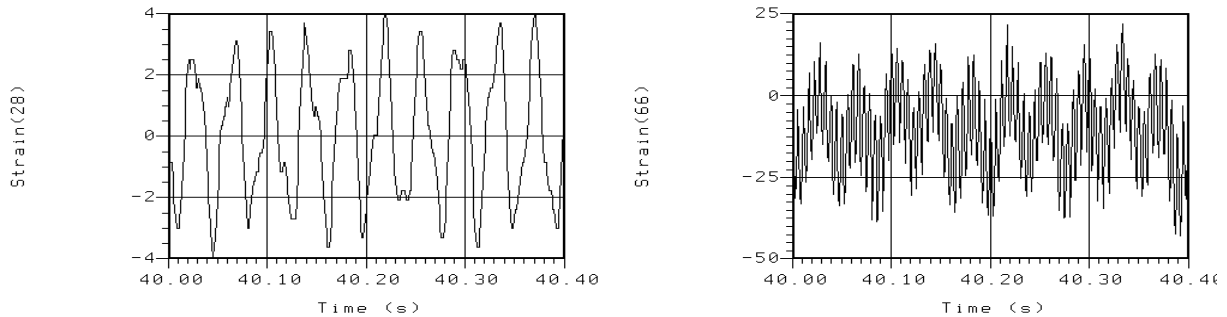
Version:
1.0

Title:

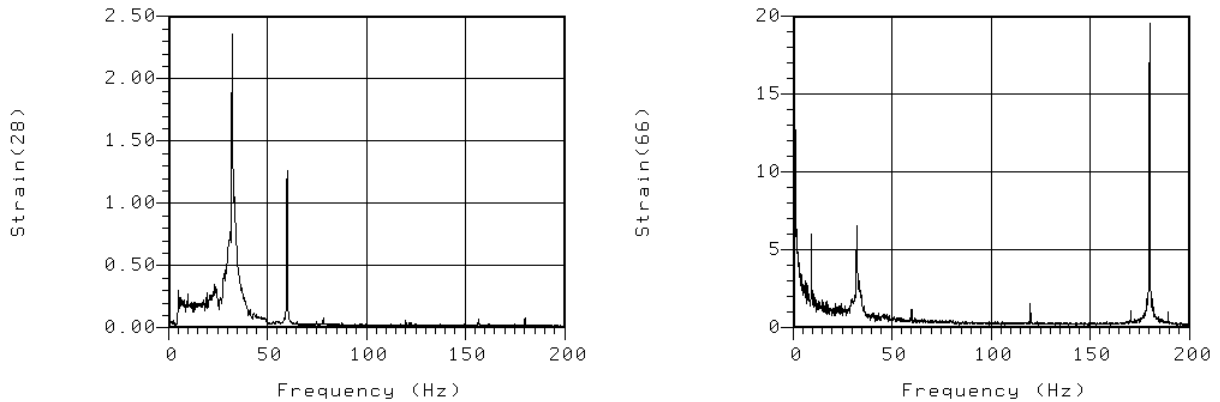
Flight Force Measurements of the Gamma-Ray Large Area Space Telescope / Delta II Flight

Page #:
53 of 226

spacecraft and a 60 Hz spike, while the noisy channel is dominated by electrical noise at 180, 120, and 60 Hz, and a sizeable DC offset. This was typical for all noisy strain channels.



A Sample of Strain Gage Data – Unfiltered – From Run Z18



Spectral Density of the Strain

Figure 6.2-14. Two Strain Channels from Run Z18



**NASA Engineering and Safety Center
Technical Assessment Report**

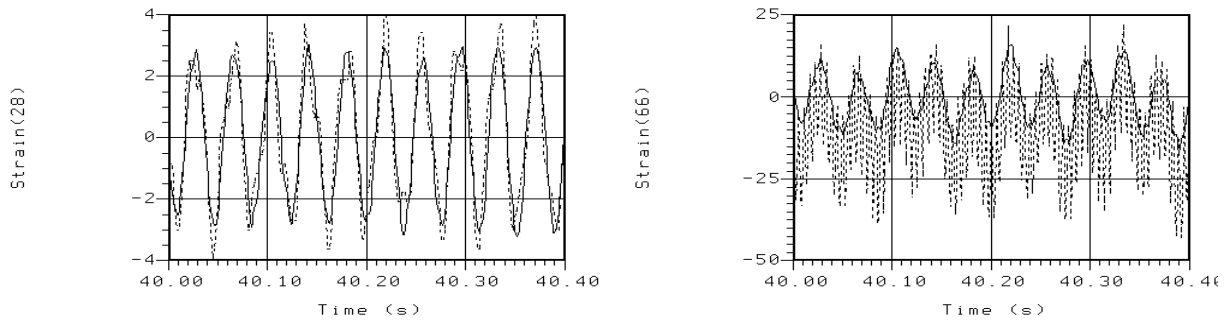
Document #:
**NESC-RP-
06-071**

Version:
1.0

Title:

**Flight Force Measurements of the Gamma-Ray Large
Area Space Telescope / Delta II Flight**

Page #:
54 of 226



A Sample of Strain Gage Data – Filtered – from Run Z18

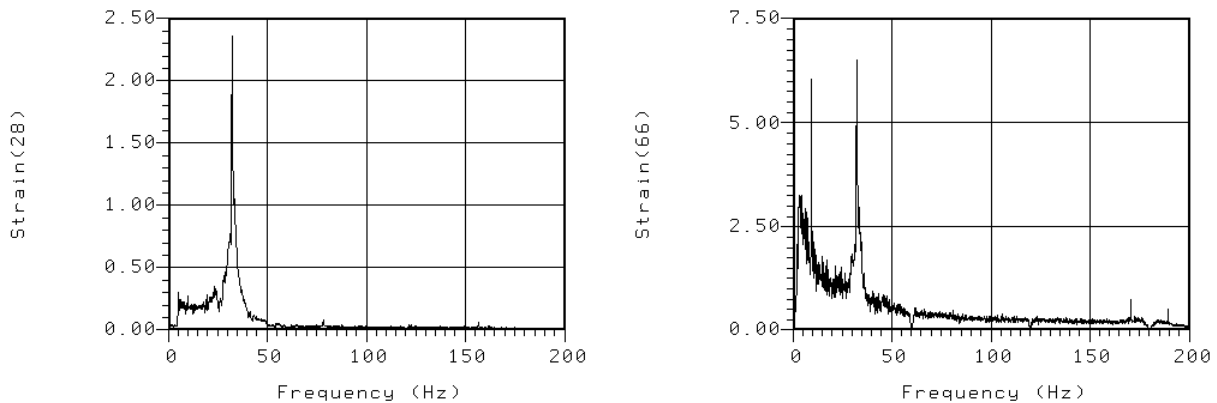


Figure 6.2-15. Spectral Density of the Strain Measurements

Applying filters to this data created Figure 6.2-16 for the time history and Figure 6.2-17 for its spectral density. The transients show the unfiltered strain (dashed line) and the filtered strain (solid line) superimposed. The fourth order filters used on all strain data were:

- Low-pass (LP) at 170 Hz
- Band-pass (BP) at 120 Hz
- BP at 60 Hz
- High-pass (HP) at 2 Hz

The data acquisition used a 200 Hz LP filter. When the data was filtered there was a phase shift so that forces generated from this strain data may not be phased with those from the force gages. This appears to be unavoidable, but is a sufficiently small effect to be un-noticed in Figure 6.2-18.

Following the changes discussed above, the test data was ready for examination. Figure 6.2-16 shows the form and type. From run 23, an X-axis sweep, a few channels are shown. The dominant mode is at 10 Hz and the test duration was 77 seconds.



**NASA Engineering and Safety Center
Technical Assessment Report**

Document #:
**NESC-RP-
06-071**

Version:
1.0

Title:

**Flight Force Measurements of the Gamma-Ray Large
Area Space Telescope / Delta II Flight**

Page #:
55 of 226

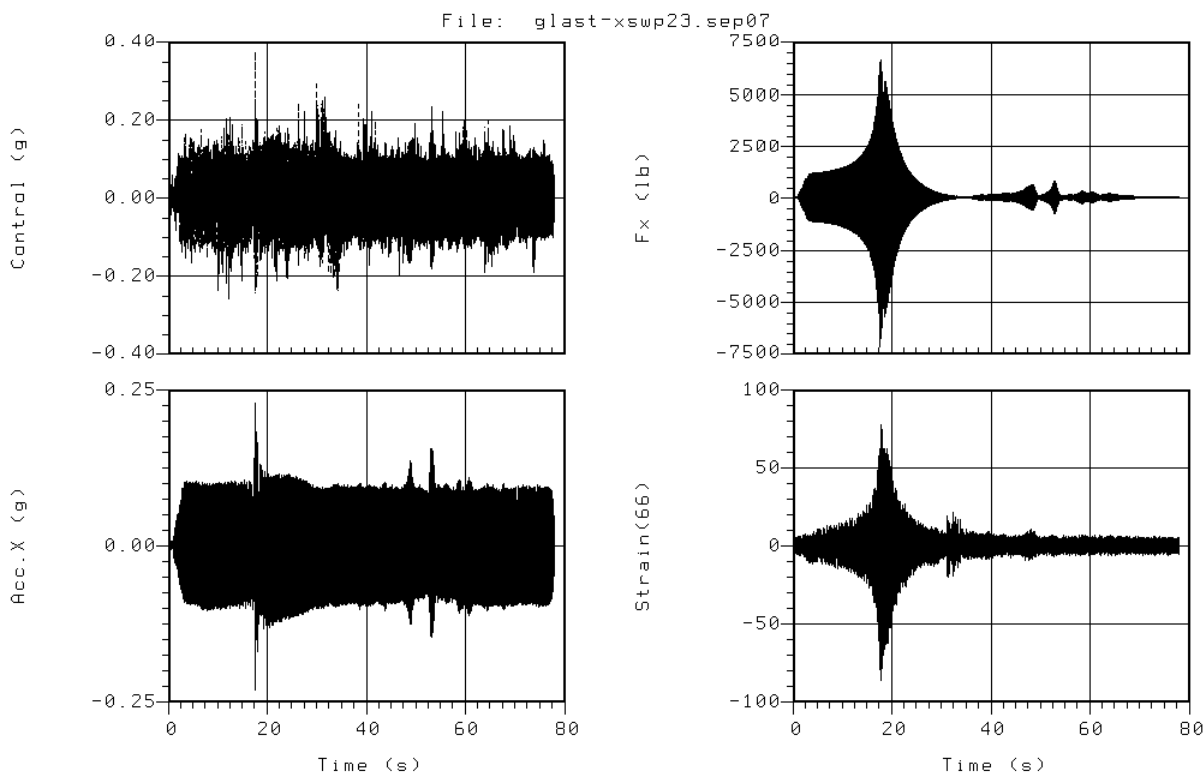


Figure 6.2-16. A Sample of the Data – Run X23

From run Z18, a vertical sine sweep from 5 to 150 Hz, a few channels are shown in Figure 6.2-17. Notice the results are plotted versus frequency, not time. The two control channels are slightly ragged as expected, and the fundamental Z-mode at 33 Hz is evident.



Title:

**Flight Force Measurements of the Gamma-Ray Large
Area Space Telescope / Delta II Flight**

Page #:
56 of 226

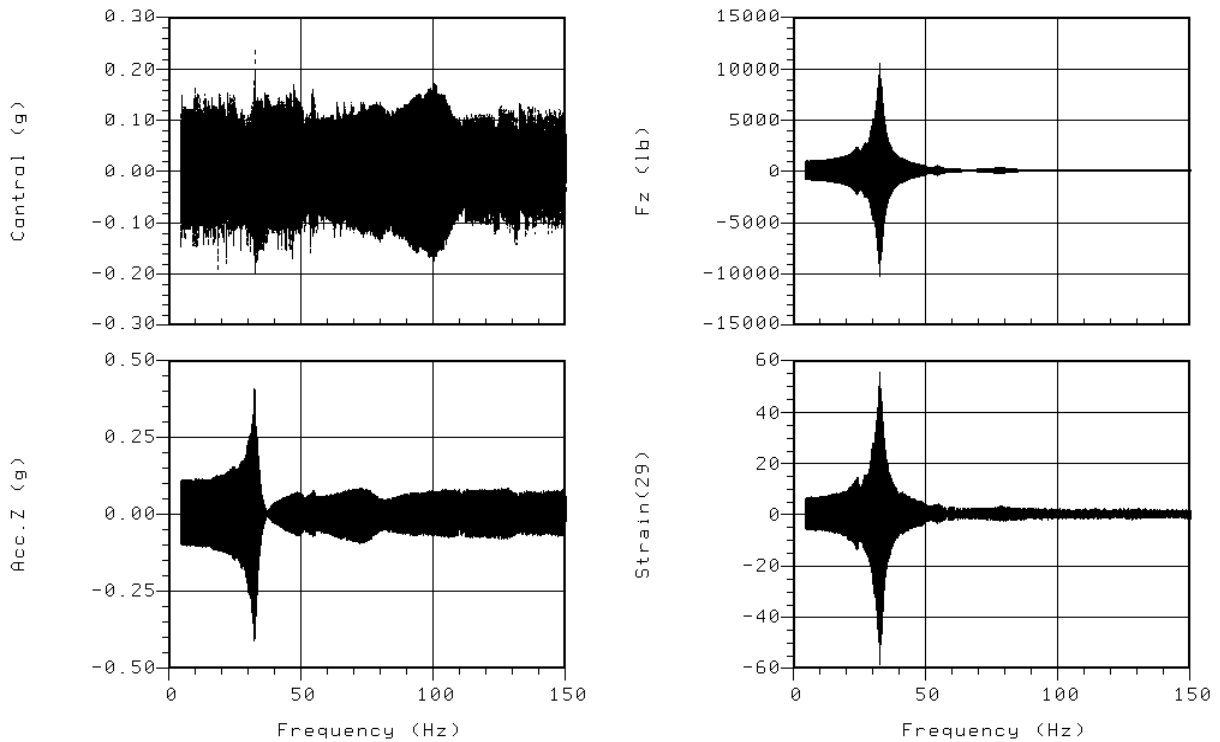


Figure 6.2-17. A Sample of the Data – Run Z18

This run was interrupted for about 15 seconds when the shaker tried to drive through the Z-mode, so a time history plot was unavailable. Zooming in on a time span close to the peak is shown in Figure 6.2-18. Notice that most signals are nearly clean sinusoids, but the control accelerometers are noisy, apparently trying to keep up with the dynamic spacecraft.



Title:

Flight Force Measurements of the Gamma-Ray Large Area Space Telescope / Delta II Flight

Page #:
57 of 226

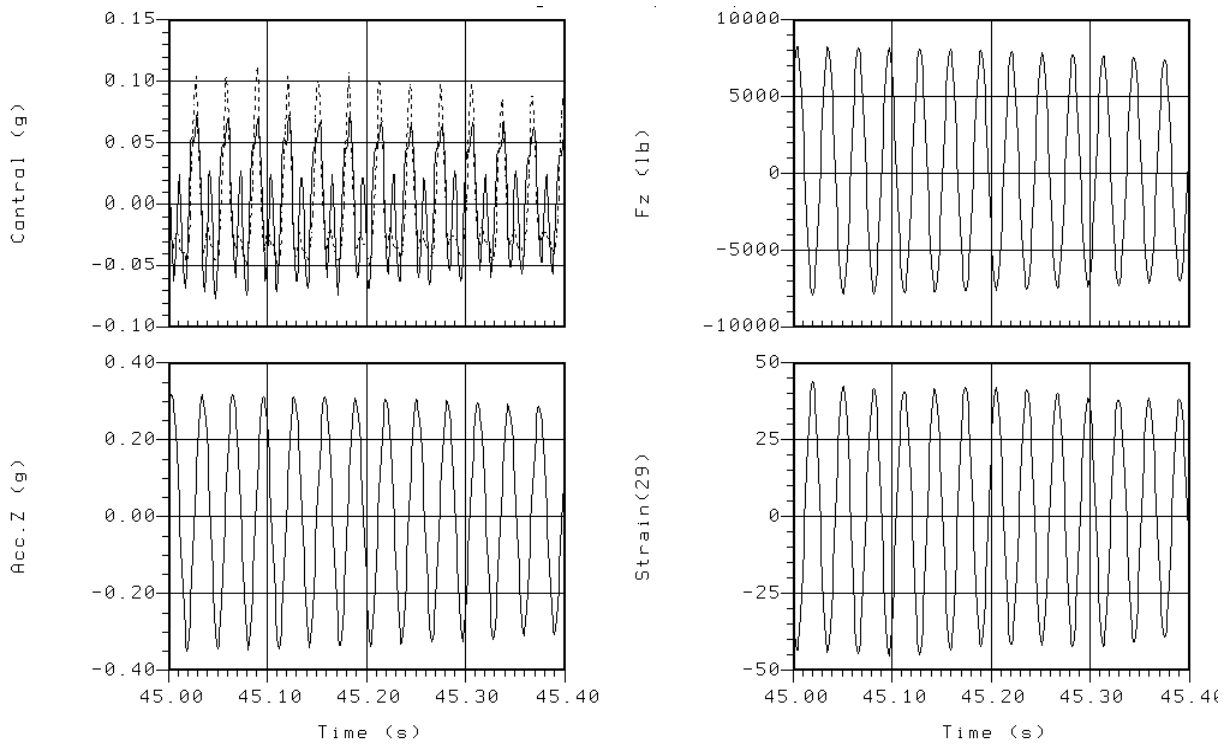


Figure 6.2-18. Zoom In on the Data Plotted

Comparisons between the analytical model of the test setup and the test itself begin with the natural frequencies. The fundamental X-mode showed two peaks due to solar array interaction with the basic bus and has a range of natural frequencies shown in Table 6.2-10.

Table 6.2-10. Natural Frequencies of the Fundamental Modes

Mode	From the Test Data (Hz)	From GLAST-PAF Dynamic Model (Hz)
X Bending	9.6 – 10.1	10.4
Y Bending	10.3	11.1
Z Axial	33.1	31.6

For reference, the maxima were measured during the low level runs (the ones used for data processing). Notice that the strain varied greatly from strut to strut even for the axial (Z) sweep, and the shear strain is generally lower than the axial strain as shown in Table 6.2-11.

	NASA Engineering and Safety Center Technical Assessment Report	Document #:	Version:
		NESC-RP-06-071	1.0
Title: Flight Force Measurements of the Gamma-Ray Large Area Space Telescope / Delta II Flight			Page #: 58 of 226

Table 6.2-11. Maxima Measured in the Low Level Sweeps

	X Sweep (lateral)	Y Sweep (lateral)	Z Sweep (thrust)
Max. Drive Acc. (g)	0.15	0.17	0.17
Max. I/F Force (lb)	7175	7099	9344
Max. Axial Strut 1 (μ)	130	342	83
Strain Strut 2	145	235	66
Strut 3	281	134	66
Strut 4	237	158	72
Strut 5	141	301	71
Strut 6	154	228	66
Strut 7	305	131	72
Strut 8	237	145	73
Max. Shear Strut 1 (μ)	51	92	41
Strain Strut 2	86	184	71
Strut 3	125	39	44
Strut 4	190	81	102
Strut 5	48	83	52
Strut 6	90	180	71
Strut 7	96	41	42
Strut 8	169	77	63

6.2.7 Calculation of Impedance

The term impedance as used within this report is the acceleration impedance, or the interface force divided by the interface acceleration. For the Z-axis test, the accelerometers in the TPAF were incorrectly placed at the upper ring by the GLAST interface points, instead of at the lower ring. For this test, the average shaker control was used for interface acceleration.

Only the impedance function magnitude is presented in this section, though they are complex functions in a 6x6 matrix used in the equation:

$$[F(\omega)] = [W(\omega)] [A(\omega)]$$

From each sweep, 1 column was calculated in the impedance matrix [W]. In the following plots (Figures 6.2-19 through 6.2-21), the results from the GLAST spacecraft-PAF FEM are shown with damping of 2 and 3 percent, along with the impedance from the test data. Data from the FEM is included for comparison only.



Title:

Flight Force Measurements of the Gamma-Ray Large Area Space Telescope / Delta II Flight

Page #:
59 of 226

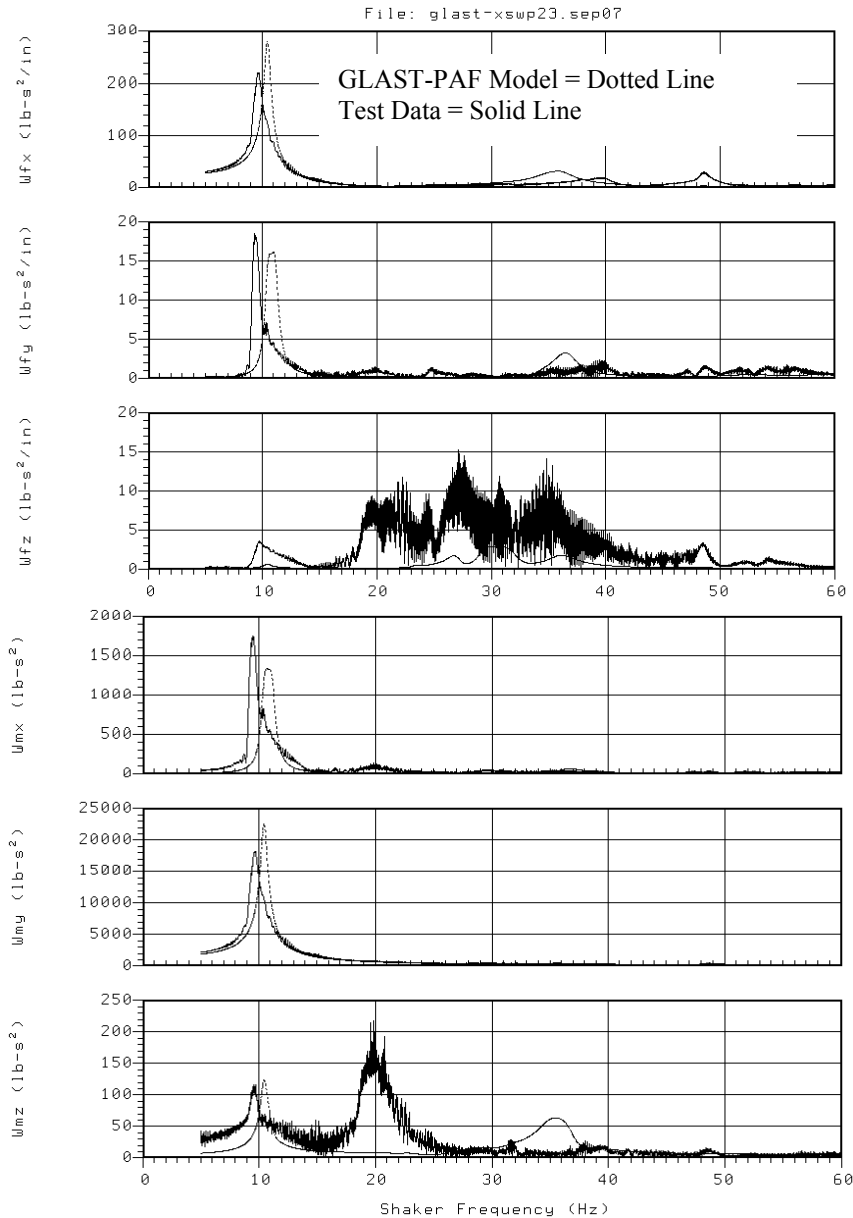


Figure 6.2-19. Impedance from the X-Axis Sweep



Title:

Flight Force Measurements of the Gamma-Ray Large Area Space Telescope / Delta II Flight

Page #:
60 of 226

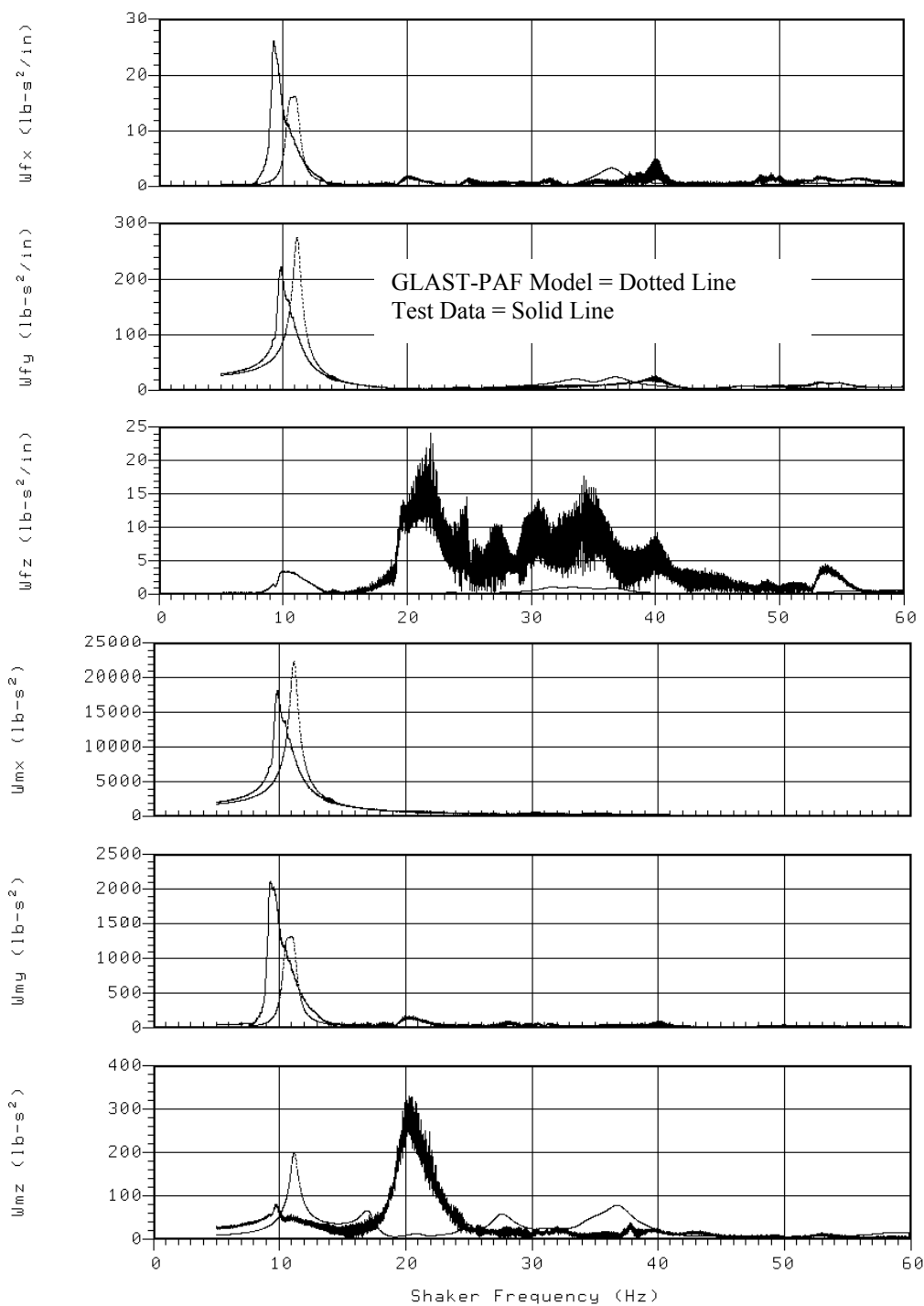


Figure 6.2-20. Impedance from the Y-Axis Sweep



NASA Engineering and Safety Center Technical Assessment Report

Document #:
**NESC-RP-
06-071**

Version:
1.0

Title:

Flight Force Measurements of the Gamma-Ray Large Area Space Telescope / Delta II Flight

Page #:
61 of 226

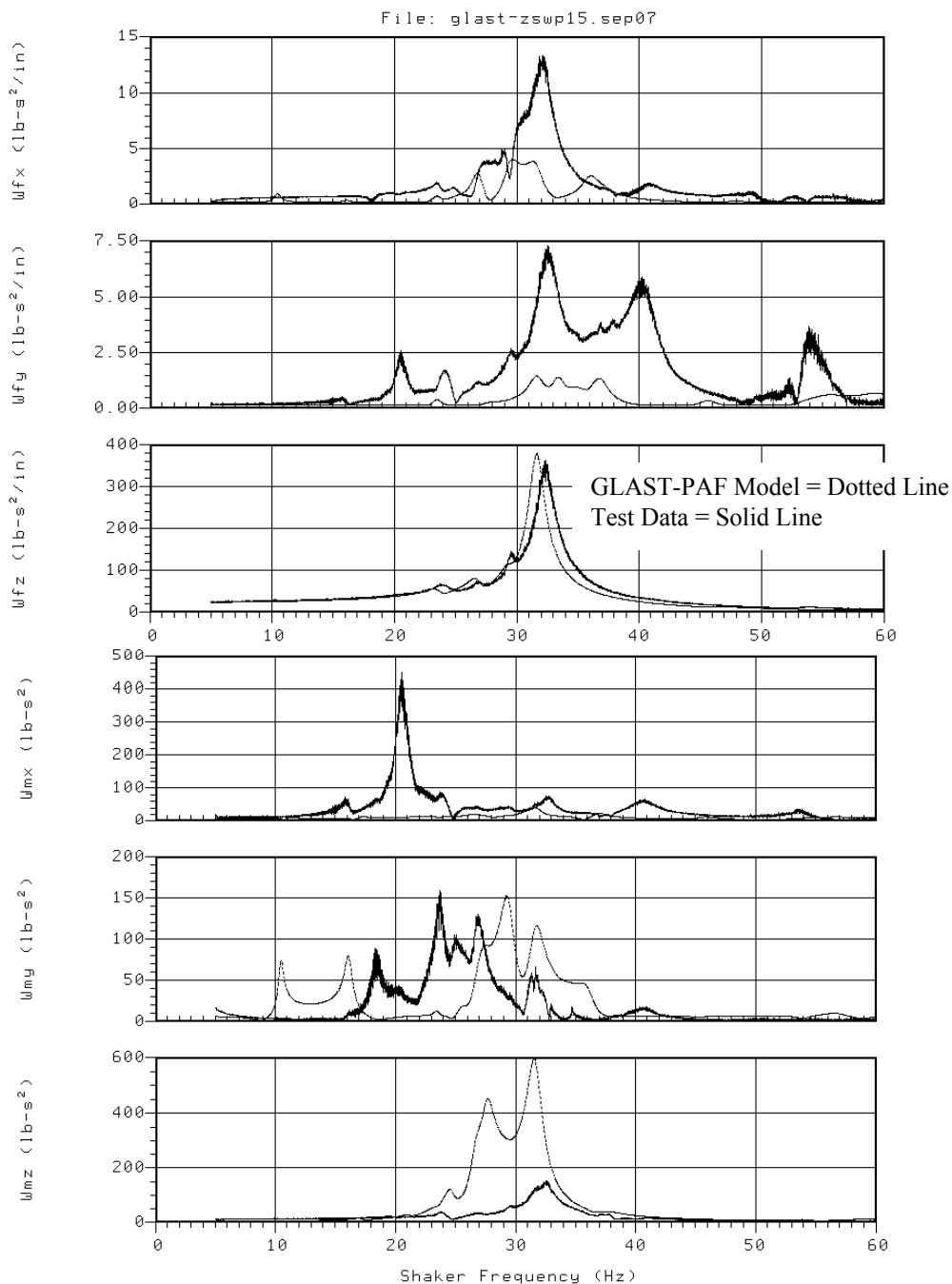


Figure 6.2-21. Impedance from the Z-Axis Sweep

	NASA Engineering and Safety Center Technical Assessment Report		Document #: NESC-RP- 06-071	Version: 1.0
	Title: Flight Force Measurements of the Gamma-Ray Large Area Space Telescope / Delta II Flight			Page #: 62 of 226

6.2.8 Calculation of Forces from Strain

The technique to convert strains into forces for the PAF is described in Reference 1. The method involves the simple calculation in the time domain:

$$[F(t)] = [E] [Strain(t)]$$

where, E = a matrix of constant coefficients

There are two ways to perform the conversion; one is the FEM Method that relies on the PAF FEM accuracy, the other is the SFM that sums the forces from each strut section at the GLAST spacecraft interface plane. For the FEM Method, the NESC team could only use the 30 clean strain gages, but found improved accuracy by using all strain gages after filtering. For the SFM, the NESC team needed at least six gages per PAF strut and used all 62 strain gages.

Validation of the strain-to-force calculation confirms:

- PAF FEM accuracy.
- Numbering and labeling schemes accuracy.
- Strain determination from the FEM accuracy.

Figures 6.2-22 through 6.2-27 show two curves on each plot, the solid line (the more ragged curve) is the force computed at the lower PAF interface from the strain measurements, and the dotted line (the smoother curve) is the measured force from the sum of the Kistler force transducers. All results are shown twice, once from the FEM Method and then from the SFM. Except for noise in the strain channels both methods produce excellent results. The error from the strain calculations at the peaks are shown on Table 6.2-12.

This is based on 62 strain gages, where the flight configuration had the full set of 64 gages.

Table 6.2-12. Difference Between Dominant Peaks from Strain and Force Gages (percent)

	X-Sweep (Lateral)		Y-Sweep (Lateral)		Z-Sweep (Axial)	
	FEM	SFM	FEM	SFM	FEM	SFM
Fx	2.99	7.06				
Fy			7.57	3.41		
Fz					2.73	0.03
Mx			9.71	6.97		
My	7.03	3.35				
Mz						



Title:

**Flight Force Measurements of the Gamma-Ray Large
Area Space Telescope / Delta II Flight**

Page #:
65 of 226

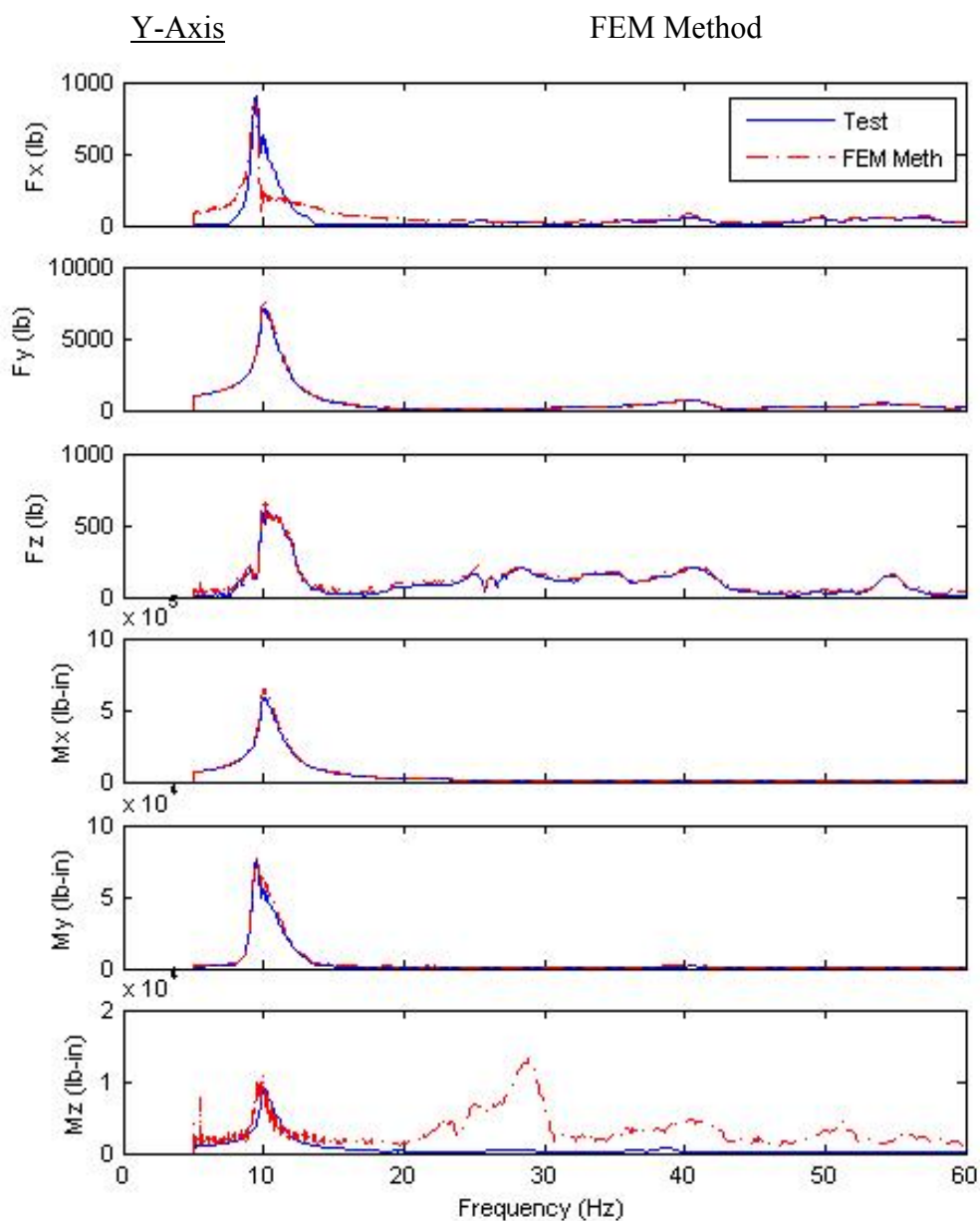


Figure 6.2-24. Forces from the FEM Method – Run Y28



Title:

**Flight Force Measurements of the Gamma-Ray Large
Area Space Telescope / Delta II Flight**

Page #:
66 of 226

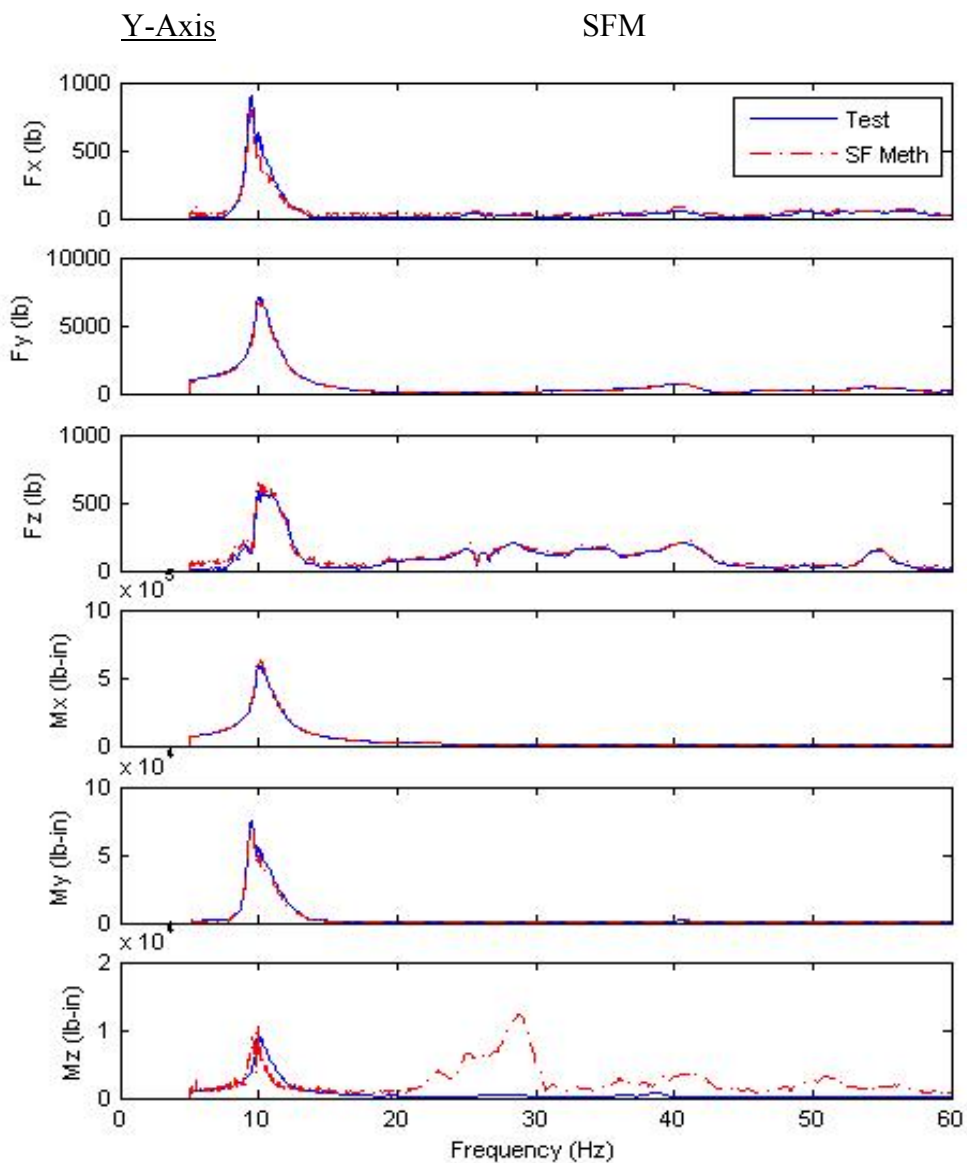


Figure 6.2-25. Forces from the SFM – Run Y28



Title:

**Flight Force Measurements of the Gamma-Ray Large
Area Space Telescope / Delta II Flight**

Page #:
67 of 226

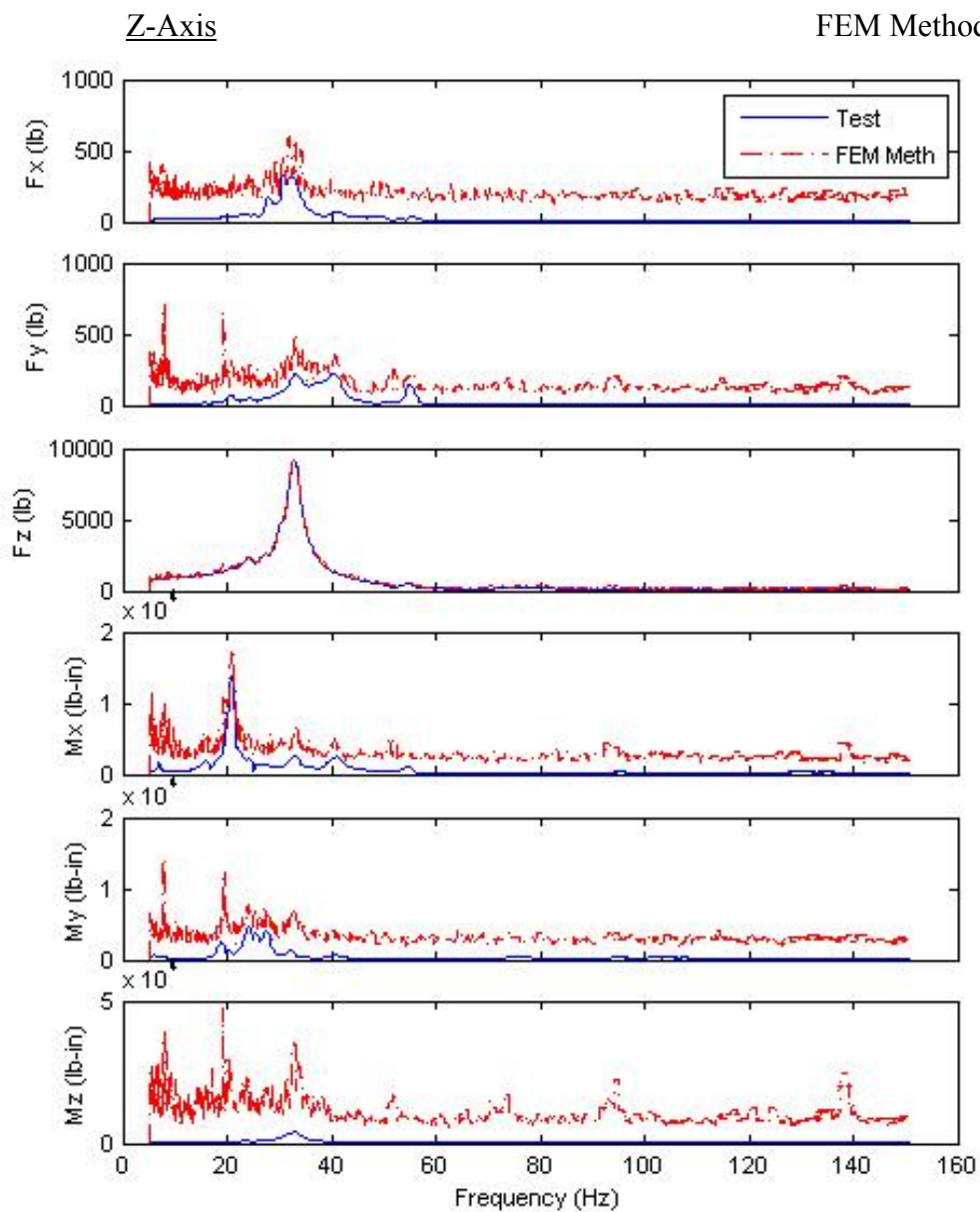


Figure 6.2-26. Forces from the FEM Method – Run Z15



Title:

Flight Force Measurements of the Gamma-Ray Large Area Space Telescope / Delta II Flight

Page #:
68 of 226

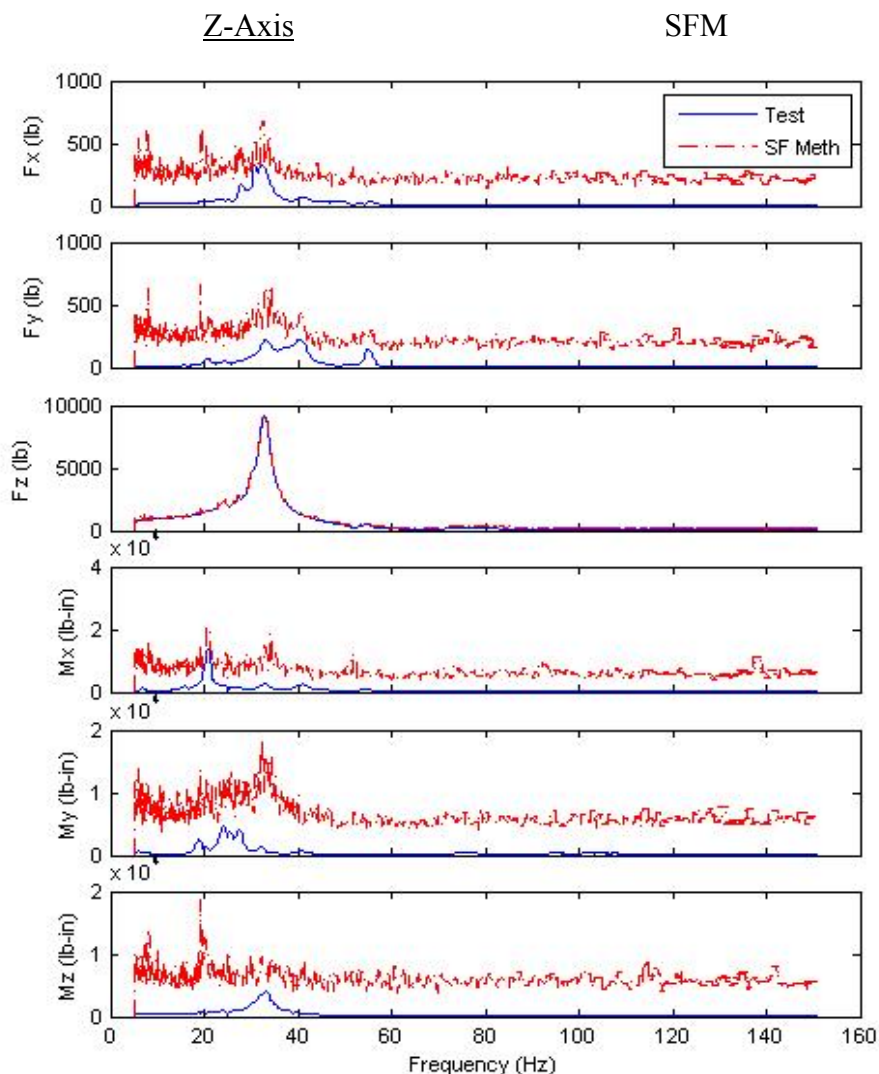


Figure 6.2-27. Forces from the SFM – Run Z15

It was concluded from these plots that both the FEM Method and the SFM are adequate to convert PAF strains into forces. This test serves as an independent check of the flight force method technique. By verifying the ability to use strain gages to measure boundary forces, the test verifies the PAF FEM, its ability to calculate strains and the accuracy of the complex numbering, and labeling scheme for the output channels.

Results normal to the shake direction are generally lost in electrical noise, a condition that should not occur in flight.

	NASA Engineering and Safety Center Technical Assessment Report	Document #: NESC-RP- 06-071	Version: 1.0
Title: Flight Force Measurements of the Gamma-Ray Large Area Space Telescope / Delta II Flight		Page #: 69 of 226	

6.3 Phase 2: Ground Static Test Validation

A test plan was generated in December 2007 [ref. 3]. Relevant portions of this test plan are presented in this report. The test description was to subject the Delta II 6915 TPAF to known static limit load forces and moments and to record strain gage measurements at various locations. The TPAF was mounted in the GSFC static load facility and connected to a mock payload where forces can be applied. Force application was by hydraulic load cell. Strain gages and displacement sensors on the PAF were monitored. The measurements were used to validate their use to indirectly determine the applied forces and moments by various NESC methods in post-test analysis.

6.3.1 Test Objectives

The test objectives were:

- 1) Verify the test configuration analytical model.
- 2) Investigate the effect of the launch vehicle flexibility at the PAF interface.
- 3) Serve as a possible replacement for the analytical model that converts strain data into force.

6.3.2 Test Article Description

The unit under test was the Delta II 6915 TPAF. This is the same TPAF that was used for the GLAST sine vibration testing and described in detail in Section 6.2.5. A mass simulator of the X-Ray Timing Experiment (XTE) spacecraft was used during static testing as a load fixture. The same four mounting locations (A, B, C, and D) used for the dynamic test shown in Figure 6.2-7 were used for the static test configuration. However, the dynamic test used a flight like interface with a center mounted separation bolt for tension load and a male conical fitting designed to carry shear load installed at each mounting interface. Each of the conical shear fittings attach through two bolt holes on either side of the mounting pad. For the static test, the separation bolt and conical shear fitting were not used and the XTE simulator mounted to interface blocks which bolted into the two holes used to attach the shear fittings at each of the PAF mounting pads. The static test was performed using the PAF FEM coordinate system shown in Figure 6.1-2.

The static load testing of the TPAF was planned in two parts. The first part was to be performed with a rigid interface at the base of the PAF. The second part was to be performed with a flexible interface to replicate the behavior of the Delta II Upper Stage. Part one of the testing with the fixed base was conducted December 17 through 19, 2007, and January 3, 2008. Part two was conducted on July 15, 2008. The results from all of the static testing performed on the TPAF are documented in reference 4.

	NASA Engineering and Safety Center Technical Assessment Report	Document #: NESC-RP- 06-071	Version: 1.0
Title: Flight Force Measurements of the Gamma-Ray Large Area Space Telescope / Delta II Flight		Page #: 70 of 226	

6.3.3 Static Testing – Fixed Base

The test setup for the first part of the TPAF static testing in a fixed-base configuration is shown in Figure 6.3-1 along with the coordinate axes used for the test. The cylinder on the bottom is the semi-rigid swivel/tilt fixture. A solid base plate was used to adapt the TPAF 68-bolt booster interface to the swivel/tilt fixture. The swivel/tilt fixture is 61 inches in diameter and approximately 22 inches high. Even though this item is stiff, the displacements of its interface ring were measured during the test by linear variable differential transformers (LVDTs). The swivel/tilt fixture allows for space to attach vertical load actuators to the XTE trunnions. The TPAF is connected to the base plate via an aluminum adaptor ring with a thickness of 2 inch, OD of approximately 64 inches, and an ID of approximately 56 inches. On top of the TPAF is the XTE Mass Simulator whose sole purpose is to act as a load fixture.



**NASA Engineering and Safety Center
Technical Assessment Report**

Document #:
**NESC-RP-
06-071**

Version:
1.0

Title:

**Flight Force Measurements of the Gamma-Ray Large
Area Space Telescope / Delta II Flight**

Page #:
71 of 226

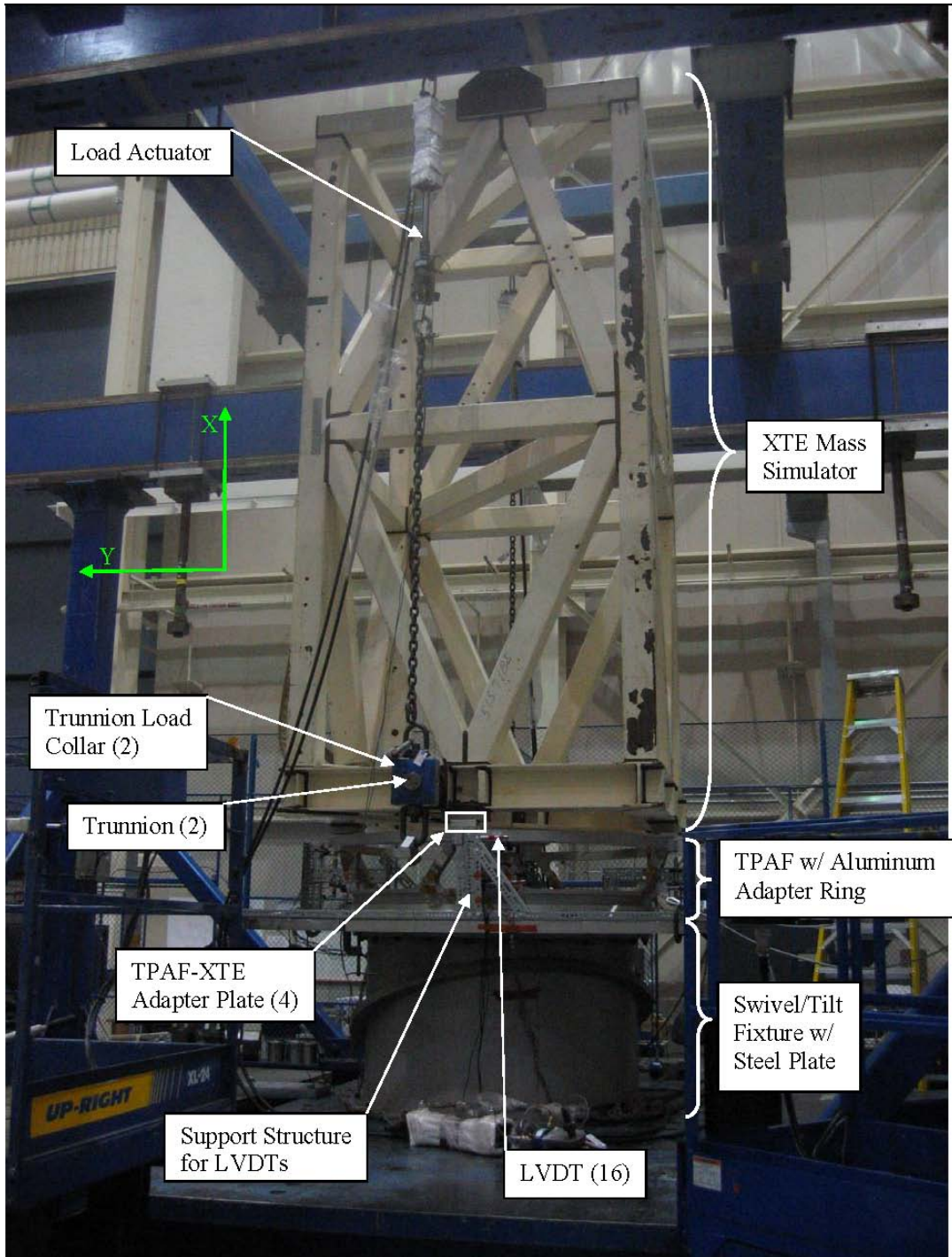


Figure 6.3-1. TPAF and XTE Mass Simulator

	NASA Engineering and Safety Center Technical Assessment Report	Document #:	Version:
		NESC-RP-06-071	1.0
Title: Flight Force Measurements of the Gamma-Ray Large Area Space Telescope / Delta II Flight		Page #: 72 of 226	

The XTE Mass Simulator was used as the load fixture. The weight of the XTE, was measured at the test site, was 5,157 pounds without its two mass plates. Figure 6.3-2 shows the lower portion of the XTE and labels the trunnions. The locations of these load points, as measured at the test site, are shown in Table 6.3-1.

Table 6.3-1. Coordinates of Trunnion Load Points

	<u>Point</u>	<u>X (in)</u>	<u>Y (in)</u>	<u>Z (in)</u>
+Z Primary Trunnion,	8159	7.0	7.0	44.31
-Z Primary Trunnion,	8160	7.0	7.0	-44.31

The XTE was partially restored for this test by removing and replacing the bolts at the trunnions, inspecting welds, and completing a stress analysis. Two trunnion load collars were fabricated for load application fittings. Each collar consisted of two halves which bolt together around a trunnion. Figure 6.3-3 shows one of the trunnion collars with load cables attached.

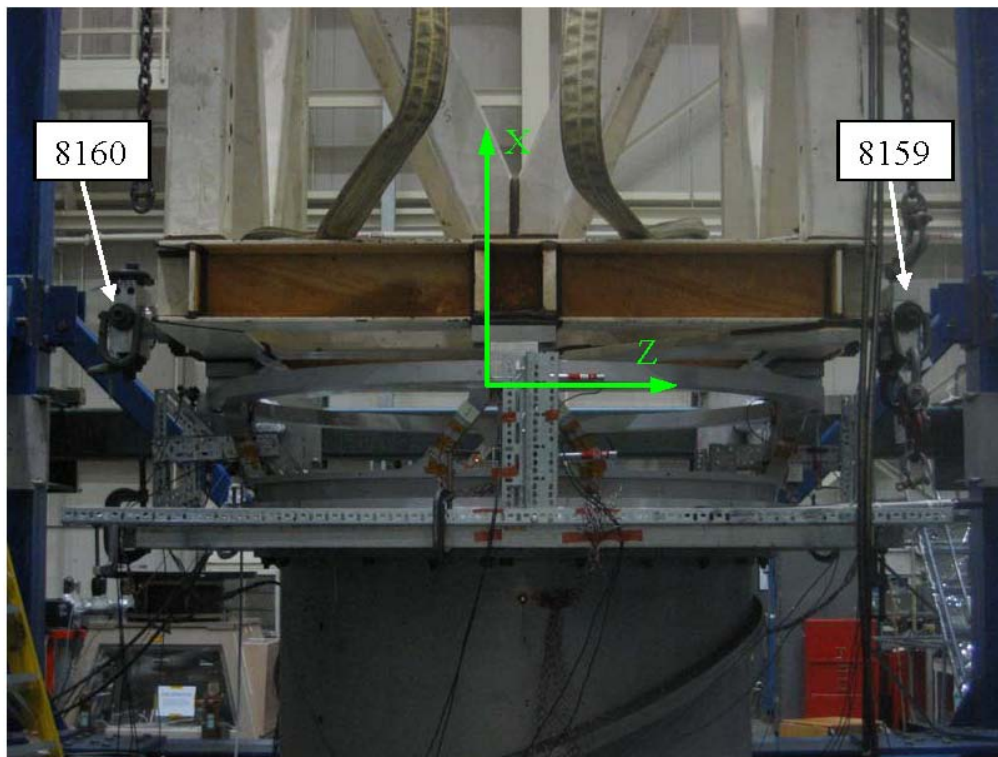


Figure 6.3-2. XTE Mass Simulator and Trunnion Labels



Title:

**Flight Force Measurements of the Gamma-Ray Large
Area Space Telescope / Delta II Flight**

Page #:
73 of 226

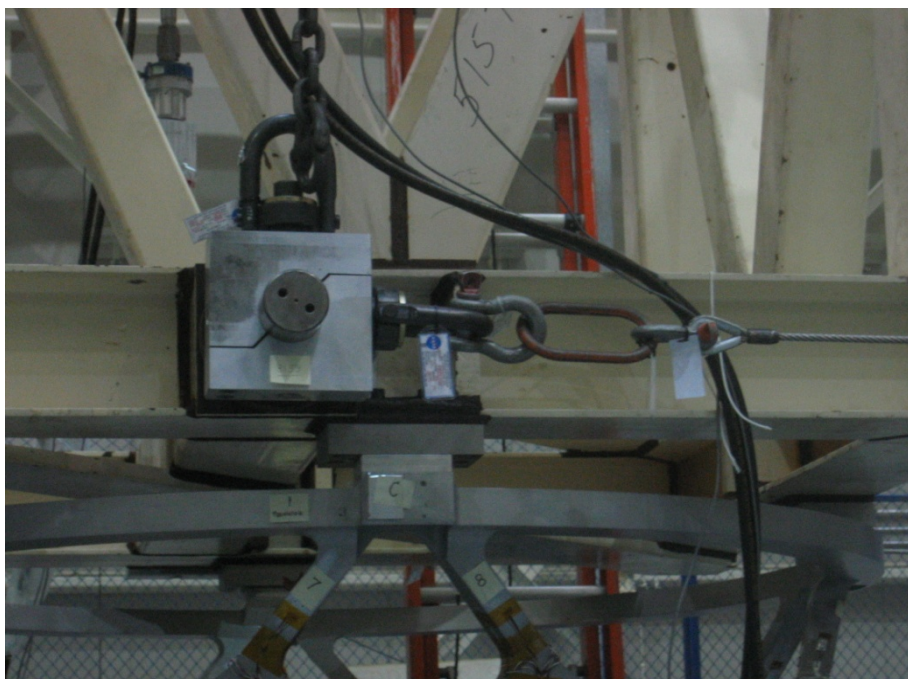


Figure 6.3-3. XTE Trunnion Load Collar

6.3.4 Static Testing – Flexible Interface with Cylindrical Extension

The second part of the static testing of the TPAF was performed on a cylindrical extension to replicate the flexibility of the Delta II Upper Stage. A model of the cylindrical extension developed for this test configuration is shown in Figure 6.3-4. The cylindrical extension replaces the swivel/tilt fixture for the second part of the test.

For this test configuration, the adaptor ring used to connect the TPAF to the swivel/tilt fixture was placed on the static test facility floor, the cylindrical extension was bolted on the adaptor ring top, the TPAF was mounted to the cylindrical extension, and finally the XTE was placed on the TPAF. A CAD model of the test configuration with the cylindrical extension is shown in Figure 6.3-5. The swivel/tilt fixture can be seen in the figure to the left of the test article. The cylindrical extension has a 57.5 inch diameter and a 36.75 inch height. The cylinder was designed to approximate the stiffness of the Delta II Upper Stage in various directions. It was not vital to have a structure with the exact stiffness properties as the Upper Stage, so the cylinder was designed to be slightly more compliant. The reason for incorporating the cylindrical extension was to show that the TPAF boundary conditions would not significantly affect the FFM methodologies for calculating forces. Figure 6.3-6 shows a picture of the test setup with the cylindrical extension in place for Load Case 19.



Title:

**Flight Force Measurements of the Gamma-Ray Large
Area Space Telescope / Delta II Flight**

Page #:
74 of 226

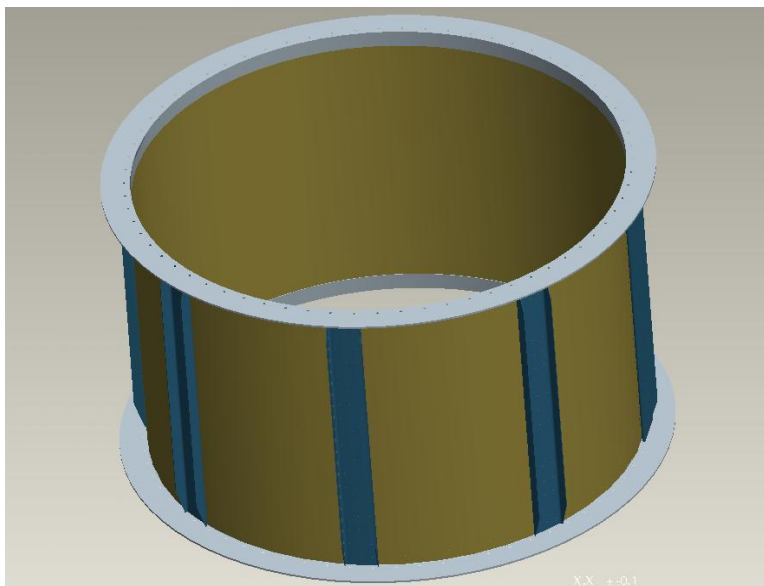


Figure 6.3-4. Cylindrical Extension

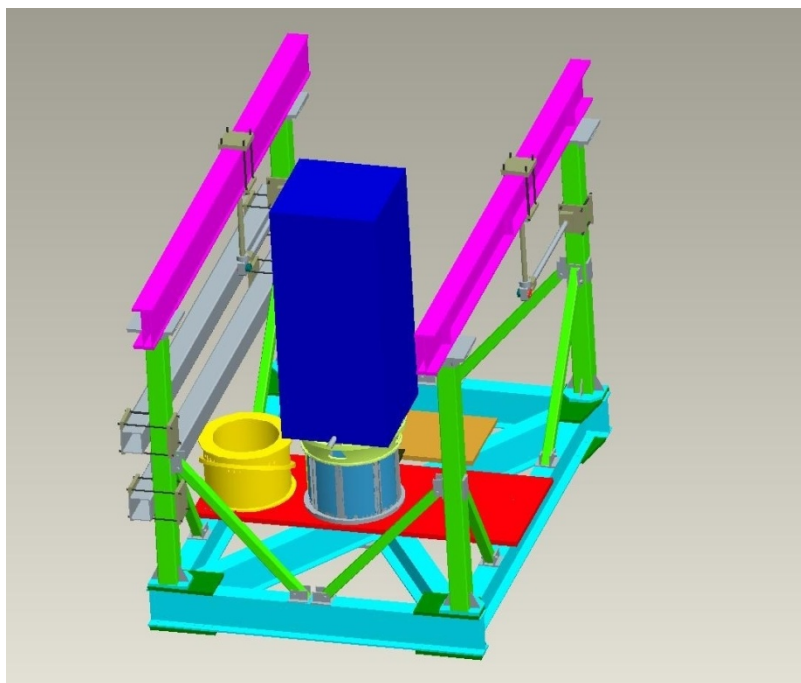


Figure 6.3-5. Configuration with Cylindrical Extension

	NASA Engineering and Safety Center Technical Assessment Report	Document #: NESC-RP- 06-071	Version: 1.0
Title: Flight Force Measurements of the Gamma-Ray Large Area Space Telescope / Delta II Flight			Page #: 75 of 226



Figure 6.3-6. Test Run 19 with the Cylindrical Extension

6.3.5 Instrumentation

Strain gage rosette instrumentation was placed on the 4 faces of each TPAF strut. As with the sine vibration testing, only two of the three rosette gages were used (shear and axial) for a total of 64 strain gage measurements. The location and orientation of the strain gages is the same as used for the GLAST sine vibration testing as defined in Section 6.2.2. The nomenclature used to identify the gages during the static test is defined in Section 6.1.3.

In addition to the strain gages, 16 LVDTs were installed at the XTE load fixture's four base points and the PAF base for part 1 of the static test with the swivel/tilt fixture in place. The LVDTs were mounted in the vertical and tangential directions to measure average X, Y, and Z-displacements at the TPAF top and bottom. At the top, they are at points A, B, C, and D from Figure 6.1-2 and are sketched on Figure 6.3-7. The full set of instrumentation channels measured during static testing of the TPAF is shown in Table 6.3-2.



**NASA Engineering and Safety Center
Technical Assessment Report**

Document #:
**NESC-RP-
06-071**

Version:
1.0

Title:

**Flight Force Measurements of the Gamma-Ray Large
Area Space Telescope / Delta II Flight**

Page #:
76 of 226

Table 6.3-2. Instrumentation Channels

Test Channel	Point Numbers	Dir.	Description	Comments
1	101	Force	Applied force	
2	102	“	Alternate applied force	
3	103	“	Alternate applied force	
4-7	18,1o,12,1i	Axial	Strut 1 strain gages	
8-11	21,2o,23,2i	“	Strut 2 “ “	
12-15	32,3o,34,3i	“	Strut 3 “ “	
16-19	43,4o,45,4i	“	Strut 4 “ “	
20-23	54,5o,56,5i	“	Strut 5 “ “	
24-27	65,6o,67,6i	“	Strut 6 “ “	
28-31	76,7o,78,7i	“	Strut 7 “ “	
32-35	87,8o,81,8i	“	Strut 8 “ “	
36-39	18,1o,12,1i	Shear	Strut 1 strain gages	
40-43	21,2o,23,2i	“	Strut 2 “ “	
44-47	32,3o,34,3i	“	Strut 3 “ “	
48-51	43,4o,45,4i	“	Strut 4 “ “	
52-55	54,5o,56,5i	“	Strut 5 “ “	
56-59	65,6o,67,6i	“	Strut 6 “ “	
60-63	76,7o,78,7i	“	Strut 7 “ “	
64-67	87,8o,81,8i	“	Strut 8 “ “	
68-69	5427	+X,-Y	LVDTs at XTE interface pad, pt. A	
70-71	8094	+X,-Z	“ B	
72-73	8092	+X,+Y	“ C	
74-75	8093	+X,+Z	“ D	
76-77	-	+X,-Y	LVDTs at TPAF base, beneath point A	
78-79	-	+X,-Z	“ B	
80-81	-	+X,+Y	“ C	
82-83	-	+X,+Z	“ D	



Title:

**Flight Force Measurements of the Gamma-Ray Large
Area Space Telescope / Delta II Flight**

Page #:
77 of 226

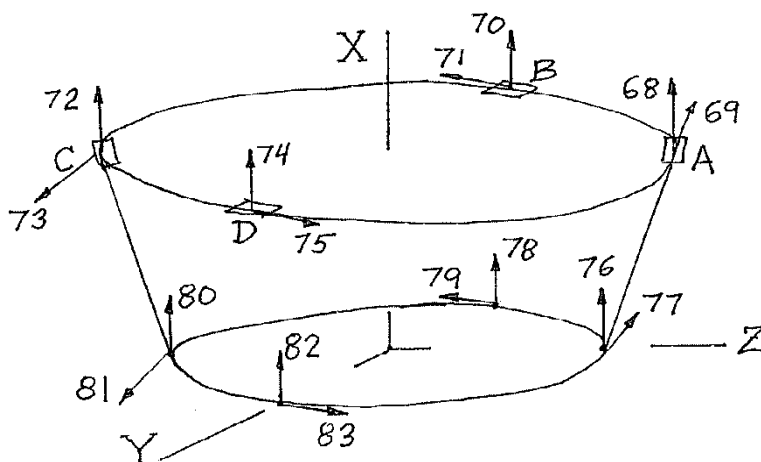


Figure 6.3-7. LVDT Locations

6.3.6 Test Levels

Not-to-exceed values were determined prior to testing based on an earlier PAF proof test, a GLAST spacecraft CLA [ref. 7] and the GLAST spacecraft sine vibration test. The static test loads were limited to 50 percent (approximately) of the loads created during the final GLAST spacecraft CLA, and to 33 percent (approximately) of the 1993 PAF proof test with the same XTE Mass Simulator. The strains were limited to 50 percent of the maximum strains achieved in the GLAST spacecraft vibrations test. These limits were set below previous load test levels for in order to avoid performing a detailed TPAF and XTE Mass Simulator stress analysis. Tables 6.3-3 and 6.3-4 show the limiting loads from these tests. During each test run, the test director monitored a strain versus applied force plot of all strain gages to verify that strains stayed within the not-to-exceed values.

Table 6.3-3. PAF Limit Loads

	GLAST CLA	50 Percent	Proof Test for XTE	33 Percent	Max. single CLA flight load event (Aero Wind at T = 40s)
Fx (axial) (lb)	26,053	13,026	92,095	30,698	20,458
Fy, Fz (lateral) (lb)	12,075	6,037	18,000	6,000	12,012
Mx (torsion) (in-lb)	46,178	23,089	-	-	44,945
My, Mz (bending) (in-lb)	766,344	383,172	1,674,000	558,000	766,344

	NASA Engineering and Safety Center Technical Assessment Report	Document #:	Version:
		NESC-RP-06-071	1.0
Title: Flight Force Measurements of the Gamma-Ray Large Area Space Telescope / Delta II Flight			Page #: 78 of 226

Table 6.3-4. Absolute Maximum Strain Limiting Values

	Maximum Strain from the GLAST Vibration Test			Not to
	(μ-strain)			Exceed
	X-Sweep	Y-Sweep	Z-Sweep	(w/o 1g)
	(Axial)	(Lateral)	(Lateral)	(μ-strain)
Axial Gages	143.4	368.8	350.9	184.4
Shear Gages	218.0	202.4	224.7	121.3

Tables 6.3-5 and 6.3-6 show test levels, interface loads, and the maximum predicted strain for both the Part 1 (Fixed Base) and Part 2 (Cylindrical Extension) portions of the static test. The test sequence of runs was selected to minimize the setup of the load actuators. For a given test run, all loads were incremented from 0 to 10, 20, 30, 50, 75, and 100 percent, then down to 75, 50, 30, 20, 10, and 0 percent of their maximum value. Although it was difficult to apply an exact load with the hydraulic hand pumps (especially when there were two or more loads being applied), the load cells did measure the actual load that was applied. After the first few test runs it became apparent that there was some “settling” occurring in the structures during loading, resulting in extremely non-linear strain plots. The change was made to the loading sequence: first load from 0 to 100 percent, back to 0 percent, then follow the incremental loading plan.

The loads for the second portion of the static test were limited by the cylindrical extension. Stress and buckling analyses were performed on the cylindrical extension to determine the maximum loading for Test Runs 11 through 20. The entire portion of the test using the cylindrical extension was performed with struts 1, 2, 5, 6, 7, and 8 using the 0.125 inch gages and struts 3 and 4 using the 0.250 inch gages.



NASA Engineering and Safety Center Technical Assessment Report

Document #:
NESC-RP-
06-071

Version:
1.0

Title:

Flight Force Measurements of the Gamma-Ray Large Area Space Telescope / Delta II Flight

Page #:
79 of 226

Table 6.3-5. Static Test Runs: Part 1 - Fixed Base

Test Run	Load Axis	Load Point	Approx. Max Pull (lb)	Max at PAF-XTE I/F		Max Strain		Notes
				Mx (in-lb)	My, Mz (in-lb)	Ax. (μ)	Shear (μ)	
1/1A	Axial +X +X	8159 8160	+7,200 +7,200	0	99,200	185	89	XTE weight = 5,157 lb
2	Bending +X -X	8159 8160	+4,500 -4,500	0	384,700	150	69	
3	Axial -X -X	8159 8160	-6,000 -6,000	0	82,700	154	74	XTE weight = 5,157 lb
3A/B	Axial/ Bending -X	8159	-6,000	0	256,500	185	92	3B uses 0.250 inch strain gages
4	Bending -X +X	8159 8160	-4,500 +4,500	0	384,700	150	69	
5	Shear +Y +Y	8159 8160	+3,000 +3,000	0	123,750	121	49	
5A/B	Shear/ Torsion +Y	8159	+3,000	128,250	20,700	95	63	5B uses 0.250 inch strain gages
6	Torsion +Y -Y	8159 8160	+540 -540	46,200	0	15	6	50 percent rule ignored b/c of low level
7	Shear -Y -Y	8159 8160	-3,000 -3,000	0	123,750	126	49	
8	Torsion -Y +Y	8159 8160	-540 +540	46,200	0	15	6	50 percent rule ignored b/c of low level
9	Combo +X +X +Y +Y	8159 8160 8159 8160	5,570 1,286 1,428 1,428	0	183,200	185	67	Combine runs 1,2,5 scaled down x 0.476
10	Combo -X -X -Y -Y	8159 8160 8159 8160	-5,260 -750 -1,500 -1,500	0	-192,600	184	66	Combine runs 3,4,7 scaled down x 0.501



**NASA Engineering and Safety Center
Technical Assessment Report**

Document #:
**NESC-RP-
06-071**

Version:
1.0

Title:

**Flight Force Measurements of the Gamma-Ray Large
Area Space Telescope / Delta II Flight**

Page #:
80 of 226

Table 6.3-6. Static Test Runs: Part 2 - Cylindrical Extension

Test Run	Load Axis	Load Point	Max. Pull (lb)	Max cylindrical extension Stress (ksi)	Max at PAF I/F			Est. Max. Strain		Notes
					Fx (kip)	Mx (kip-in)	My, Mz (kip-in)	Axial (μ)	Shear (μ)	
11	Axial +X +X	8159 8160	+7,200 +7,200	6.8	14.4	0	99.4	131	98	XTE weight = 5,157 lb
12	Bending +X -X	“ “	+1,600 -1,600	7.5	0	0	136.8	40	44	
13	Axial -X -X	“ “	-3,200 -3,200	7.5	6.4	0	44.2	58	44	XTE weight = 5,157 lb
14	Bending -X +X	“ “	-1,600 +1,600	7.5	0	0	136.8	40	44	
15	Shear +Y +Y	“ “	+1,400 +1,400	7.2	0	0	16.8	43	41	
16	Torsion +Y -Y	“ “	+540 -540	3.5	0	46.2	0	9	14	
17	Shear -Y -Y	“ “	-1,400 -1,400	7.3	0	0	16.8	43	41	
18	Torsion -Y +Y	“ “	-540 +540	3.5	0	46.2	0	9	14	
19	Combo +X +X +Y +Y	8159 8160 8159 8160	+1,800 +900 +1,800 +1,800	5.3	2.7	0	38.5	72	52	Combine runs 11,12, 15 scaled down
20	Combo -X -X -Y -Y	8159 8160 8159 8160	-1,100 -550 -1,100 -1,100	6.8	1.7	0	23.5	44	32	Combine runs 13,14, 17 scaled down

	NASA Engineering and Safety Center Technical Assessment Report	Document #: NESC-RP- 06-071	Version: 1.0
Title: Flight Force Measurements of the Gamma-Ray Large Area Space Telescope / Delta II Flight			Page #: 81 of 226

6.3.7 Change in Strain Gage Size

When the static test started, the TPAF was equipped with 0.125-inch strain gages (Vishay CEA-13-125UR-350); the FFM math models had been developed with this size strain gage. Before the end of the first part of the test, with the swivel/tilt fixture, it was determined ULA had begun outfitting the flight PAF with 0.250 inch strain gages (Vishay CEA-13-250UW-120). New test runs were created to determine that this size change had a negligible effect.

Test Runs 3A/B and 5A/B were similar to Test Runs 3 and 5, respectively (except that only the loads applied to Load Point 8159 were used). Test Runs 3A and 5A were completed with all TPAF struts using the 0.125 inch strain gages. After these runs were finished, struts 3 and 4 (the struts directly below Load Point 8159) had their strain gages changed for the 0.250 inch gages, and Test Runs 3B and 5B were then completed. The reason for only using one of the load points was that most of the load goes through the strain gages of interest. Mathematically, this makes the strain gage values on struts 3 and 4 the most important contributors to the FFM equations. The force calculations showed agreement between runs using the 0.125 inch gages (3A and 5A) and the runs using the 0.250 inch gages (3B and 5B) indicating that the change in gage size had a negligible effect on the ability to measure interface forces [ref. 4].

6.3.8 Post-Test Data Analysis

Raw data was received in the form of spreadsheets and text files. The spreadsheets contain continuous strain gage, load cell, and LVDT data updated at 1 Hz. The text files contain the same data, but at snapshots taken at the previously specified load increments.

Figure 6.3-8 is a plot of the applied forces (measured by load cell) (“ $F_{APPLIED}$ ”) and the forces calculated from strain gage data using the SFM (“ F_{SFM} ”) and FEM Method (“ F_{FEM} ”) from Test Run 1A, plotted versus strain. Whichever strain gage in a particular run had the highest strain was used as the master for the strain axis. All forces are resolved at the TPAF-XTE interface.



Title:

Flight Force Measurements of the Gamma-Ray Large Area Space Telescope / Delta II Flight

Page #:
82 of 226

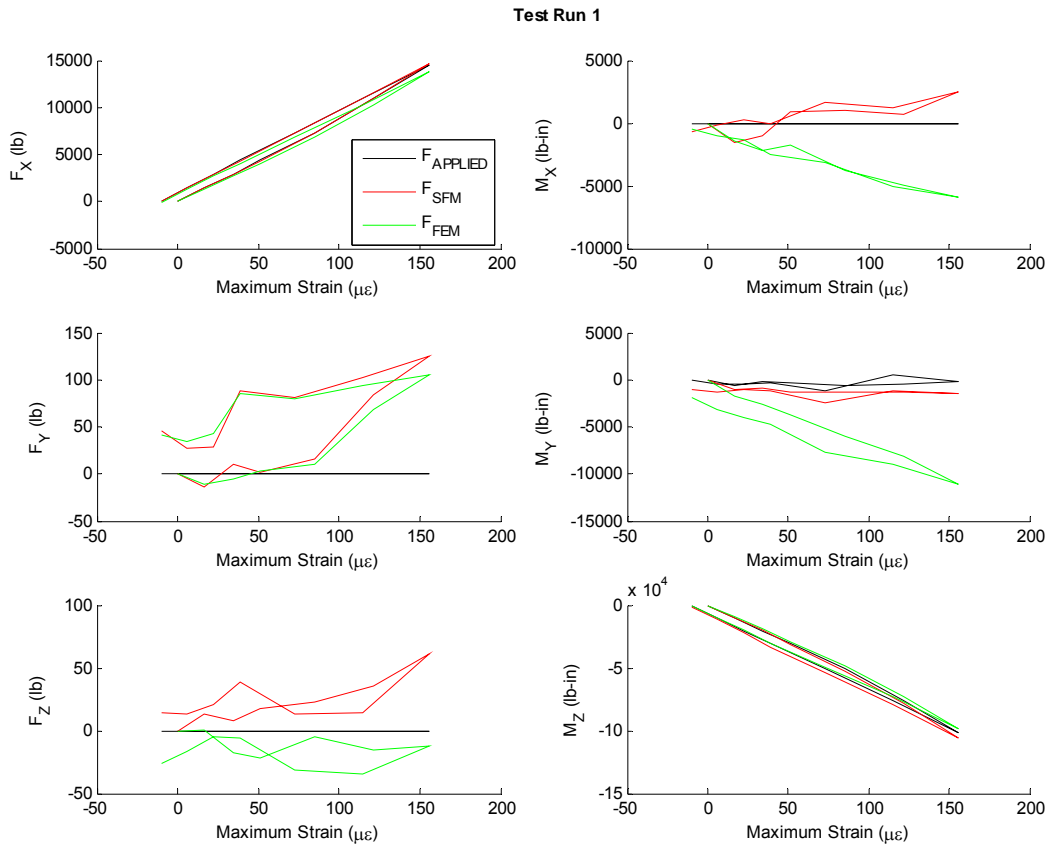


Figure 6.3-8. Force versus Strain – Test Run 1A

Note on Figure 6.3-8 the upper left plot shows excellent agreement between applied force and calculated force. In each test run there are cross-talk directions where no force was applied. The plots of the calculated forces in these directions show larger errors than in the direction of the primary applied loads and are not of concern because the magnitudes are relatively small. As Figures 6.3-9 through 6.3-12 show, the applied forces must be high enough to produce strain values of significance.

Figures 6.3-9 through 6.3-12 show the maximum error between applied and calculated load from collecting all 10 runs in Parts 1 and 2. It is important to note that until forces exceed about 700 pounds, the errors can be large due to the strain gage resolution. In all cases, the SFM was more accurate than the FEM Method. Because of PAF symmetry, the test item was not loaded in the Z-direction and lateral Z-forces are not shown in the Figures 6.3-9 through 6.2-12.



Title:

Flight Force Measurements of the Gamma-Ray Large Area Space Telescope / Delta II Flight

Page #:
83 of 226

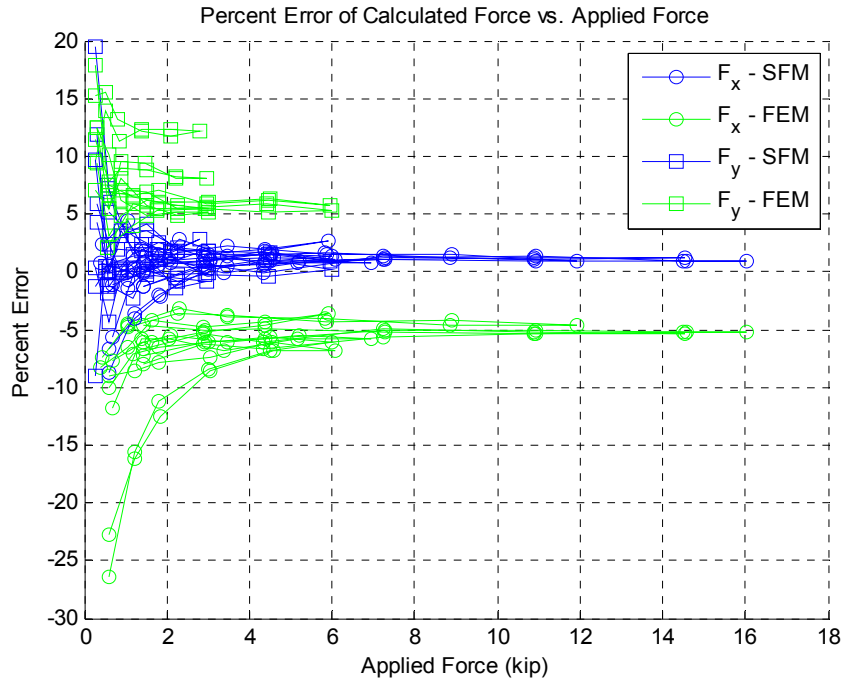


Figure 6.3-9. Force Error Plot – Fixed Base

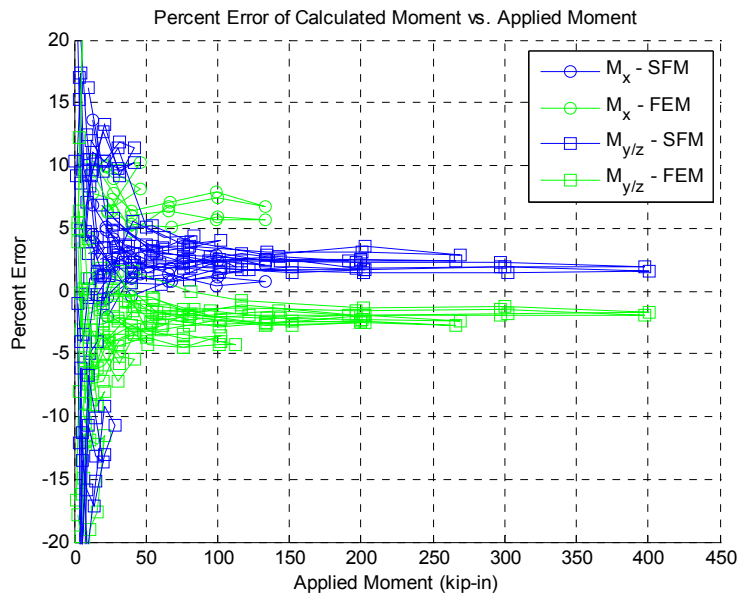


Figure 6.3-10. Moment Error Plot – Fixed Base



Title:

Flight Force Measurements of the Gamma-Ray Large Area Space Telescope / Delta II Flight

Page #:
84 of 226

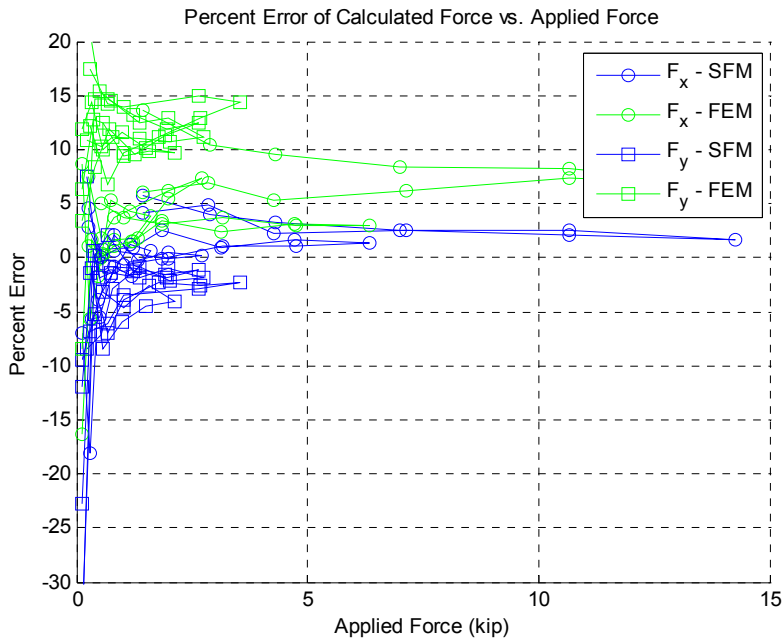


Figure 6.3-11. Force Error Plot – Flexible Base

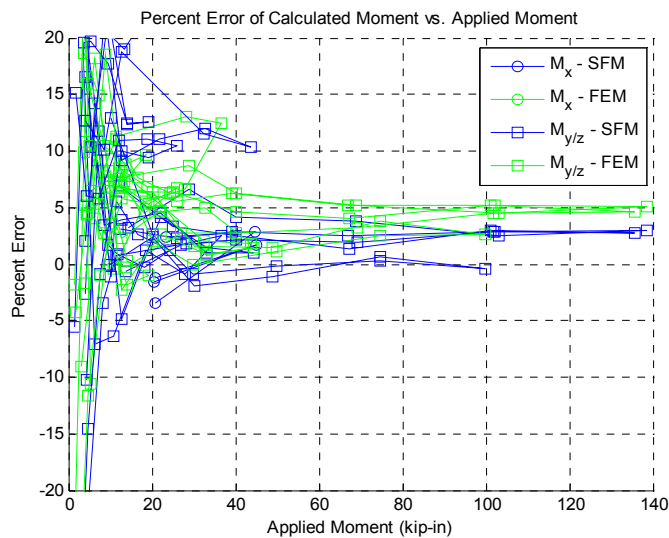


Figure 6.3-12. Moment Error Plot – Flexible Base

It can be easily found that as the test levels increase, the prediction errors decrease.

	NASA Engineering and Safety Center Technical Assessment Report	Document #:	Version:
		NESC-RP-06-071	1.0
Title: Flight Force Measurements of the Gamma-Ray Large Area Space Telescope / Delta II Flight		Page #: 85 of 226	

6.3.9 Static Tests Summary

The tests were expertly conducted and successfully completed by Analex. Data was delivered in an easy-to-read, understood format. The test revealed the accuracy that can be expected by the strain-based predictive methods. At the low force end, noise and strain resolution limited the accuracy. However as loads increased, the predictions improved. The general rule of thumb is described in Table 6.3-7 for approximate limits.

Table 6.3-7. Approximate Prediction Accuracy

	Maximum Desired Error (percent)	Minimum Predicted Force		Minimum Predicted Moment		Method of Solution
		Axial (lb)	Lateral (lb)	Bending (lb-in)	Torsion (lb-in)	
On a Rigid Base	10	500	500	25,000	25,000	SFM
		500	2800	25,000	30,000	FEM
	5	800	800	40,000	30,000	SFM
		11,000	6000	45,000	50,000	FEM
On a Flexible Base	10	500	500	45,000	15,000	SFM
		3500	4000	45,000	30,000	FEM
	5	2500	1800	45,000	20,000	SFM
		N.A.	N.A.	70,000	N.A.	FEM

N.A. = Not Achieved

Table 6.3-7 (static test) and Table 6.2-12 (dynamic test) confirm the viability of using the 6915 PAF instrumented with strain gages to measure interface forces where the accuracy goal was set at 10 percent (20 percent worst case). The static and dynamic test results show that using the SFM for flight predictions would reasonably provide 5 percent accuracy, 10 percent worst case, so long the predicted peak forces meet minimum values (Table 6.3-7).

6.4 Phase 4: Procurement of Flight System and Flight Data

The Critical Design Review (CDR) of the SFI package is summarized in reference 8. Relevant material from the CDR is presented herein. The CDR objectives were to obtain the Kennedy Space Center (KSC) Chief Engineer's Office and KSC customer concurrence for the following:

- A NASA-requested Delta II payload-to-launch vehicle FFM SFI system critical design.
- Implementation of the aforementioned SFI system components on the Delta II GLAST spacecraft PAF and Second Stage.

The package includes the following SFI aspects:

	NASA Engineering and Safety Center Technical Assessment Report	Document #: NESC-RP- 06-071	Version: 1.0
Title: Flight Force Measurements of the Gamma-Ray Large Area Space Telescope / Delta II Flight		Page #: 86 of 226	

Strain Gage Range and Resolution Requirements
Telemetry System Design, Battery Margin Assessment
Calibration and Checkout Plans
Electrical Packaging Design
Electromagnetic Interference (EMI) Qualification Assessment
Mechanical/Structural Drawing Changes Required
Estimated Vehicle Performance Impact
Hardware Attachment to Launch Vehicle Structural Integrity
Summary/Conclusion

The total number of SFI channels installed on the GLAST spacecraft/Delta II 6915 PAF was:

Strain gages channels	64
<u>Accelerometers channels</u>	<u>12</u>
TOTAL	76

The schedule major milestones were:

- Authority to Proceed (ATP) for Long-Lead Material Procurement, February 28, 2007
- ATP ((Original Scope of Work (SOW)), April 5, 2007
- ATP (Revised SOW), November 8, 2007
- Avionics Engineering Review Board (ERB), December 7, 2007
- Joint ULA/NASA-KSC CDR/ERB, January 20, 2008
- PAF Installations/Checkout Complete (at Boeing Huntington Beach), February 22, 2008
- PAF Delivery to Launch Site, April 17, 2008
- Strain Gage Calibration (at spacecraft/PAF mate), April 23, 2008
- GLAST vehicle ILC
- Flight date, June 12, 2008

	NASA Engineering and Safety Center Technical Assessment Report	Document #: NESC-RP- 06-071	Version: 1.0
Title: Flight Force Measurements of the Gamma-Ray Large Area Space Telescope / Delta II Flight		Page #: 87 of 226	

6.4.1 Strain Gage Range and Resolution Requirements

Unit load case strain level estimates at proposed strain gage locations were determined by Strength:

- Axial load = 1,000 lbs / leg in tension/compression
- On leg: Axial strain = 70 $\mu\text{in/in}$ (along leg direction)

In-flight loading from CLA and MECO analysis was estimated by Loads and Dynamics:

- Upper and lower bounds were determined by Strength based on material capability:
 - $\pm 2,400 \mu\text{in/in}$ for aluminum 2019-TXXX
- Resolution was determined based on high frequency MECO loading
 - $\pm 40 / 10 = \pm 4 \mu\text{in/in}$

In summary:

- Strain range: $\pm 2,400 \mu\text{in/in}$
- Required Minimum Resolution: $\pm 4 \mu\text{in/in}$ (± 0.2 percent of range)
- Delivered System Resolution: $\pm 1.2 \mu\text{in/in}$

6.4.2 Measurements Requested

The SFI required for the GLAST mission was:

- WRO L-NLS-1100-271 R1 dated November 8, 2007
 - Non-Launch Services Task Order NLSB-271R1
 - 76 Required measurements
- 64 Strain Measurements,
 - 32 Rosette Style Gages
 - Frequency Response 0 to 200 Hz, Flat within 1 dB
- 12 Accelerometers,
 - 4 Tri-axial Accelerometers
 - Aligned to thrust, tangential, and radial axes of vehicle
 - TM System Frequency Content to 200 Hz
- EMI Qualification Test on SFI Transmitter

6.4.3 Flight System and Data Summary

The system design for a Delta II payload-to-launch vehicle FFM SFI system was presented.

- System components to be installed on GLAST spacecraft/Delta II 6915 PAF and Second Stage.

	NASA Engineering and Safety Center Technical Assessment Report	Document #: NESC-RP- 06-071	Version: 1.0
Title: Flight Force Measurements of the Gamma-Ray Large Area Space Telescope / Delta II Flight			Page #: 88 of 226

- System incorporates mature design practices and will incorporate fully test-qualified components.
- Addition of SFI system introduces no significant risk to Delta II primary flight systems.

A special instrumentation package was procured to meet the requirements of the FFMs assessment and does not introduce significant risk on the GLAST spacecraft. Figures 6.4-1 through 6.4-3 show photos of the installed strain gages and accelerometers on the GLAST PAF.

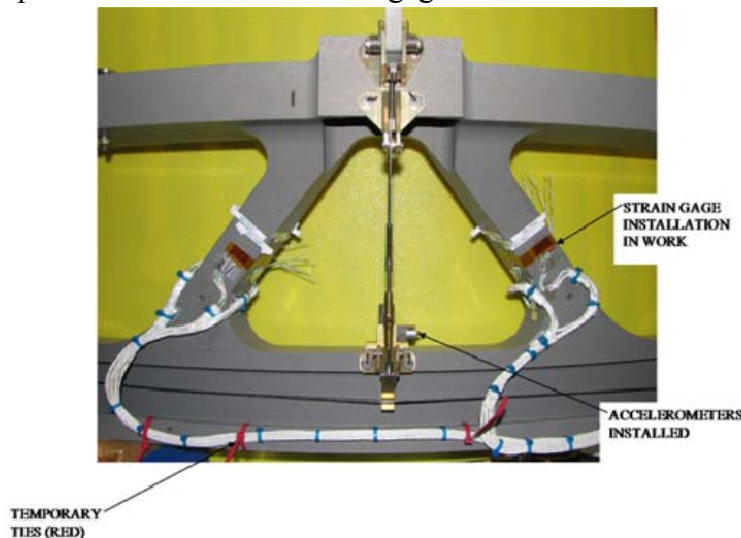


Figure 6.4-1. Flight PAF with Strain Gages and Accelerometers Installed

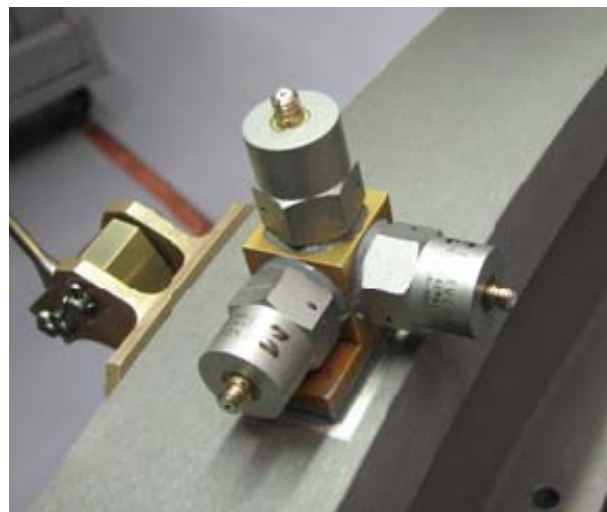


Figure 6.4-2. Accelerometer Installation



Title:

**Flight Force Measurements of the Gamma-Ray Large
Area Space Telescope / Delta II Flight**

Page #:
89 of 226



Figure 6.4-3. Close-up of Strain Gage Installation

The strain gages installed on the PAF for the GLAST flight were the same type as were used in the TPAF static and dynamic ground testing. These were independently selected by ULA for use in instrumenting the flight PAF based on the manufacturers recommendation for this type of aluminum structure. The flight gages were 0.250 inch while most of the dynamic and static testing was performed with 0.125-inch gages. However, additional static load testing was performed using the same 0.250-inch gages to verify that the larger gage size does not affect the ability to accurately measure interface loads. This is discussed in Section 6.3.7.

	NASA Engineering and Safety Center Technical Assessment Report	Document #: NESC-RP- 06-071	Version: 1.0
Title: Flight Force Measurements of the Gamma-Ray Large Area Space Telescope / Delta II Flight			Page #: 90 of 226

6.5 Phase 5: Flight Data Flight Processing and Flight Reconstruction

The preferred method developed for flight force prediction is the SFM, which had the best accuracy based on ground tests. However, the FEM and Impedance Methods were also evaluated as part of this activity. The events that drive design loads on a Delta II vehicle are Liftoff, Airloads, and MECO, which are the main focus of the reconstruction effort. However, MECO has never previously been successfully reconstructed and an Airloads reconstruction is a complex process that could not be completed within the assessment schedule. These two events were evaluated with basedrive analyses using the actual measured accelerations. Only Liftoff was reconstructed as a CLA.

Several different methods were used for flight reconstruction and force prediction for comparison with the measured flight forces as part of this study. They are described briefly as follows:

- a) **Full coupled loads reconstruction** is a dynamic response analysis of the coupled system (launch vehicle and payload models) using forcing functions similar to the CLA process, except the forcing functions are modified to reflect the parameters measured on the specific flight of interest. This is intended to remove the statistical uncertainty that is part of a standard load cycle. Typically the reconstruction analysis is a linear multi-input multi-output process. The Liftoff analysis is performed in the time domain while the Airloads analysis is a combination of time domain (gust) and frequency domain (buffet) solutions. As previously noted, it was only possible to perform a full flight reconstruction analysis of the Liftoff event as part of the FFM study.
- b) **Basedrive reconstruction** is an analysis in which the payload model is driven at a single 6 d-o-f grid at the PAF base. The 6 input accelerations (three translations and three rotations) at the drive point are derived from measured flight time histories. This is a linear single-point input (6 accelerations at drive point) multi-point output analysis. Two different configurations of the GLAST spacecraft were used in the basedrive reconstruction analysis. The first configuration used the VCLA model with a constant damping of two percent for all modes. The VCLA spacecraft model had been verified by a traditional fixed base modal survey in which the mode shapes and frequencies were identified and the spacecraft FEM was adjusted to correlate the corresponding modes within standard requirements. The second basedrive configuration was an updated version of the VCLA model which had been modified to directly match the data from the GLAST sine vibration test. In addition, the damping schedule derived from the sine vibration test data was used for this analysis configuration. The basedrive results for both model configurations are discussed under Data Analysis (Section 7.0)

	NASA Engineering and Safety Center Technical Assessment Report	Document #: NESC-RP- 06-071	Version: 1.0
Title: Flight Force Measurements of the Gamma-Ray Large Area Space Telescope / Delta II Flight		Page #: 91 of 226	

- c) **The Impedance Method** uses ground-test measured translational impedances from dynamic testing of the spacecraft and PAF, and model-based rotational impedances (to account for rotational terms that cannot be obtained in a standard shaker test). The GLAST model used to derive the rotational impedance terms is the VCLA model which had been updated based on data from the sine vibration test. This test-correlated GLAST model was adjusted to match the measured frequency and damping results from the sine test. The model used in these calculations is the “Impedance Correlated” model described in Section 6.2. The flight measured input accelerations are transformed to the frequency domain by a Fourier transform. The resulting acceleration spectra are multiplied by the impedance functions to produce the interface force spectra. The interface force spectra are converted to force time histories by an inverse Fourier transform. Thus, this method is also a linear, single-input (six accelerations at a single drive point), multi-output analysis.

In the special flight data system implemented on the Delta II for this assessment, the accelerometers are alternating current (AC) coupled and the strain gages are direct current (DC) coupled. This means that the accelerometers measure only the dynamic response while the strain gages measure the total response (steady state plus dynamic). An additional accelerometer on the Delta II Avionics Section (standard instrumentation), which is DC coupled, measured the steady state thrust acceleration.

6.5.1 Flight Summary and Vehicle Description

The GLAST mission (Delta 333) was launched from the Cape Canaveral Air Force Station (CCAFS) (SLC 17B) on June 11, 2008 at 12:05:00.521 Eastern Daylight Time. The Delta II Model 7920H-10C launch vehicle successfully placed the GLAST spacecraft into the required orbit. Figure 6.5-1 shows the GLAST spacecraft on the Delta II vehicle during fairing mate. Figure 6.5-2 shows the GLAST launch.



NASA Engineering and Safety Center Technical Assessment Report

Document #:
**NESC-RP-
06-071**

Version:
1.0

Title:

**Flight Force Measurements of the Gamma-Ray Large
Area Space Telescope / Delta II Flight**

Page #:
92 of 226



Figure 6.5-1. GLAST Spacecraft on Delta II Vehicle During Fairing Mate

The Delta II vehicle consisted of the extended tank liquid oxygen (LOX)/RP-1 booster with thrust augmentation provided by 9 graphite epoxy solid motors (GEMs) and a hypergolic Second Stage. This was the first flight of the Delta II heavy vehicle with the 10-foot diameter (10C) fairing.

The dynamic data acquisition system consisted of 12 Pulse Code Modulation (PCM) flight instrumentation channels with a special instrumentation suite of 12 accelerometers and 64 strain gages on the PAF. All dynamic instrumentation channels functioned satisfactorily, except for the Second Stage engine head accelerometer, which was invalid from Liftoff through Second Engine Cutoff (SECO) 2.

	NASA Engineering and Safety Center Technical Assessment Report	Document #: NESC-RP- 06-071	Version: 1.0
Title: Flight Force Measurements of the Gamma-Ray Large Area Space Telescope / Delta II Flight			Page #: 93 of 226



Figure 6.5-2. GLAST/Delta II 7920H-10C Launch

A summary of the sequence of events for the GLAST mission is presented in Table 6.5-1. The table compares the Best Estimated Trajectory (BET) predictions with the actual event times as measured on the flight instrumentation. As can be seen, all events occurred close to their predicted times through MECO. Actual event times following MECO differed slightly from predicted times as a result of guidance adjustments required to compensate for off-nominal booster performance. It should be noted that the actual flight times shown were extracted from the standard flight instrumentation and may be different from the data shown for the SFI.

A post flight analysis report was prepared by ULA [ref. 9]. Relevant portions of that report are presented in the following sections.



**NASA Engineering and Safety Center
Technical Assessment Report**

Document #:
**NESC-RP-
06-071**

Version:
1.0

Title:

**Flight Force Measurements of the Gamma-Ray Large
Area Space Telescope / Delta II Flight**

Page #:
94 of 226

Table 6.5-1. Sequence of Events Summary

Event	Time after Liftoff (sec)	
	BET Predicted	Actual
Liftoff	0.0	0.0
Ground Ignited Solid Motors (3) Burnout	77.0	75.2
Ground Ignited Solid Motors (3) Burnout	77.4	75.6
Altitude Ignited Solid Motors (3) Ignition	79.0	79.0
Jettison (3) Ground Ignited Solid Motors	80.5	80.5
Jettison (3) Ground Ignited Solid Motors	81.5	81.5
Altitude Ignited Solid Motors (3) Burnout	155.3	154.1
Jettison (3) Altitude Ignited Solid Motors	159.5	159.5
Main Engine Cutoff (MECO)	264.6	264.9
Stage I-II Separation	273.0	274.0
Stage II Ignition	278.5	279.5
Jettison Fairing	283.0	283.5
First Cutoff - Stage II (SECO 1)	616.8	629.9
Stage II Restart Ignition	4091.0	4093.7
Second Cutoff - Stage II (SECO 2)	4156.8	4163.6
Release Second Set of Separation Nuts	4475.0	4477.7
Spacecraft Separation / Secondary Latch Release	4504.0	4506.7

6.5.2 Dynamic Environments

The following excerpt summarizing the flight dynamic environments was taken from the post-flight analysis report, [ref. 9]:

“All dynamic data from Delta 333, GLAST, were reviewed from liftoff through spacecraft separation and during second stage engine depletion burn. This was the first flight of a Delta II heavy vehicle with a 10C fairing. Liftoff and transonic random vibration levels were as predicted for this vehicle, except that transonic random vibration measured by the Redundant Inertial Flight Controller Assembly (RIFCA) input accelerometer exceeded the RIFCA MPE slightly at 10 Hz; this does not adversely affect the qualification status of any guidance section component. The second stage engine head accelerometer was invalid through SECO 2, but was valid after that. All other dynamic environments were normal and similar to previous comparable Delta II missions.”

6.5.3 Meteorological Conditions

The following summary of launch time weather conditions was taken from the post-flight report, [ref. 9]:



**NASA Engineering and Safety Center
Technical Assessment Report**

Document #:
**NESC-RP-
06-071**

Version:
1.0

Title:

**Flight Force Measurements of the Gamma-Ray Large
Area Space Telescope / Delta II Flight**

Page #:

95 of 226

A synopsis of the launch time weather follows: (Weather observations provided by the 45th SW Weather Squadron)

	<u>KSC Weather Station (SLF)</u>	<u>CCAFS Weather Station (XMR)</u>
Clouds	SCT110 FEW025 BKN110 BKN280	FEW033 SCT120 BKN250
Visibility	10 MILES	10 MILES
Temp/Dew Point	82 F / 73 F	84 F / 73 F
Relative Humidity	74%	70%
Pressure	30.08 Ins Hg	30.06 Ins Hg
Present Weather	none	none
Wind Direction / Speed Tower 0002 (90 ft level)		NW sensor --> 047 / 09 G 12 KTS
Wind Direction / Speed Tower 0002 (54 ft level)		NW sensor --> 048 / 08 G 12 KTS
Temperature / Dew Point / Relative		83 F / 73 F / 72%

6.5.4 First Stage Flight

The following paragraphs summarize the data provided in the post-flight data report [ref. 9] for the First Stage flight.

The main engine gimbal block accelerometer (EV005DX) monitored the thrust axis vehicle excitations and transients in the First Stage engine section. The gimbal block accelerometer data were filtered using a filter with 0.7 dB rolloff at 120 Hz to minimize the high frequency engine noise and to maintain data consistency with the established database. The Liftoff shock transient of the RS-27A main engine was nominal with a peak amplitude of 14.0 g(o-p) measured at the main engine gimbal block. In comparison, the average for 114 Delta II vehicles is 14.5 g(o-p) and the maximum for all Delta II vehicles is 21.0 g(o-p) as recorded on D229, Radarsat. The GLAST Liftoff shock spectrum was nominal compared to a calculated P95/50 of 84 RIFCA vehicles.

The Liftoff and transonic random vibration environments were evaluated by the RIFCA input accelerometer (GV004AX) located on the SSGS crossbeam. The Liftoff and transonic acceleration histories for GLAST spacecraft were compared to those for D323, THEMIS, a 7925-10C vehicle launched from CCAFS Pad 17B. Though both of these vehicles launched from the same pad and have similar vehicle configurations, the GEMs on a Delta II heavy vehicle have more thrust, and therefore the Liftoff environment for the GLAST spacecraft was expected to be somewhat higher than that of THEMIS. The spectral data analysis of the GLAST spacecraft Liftoff environment measured by the RIFCA input accelerometer showed that it was

	NASA Engineering and Safety Center Technical Assessment Report	Document #: NESC-RP- 06-071	Version: 1.0
Title: Flight Force Measurements of the Gamma-Ray Large Area Space Telescope / Delta II Flight			Page #: 96 of 226

generally higher than that of THEMIS, but within the P95/50 liftoff environment from 7925-9.5 missions, as predicted prior to flight. The transonic environment measured by the RIFCA input accelerometer for the GLAST spacecraft was comparable with those measured on 7420-10C missions, as expected prior to flight, except near 10 Hz. The Liftoff and transonic acceleration environments for the GLAST spacecraft were below the RIFCA Maximum Predicted Environment (MPE), except that the transonic environment slightly exceeds the RIFCA MPE at 10 Hz. This does not affect the qualification status of any component in the Guidance Section, since none are sensitive to dynamic excitation in this frequency range. Note that the Liftoff and transonic spectra for the RIFCA input accelerometer for the GLAST spacecraft were created by a non-standard process, generating spectra in 2 Hz bandwidth and then combining them to get 10 Hz bandwidth results. This was performed to reduce smoothing of the spectra, so that high low-frequency (below 5 Hz) sine levels seen on GLAST spacecraft did not unduly influence the 10 Hz spectral point.

The fairing microphone (GV002AX) was located inside the composite payload fairing at Station 360 in Quad II. The Liftoff and transonic microphone pressure histories for the GLAST spacecraft were compared with D323, THEMIS, a 7925-10C vehicle launched from CCAFS Pad 17B. Generally, the liftoff acoustics for the GLAST spacecraft were higher than for THEMIS, which was expected prior to flight. The GLAST spacecraft acoustics were within the mission specification.

The low frequency lateral axis responses measured during transonic flight at the triaxial crossbeam pitch and yaw accelerometers were significantly higher than levels measured on D323, THEMIS. The peak levels were 0.56 g(o-p) measured at the triaxial crossbeam pitch accelerometer (GV006DX), and 0.61 g(o-p) measured at the triaxial crossbeam yaw accelerometer (GV007DX). It is likely that this difference is due to the Delta II GEMs utilized for the GLAST mission.

Ordnance thrusters were used to separate the six ground-ignited GEMS and three air-ignited GEMS in a 6+3 firing sequence. The ground-ignited motors separated at T+80.5 seconds (motors 1, 2, and 3) and T+81.5 seconds (motors 7, 8, and 9) as indicated by the vehicle lateral responses. The low frequency transient responses induced by the ground ignited motor separation were lower than those on D323, THEMIS, with peak levels of 0.08 g(o-p) at 20 Hz in the pitch axis, and 0.08 g(o-p) at 17 Hz in the yaw axis. Peak levels for the separation of the air ignited motors (motors 4, 5, and 6) at T+147.3 seconds were comparable to those from GPS missions (7925-9.5 vehicles. The air ignited motors separation had peak levels of 0.79 g(o-p) in the pitch axis and 0.67 g(o-p) in the yaw axis.

	NASA Engineering and Safety Center Technical Assessment Report	Document #: NESC-RP- 06-071	Version: 1.0
Title: Flight Force Measurements of the Gamma-Ray Large Area Space Telescope / Delta II Flight			Page #: 97 of 226

The first pre-MECO oscillations for the GLAST spacecraft of 3.2 g(o-p) at the main engine gimbal block are normal and similar to those for D327, DAWN (which used the same First Stage engine configuration). There were no second pre-MECO oscillations.

The low-level thrust axis oscillations at the main engine gimbal block were nominal. The peak amplitudes of the oscillations were 0.52 g(o-p) at 17 Hz and 0.20 g(o-p) at 17 Hz measured at the main engine gimbal block and the SSGS, respectively. These levels were within the maximum amplitudes of 1.4 g(o-p) at the gimbal block and 0.48 g(o-p) at the SSGS.

The PAF thrust accelerometer (GA055HX) encountered a combined steady state and dynamic acceleration level of 5.4 g prior to MECO. The combined steady state and dynamic acceleration level measured on GLAST spacecraft was within the mission specification of 6.6 g (steady state). The MECO shock transient measured at the main engine gimbal block was normal with a peak amplitude of 18.9 g(o-p). In comparison to previous Delta II missions with an RS-27A engine and a 0.067-inch Main Oxidizer Valve (MOV) pneumatic orifice with proper edge break, the MECO shock transient for GLAST spacecraft was nominal. The GLAST spacecraft MECO shock response spectrum at the main engine gimbal block was within the calculated P95/50 level 22 Delta II missions that flew similar engine configurations. The RIFCA MECO shock response spectrum comparison shows that the GLAST spacecraft response was within a P95/50 of 38, 50-system engine missions, though it exceeds the RIFCA Maximum Predicted Environment (MPE) near 120 Hz.

6.5.5 Second Stage Flight

The following paragraphs summarize the data provided in the post-flight report [ref. 9] for the Second Stage flight.

The peak shock levels occurred during First and Second Stage separation in the SSGS. It is likely that the peak shock levels at the engine head occurred at Second Stage ignition, but this could not be confirmed since the engine head accelerometer was invalid through SECO 2. The GLAST spacecraft First to Second Stage separation shock level at the RIFCA input accelerometer was nominal at 13.9 g(o-p). The GLAST spacecraft First to Second Stage separation shock response spectrum measured by the RIFCA input accelerometer was nominal with prior missions that flew the 10C composite payload fairing.

The Second Stage engine ignition shock transient is typically assessed at the Second Stage engine head, but this measurement was invalid on GLAST mission through SECO 2. The Second Stage ignition transient had a nominal magnitude on the SSGS accelerometers.

The fairing separation for the 10C fairing consisted of one bolt detonation shock, followed 1 second later by the fairing separation shock. The shock spectrum for fairing separation at the RIFCA input accelerometer exceeds both the RIFCA MPE and the P95/50 of 35 missions with



**NASA Engineering and Safety Center
Technical Assessment Report**

Document #:
**NESC-RP-
06-071**

Version:
1.0

Title:

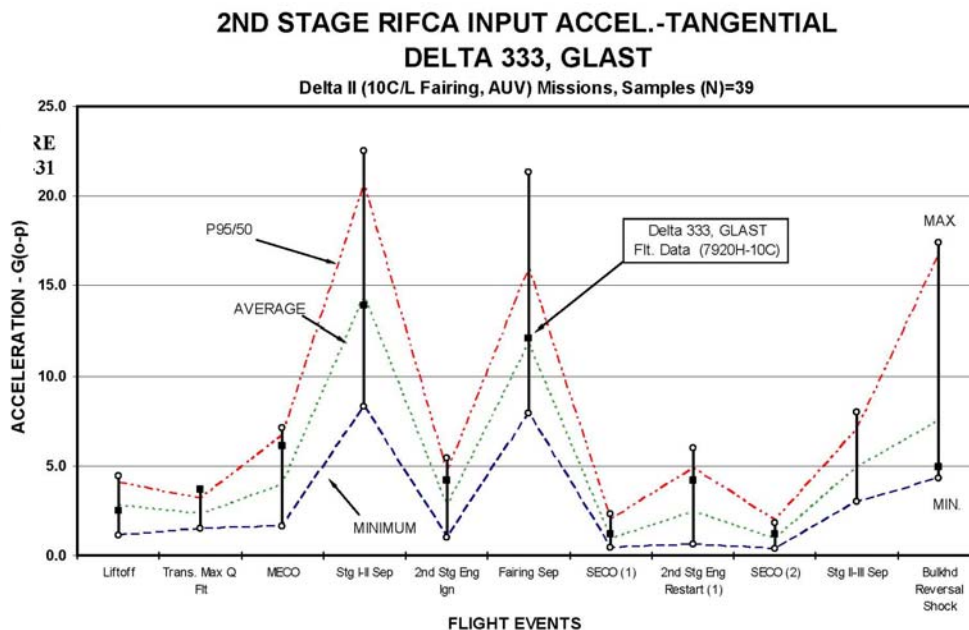
**Flight Force Measurements of the Gamma-Ray Large
Area Space Telescope / Delta II Flight**

Page #:
98 of 226

10C fairings at 100 Hz. However, this does not adversely affect the RIFCA qualification status. There was no fairing re-contact observed after fairing separation for GLAST mission. The dynamic excitations during the first two Second Stage engine burns had normal magnitudes on the SSGC accelerometers.

Spacecraft separation consisted of 4 separation nuts detonating two at a time, with the two detonations being 1 second apart at T+4476.7 and T+4477.7 seconds, and a secondary latch release at T+4506.7 seconds. Transients from separation nut detonation, secondary latch actuation, and Second Stage retro firing on GLAST spacecraft were nominal. The Second Stage restart 2 event was nominal at 12.7 g(o-p), and the SECO 3 event was nominal at 6.8 g(o-p). The Second Stage restart 3 transient of 22.0 g(o-p) was nominal, as was the depletion transient at 2.7 g(o-p). Following depletion, the bulkhead reversal shock was observed at T+6634.9 seconds and was normal with amplitudes of 5.6 g(o-p) and 4.9 g(o-p) measured at the engine head and RIFCA accelerometers, respectively.

Figure 6.5-3 summarizes the flight data events measured by the RIFCA input accelerometer. All dynamic environments were nominal for events when compared to similar Delta II missions. Liftoff accelerations for the GLAST spacecraft show average values, transonic / maximum Q, and MECO show GLAST reached approximately the P 95/50 values.





Title:

Flight Force Measurements of the Gamma-Ray Large Area Space Telescope / Delta II Flight

Page #:
99 of 226

Figure 6.5-3. ULA Statistical Description of the GLAST Flight Events

7.0 Data Analysis

7.1 Flight Data Acquisition System

7.1.1 Data Acquisition System and Channels

The SFI data acquisition system and its downlink were designed, installed, and tested by ULA, [ref. 8]. All signals were sent to an on-board, modified Sub Master Telemetry Unit (SMTU), and transmitted by S-band to the ground stations. The parameters of the data acquisition system are shown in 7.1-1.

Table 7.1-1. Data Acquisition System Parameters

Number of channels:	77
Sample rate (Hz):	1000 (frequency cutoff 250)
Power required (V):	28
PCM format:	12 bit words

The data acquisition system underwent complete thermal-vacuum and random vibration testing.

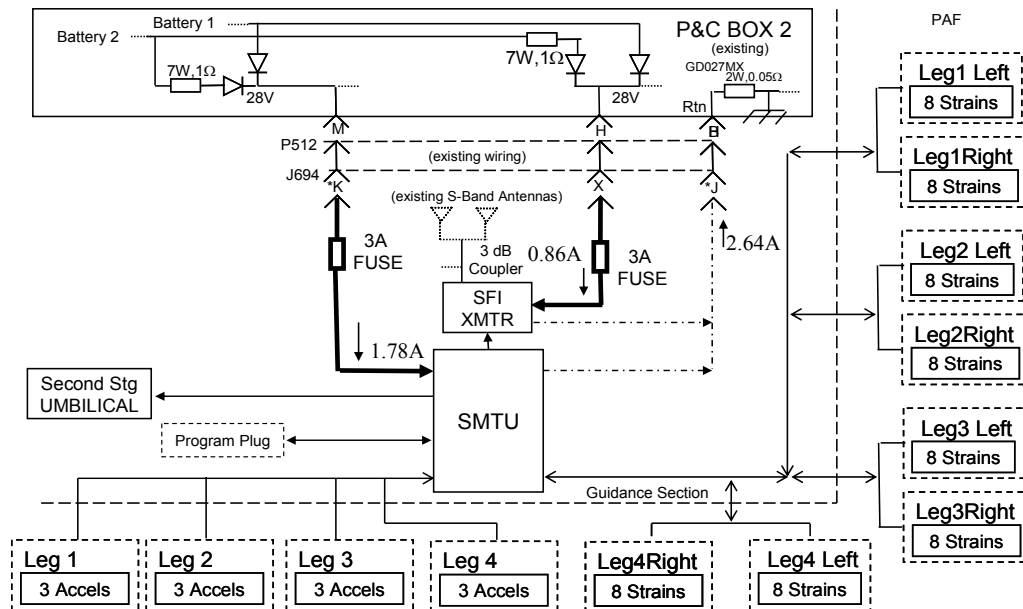


Figure 7.1-1. GLAST SFI Block Diagram

	NASA Engineering and Safety Center Technical Assessment Report	Document #: NESC-RP- 06-071	Version: 1.0
Title: Flight Force Measurements of the Gamma-Ray Large Area Space Telescope / Delta II Flight		Page #: 100 of 226	

There were two maps for the instrumentation that relate the ULA strain gage locations to those used by the FFM matrices, one for before launch when the GLAST spacecraft was being connected to the Delta II launch vehicle, and the second for use during pre-launch and flight. Tables 7.1-2 and 7.1-3 provide the mapping between the flight data channels and the FFM channels.



**NASA Engineering and Safety Center
Technical Assessment Report**

Document #:
**NESC-RP-
06-071**

Version:
1.0

Title:

**Flight Force Measurements of the Gamma-Ray Large
Area Space Telescope / Delta II Flight**

Page #:

101 of 226

Table 7.1-2. Strain Gage Mapping for the Static Measurements

ULA Gages			FFM Gages		ULA Gages			FFM Gages	
Nr.	ID	Label	Nr.	Label	Nr.	ID	Label	Nr.	Label
1	GS096DX	1 L L 1	57	7 6 S	33	GS056DX	3 L L 1	41	3 2 S
2	GS107DX	1 L L 2	25	7 6 A	34	GS067DX	3 L L 2	9	3 2 A
3	GS074DX	1 L N 1	60	7 i S	35	GS043DX	3 L N 1	44	3 i S
4	GS085DX	1 L N 2	28	7 i A	36	GS045DX	3 L N 2	12	3 i A
5	GS052DX	1 L R 1	59	7 8 S	37	GS102DX	3 L R 1	43	3 4 S
6	GS063DX	1 L R 2	27	7 8 A	38	GS113DX	3 L R 2	11	3 4 A
7	GS030DX	1 L U 1	58	7 o S	39	GS080DX	3 L U 1	42	3 o S
8	GS041DX	1 L U 2	26	7 o A	40	GS091DX	3 L U 2	10	3 o A
9	GS086DX	1 R L 1	61	8 7 S	41	GS046DX	3 R L 1	45	4 3 S
10	GS097DX	1 R L 2	29	8 7 A	42	GS057DX	3 R L 2	13	4 3 A
11	GS064DX	1 R N 1	64	8 i S	43	GS114DX	3 R N 1	48	4 i S
12	GS075DX	1 R N 2	32	8 i A	44	GS035DX	3 R N 2	16	4 i A
13	GS042DX	1 R R 1	63	8 1 S	45	GS092DX	3 R R 1	47	4 5 S
14	GS053DX	1 R R 2	31	8 1 A	46	GS103DX	3 R R 2	15	4 5 A
15	GS110DX	1 R U 1	62	8 o S	47	GS070DX	3 R U 1	46	4 o S
16	GS031DX	1 R U 2	30	8 o A	48	GS081DX	3 R U 2	14	4 o A
17	GS076DX	2 L L 1	33	1 8 S	47	GS036DX	4 L L 1	49	5 4 S
18	GS087DX	2 L L 2	1	1 8 A	50	GS047DX	4 L L 2	17	5 4 A
19	GS054DX	2 L N 1	36	1 i S	51	GS104DX	4 L N 1	52	5 i S
20	GS065DX	2 L N 2	4	1 i A	52	GS115DX	4 L N 2	20	5 i A
21	GS032DX	2 L R 1	35	1 2 S	53	GS082DX	4 L R 1	51	5 6 S
22	GS043DX	2 L R 2	3	1 2 A	54	GS093DX	4 R L 2	19	5 6 A
23	GS100DX	2 L U 1	34	1 o S	55	GS060DX	4 L U 1	50	5 o S
24	GS111DX	2 L U 2	2	1 o A	56	GS071DX	4 L U 2	18	5 o A
25	GS066DX	2 R L 1	37	2 1 S	57	GS116DX	4 R L 1	53	6 5 S
26	GS077DX	2 R L 2	5	2 1 A	58	GS037DX	4 R L 2	21	6 5 A
27	GS044DX	2 R N 1	40	2 i S	59	GS094DX	4 R N 1	56	6 i S
28	GS055DX	2 R N 2	8	2 i A	60	GS105DX	4 R N 2	24	6 i A
29	GS112DX	2 R R 1	39	2 3 S	61	GS072DX	4 R R 1	55	6 7 S
30	GS033DX	2 R R 2	7	2 3 A	62	GS083DX	4 R R 2	23	6 7 A
31	GS090DX	2 R U 1	38	2 o S	63	GS050DX	4 R U 1	54	6 o S
32	GS101DX	2 R U 2	6	2 o A	64	GS061DX	4 R U 2	22	6 o A



**NASA Engineering and Safety Center
Technical Assessment Report**

Document #:
**NESC-RP-
06-071**

Version:
1.0

Title:

**Flight Force Measurements of the Gamma-Ray Large
Area Space Telescope / Delta II Flight**

Page #:

102 of 226

Table 7.1-3. Flight Instrumentation Channels

Flight Gages			FFM Gages		Flight Gages			FFM Gages	
Nr.	ID	Label	Nr.	Label	Nr.	ID	Label	Nr.	Label
1	Time	(sec)	-	-	42	GS085DX	1 L N 2	28	7 i A
2	GS030DX	1 L U 1	58	7 o S	43	GS086DX	1 R L 1	61	8 7 S
3	GS031DX	1 R U 2	30	8 o A	44	GS087DX	2 L L 2	1	1 8 A
4	GS032DX	2 L R 1	35	1 2 S	45	GS090DX	2 R U 1	38	2 o S
5	GS033DX	2 R R 2	7	2 3 A	46	GS091DX	3 L U 2	10	3 o A
6	GS034DX	3 L N 1	44	3 i S	47	GS092DX	3 R R 1	47	4 5 S
7	GS035DX	3 R N 2	16	4 i A	48	GS093DX	4 L R 2	19	5 6 A
8	GS036DX	4 L L 1	49	5 4 S	49	GS094DX	4 R N 1	56	6 i S
9	GS037DX	4 R L 2	21	6 5 A	50	GS096DX	1 L L 1	57	7 6 S
10	GS041DX	1 L U 2	26	7 o A	51	GS097DX	1 R L 2	29	8 7 A
11	GS042DX	1 R R 1	63	8 1 S	52	GS100DX	2 L U 1	34	1 o S
12	GS043DX	2 L R 2	3	1 2 A	53	GS101DX	2 R U 2	6	2 o A
13	GS044DX	2 R N 1	40	2 i S	54	GS102DX	3 L R 1	43	3 4 S
14	GS045DX	3 L N 2	12	3 i A	55	GS103DX	3 R R 2	15	4 5 A
15	GS046DX	3 R L 1	45	4 3 S	56	GS104DX	4 L N 1	52	5 i S
16	GS047DX	4 L L 2	17	5 4 A	57	GS105DX	4 R N 2	24	6 i A
17	GS050DX	4 R U 1	54	6 o S	58	GS107DX	1 L L 2	25	7 6 A
18	GS052DX	1 L R 1	59	7 8 S	59	GS110DX	1 R U 1	62	8 o S
19	GS053DX	1 R R 2	31	8 1 A	60	GS111DX	2 L U 2	2	1 o A
20	GS054DX	2 L N 1	36	1 i S	61	GS112DX	2 R R 1	39	2 3 S
21	GS055DX	2 R N 2	8	2 i A	62	GS113DX	3 L R 2	11	3 4 A
22	GS056DX	3 L L 1	41	3 2 S	63	GS114DX	3 R N 1	48	4 i S
23	GS057DX	3 R L 2	13	4 3 A	64	GS115DX	4 L N 2	20	5 i A
24	GS060DX	4 L U 1	50	5 o S	65	GS116DX	4 R L 1	53	6 5 S
25	GS061DX	4 R U 2	22	6 o A	66	GV201D0	Pad 1 axial		Accel.
26	GS063DX	1 L R 2	27	7 8 A	67	GV212D1	Pad 2 tangential		
27	GS064DX	1 R N 1	64	8 i S	68	GV223D2	Pad 3 radial		
28	GS065DX	2 L N 2	4	1 i A	69	GV304D0	Pad 4 axial		
29	GS066DX	2 R L 1	37	2 1 S	70	GV311D1	Pad 1 tangential		
30	GS067DX	3 L L 2	9	3 2 A	71	GV322D2	Pad 2 radial		
31	GS070DX	3 R U 1	46	4 o S	72	GV403D0	Pad 3 axial		
32	GS071DX	4 L U 2	18	5 o A	73	GV414D1	Pad 4 tangential		
33	GS072DX	4 R R 1	55	6 7 S	74	GV421D2	Pad 1 radial		Accel.
34	GS074DX	1 L N 1	60	7 i S	75	GV502D0	Pad 2 axial		
35	GS075DX	1 R N 2	32	8 i A	76	GV513D1	Pad 3 tangential		
36	GS076DX	2 L L 1	33	1 8 S	77	GV524D2	Pad 4 radial		
37	GS077DX	2 R L 2	5	2 1 A					
38	GS080DX	3 L U 1	42	3 o S					
39	GS081DX	3 R U 2	14	4 o A					
40	GS082DX	4 L R 1	51	5 6 S					
41	GS083DX	4 R R 2	23	6 7 A					

	NASA Engineering and Safety Center Technical Assessment Report	Document #: NESC-RP- 06-071	Version: 1.0
Title: Flight Force Measurements of the Gamma-Ray Large Area Space Telescope / Delta II Flight		Page #: 103 of 226	

The naming convention used in the mapping tables is defined in Table 7.1-4.

Table 7.1-4. ULA and FFM Strain Gage Naming Convention

ULA Strain Name -	1 st number = 1 2 3 or 4 for Delta PAF leg/pad number
	2 nd letter = L R for Left or Right strut looking inward
	3 rd letter = U R N L for outward, right, inward, left face
	4 th number = 1 2 for shear or axial gage
FFM Strain Name -	1 st number = strut (leg) number
	2 nd letter = 2 i o 8 for facing strut 2, inside, outside, strut 8
	3 rd letter = S A for shear or axial gage

7.1.2 Pre-Flight Static Measurements

Before flight, the strain gages were monitored while the GLAST spacecraft was being fitted to the PAF. These static results were recorded by the flight data acquisition system. They were used to determine if the strain gages could predict the GLAST spacecraft weight with PAF in the flight configuration. In Table 7.1-5, the load is the change in reading from the overhead hydroset while the GLAST spacecraft was mated to the PAF (except in the final two columns where “Load” refers to procedure numbers used by ULA). The two prediction methods (FEM and SFM) used to calculate interface forces are described in Section 6.1.

	NASA Engineering and Safety Center Technical Assessment Report	Document #:	Version:
		NESC- RP-06-071	1.0
Title: Flight Force Measurements of the Gamma-Ray Large Area Space Telescope / Delta II Flight			Page #: 104 of 226

*Table 7.1-5. Static Pre-Flight Data Results**
(GLAST Coordinates, Z is Axial)

Day and Time	135 13:24	135 16:08	135 16:31	140 18:36	143 17:11
Temperature, PAF Leg 1, °F	~69.6	~69.6	~69.6	~64	~65
Temperature, PAF Leg 3, °F	~69.5	~69.5	~69.5	~62.5	~63
Load, lb	500	9500	9631	E1011	F6 T2

Computed from Strain Gage Readouts:

FEM	Fx (lb)	342	455	458	219	762
Method	Fy (lb)	75	102	94	74	65
	Fz (lb)	-2,167	-9,340	-9,327	-9,715	-10,697
	Mx (lb-in)	-6,432	-9,470	-8,550	-6,264	-3,528
	My (lb-in)	-22,649	-14,626	-12,121	-4,557	-15,891
	Mz (lb-in)	-15,306	5,704	6,589	10,394	-2,113
Summed	Fx (lb)	154	193	201	80	677
Force Method	Fy (lb)	44	35	8	-25	79
	Fz (lb)	-1,684	-9,669	-9,667	-9,685	-10,407
	Mx (lb-in)	-2,079	-2,871	-1,958	-736	772
	My (lb-in)	-15,979	-8,855	-6,539	-2,727	-10,515
	Mz (lb-in)	-4,859	-2,735	-1,568	-155	-10,411

*Weight of Spacecraft plus PAF = 9643 pounds

The note in this table refers to the axial forces (Fz) compared to the load values, the differences between the two prediction methods, and the change in Fz when the temperature has changed on days 140 and 143. For the 500-pound load, the predicted forces are not accurate. Generally, the SFM appears better than the FEM Method.

7.2 Flight Data

Roughly one month after the GLAST flight, the data acquired by the SFI system was provided to the NESC team by ULA. Much of the initial data processing of this flight data was performed by Bill Haile at ATK Space Division and summarized in a report entitled “FFM Reconstruction of the GLAST Flight Loads” [ref. 11]. There were three major flight data sets “TEL4_SFI”, “AE_SFI”, and “ANT_AE_SFI” provided by ULA. Each data channel had its own independent file, so there are 64 strain data files and 12 accelerometer files in each set. The data included data dropouts, the timing of which varied channel. For strain gage 1, a sample dropout is shown in Figure 7.2-1 as a 1400 $\mu\epsilon$ spike. Notice the duration was about 0.025 seconds. Other data dropouts lasted as long as 0.030 seconds, but most were of short duration (<0.005 seconds).

	NASA Engineering and Safety Center Technical Assessment Report	Document #:	Version:
		NESC- RP-06-071	1.0
Title: Flight Force Measurements of the Gamma-Ray Large Area Space Telescope / Delta II Flight		Page #: 105 of 226	

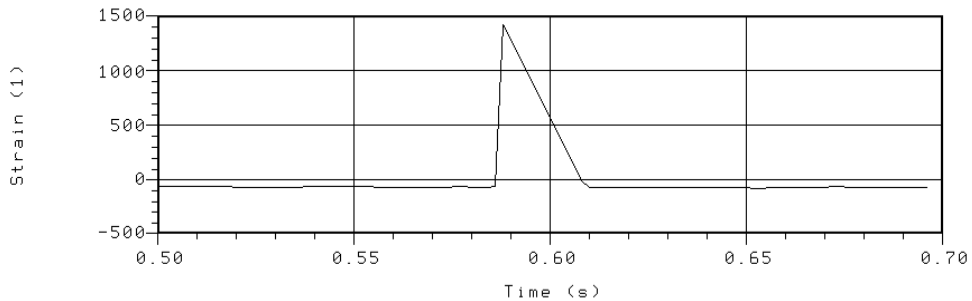


Figure 7.2-1. Sample Data Dropout

The AE_SFI dataset had a time stamp that was 0.2081 seconds ahead of TEL4_SFI, so this time increment was subtracted from the AE_SFI dataset before use. Dropouts were removed by eliminating them from the time record, leaving unequal time steps, and then interpolating back in 2 ms steps. For the channel shown in Figure 7.2-1, the result of this technique is shown in Figure 7.2-3. Note the vertical scale differences between the Figures 7.2-2 and 7.2-3.

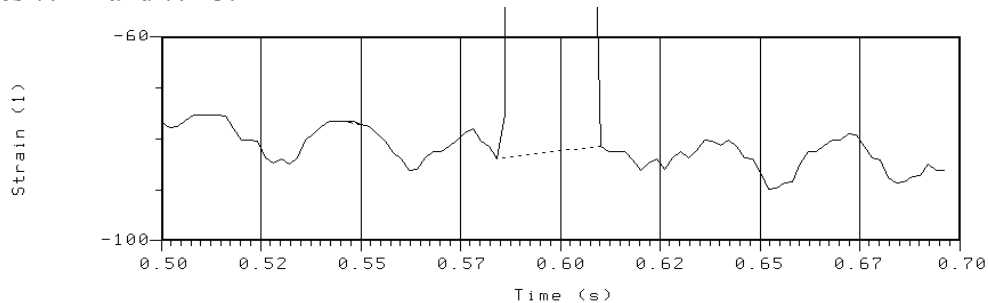


Figure 7.2-2. Data Dropout Before and After Removal

Table 7.2-1 shows which dataset was used in the analysis of a given flight event. Dropouts needed to be removed from the TEL4_SFI dataset only during the Liftoff event. The remaining datasets contained no dropouts for event for which they were used.

Table 7.2-1. Datasets Used for Various Events

Event	Event Time (seconds)	Dataset Used
Liftoff	T-1 to T+3	TEL4_SFI
Max Air Loads	T+10 to T+50	TEL4_SFI
MECO	T+260 to T+270	TEL4_SFI
S1/S2 Separation	T+271 to T+290	AE_SFI
S2 Cutoff	T+621 to T+629	ANT_AE_SFI

If a drop out was interpolated, the maxima obtained was checked that it did not occur during that time interval. For the Liftoff, Airloads, and MECO, the maxima did not occur

	NASA Engineering and Safety Center Technical Assessment Report	Document #:	Version:
		NESC- RP-06-071	1.0
Title: Flight Force Measurements of the Gamma-Ray Large Area Space Telescope / Delta II Flight		Page #: 106 of 226	

in the interval. In addition, the data analysis examined the time domain transient shapes comparison and frequency domain characteristics.

Regarding the flight accelerometer, some data was noisy. Plotted in Figure 7.2-3 are the 12 accelerometer channels during a high load flight portion from T+30 to 31 seconds. The accelerometers that have a +X component are plotted first, then those with a -X component, and finally those in the axial (Z) direction. The axial acceleration is saturated with noise, whether this response was real or electronic remains uncertain.

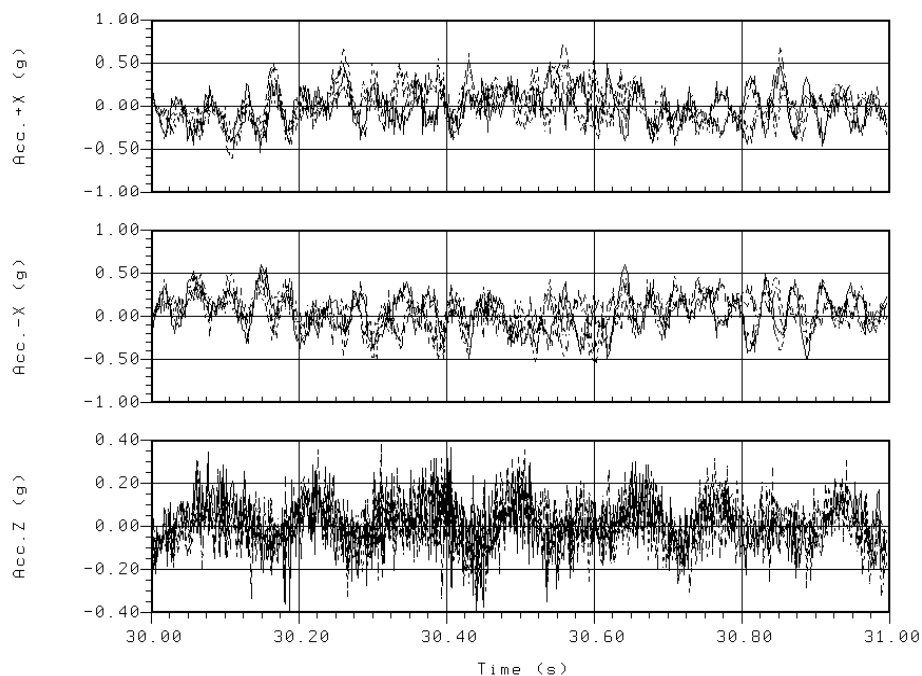


Figure 7.2-3. Accelerometer Channels Showing High Frequency Noise

After processing the data through a 120 Hz LP filter, some of the noise is smoothed. Results are shown below for the same data as plotted in Figure 7.2-5. Most of the reduction is in the axial channels. This filtering was performed for information only as the data was used without filtering.

	NASA Engineering and Safety Center Technical Assessment Report	Document #:	Version:
		NESC- RP-06-071	1.0
Title: Flight Force Measurements of the Gamma-Ray Large Area Space Telescope / Delta II Flight			Page #: 107 of 226

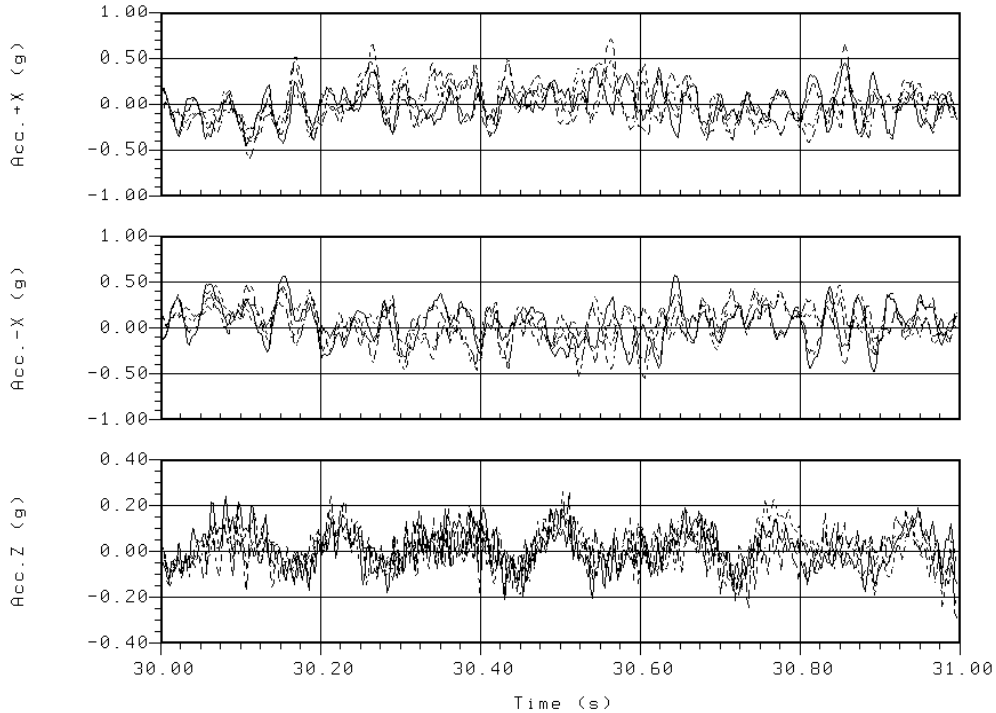


Figure 7.2-4. Accelerometer Channels After 120 Hz LP Filter

Because the strain gages changed temperature during the flight, an absolute result cannot be obtained; only the change from Liftoff can be estimated. Thus, the average value during the initial second before Liftoff (between T-5 and -4 seconds) was used for the local null of all gages. Note that a 1 °F bulk temperature rise causes every strain gage to register 14 $\mu\epsilon$, which results in an apparent overall 2,942 pound axial force change. Estimated temperatures for the GLAST spacecraft during flight are shown in Figure 7.2-5. Based on this figure, temperature appears to be nearly constant for the first 300 seconds, through Second Stage ignition. By SECO, approximately 600 seconds into flight, the temperature change effects the strain gages.

	NASA Engineering and Safety Center Technical Assessment Report	Document #:	Version:
		NESC- RP-06-071	1.0
Title: Flight Force Measurements of the Gamma-Ray Large Area Space Telescope / Delta II Flight			Page #: 108 of 226

GLAST Mission 2nd Stage - DTO Reset
Hot Case, 5/16/08 Launch, 53°F PLF Air, SC Separation @ 4500 Sec.

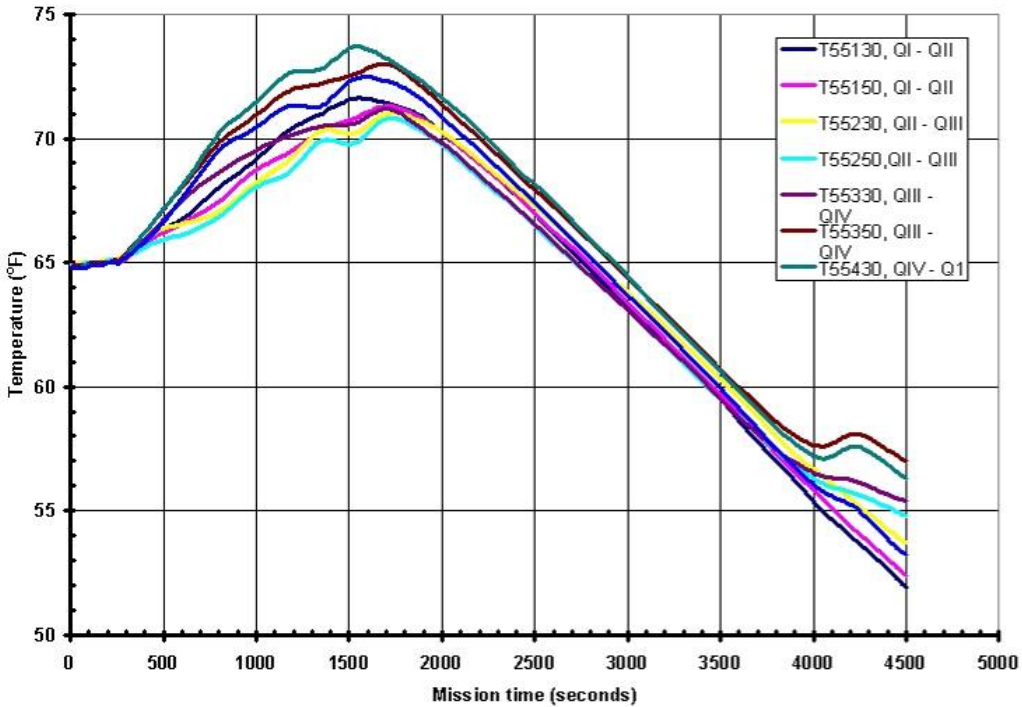


Figure 7.2-5. Estimated Flight Temperatures

Finally, it is noted that while the strain gages were DC coupled and did accurately capture the steady-state thrust forces, the accelerometers were AC coupled so the quasi-static thrust acceleration was not detected. This includes the initial 1 g acceleration prior to Liftoff that can be seen in Figure 7.2-5. In addition, the SFI data acquisition system was designed with a 0.5 Hz HP filter on all of the accelerometer data. This filter is not able to respond quickly enough to accurately characterize flight events that have a rapid change of acceleration such as in the thrust directions for Liftoff and MECO. As a result, the acceleration data in the thrust axis for these flight events show an artifact of the HP filtering in which the data appears to have an offset such that it does not oscillate about 0, but rather over- and under-shoots the acceleration level and returns to 0 in roughly 2 seconds, which is the period of the HP filter. This effect can be seen in Figures 7.2-6 and 7.2-44.

	NASA Engineering and Safety Center Technical Assessment Report	Document #:	Version:
		NESC- RP-06-071	1.0
Title: Flight Force Measurements of the Gamma-Ray Large Area Space Telescope / Delta II Flight		Page #: 109 of 226	

7.2.1 Liftoff Summary

The data processing was initiated by calculating an average strain for each gage in the time interval from T-5 to T-4 seconds in order to provide the initial conditions corresponding to the net GLAST spacecraft and PAF weight under 1 g. Therefore, the strain vector utilized in the prediction at each time step is the strain set at the time step minus the average strain set, then the net weight was added in the thrust direction force.

$$\varepsilon(t)_i = \varepsilon(t)_i - \varepsilon(t)_{avg}$$

$$F_z(t)_i = F_z(t)_i + \text{net weight}$$

The time interval evaluated for the Liftoff begins at T-1 second and extends to T+3 seconds. To begin the description of this event, accelerations will be presented and then forces. The 12 accelerations measured during the ascent were reduced to 6 components, 3 translational and 3 rotational accelerations at the PAF to Delta II interface to be used on the basedrive reconstruction and Impedance Methods (basedrive and Fourier).

Figures 7.2-6 through 7.2-10 show acceleration time histories and shock response spectra (SRS) for Liftoff. It should be noted in Figure 7.2-8 that the thrust axis acceleration data contains a low-frequency artifact of the HP filter built into the data acquisition system as discussed in Section 7.2. The artifact appears as an offset to the AC coupled accelerometer data such that it does not oscillate about zero.

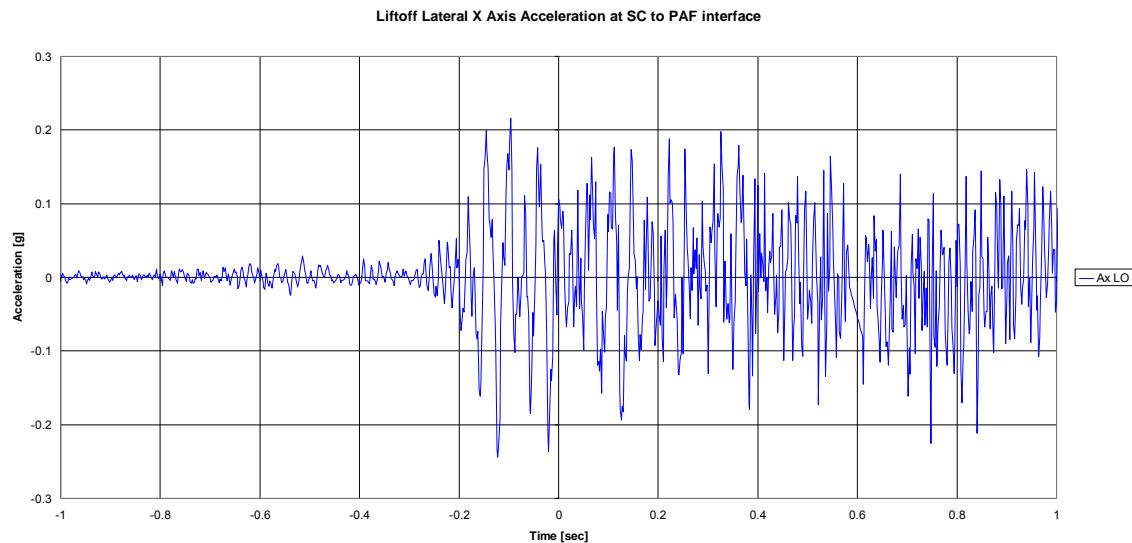


Figure 7.2-6. Liftoff Lateral X Acceleration

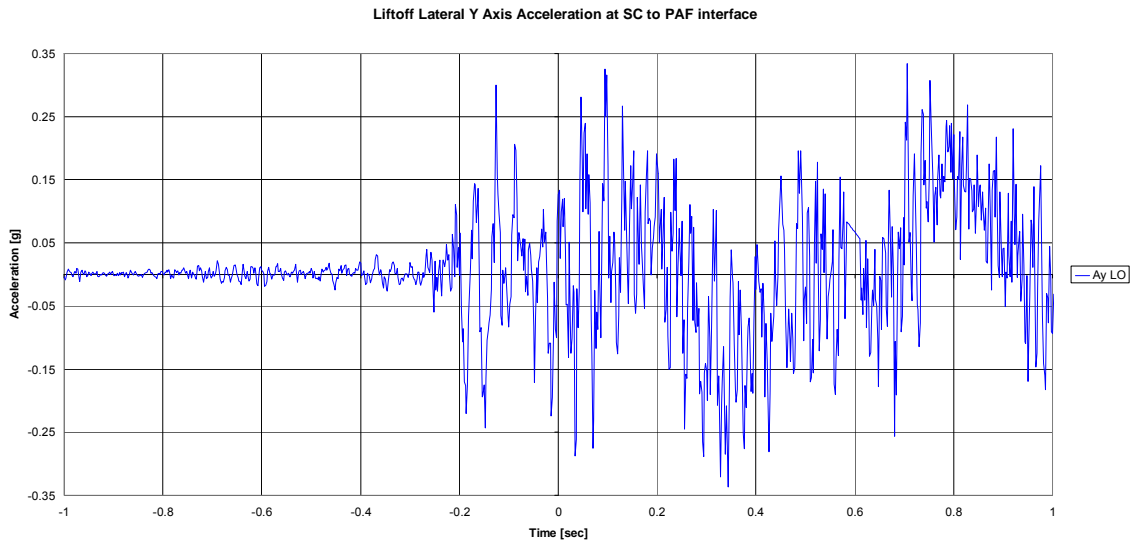


Figure 7.2-7. Liftoff Lateral Y Acceleration

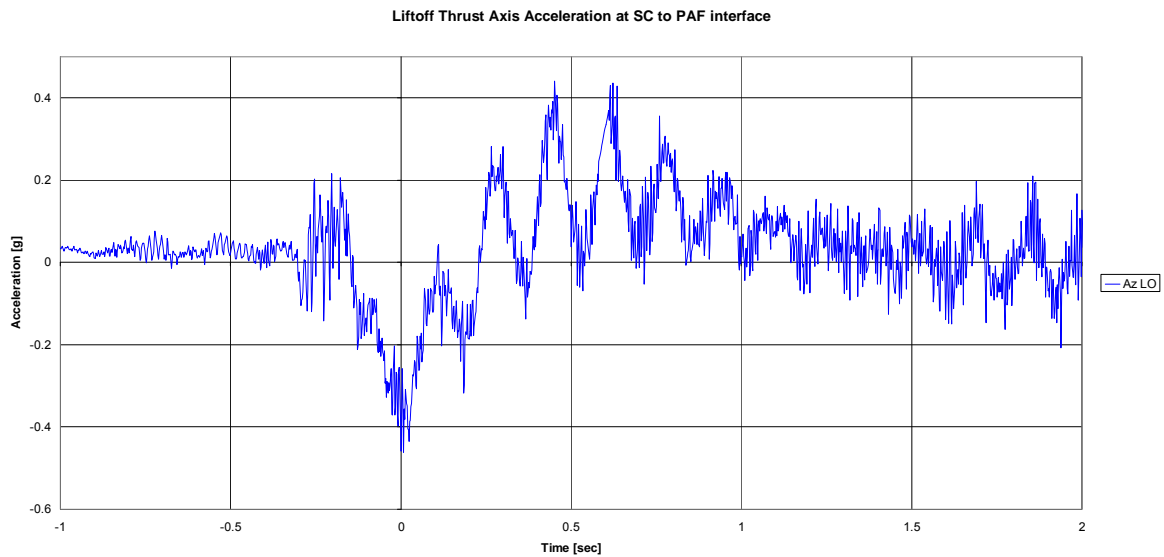


Figure 7.2-8. Liftoff Thrust Axis Acceleration at SC to PAF Interface



Title:

**Flight Force Measurements of the Gamma-Ray Large
Area Space Telescope / Delta II Flight**

Page #:
111 of
226

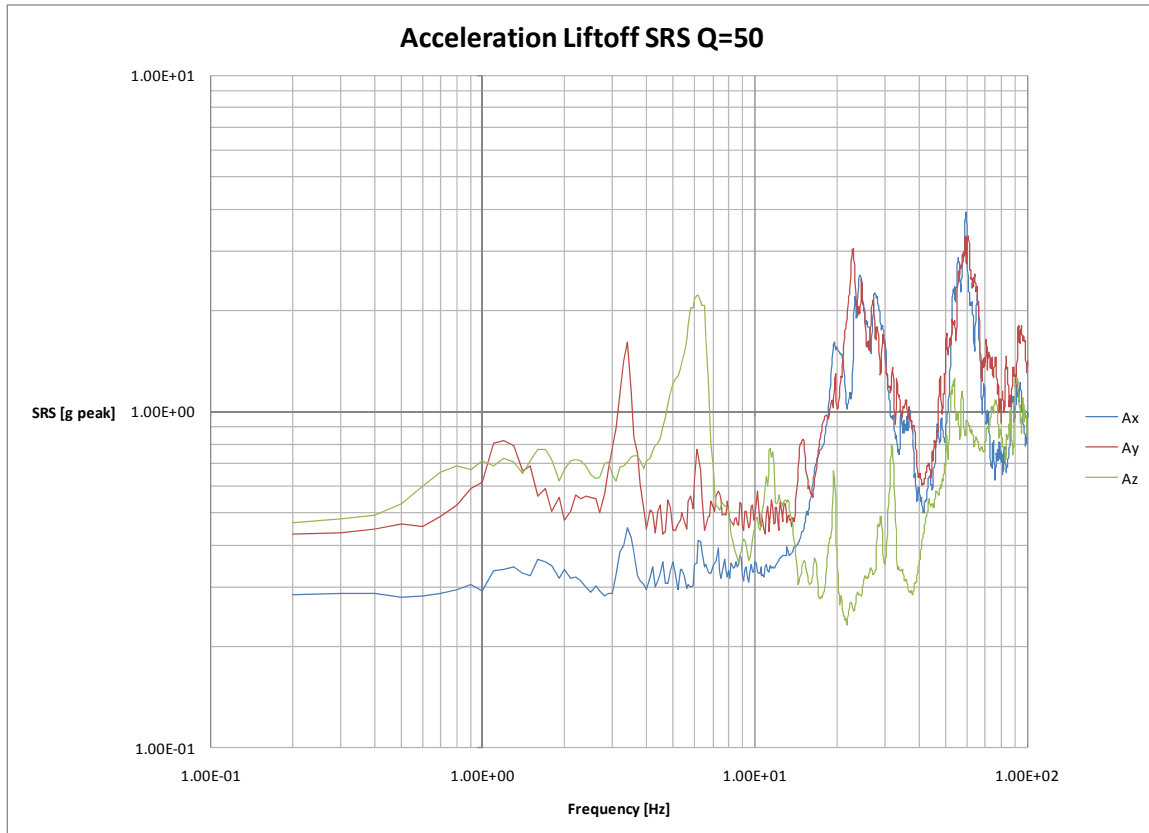


Figure 7.2-9. Acceleration at Liftoff: SRS Q=50

	NASA Engineering and Safety Center Technical Assessment Report	Document #:	Version:
		NESC- RP-06-071	1.0
Title: Flight Force Measurements of the Gamma-Ray Large Area Space Telescope / Delta II Flight		Page #: 112 of 226	

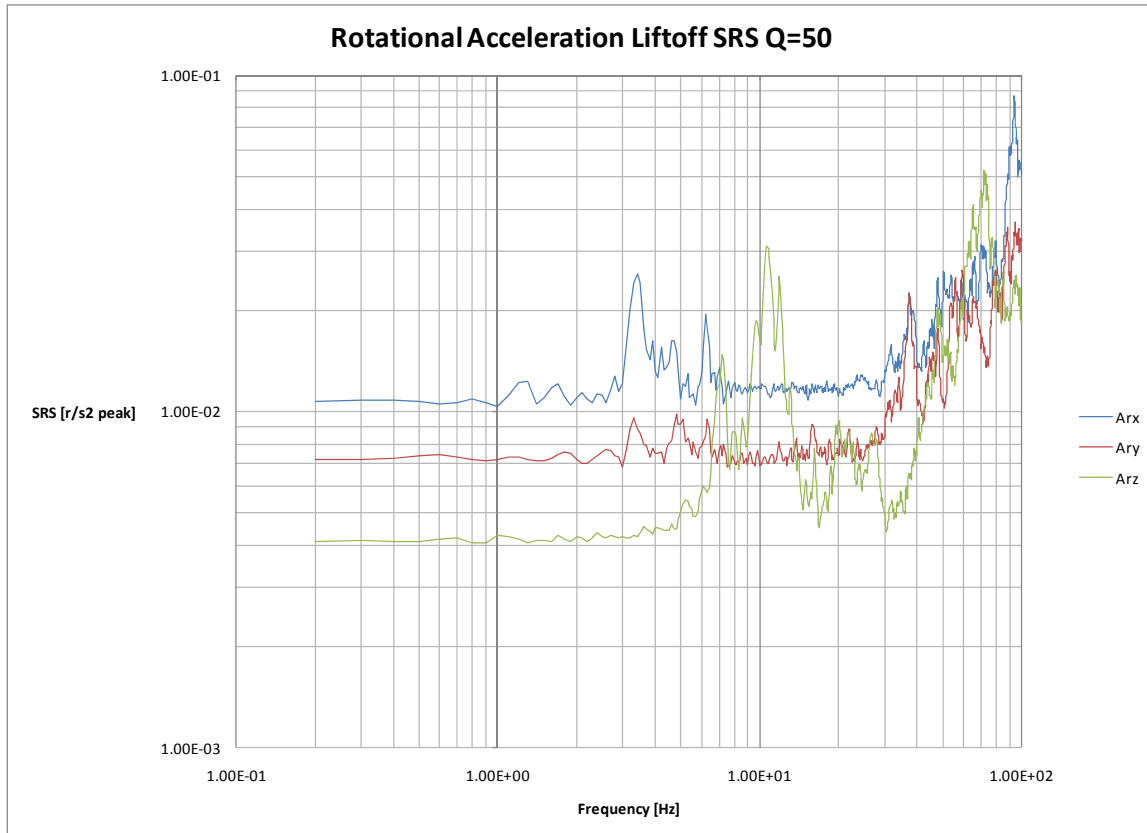


Figure 7.2-10. Rotational Accelerations at Liftoff: SRS Q=50

Review of the liftoff SRS results in Figures 7.2-9 and 7.2-10 shows the following trends:

- The lateral and overturning accelerations show frequency content at the coupled system (Delta II launch vehicle and GLAST spacecraft) first bending mode around 3 Hz. There are no predicted GLAST spacecraft modes in that range.
- Significant angular accelerations exist to at least 100 Hz, the limit of our dynamic model.
- The thrust axis acceleration shows a dominant 6 Hz content. This is not a predicted GLAST spacecraft axial mode.

Figure 7.2-11 shows the acceleration measured at Liftoff on the Delta II standard avionics DC accelerometer. Different LP filters were applied to the data and a 2 Hz LP was selected as the best representation of the steady state acceleration throughout the Liftoff event. The results of processing the thrust data with 1 and 2 Hz LP filters is shown in Figure 7.2-11.

	NASA Engineering and Safety Center Technical Assessment Report	Document #: NESC- RP-06-071	Version: 1.0
		Title: Flight Force Measurements of the Gamma-Ray Large Area Space Telescope / Delta II Flight	

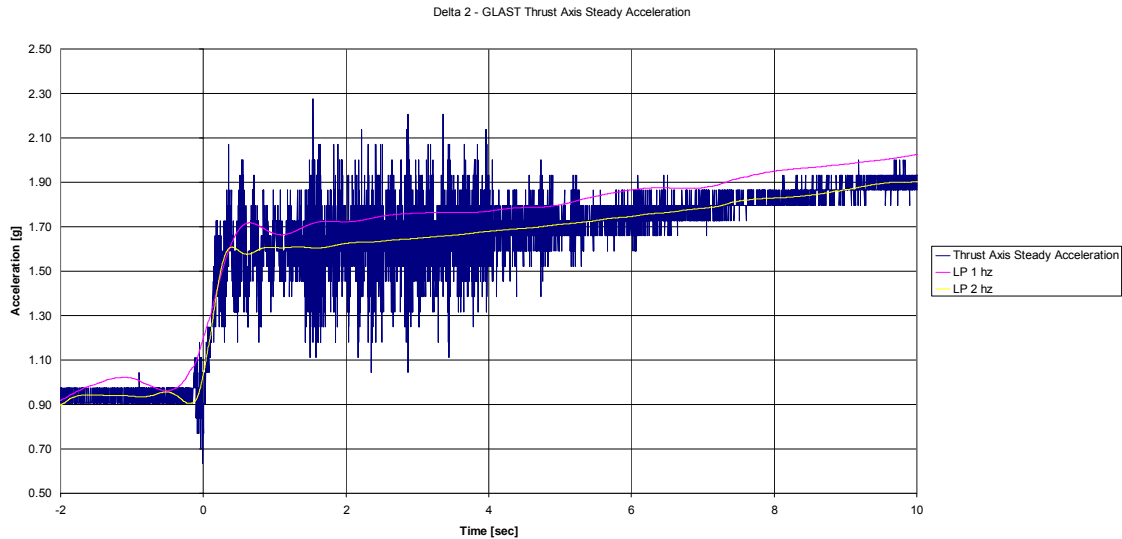


Figure 7.2-11. Delta II/GLAST Thrust Axis Steady Acceleration

The steady-state thrust force is calculated by applying a 2 Hz LP filter on the SFM force. Figure 7.2-12 shows the full and steady state thrust axis forces. The SFM is measuring the spacecraft and PAF weight until before the ignition transients (main engine and then GEMs) begin close to T=0.

The same steady state force can be calculated by multiplying the filtered acceleration shown in Figure 7.2-11 times the weight of the GLAST SC + PAF. Please note that the SFI package has a 0.24 second time offset with respect to the standard on-board instrumentation package.

	NASA Engineering and Safety Center Technical Assessment Report	Document #:	Version:
		NESC- RP-06-071	1.0
Title: Flight Force Measurements of the Gamma-Ray Large Area Space Telescope / Delta II Flight		Page #: 114 of 226	

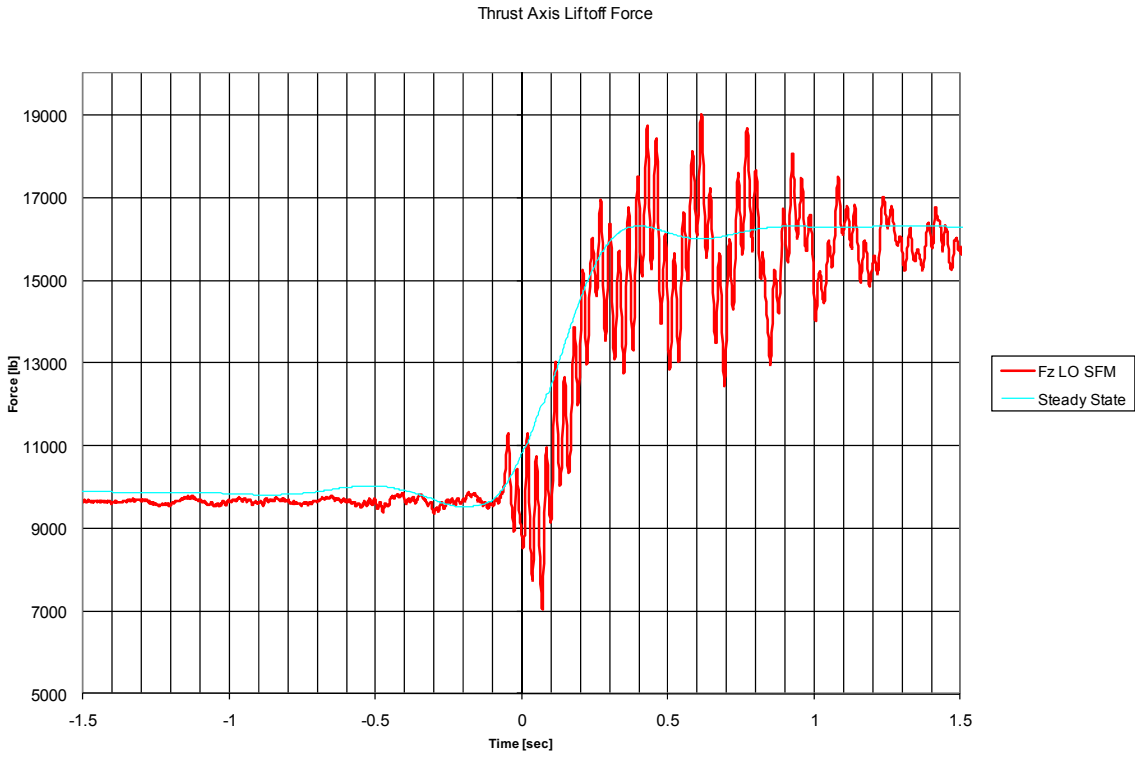


Figure 7.2-12. Liftoff Thrust Predicted Force and Steady State

Figure 7.2-13 shows the dynamic portion of the axial force as predicted from the SFM, with Figure 7.2-14 indicating the corresponding spectra.



**NASA Engineering and Safety Center
Technical Assessment Report**

Document #:
**NESC-
RP-06-071**

Version:
1.0

Title:

**Flight Force Measurements of the Gamma-Ray Large
Area Space Telescope / Delta II Flight**

Page #:
115 of
226

Thrust Axis Liftoff Force: Dynamic

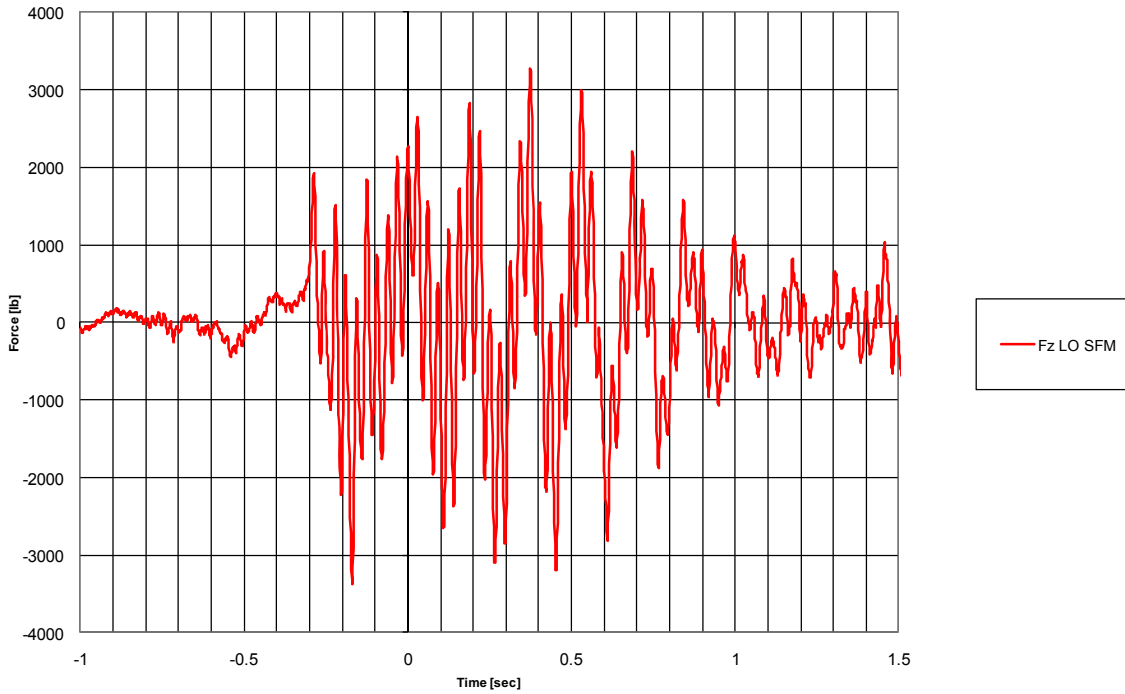


Figure 7.2-13. Thrust Axis Liftoff Force: Dynamic

	NASA Engineering and Safety Center Technical Assessment Report	Document #:	Version:
		NESC- RP-06-071	1.0
Title: Flight Force Measurements of the Gamma-Ray Large Area Space Telescope / Delta II Flight		Page #: 116 of 226	

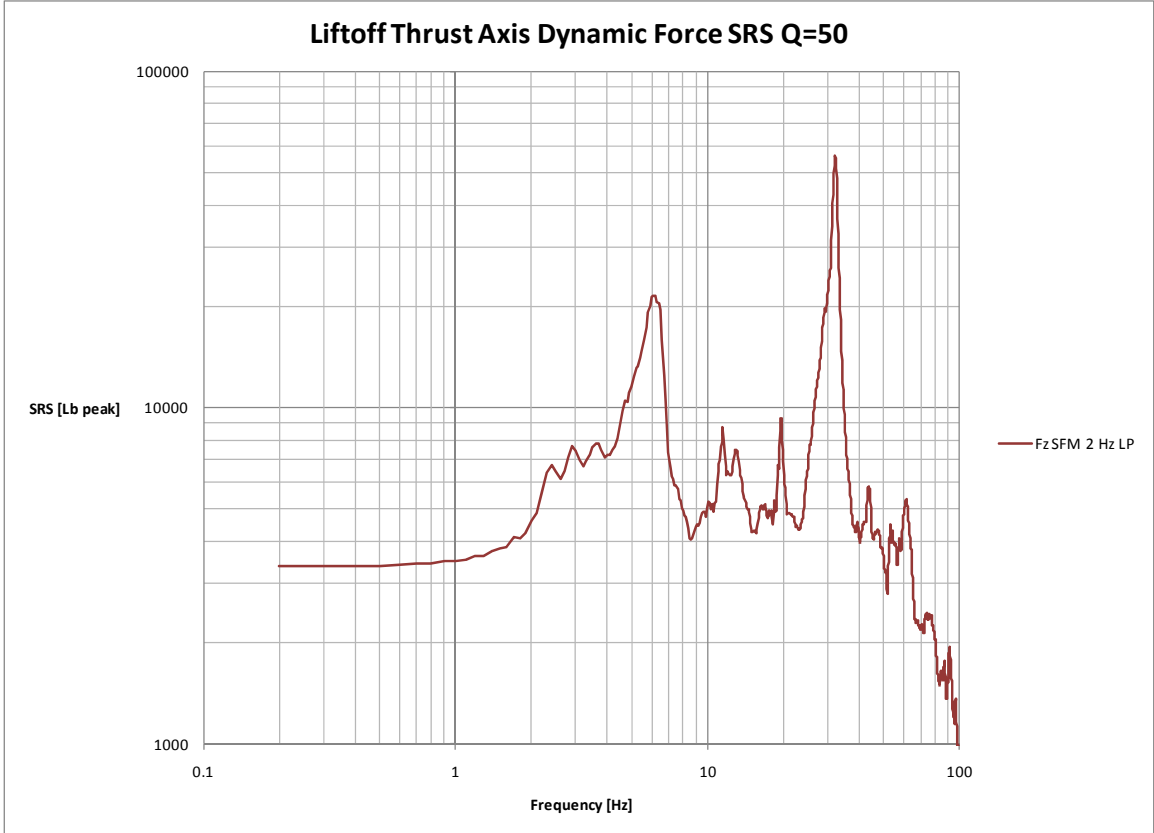


Figure 7.2-14. Force Z Liftoff: SRS Q=50

The predicted force peaks at 6 Hz where the input acceleration peaks (forcing function and coupled system related) and around 32 Hz (GLAST spacecraft dominant mode). Figures 7.2-15 and 7.2-16 show the SFM predicted lateral forces and moments, with Figures 7.2-17 and 7.2-18 indicating the corresponding spectra.

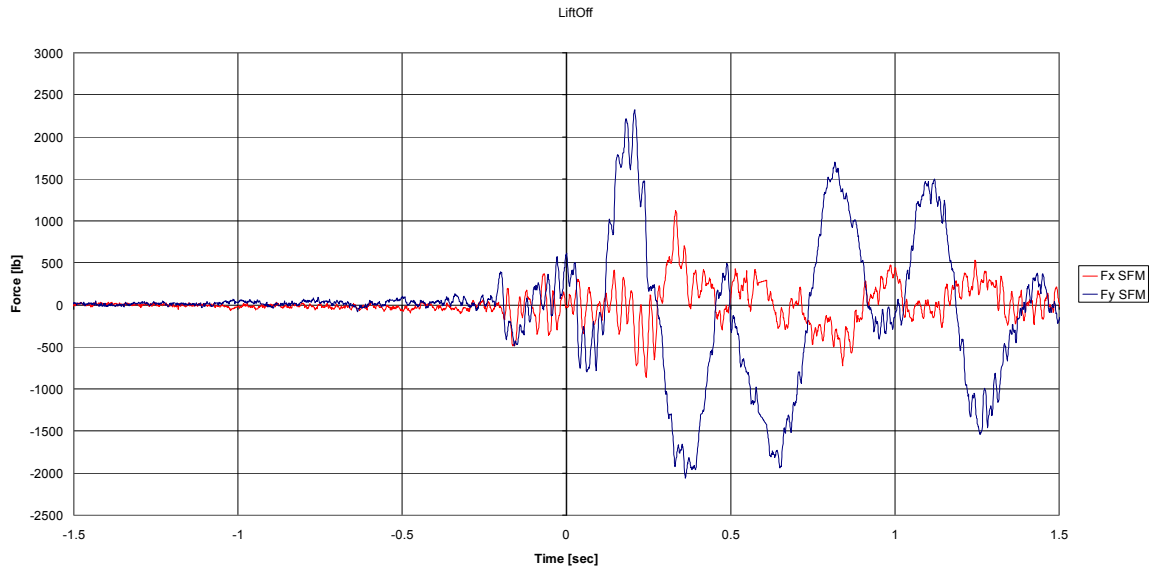


Figure 7.2-15. Liftoff Lateral Forces

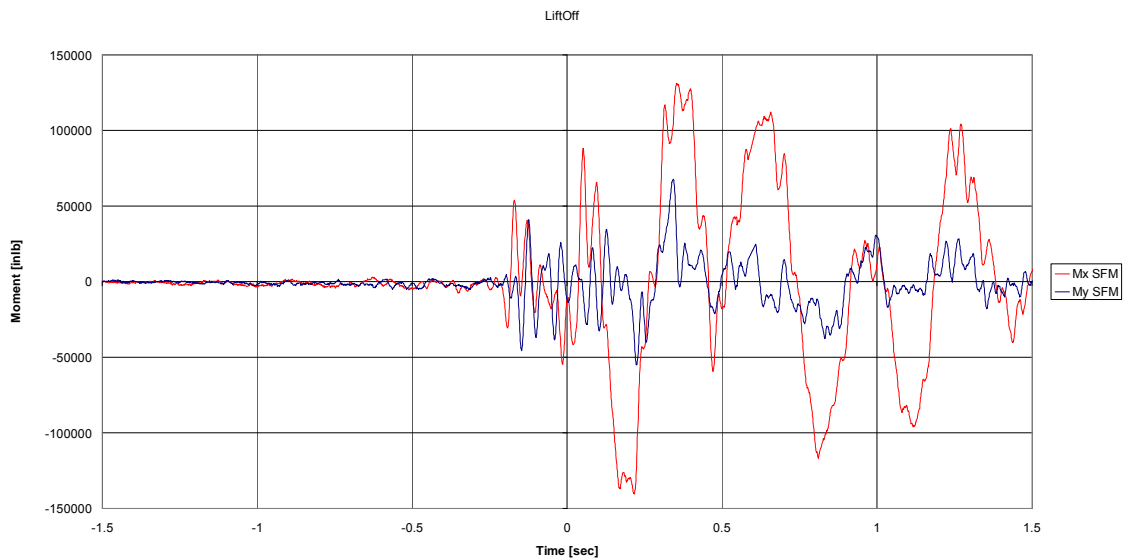


Figure 7.2-16. Liftoff Lateral Moments

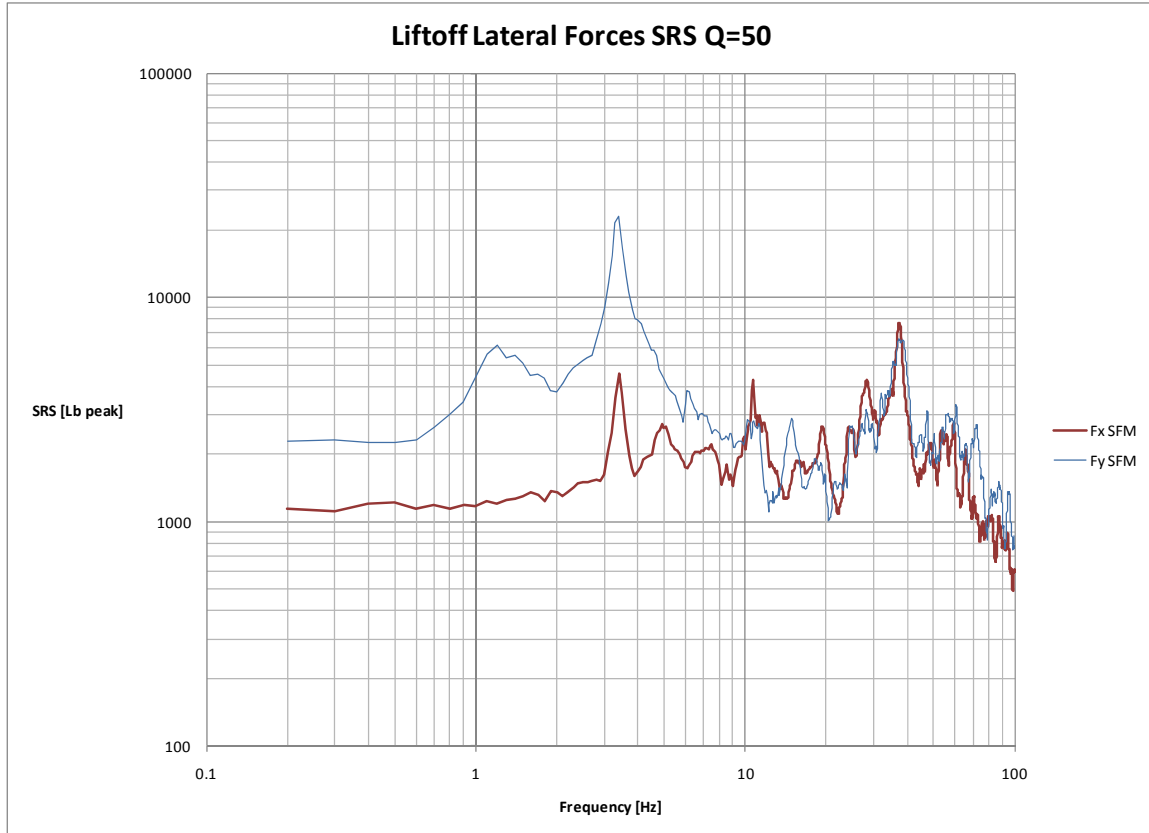


Figure 7.2-17. Lateral Forces SRS

	NASA Engineering and Safety Center Technical Assessment Report	Document #:	Version:
		NESC- RP-06-071	1.0
Title: Flight Force Measurements of the Gamma-Ray Large Area Space Telescope / Delta II Flight		Page #: 119 of 226	

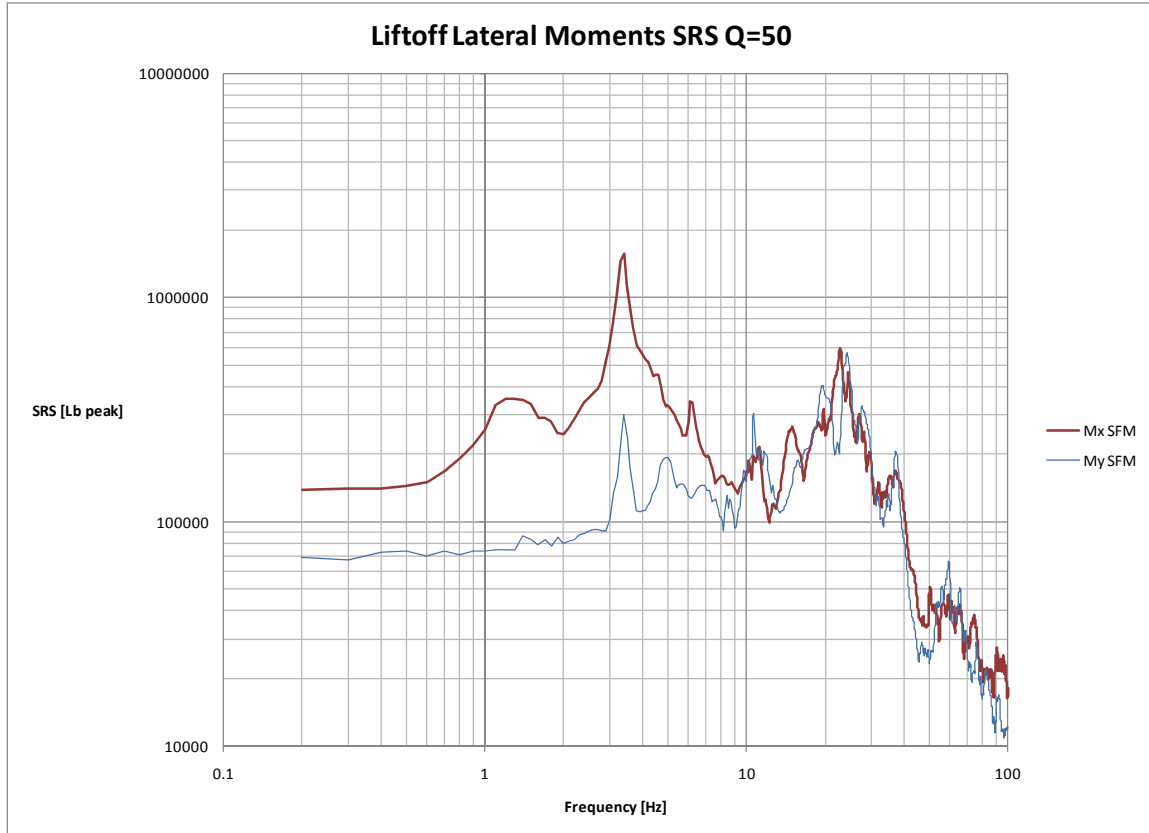


Figure 7.2-18. Liftoff Lateral Moments SRS

The SRS processing of the Liftoff interface force time histories based on the SFM approach show the following trends:

- F_y is higher than F_x , $M_x > M_y$, and the frequency contents are similar.
- The overturning moment's main frequency content is at the coupled system (~ 3 Hz) frequency and not at the GLAST spacecraft first lateral fundamentals (~ 10 Hz).

Torsional moments and respective spectra are shown in Figures 7.2-19 and 7.2-20.



**NASA Engineering and Safety Center
Technical Assessment Report**

Document #:
**NESC-
RP-06-071**

Version:
1.0

Title:

**Flight Force Measurements of the Gamma-Ray Large
Area Space Telescope / Delta II Flight**

Page #:
120 of
226

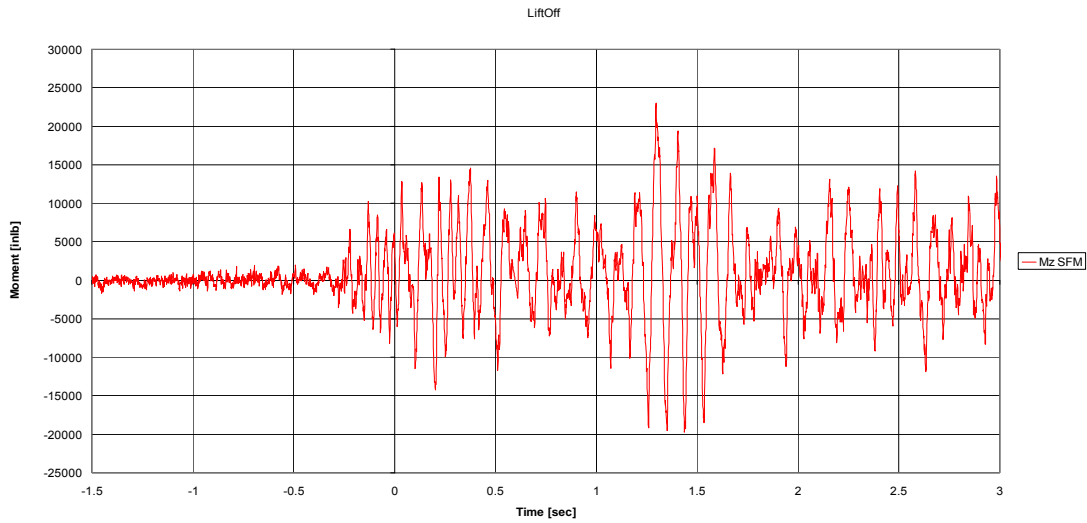


Figure 7.2-19. Liftoff Torsional Moment

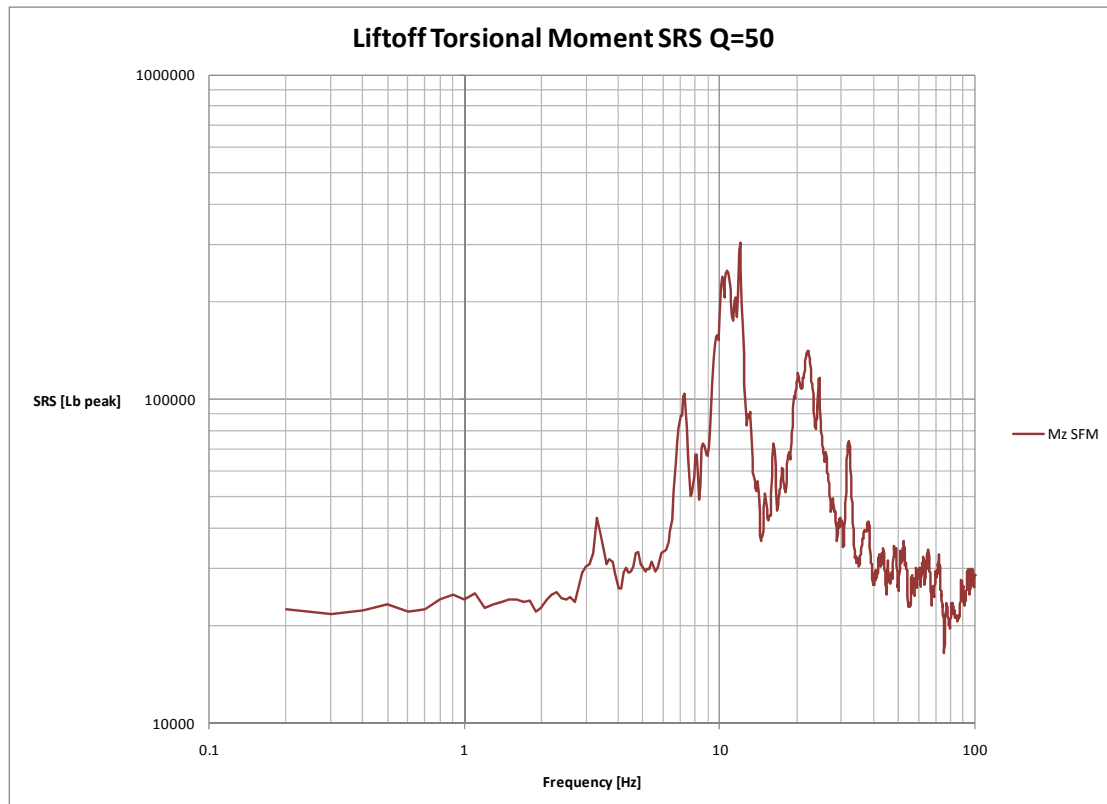


Figure 7.2-20. Liftoff Torsional Moment SRS

	NASA Engineering and Safety Center Technical Assessment Report				Document #: NESC- RP-06-071	Version: 1.0
	Title: Flight Force Measurements of the Gamma-Ray Large Area Space Telescope / Delta II Flight					

Figure 7.2-20 shows that the predominant frequency content for the torsional moment is around 10 Hz corresponding to the primary torsional mode of the launch vehicle and spacecraft stack. Table 7.2-2 shows the maximum forces predicted by the SFM during Liftoff.

Table 7.2-2. Liftoff Maximum Predicted Forces

	Maximum	Time	Maximum	Time	Maximum	Time	Maximum	Time	Maximum	Time	Maximum	Time
Method	Fx [lb]	[sec]	Fy [lb]	[sec]	Fz [lb]	[sec]	Mx [inlb]	[sec]	My [inlb]	[sec]	Mz [inlb]	[sec]
SFM: total	1121	0.333	2321	0.208	19004	0.374	140668	0.216	67612	0.343	22984	1.296
dynamic					3374	-0.170						

Following the general guideline for SFM prediction errors resulting from ground tests, all forces and moments predicted at Liftoff meet the 5 percent prediction error, except for the Fx that only obtains the 10 percent value. Acceptable results are not expected until substantial forces and moments have been produced.

7.2.2 Airloads

Airloads for the Delta II launch vehicle occurs between approximately T+20 to +50 seconds into flight and covers the transonic and Max-Q flight regimes. The events associated with Airloads are typically drivers for the maximum lateral loading on the spacecraft and produce the highest bending moments at the spacecraft separation plane. For the GLAST mission, the data during the Airloads flight time did not contain data dropouts in either the strain or acceleration data.

7.2.2.1 Airloads Interface Accelerations

For Airloads, the 12 accelerometer channels were resolved into 6 net interface acceleration components (3 translational and 3 rotational) representing the acceleration at the PAF to Delta II interface. These 6 accelerations represent the average acceleration at the launch vehicle centerline and were used as input for the basedrive and Impedance Methods discussed in Section 7.3.

The translational accelerations for the lateral axes corresponding to the Airloads flight time are shown in Figure 7.2-21. The thrust acceleration is displayed in Figure 7.2-22 and the maximum rotational acceleration is shown in Figure 7.2-23.

	NASA Engineering and Safety Center Technical Assessment Report	Document #:	Version:
		NESC- RP-06-071	1.0
Title: Flight Force Measurements of the Gamma-Ray Large Area Space Telescope / Delta II Flight			Page #: 122 of 226

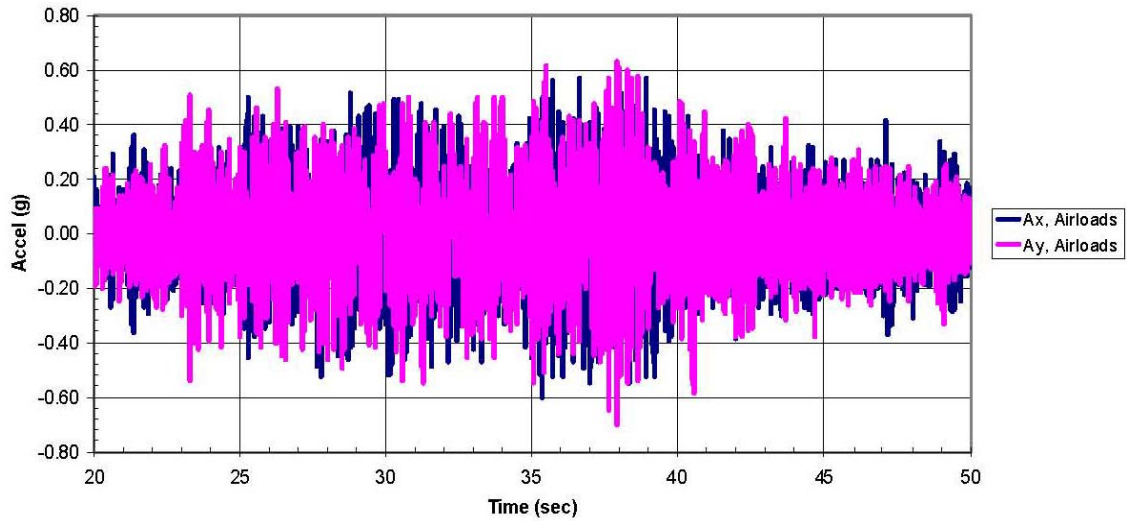


Figure 7.2-21. Airloads Net Acceleration – Lateral Axes

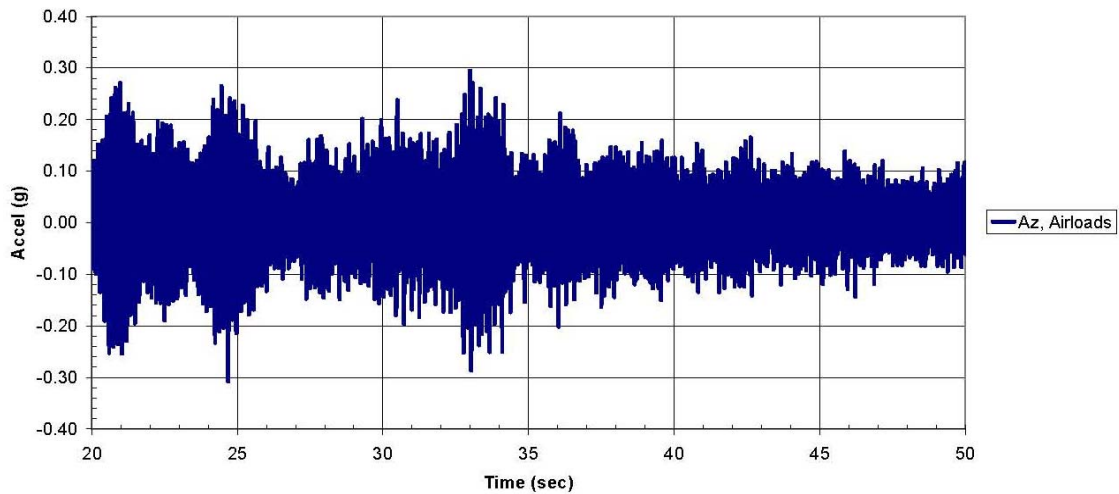


Figure 7.2-22. Airloads Thrust Axis Acceleration

	NASA Engineering and Safety Center Technical Assessment Report	Document #:	Version:
		NESC- RP-06-071	1.0
Title: Flight Force Measurements of the Gamma-Ray Large Area Space Telescope / Delta II Flight			Page #: 123 of 226

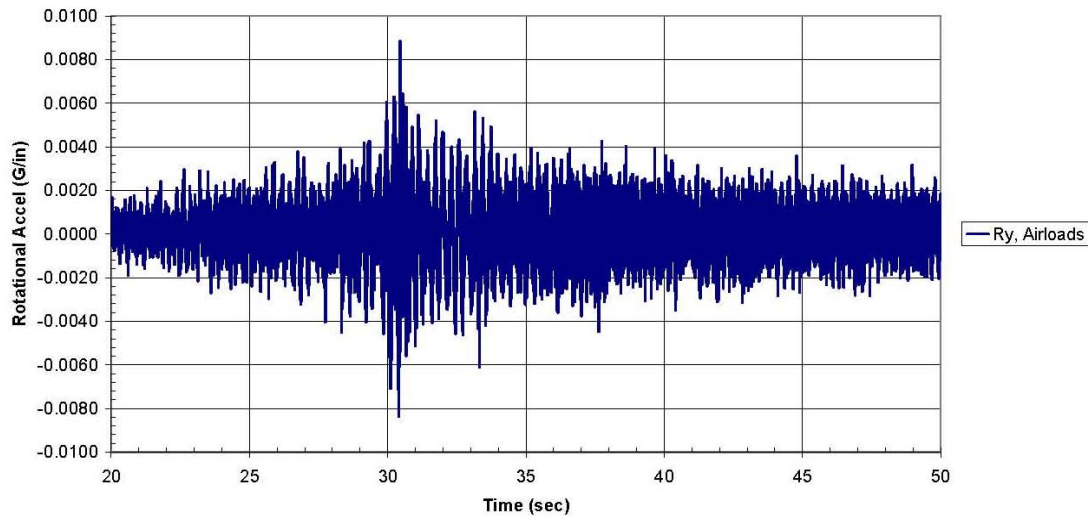


Figure 7.2-23. Airloads Rotational Acceleration about Y- Axis (Ry)

Figures 7.2-21 and 7.2-22 show that the lateral acceleration peaks between T+35 to +40 seconds, while the maximum dynamic thrust acceleration peaks at approximately T+33 seconds. The peak rotational acceleration occurs earlier between T+30 to +31 seconds. The peak Airloads accelerations measured by the SFI accelerometers are shown in Table 7.2-3.

Table 7.2-3. Peak Centerline Accelerations Measured at Airloads

Max	Time	Max	Time	Max	Time	Max	Time	Max	Time	Max	Time
Ax (g)	sec	Ay (g)	sec	Az (g)	sec	Rx (rad/sec ²)	sec	Ry (rad/sec ²)	sec	Rz (rad/sec ²)	sec
0.6	35.359	0.71	37.935	0.31	24.68	2.85	30.163	3.41	30.449	8.83	33.215

The Airloads SRS for the centerline accelerations are shown in Figures 7.2-24 and 7.2-25. The translational acceleration in the lateral axes has predominant frequency content in the 20 to 35 Hz range. The vehicle bending modes at approximately 1.5 and 3.5 Hz can also be seen in the SRS processing of the lateral axis acceleration data. The data for the thrust axis shows the low-frequency vehicle modes at approximately 7 and 11 Hz. There is little frequency content in the thrust axis above 15 Hz. The Airloads rotational accelerations predominantly have a frequency content around 10 Hz and below. The 10 Hz torsional mode of the launch vehicle stack can be seen in the rotational acceleration about the Z (thrust) axis. The data shows that the rotational accelerations have minimal frequency content above 20 Hz.

	NASA Engineering and Safety Center Technical Assessment Report	Document #:	Version:
		NESC- RP-06-071	1.0
Title: Flight Force Measurements of the Gamma-Ray Large Area Space Telescope / Delta II Flight			Page #: 124 of 226

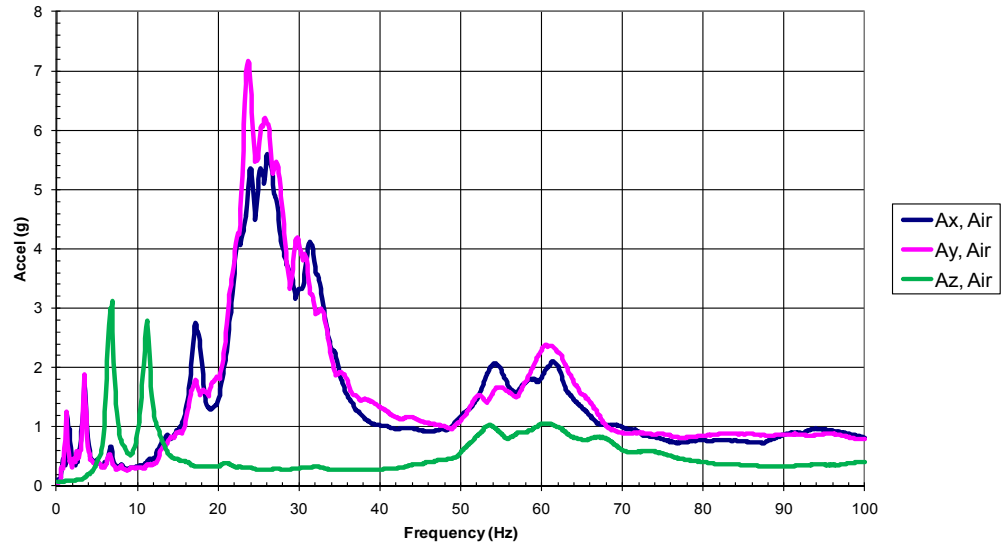


Figure 7.2-24. Airloads Translational Acceleration SRS (Q=20)

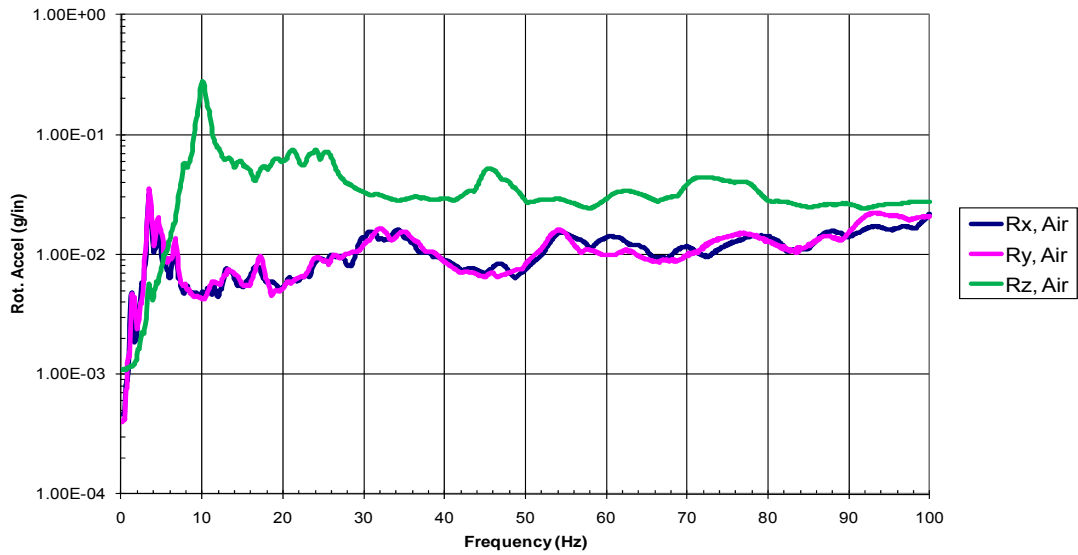


Figure 7.2-25. Airloads Rotational Acceleration SRS (Q=20)

7.2.2.2 Airloads Interface Forces

The maximum forces and moments calculated at the GLAST spacecraft to PAF interface during the Airloads flight time using the SFM and FEM Methods are shown in Table 7.2-4. It should be noted that prior to calculating the forces, the gages were nulled for the initial 1 g state at by subtracting the pre-launch strains (average from T-5 to -4).

	NASA Engineering and Safety Center Technical Assessment Report	Document #:	Version:
		NESC- RP-06-071	1.0
Title: Flight Force Measurements of the Gamma-Ray Large Area Space Telescope / Delta II Flight			Page #: 125 of 226

The measured weight of 9,643 pounds was then added to the calculated thrust axis force to arrive at the values shown in the table.

Table 7.2-4. Airloads Interface Forces Calculated from Measured Strains

Method	Maximum Fx (lb)	Time sec	Maximum Fy (lb)	Time sec	Maximum Fz (lb)	Time sec	Maximum Mx (in-lb)	Time sec	Maximum My (in-lb)	Time sec	Maximum Mz (in-lb)	Time sec
SFM	4596.5	32.444	4694.9	32.115	24581.8	21.19	288019.2	29.015	358478.7	32.443	247628.6	33.214
FEM	4663.8	32.444	4766.1	32.115	24577.5	21.19	290330.5	29.015	364071.0	32.443	247498.2	33.214

The data in Table 7.2-4 shows agreement between the SFM and FEM Method results calculated based on the measured strain data. The SFM was selected as the baseline for comparison because it showed less sensitivity to boundary conditions (see Sections 6.2 and 6.3). Plots of the interface forces calculated from the measured strains using the SFM approach are shown in the Figures 7.2-26 and 7.2-27.

Figure 7.2-25 shows that the lateral forces measured during the Airloads flight time. The measured accelerations between the two lateral axes are similar with the peak absolute value occurring within 0.3 seconds of each other.

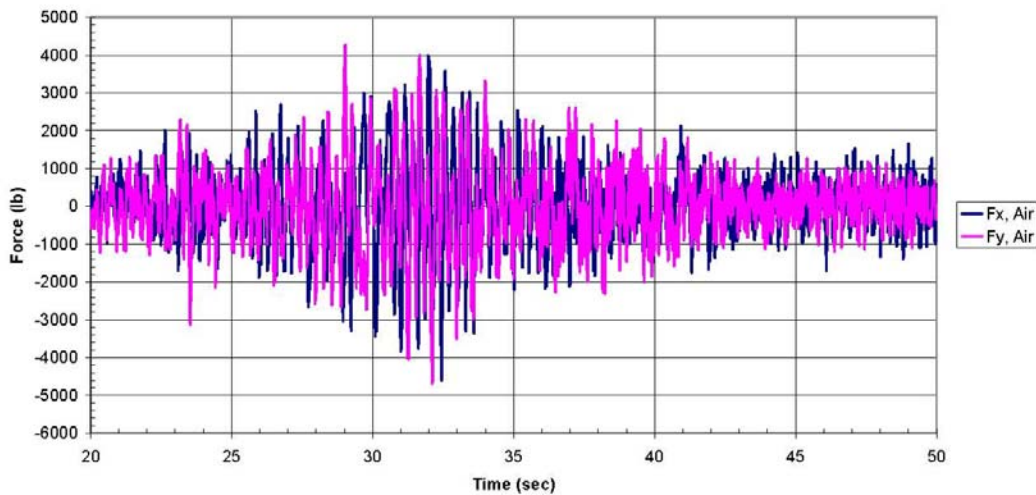


Figure 7.2-26. Airloads Lateral Forces Calculated Using SFM

Figure 7.2-27 shows the calculated SFM thrust axis force for the Airloads flight time. Also shown on this plot is the steady-state thrust force calculated based on a DC accelerometer mounted at the SSGS. As can be seen from the figure, there is agreement between the thrust forces calculated by the SFM approach as compared to the independently measured thrust acceleration converted to forces based on GLAST spacecraft weight (9,643 pounds).

	NASA Engineering and Safety Center Technical Assessment Report	Document #:	Version:
		NESC- RP-06-071	1.0
Title: Flight Force Measurements of the Gamma-Ray Large Area Space Telescope / Delta II Flight			Page #: 126 of 226

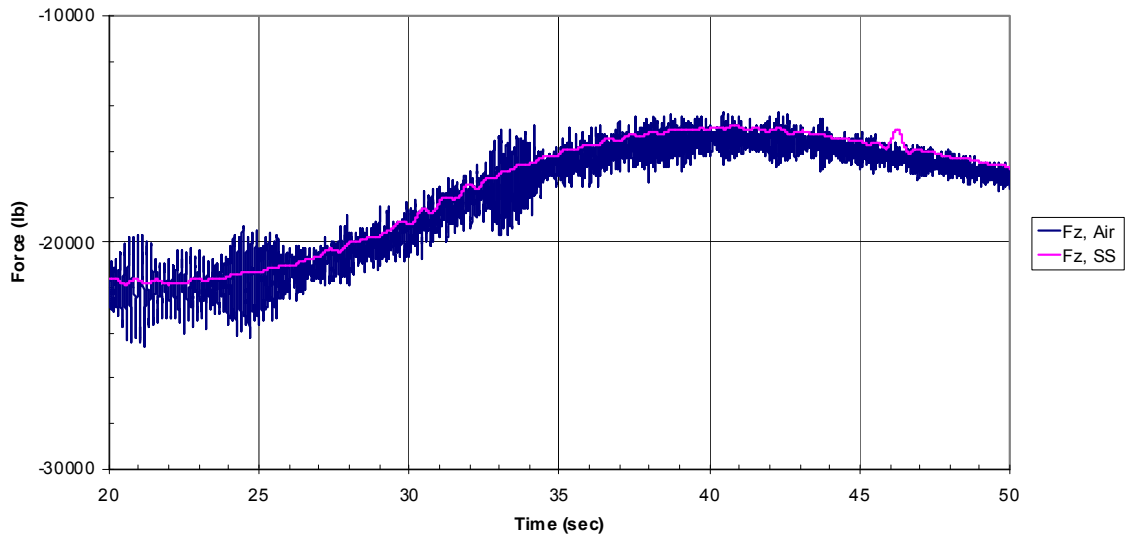


Figure 7.2-27. Airloads Thrust Force Calculated Using SFM

The moments calculated using the SFM are shown in Figure 7.2-28. The lateral moments (Mx and My) are the highest measured of all flight events with the maximum of 358,479 in-lbs occurring about the Y-axis at approximately T+32.5 seconds. The torsional moment at 247,629 in-lbs was higher than expected based on coupled loads predictions, and approximately on the same order as Mx.

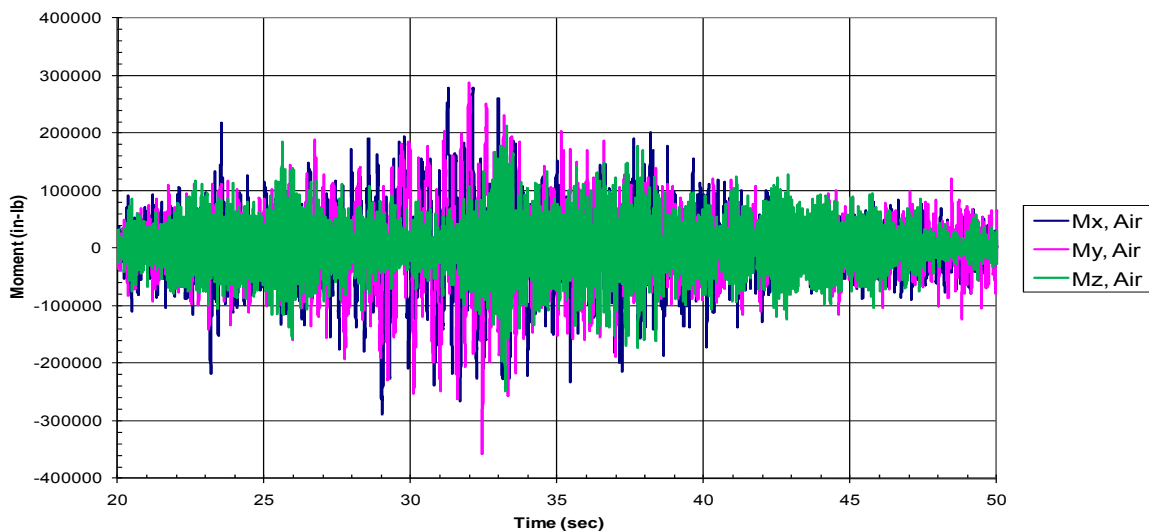


Figure 7.2-28. Airloads Moments Calculated using SFM

	NASA Engineering and Safety Center Technical Assessment Report	Document #:	Version:
		NESC- RP-06-071	1.0
Title: Flight Force Measurements of the Gamma-Ray Large Area Space Telescope / Delta II Flight		Page #: 127 of 226	

The corresponding SRS curves ($Q=20$) for the interface forces calculated using the SFM are shown in Figures 7.2-29 and 7.2-30. The SRS of the thrust axis force shows the offset associated with a quasi-static force of 24,582 pounds corresponding to a steady-state acceleration of approximately 2.5 g at the start of the Airloads flight time. The lateral forces peak around 3.5 Hz corresponding to the second bending mode of the coupled launch vehicle/spacecraft system. The thrust axis forces peak at around 7 Hz, but also have strong frequency content at 11 Hz corresponding to the launch vehicle stack axial modes. The spacecraft axial mode at 31 Hz can also be seen in the thrust axis data. Some similar trends can be seen in the SRS processing of the moments shown in Figure 7.2-30. The lateral moments show the stack bending modes at 1.5 and 3.5 Hz. The stack torsional mode at 10 Hz can be seen in the moment about the thrust axis (M_z). The moments show frequency content out to about 30 Hz with strong peaks in the 20 to 30 Hz range. All of the forces and moments show minimal frequency content above 35 Hz, while the measured acceleration data shows frequency content in the 50 to 70 Hz range.

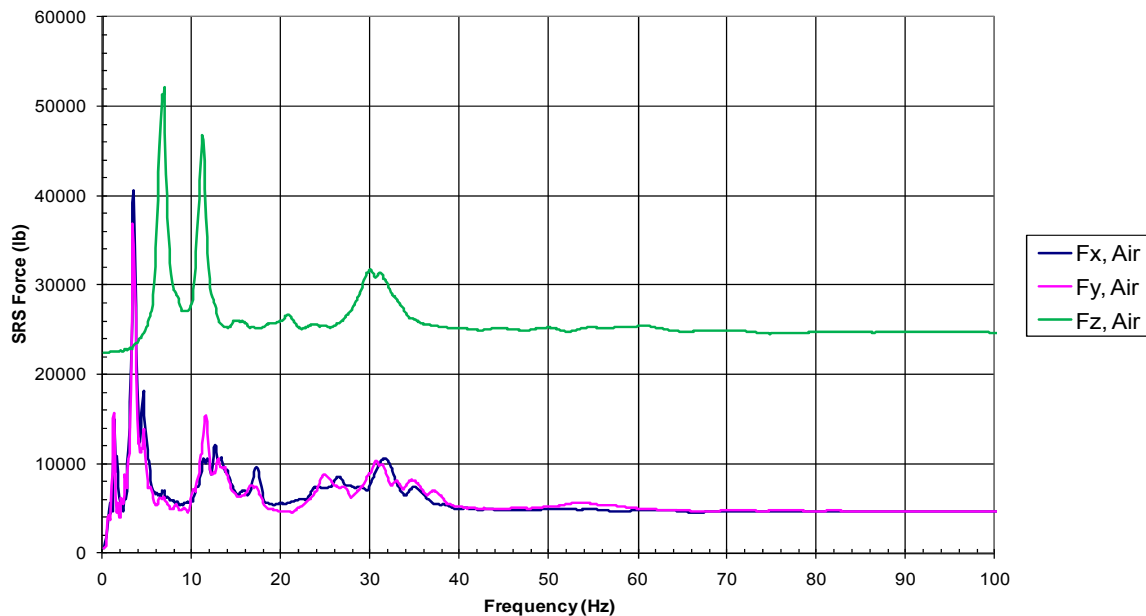


Figure 7.2-29. Airloads Force SRS Plots ($Q=20$)

	NASA Engineering and Safety Center Technical Assessment Report	Document #:	Version:
		NESC- RP-06-071	1.0
Title: Flight Force Measurements of the Gamma-Ray Large Area Space Telescope / Delta II Flight		Page #: 128 of 226	

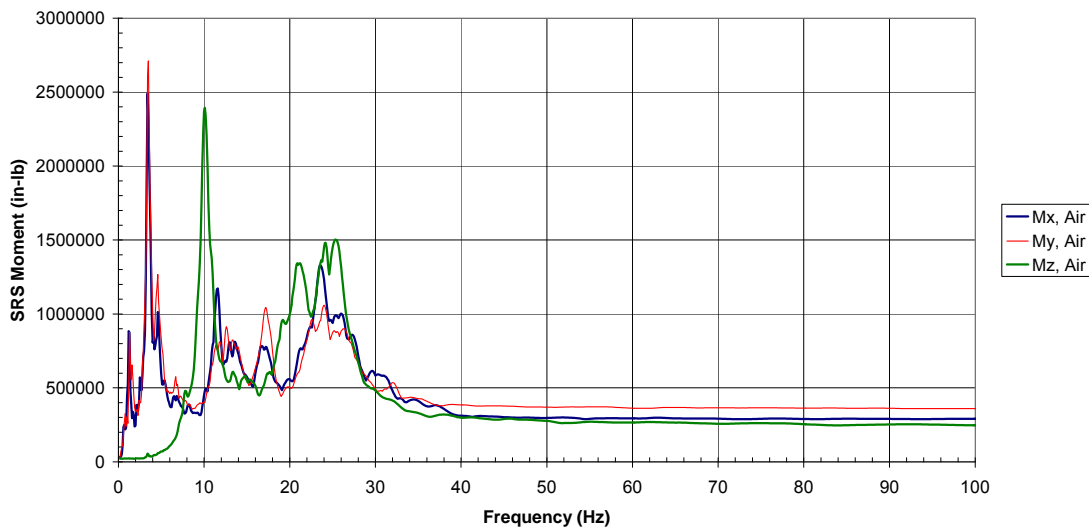


Figure 7.2-30. Airloads SRS Moments (Q=20)

The accelerations and interface forces measured by the SFI system during Airloads are consistent with what was expected for this flight time. The SFM forces measured in the thrust axis shows agreement with the steady-state acceleration measured by the DC accelerometer at the SSGS.

7.2.2.3 Airloads Summary

- The Airloads event occurs on the GLAST flight from T+20 to +50 seconds. SRS processing of the lateral axis acceleration data shows peak frequency content in the 20 to 35 Hz range.
- SRS processing of the thrust axis acceleration data shows peaks corresponding to stack modes at approximately 7 and 11 Hz. All thrust axis frequency content is below 15 Hz.
- SRS processing of rotational acceleration data about the lateral axes show peak frequency content at 3.5 Hz corresponding to the second bending mode of the vehicle. The rotational acceleration about the thrust axis peaks at 10 Hz which corresponds to the launch vehicle torsional mode.
- SFM and FEM Method results showed agreement for the calculated forces.
- Measured thrust force using SFM agrees with measured steady-state acceleration.
- Lateral moments measured during Airloads are the highest for all flight events.
- SRS processing of lateral forces (Fx and Fy) show predominant frequency content at 3.5 Hz corresponding to second bending mode of the launch vehicle.
- Thrust axis force SRS shows effect of a 2.5 g steady-state thrust as an offset.

	NASA Engineering and Safety Center Technical Assessment Report	Document #:	Version:
		NESC- RP-06-071	1.0
Title: Flight Force Measurements of the Gamma-Ray Large Area Space Telescope / Delta II Flight		Page #: 129 of 226	

- Thrust axis force SRS shows vehicle axial modes at 7 and 11 Hz and GLAST spacecraft thrust mode at 31 Hz.
- SRS processing of lateral moments shows peak moment occurs at 3.5 Hz corresponding to the second bending mode of the launch vehicle.
- SRS processing of the moment about the thrust axis (Mz) shows peak occurs at 10 Hz corresponding to the torsional mode of the launch vehicle.
- All moments including torsion show frequency content in the 15 to 30 Hz range.
- All forces and moments have minimal frequency content above 35 Hz while acceleration data shows frequency content in the 50 to 70 Hz range.

7.2.3 Main Engine Cutoff (MECO)

The MECO for the GLAST mission occurred at approximately T+264.9 seconds as measured by the SFI accelerometers. The acceleration and strain measurements recorded during MECO did not include any data drops.

There are several events associated with MECO consisting of first and second pre-MECO, prior-to-MECO, and the MECO shock transient event. The first and second pre-MECO events are periods of sustained sinusoidal vibration that occur about a minute prior to the engine shutdown as the fuel in the first stage is depleted. The first pre-MECO event tends to have frequency content in the 25 to 30 Hz range and can last up to 20 seconds. The second pre-MECO is similar in nature to the first pre-MECO event, only it tends to be shorter in duration and have frequency content in the 30 to 35 Hz range. For the GLAST mission, the first pre-MECO occurred at T+179 seconds, and lasted for approximately 13 seconds with a primary frequency content of 27 Hz. There was no second pre-MECO event measured for the GLAST mission. The average lateral acceleration measured at the PAF base by the SFI accelerometers is shown in Figure 7.2-31.

The prior-to-MECO event is an 18 Hz oscillation that corresponds to the launch vehicle fundamental axial mode and is excited by the depletion of fuel just prior to the engine shutting down during the period of maximum steady-state acceleration. On the GLAST mission, this low-frequency oscillation can be seen on the SFI thrust accelerometers as shown in Figure 7.2-32. The prior-to-MECO is the sinusoidal vibration that begins around T+263.5 seconds and builds to approximately 0.2 g just before MECO. This 0.2 g peak sinusoidal vibration occurs during the maximum steady state thrust, which at MECO was 5.2 g for an overall combined acceleration at the PAF base of 5.4 g. Both the pre-MECO and prior-to-MECO events are typically not considered drivers for payload design. These events are not covered in the standard CLA performed for the Delta II launch vehicle unless the payload has critical modes in the event frequency ranges. The GLAST mission did not have critical modes in the frequency ranges associated with pre-MECO or prior-to-MECO such that CLA load cases were not run and the spacecraft

	NASA Engineering and Safety Center Technical Assessment Report	Document #:	Version:
		NESC- RP-06-071	1.0
Title: Flight Force Measurements of the Gamma-Ray Large Area Space Telescope / Delta II Flight		Page #: 130 of 226	

responses were considered to be covered by the standard load cases for Liftoff and Airloads. The peak thrust acceleration during MECO is specified for payload design as a static limit load.

Figure 7.2-32 is the MECO shock transient event. For the GLAST mission, this event starts at T+265.1 seconds and lasts for approximately 0.2 seconds. The MECO shock transient event is a short duration transient that occurs just after MECO as a result of residual pressure transients as the valves are closed and the LOX and fuel are depleted. The MECO shock transient event is a relatively high frequency event (80 to 140 Hz). The low-frequency vibration events associated with MECO (pre-MECO and prior-to-MECO) have been defined and characterized since the early development of the Delta II launch vehicle. The MECO shock transient event is a recently recognized flight event (since 2002). The relatively high frequency nature of the MECO shock transient event has made it difficult to predict payload responses, as the launch vehicle and payload models have not been correlated in this frequency range. Attempts at developing a coupled loads simulation have not been successful in matching flight data, primarily due to the complexity of accurately simulating the behavior of a coupled launch vehicle/spacecraft system. It should be noted that the time history data shown in Figure 7.2-32 exhibits the same filtering artifact seen in the Liftoff thrust data due to the use of a 0.5 Hz HP filter in the SFI data acquisition for the accelerometer channels.

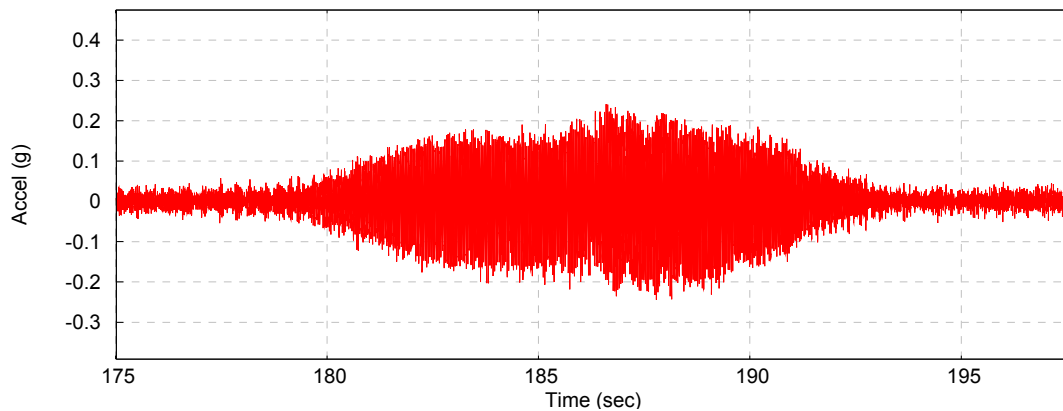


Figure 7.2-31. First Pre-MECO Lateral Acceleration

The simulation technique used for the MECO Shock Transient event has been to take measured accelerations at the PAF base from the standard measurement package flown on the Delta II vehicle and derive a set of input accelerations that can be used to basedrive the coupled spacecraft-PAF system with equivalent sine input. This has typically resulted in high responses on the payload side, but it has not been clear how realistic this analysis technique has been or how realistic the predicted responses are on

	NASA Engineering and Safety Center Technical Assessment Report	Document #:	Version:
		NESC- RP-06-071	1.0
Title: Flight Force Measurements of the Gamma-Ray Large Area Space Telescope / Delta II Flight		Page #: 131 of 226	

the spacecraft. Therefore, one of the goals of this assessment was to obtain a better understanding of the MECO Shock Transient event by evaluating the measured interface forces during that flight time. The following sections which cover the measured accelerations and forces measured during the MECO flight time focus on the MECO Shock Transient event.

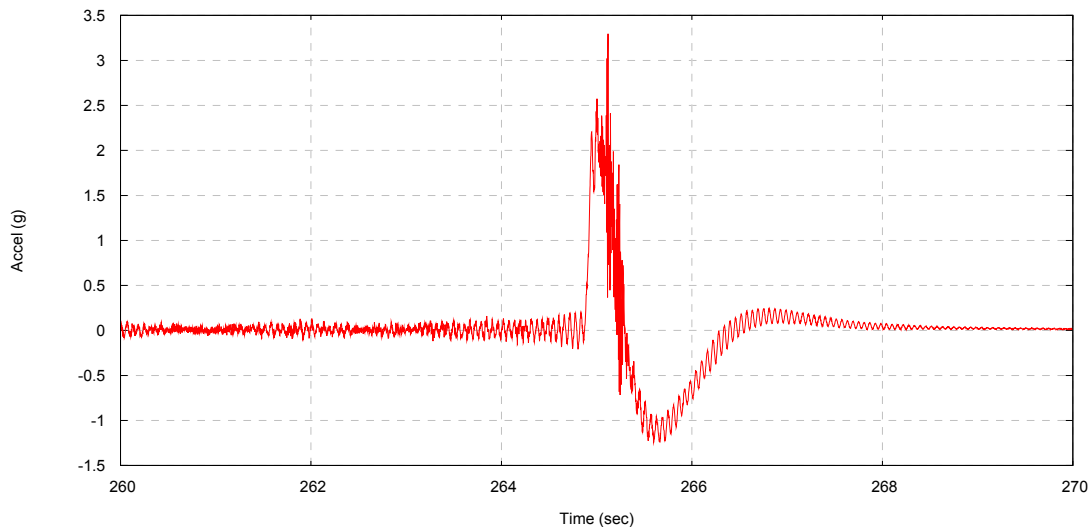


Figure 7.2-32. Prior-to-MECO and MECO Transient Thrust Acceleration

7.2.3.1 MECO Accelerations

The translational accelerations measured by the SFI accelerometers for the lateral axes corresponding to MECO are shown in Figure 7.2-33. The time period from T+ 264.5 to +266.5 seconds was processed. Like previous events, the acceleration data shown has been transformed from the 12 SFI accelerometer channels (three per leg) at the PAF base to the launch vehicle centerline. This time period was selected because it captures both the prior-to-MECO sinusoidal behavior, the actual engine shutdown, and the MECO transient behavior. It can be seen in Figure 7.2-34 that the peak dynamic acceleration in the lateral axes is about 0.5 g and corresponds to the MECO Transient Shock event.

	NASA Engineering and Safety Center Technical Assessment Report	Document #:	Version:
		NESC- RP-06-071	1.0
Title: Flight Force Measurements of the Gamma-Ray Large Area Space Telescope / Delta II Flight			Page #: 132 of 226

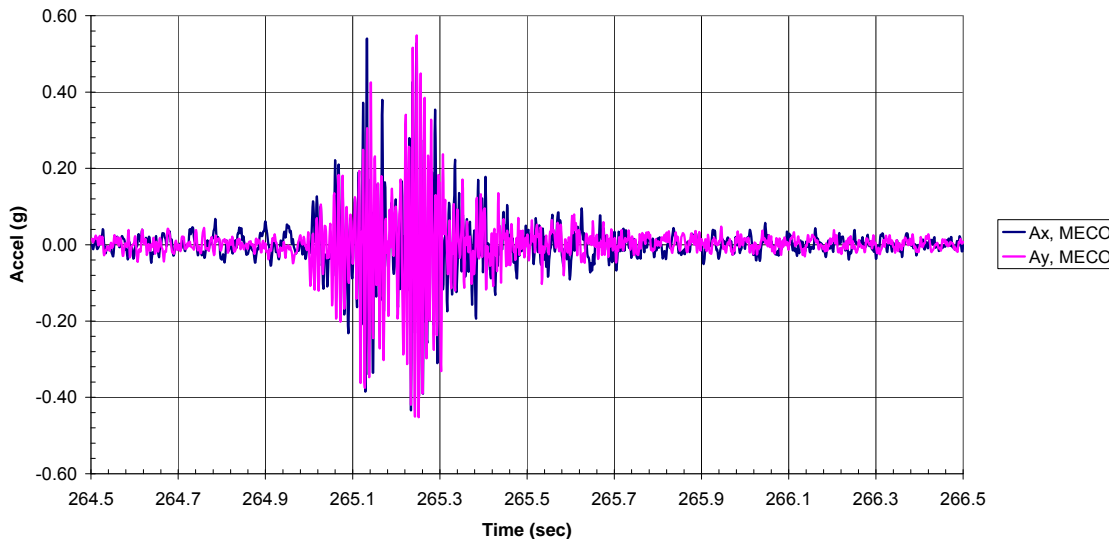


Figure 7.2-33. Lateral Net Acceleration at MECO

The thrust acceleration corresponding to the GLAST mission MECO flight time is shown in Figure 7.2-34. The thrust acceleration is AC coupled in that it does not measure the steady-state acceleration. It can be seen from this figure that there is an artifact in the thrust acceleration data which occurs when the thrust levels drop rapidly from around 5.5 to 0 g when the engine shuts down. The acceleration jumps from 0 to around 2 g and then slowly returns to 0 g over a period of about 2 seconds. This is due to the use of a 0.5 Hz HP filter in the SFI data acquisition system for the accelerometer channels. The HP filter cannot handle a very rapid change in the steady-state acceleration which results in an offset in the time history data. The data shown in Figure 7.2-34 is what was received from ULA with no additional filtering applied.

	NASA Engineering and Safety Center Technical Assessment Report	Document #:	Version:
		NESC- RP-06-071	1.0
Title: Flight Force Measurements of the Gamma-Ray Large Area Space Telescope / Delta II Flight			Page #: 133 of 226

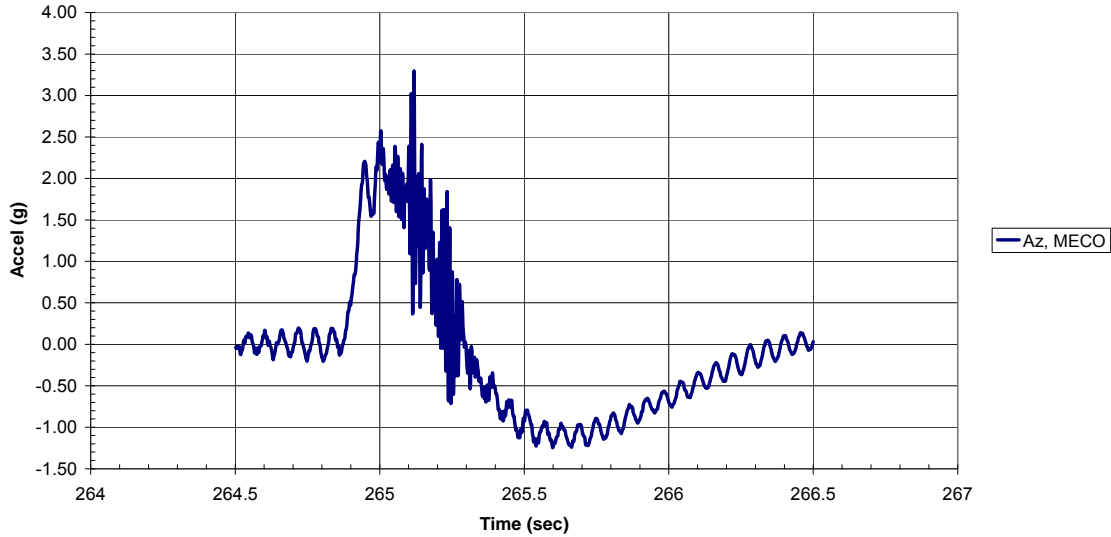


Figure 7.2-34. Thrust Axis Net Acceleration at MECO

Table 7.2-5. Peak Centerline Accelerations Measured at MECO

Max	Time	Max	Time	Max	Time	Max	Time	Max	Time	Max	Time
Ax (g)	sec	Ay (g)	sec	Az (g)	sec	Rx (rad/sec ²)	sec	Ry (rad/sec ²)	sec	Rz (rad/sec ²)	sec
0.54	265.133	0.55	265.247	3.3	265.119	5.4	265.247	3.87	265.147	4.43	265.172

The SRS for the centerline accelerations measured at MECO are shown in Figures 7.2-35 and 7.2-36. It can be seen from these figures that the predominant frequency content for the MECO Shock Transient event occurs in the 100 to 130 Hz range. The thrust axis SRS (Az) also shows the longitudinal launch vehicle mode at 18 Hz and the HP filtering artifact at 0.5 Hz. All of the acceleration data shows minimal frequency content below 60 Hz with the exception of the 18 Hz vehicle thrust axis mode.

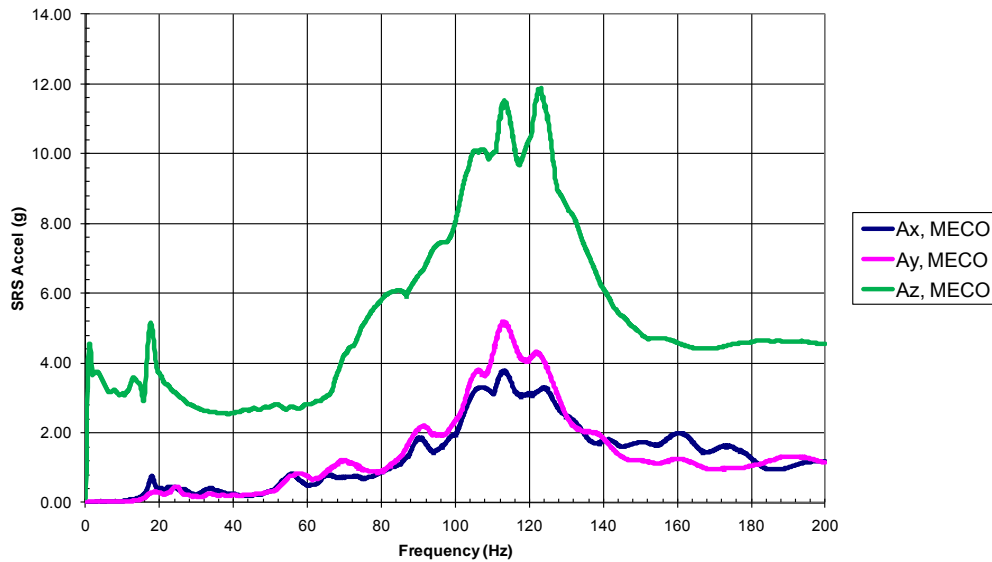


Figure 7.2-35. MECO Translational Acceleration SRS (Q=20)

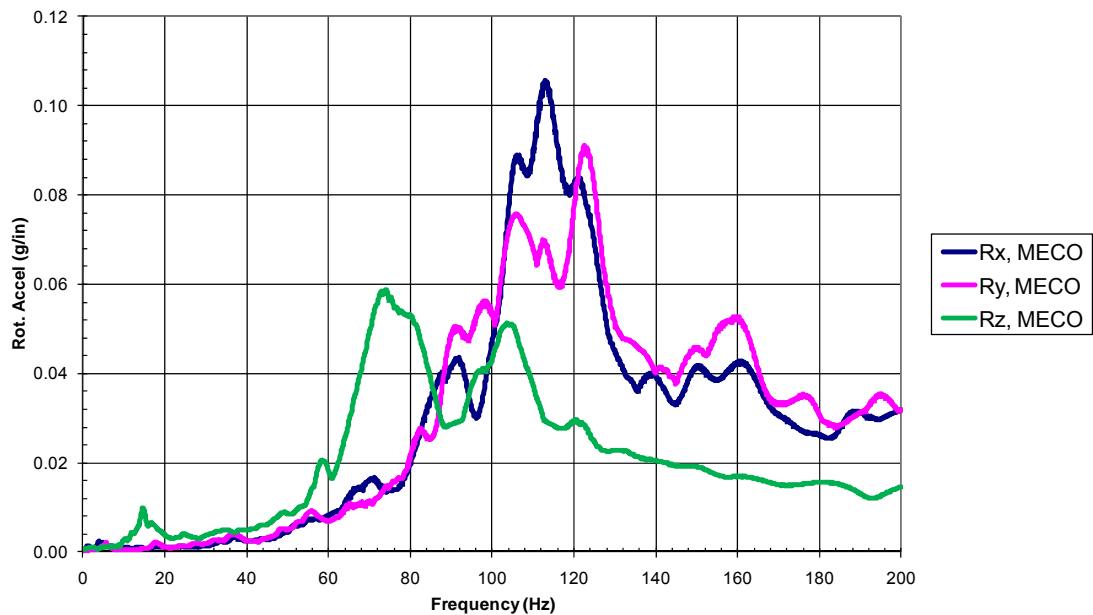


Figure 7.2-36. MECO Rotational Acceleration SRS (Q=20)

	NASA Engineering and Safety Center Technical Assessment Report	Document #:	Version:
		NESC- RP-06-071	1.0
Title: Flight Force Measurements of the Gamma-Ray Large Area Space Telescope / Delta II Flight			Page #: 135 of 226

7.2.3.2 MECO Interface Forces

Based on the strain measurements, the maximum (absolute) forces and moments calculated at the GLAST spacecraft interface using the SFM and FEM Method are shown in Table 7.2-6. A similar process described for Airloads was used with the MECO strain data in which the strains were nulled by removing the 1g strain field and adding back the static payload weight of 9,643 pounds.

Table 7.2-6. MECO Interface Forces Calculated from Measured Strains

Method	Maximum Fx (lb)	Time sec	Maximum Fy (lb)	Time sec	Maximum Fz (lb)	Time sec	Maximum Mx (in-lb)	Time sec	Maximum My (in-lb)	Time sec	Maximum Mz (in-lb)	Time sec
SFM	494.7	265.235	394.4	265.578	52520.5	264.804	27017.3	263.941	26941.3	265.259	20339.6	262.751
FEM	514.1	265.235	402.8	265.578	52512.5	264.804	28064.5	263.941	27332.7	265.01	24336.6	262.751

Figures 7.2-37 through 7.2-39 show the time history plots of the interface forces calculated during the MECO flight time using the SFM. The absolute maximums from these plots correspond to the first row of Table 7.2-6.

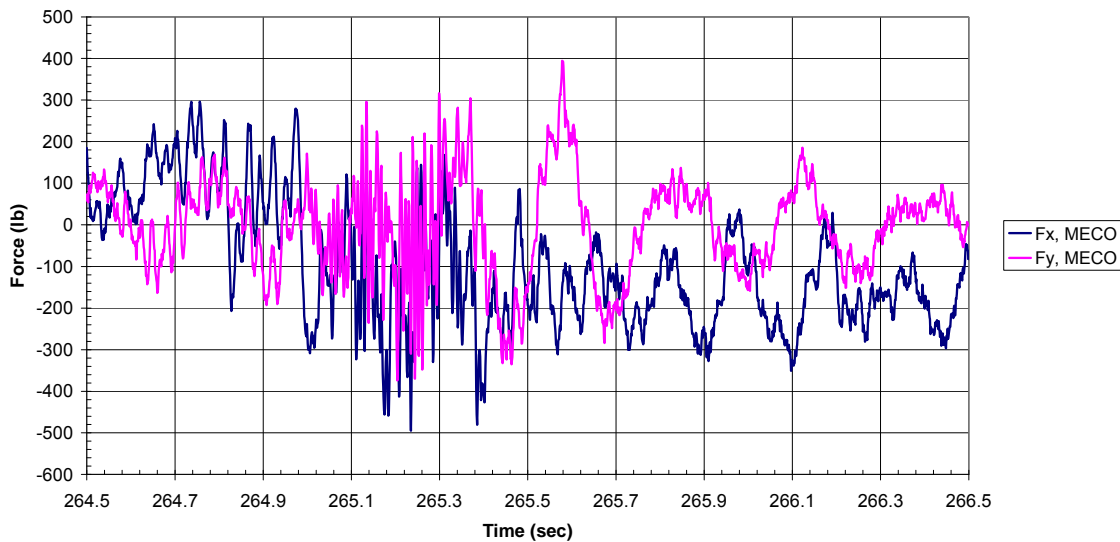


Figure 7.2-37. MECO Lateral Forces Calculated using SFM

Figure 7.2-38 shows the thrust axis force for the MECO flight time. Also shown in the plot is the steady-state thrust force calculated based on the SSGS DC accelerometer which has been LP filtered at 2 Hz and multiplied by the flight weight of 9,643 pounds.

	NASA Engineering and Safety Center Technical Assessment Report	Document #:	Version:
		NESC- RP-06-071	1.0
Title: Flight Force Measurements of the Gamma-Ray Large Area Space Telescope / Delta II Flight		Page #: 136 of 226	

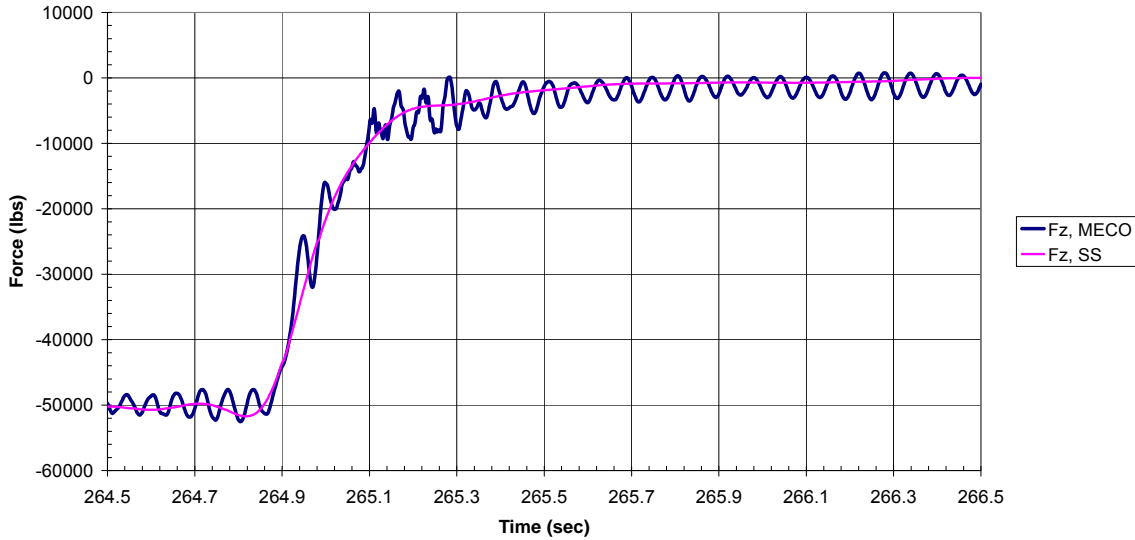


Figure 7.2-38. MECO Thrust Forces Calculated using SFM

Figure 7.2-38 shows there is agreement between the thrust forces calculated by the SFM as compared with the independently measured steady state acceleration. It can be seen that the maximum steady-state force at the start of the measurement period was 50,239 pounds. This force corresponds to an acceleration level of $50,239/9,643 = 5.2$ g and that the acceleration level goes from 5.2 to less than 1 g in approximately 0.2 seconds. It can be seen from this data that MECO occurs at 264.9 seconds. Figure 7.2-39 shows the lateral moments (M_x and M_y) and the torsional moment (M_z) measured during MECO.

	NASA Engineering and Safety Center Technical Assessment Report	Document #:	Version:
		NESC- RP-06-071	1.0
Title: Flight Force Measurements of the Gamma-Ray Large Area Space Telescope / Delta II Flight		Page #: 137 of 226	

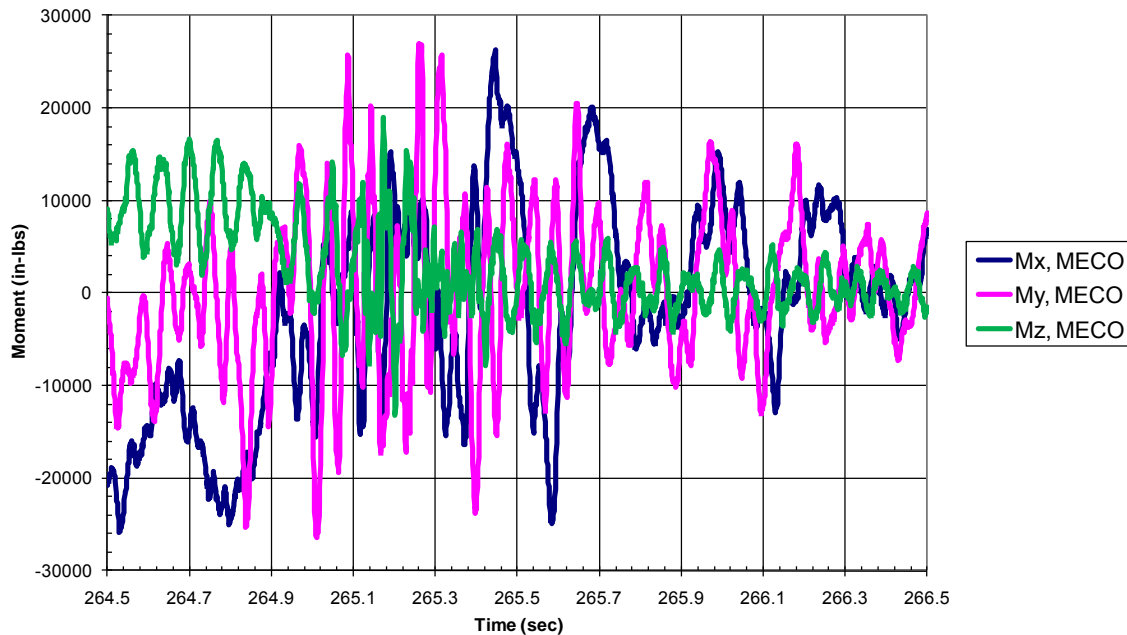


Figure 7.2-39. MECO Moments Calculated Using SFM

The SRS curves ($Q=20$) for MECO forces are shown in Figures 7.2-40 through 7.2-43. The SRS results for the lateral forces shown in Figure 7.2-39 indicates that the Y-axis force has predominant frequency content just below 120 Hz, which corresponds to the frequency range of the high Y-axis acceleration and rotational acceleration about the X-axis. The 3.5 Hz launch vehicle bending mode can be seen in the lateral response for both axes. The thrust data shown in Figure 7.2-41 has predominant frequency content at 18 Hz. This value is the launch vehicle longitudinal frequency at MECO, but the curve is relatively flat above 30 Hz. This indicates that the forces associated with the MECO Shock Transient event are small compared to the forces associated with the steady-state acceleration. Figure 7.2-42 shows the SRS of the same data filtered from 30 to 150 Hz to remove the steady-state thrust and prior-to-MECO oscillations at 18 Hz. This data now shows the effect of the MECO Shock Transient event with a peak at 113 Hz and significant frequency content around 80 Hz associated with axial modes of the spacecraft. The fundamental axial mode of the spacecraft can also be seen around 30 Hz. The SRS plot of the moments associated with MECO shown in Figure 7.2-43 indicates that the moments at the interface are primarily driven by the low-frequency launch vehicle bending modes and that the moments associated with the MECO Shock Transient in the 80 to 140 Hz range are relatively small in comparison to the low-frequency response. The high moment about the Y-axis at 18 Hz most likely indicates bending-axial coupling of the spacecraft at the longitudinal mode of the vehicle.



Title:

**Flight Force Measurements of the Gamma-Ray Large
Area Space Telescope / Delta II Flight**

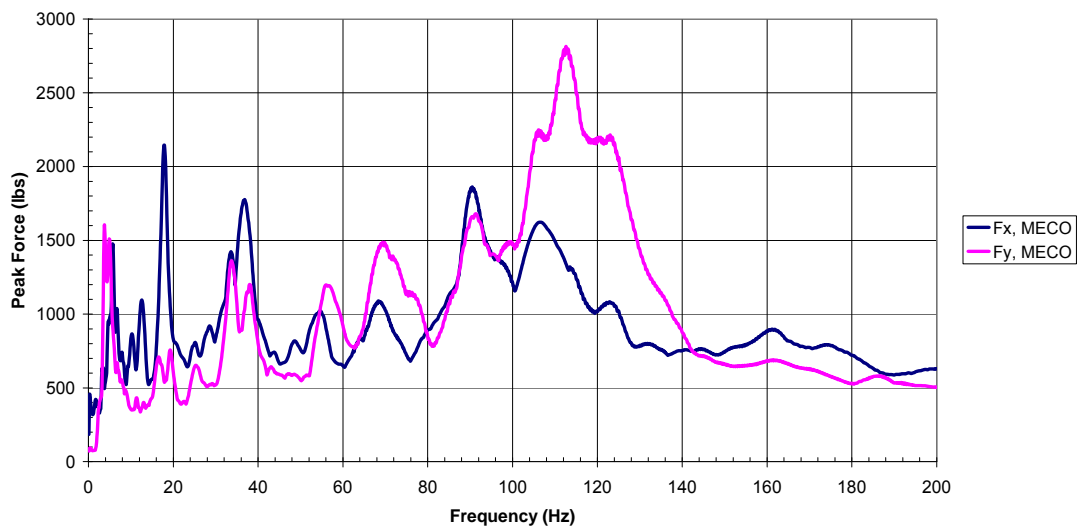


Figure 7.2-40. Lateral MECO SRS Forces (Q=20)

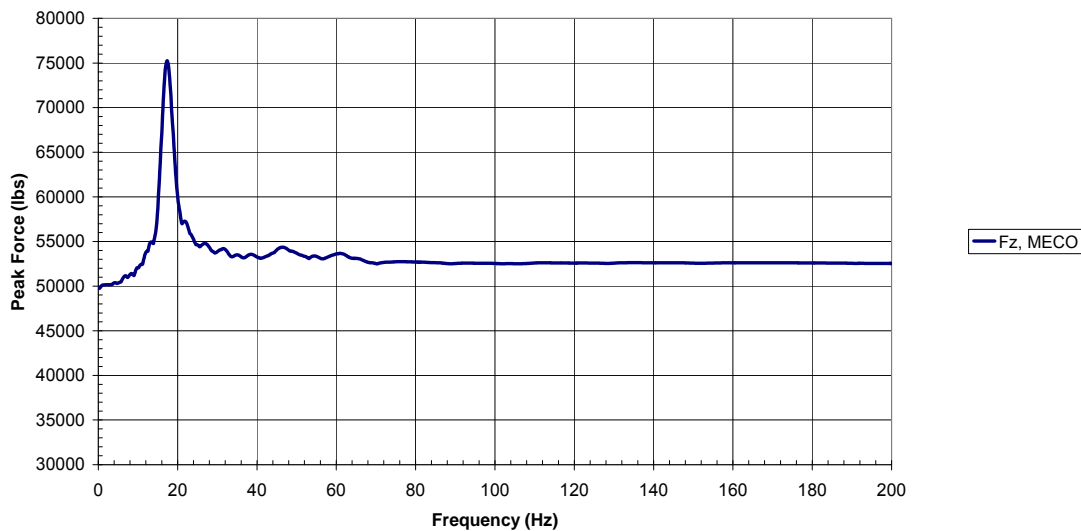


Figure 7.2-41. Thrust MECO SRS Force (Q=20)

	NASA Engineering and Safety Center Technical Assessment Report	Document #: NESC- RP-06-071	Version: 1.0
		Title: Flight Force Measurements of the Gamma-Ray Large Area Space Telescope / Delta II Flight	

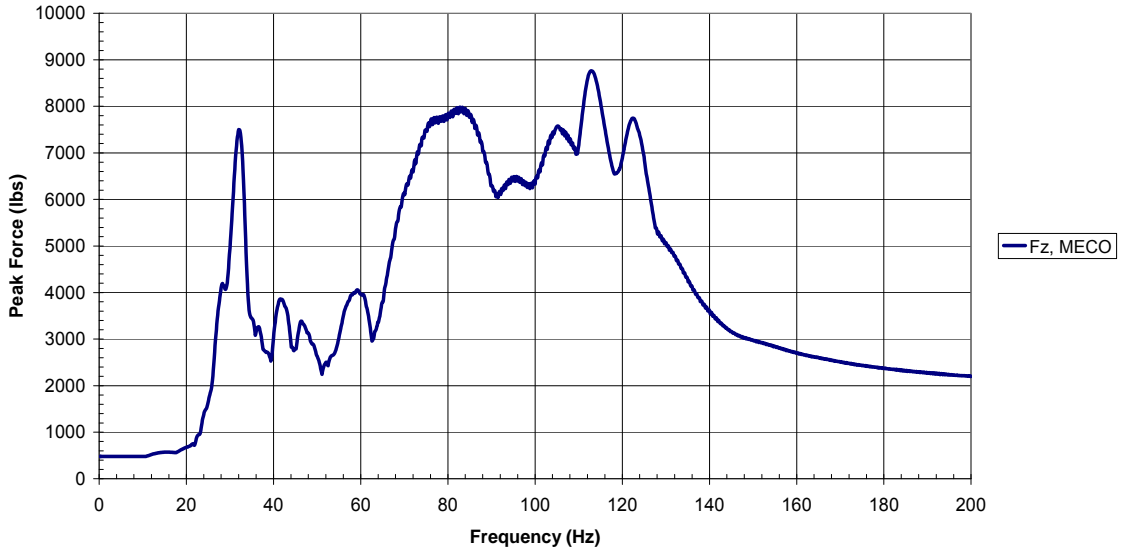


Figure 7.2-42. Thrust MECO SRS Force (Q=20) Filtered 30 – 150 Hz

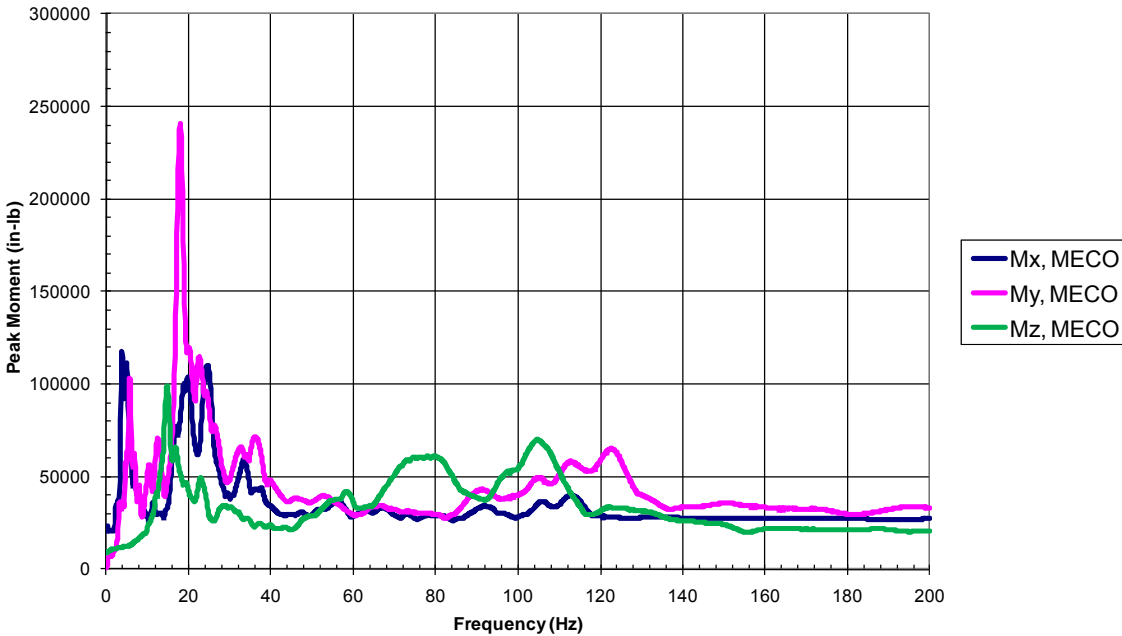


Figure 7.2-43. MECO SRS Moments (Q=20)

	NASA Engineering and Safety Center Technical Assessment Report	Document #:	Version:
		NESC- RP-06-071	1.0
Title: Flight Force Measurements of the Gamma-Ray Large Area Space Telescope / Delta II Flight		Page #: 140 of 226	

7.2.3.3 MECO Summary

- Data was process from T+264.5 to +266.5 seconds to capture prior-To-MECO and MECO Shock Transient events.
- MECO Shock Transient event starts at T+265.1 seconds and last for approximately 0.2 seconds.
- The peak lateral and thrust accelerations occur during the MECO Shock Transient event.
- The thrust axis acceleration data contains artifact associated with 0.5 Hz HP filtering of engine shutdown.
- Lateral axis acceleration SRS processing shows predominant frequency content in the 100 to 120 Hz range consistent with data for MECO Shock Transient Event from prior Delta II flights.
- Thrust axis acceleration SRS processing shows predominant frequency content in the 100 to 130 Hz range. The SRS for the thrust axis also shows the vehicle primary axial mode at 18 Hz and a mode at 0.5 Hz due to the HP filtering artifact.
- There is agreement between results from the SFM and the FEM Method.
- Measured thrust forces based on the SFM shows agreement with measured steady-state acceleration.
- SRS processing of the Y-axis forces shows predominant frequency content in the 100 to 120 Hz range.
- SRS processing of the X-axis shows frequency content at 90 and 110 Hz, but is not as dominant. The peak X-axis force occurs at 18 Hz due to coupling with the primary axial mode of the launch vehicle.
- SRS of the X and Y lateral forces show peaks at 3.5 Hz corresponding to the 2nd vehicle lateral bending mode, but this is not the dominate force for either axis.
- SRS of the unfiltered thrust forces show primarily the 18 Hz launch vehicle axial mode. The SRS curve is flat above 20 Hz because the forces generated by the steady-state thrust plus dynamic content of the prior-to-MECO event envelope the forces at higher frequencies.
- SRS processing of the thrust axis force data filtered from 30 to 150 Hz shows responses at 113 Hz due to the MECO Shock Transient event and at 80 Hz due to axial modes of the spacecraft. The fundamental axial mode of the spacecraft can also be seen in the filtered data at 31 Hz.
- SRS processing of the moments shows that they primarily have frequency content below 25 Hz with the 18 Hz axial launch vehicle mode dominant in the moment about the Y-axis due to axial/bending coupling. The 3.5 Hz lateral launch vehicle bending mode is seen in both lateral moments (Mx and My).

	NASA Engineering and Safety Center Technical Assessment Report	Document #:	Version:
		NESC- RP-06-071	1.0
Title: Flight Force Measurements of the Gamma-Ray Large Area Space Telescope / Delta II Flight		Page #: 141 of 226	

7.2.4 Other Flight Events

In addition to processing the acceleration and force data for Liftoff, Airloads, and MECO which are considered the major load drivers for the spacecraft, several other flight events were processed. The forces at the payload interface were calculated for First – Second Stage Separation, Second Stage Ignition, Fairing Separation, and SECO. This was done primarily as a check of the methodology and to verify that the interface forces associated with these flight events were enveloped by the standard flight events that are evaluated as part of the normal payload design/analysis/test cycle.

Figure 7.2-44 shows the thrust acceleration forces calculated during the flight time that covers First-Second Stage Separation (T+274 seconds), Second Stage Ignition (T+279.5 seconds), and Fairing Separation (T+283.5 seconds). Each of these events can be seen in the thrust data. Figure 7.2-45 shows the thrust axis forces for SECO, which occurred at T+629.9 seconds.

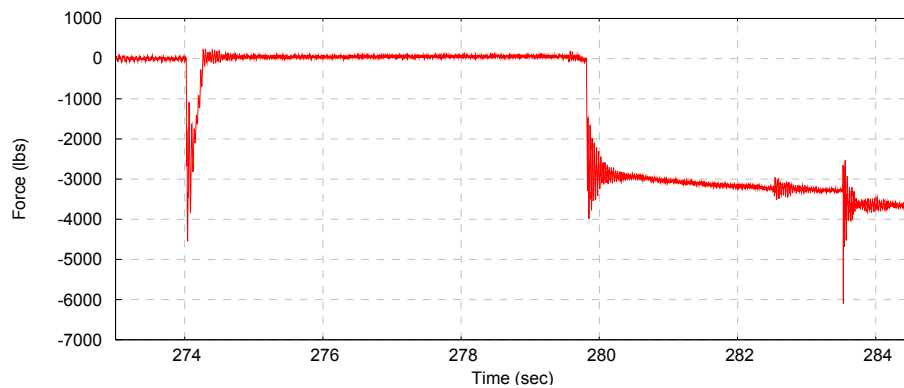


Figure 7.2-44. Thrust Axis Forces SI-2 Separation, Stage II Ignition, and Fairing Separation (SFM)

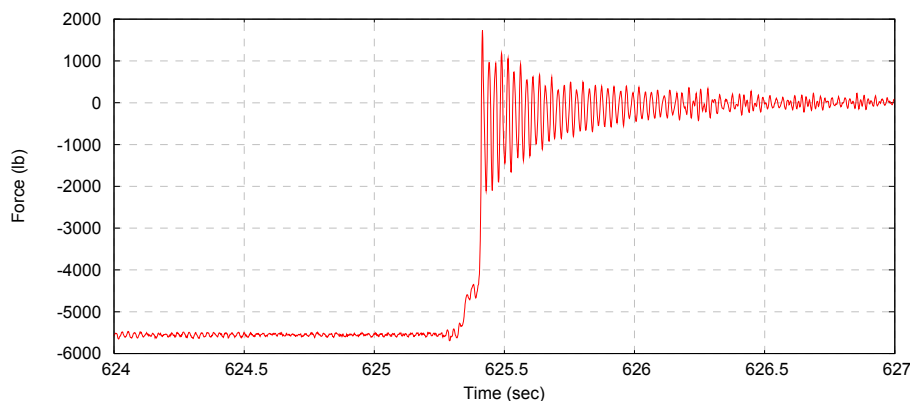


Figure 7.2-45. Thrust Axis Force at SECO (SFM)

	NASA Engineering and Safety Center Technical Assessment Report	Document #:	Version:
		NESC- RP-06-071	1.0
Title: Flight Force Measurements of the Gamma-Ray Large Area Space Telescope / Delta II Flight		Page #: 142 of 226	

The absolute maximum forces measured during these flight events are summarized in Tables 7.2-7 and 7.2-8. Table 7.2-7 shows the forces calculated using the SFM approach while Table 7.2-8 shows the forces calculated using the FEM Method. It can be seen from these tables that both methods show agreement between the calculated force levels.

Table 7.2-7. SFM Results for Other Flight Events

Event	Fx (lbs)	Fy (lbs)	Fz (lbs)	Mx (in-lbs)	My (in-lbs)	Mz (in-lbs)
S1Sep	168.40	490.85	4556.70	53763.00	9785.30	6948.70
S1Ign	423.56	364.41	3993.20	9229.30	11289.00	10160.00
Fair Sep	399.89	443.73	6104.00	20683.00	22543.00	30752.00
SECO	175.00	125.25	5693.40	12971.00	14513.00	5108.40
Max	423.56	490.85	6104.00	53763.00	22543.00	30752.00

Table 7.2-8. FEM Results for Other Flight Events

Event	Fx (lbs)	Fy (lbs)	Fz (lbs)	Mx (in-lbs)	My (in-lbs)	Mz (in-lbs)
S1Sep	170.01	488.57	4557.30	54443.00	10212.00	6830.10
S1Ign	420.79	368.96	3982.20	9507.90	11611.00	10871.00
Fair Sep	405.79	442.67	6101.80	21139.00	22309.00	31185.00
SECO	170.99	127.59	5697.80	12927.00	14398.00	5239.60
Max	420.79	488.57	6101.80	54443.00	22309.00	31185.00

The results from these tables show that the forces and moments associated with these additional flight events are almost an order or magnitude less than the interfaces loads developed during Liftoff and Airloads. The maximum loads due to Second Stage ignition and Fairing Separation are roughly the same order of magnitude as the maximum loads predicted for MECO.

7.3 Verification Coupled Loads Analysis (VCLA)

The VCLA for the GLAST mission was completed in October 2007. The VCLA results are documented in the ULA report entitled "GLAST-Delta 7920H Verification Loads Cycle Dynamic Results Analysis (Rev 1) [ref. 7]". This report documents the structural dynamic response analysis performed to determine the maximum expected dynamic accelerations, displacements, and loads for the GLAST spacecraft during launch.

The dynamic portion of the payload design or verification CLA (or base drive analysis) outputs are typically increased by a dynamic uncertainty factor (DUF) to account for the maturity of the design, fidelity of the dynamic model, and level of test correlation. Typically at PDR a factor of 1.4 or 1.5 is applied to the dynamic responses. The factor is usually reduced to 1.25 by CDR when the design has been frozen and the model is mature. The DUF may be further reduced to 1.1 or 1.0 after successful test-correlation of

	NASA Engineering and Safety Center Technical Assessment Report	Document #:	Version:
		NESC- RP-06-071	1.0
Title: Flight Force Measurements of the Gamma-Ray Large Area Space Telescope / Delta II Flight		Page #: 143 of 226	

the payload dynamic model. For the GLAST Project, the payload model used for the VCLA had been verified by a traditional modal survey. Thus, the VCLA results cited in this report reflect a DUF of 1.0. Note that the GLAST VCLA model with the PAF was further correlated based on measured impedance data from the GLAST shaker testing performed after completion of the VCLA.

7.3.1 VCLA Liftoff Analysis

The liftoff analysis consists of a time integrated transient response from the flight time of T-0.865 seconds (main engine ignition) to T+1.135 seconds. The integration for response was performed in three steps corresponding to the flight conditions:

1. Prelaunch, in which the vehicle is resting on the pad and is connected to the pad in all six d-o-f ($x, y, z, \theta_x, \theta_y, \theta_z$);
2. Liftoff, in which the vehicle is moving off the pad, but has not cleared the launch mount shear pins, and is connected to the pad in the y, z, θ_x d-o-f, but free in x, θ_y , and θ_z ;
3. Free-flight, in which the vehicle is clear of the pad.

At each step, the pad reaction forces are calculated and applied to the next step. Non-linear corrections are made to the lateral pad reactions during the liftoff step to simulate slippage on the shear pins as the vehicle ascends.

The Delta II liftoff dynamic response analysis considers four sources of vehicle excitation:

1. Ignition thrust transients of the main engine and 6 GEMs
2. Lateral ignition induced overpressure forces
3. Lateral ground wind forces
4. Launch vehicle to pad interaction during Liftoff

The ignition thrust of the RS-27A 12:1 main engine was derived from the RS-27 8:1 main engine chamber pressure time histories from 7 Delta 6925 flights. These pressures were converted to net thrust for each flight and adjusted to a mean + 3-sigma level according to the pressure variance. The 3-sigma RS-27 8:1 thrust level was then adjusted to a 3-sigma RS-27A 12:1 thrust level by accounting for the difference in exhaust gas expansion at sea level. The ignition thrust of the 46-inch GEM was derived using static fire test data.

The ignition overpressures on the launch pad B were a result of inlet wave pressures originating near the launch deck and include exit wave pressures resulting from the addition of a 150-foot long launch duct. The inlet wave forces were derived from Delta II 6925. The Delta II 6925 overpressure forces were adjusted to reflect Delta II 7925H

	NASA Engineering and Safety Center Technical Assessment Report	Document #: NESC- RP-06-071	Version: 1.0
Title: Flight Force Measurements of the Gamma-Ray Large Area Space Telescope / Delta II Flight		Page #: 144 of 226	

characteristics. These forces have frequency content to 40 Hz. The exit wave forces were derived from analytical calculations of the pressure at the launch duct exit and flight data from launch vehicles with similar ducts.

The ground wind forces applied to the Delta II 7920H-10 launch vehicle were derived from vehicle lateral drag coefficients and an assumed boundary layer velocity distribution. In the GEM region, drag force was applied to the motors and the booster. Forces were applied only to those GEMs having frontal area to the upstream wind direction.

Sixteen independent liftoff cases were analyzed in two sets for each launch pad, resulting in a total of 32 liftoff cases. Figures 7.3-1 through 7.3-4 compare the data measured for the GLAST mission during liftoff with the comparable results from the Liftoff analysis. The data is shown for the liftoff case that produced the maximum acceleration or force for the particular direction being compared. The VCLA data is then compared with the corresponding measured values from the SFI system either centerline accelerations or forces calculated using the SFM.

Figure 7.3-1 and Figure 7.3-2 show a comparison for the Y-axis and the Z-axis (thrust) accelerations at the PAF base. Because the coupled loads are intended to cover a 3-sigma level input, it is expected that the acceleration levels predicted by the VCLA should be greater than those measured directly by the SFI accelerometers. The corresponding force comparisons at the GLAST spacecraft separation plane are shown in Figure 7.3-3 and 7.3-4. It can be seen that the VCLA forces over-predict the interface forces measured during flight and consistent with the amount of over-prediction seen in the acceleration results for the Y and Z axes.

	NASA Engineering and Safety Center Technical Assessment Report	Document #:	Version:
		NESC- RP-06-071	1.0
Title: Flight Force Measurements of the Gamma-Ray Large Area Space Telescope / Delta II Flight			Page #: 145 of 226

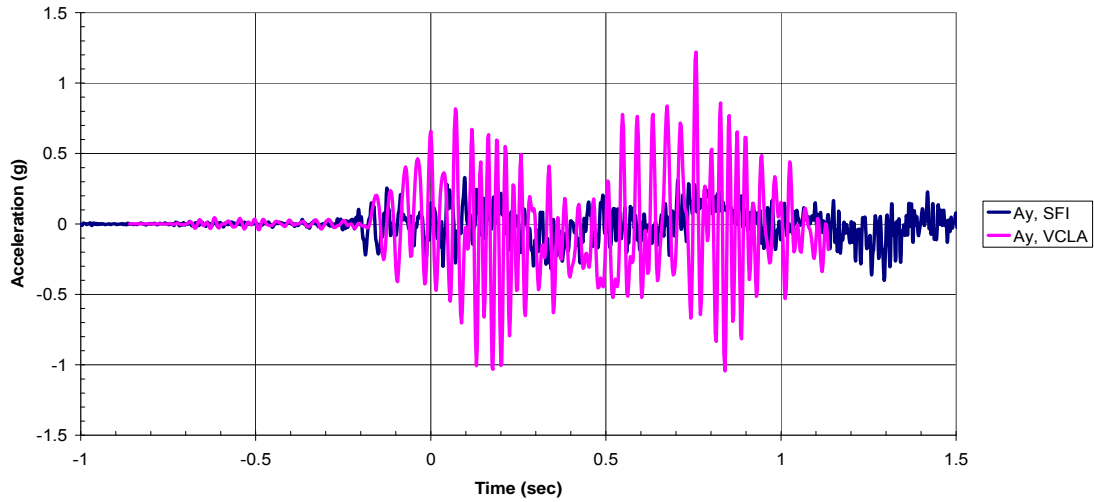


Figure 7.3-1. VCLA Y-Axis Liftoff Acceleration (Load Case = 27) versus SFI Data

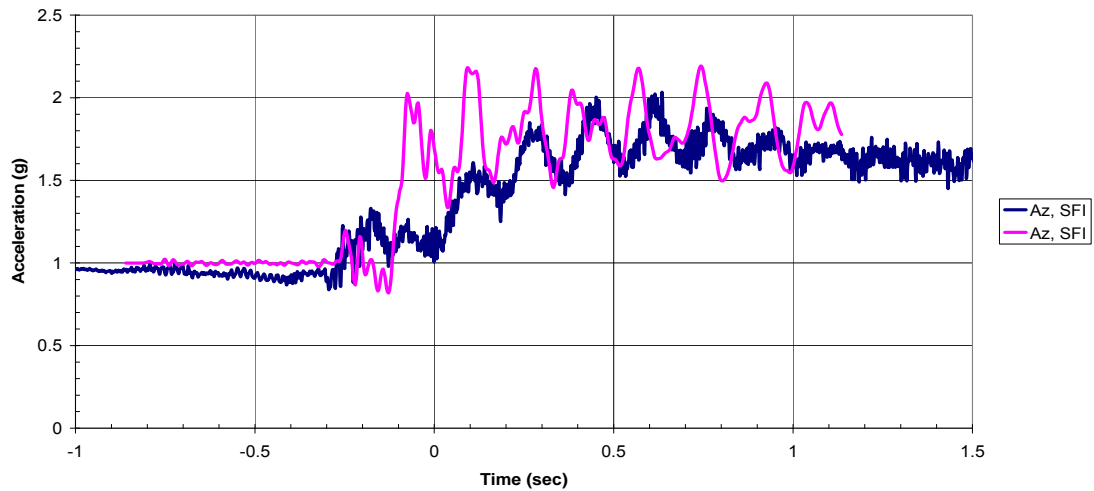


Figure 7.3-2. VCLA Z-Axis Liftoff Acceleration (Load Case = 18) versus SFI Data

	NASA Engineering and Safety Center Technical Assessment Report	Document #:	Version:
		NESC- RP-06-071	1.0
Title: Flight Force Measurements of the Gamma-Ray Large Area Space Telescope / Delta II Flight		Page #: 146 of 226	

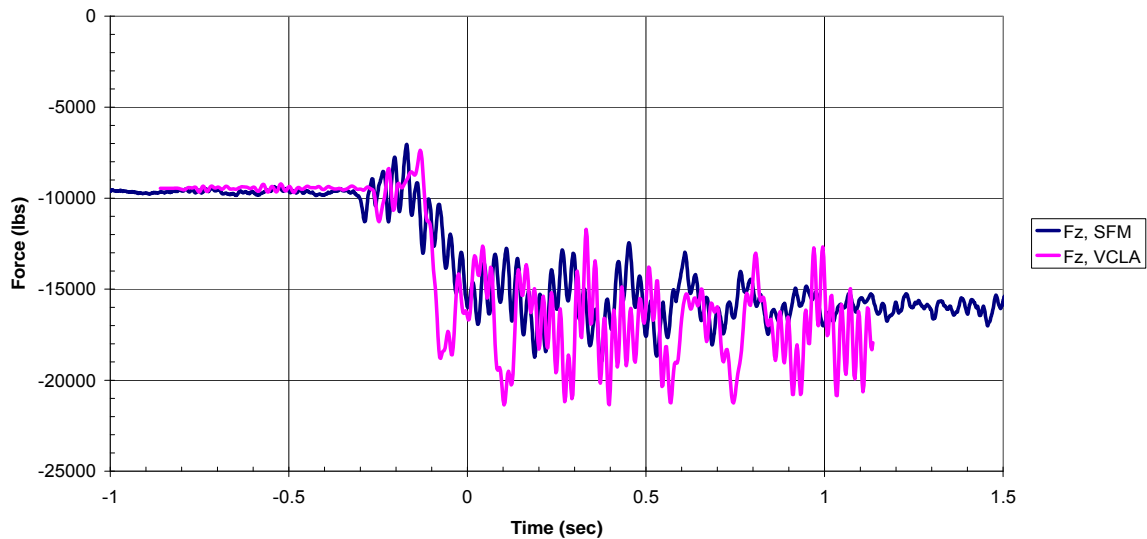


Figure 7.3-3. VCLA Z-Axis Liftoff Force (Load Case = 18) versus SFM

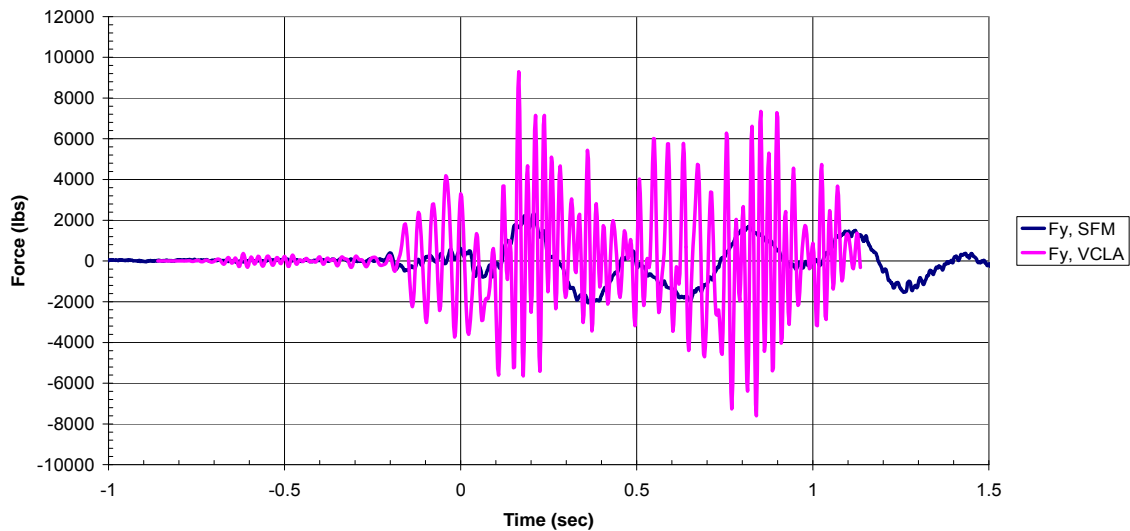


Figure 7.3-4. VCLA Y-Axis Liftoff Force (Load Case = 23) versus SFM

Table 7.3-1 shows an overall comparison between the maximum accelerations and forces predicted by the VCLA for Liftoff with the same quantities measured by the SFI system. The table shows that while both accelerations and forces calculated by the VCLA over-predict the comparable quantities measured during flight, the forces tend to show a larger relative over-prediction compared to the accelerations. This would indicate that if the

	NASA Engineering and Safety Center Technical Assessment Report	Document #:	Version:
		NESC- RP-06-071	1.0
Title: Flight Force Measurements of the Gamma-Ray Large Area Space Telescope / Delta II Flight		Page #: 147 of 226	

VCLA results were scaled to match the peak accelerations measured during flight, the CLA would over-predict the interface forces and moments.

Table 7.3-1. Comparison of VCLA Predictions versus Measured SFI Data for Liftoff

	X (g)	Y (g)	Z (g)	Rx (rad/sec ²)	Ry (rad/sec ²)	Rz (rad/sec ²)
VCLA	0.757	1.5	2.243	5.064	3.357	1.549
SFI	0.285	0.401	2.034	4.437	2.545	1.464
	166%	274%	10%	14%	32%	6%
	Fx (lbs)	Fy (lbs)	Fz (lbs)	Mx (in-lbs)	My (in-lbs)	Mz (in-lbs)
VCLA	5477	9454.6	22887.9	385609	328252	25808
SFI	1121	2321	19004	140658	67612	22984
	389%	307%	20%	174%	385%	12%

To put the CLA results into perspective, assume a typical expendable launch vehicle (ELV) coefficient of variation (COV) of 1/3. COV is the relationship between the standard deviation and the mean. Further assuming the CLA results to be a 3-sigma value, then the following relationships can be defined:

- a) If the GLAST flight interface loads for the particular load event are assumed to be the mean of several flights, then the CLA result should predict values which are twice the mean (i.e., the CLA results would be 100 percent greater than the actual flight level).
- b) If the flight interface loads for a particular load event are assumed to be at the 1-sigma level among several flights, then the CLA result should reflect loads which are 1.5 times the mean (i.e., the CLA results would be 50 percent over the actual flight loads).

Under the assumptions described in the previous paragraph (assuming that the actual GLAST spacecraft interface loads were between the mean and 1-sigma), the CLA loads conservatism would therefore be expected to be 1.5 to 2.0 times over what was measured during flight. Based on the data shown in Table 7.3-1, Fx, Fy, and My have been over-predicted by the VCLA, and Fz and Mz have been under-predicted. Fz includes the steady state thrust force, which is a predictable value on each flight such that one would expect the thrust forces to show agreement with the CLA prediction. The most noticeable under-prediction would be for Mz. It should be noted that the relationship between this flight and others in terms of load is not known.

	NASA Engineering and Safety Center Technical Assessment Report	Document #:	Version:
		NESC- RP-06-071	1.0
Title: Flight Force Measurements of the Gamma-Ray Large Area Space Telescope / Delta II Flight		Page #: 148 of 226	

To continue this line of thinking and from the ULA report [ref. 9], the NESC team approximated this from the comparison of the GLAST peak accelerations flight with previous flights. For Liftoff, the data suggest that GLAST spacecraft accelerations have been average. In any case, that F_x , F_y , and M_y show 300 to 400 percent, while F_z and M_z were 10 to 20 percent is an indication that at least one of the two groups in the VCLA were too high or low as 3-sigma predictions.

Based on the Delta II / GLAST spacecraft ULA Post-Flight report [ref. 9], the acceleration levels measured during Liftoff on this flight reached mean levels based on data from 39 similar Delta II (10C/L Fairing, AUV) flights (See Figure 6.5-1). Therefore, it was assumed that the loads measured in flight (SFM) during Liftoff also reflect the mean of those 39 flights.

Using the typical COV of 1/3, which estimated the P99/90 load the CLA predicted as:

$$P99/90 = \mu + k_{99/90/39} \sigma = \mu(1 + K_{99/90/39} * 1/3)$$

The plot of single tolerance factors (STF) for P99/90 is presented in figure 7.3-5. For the GLAST flight, $n=39$.

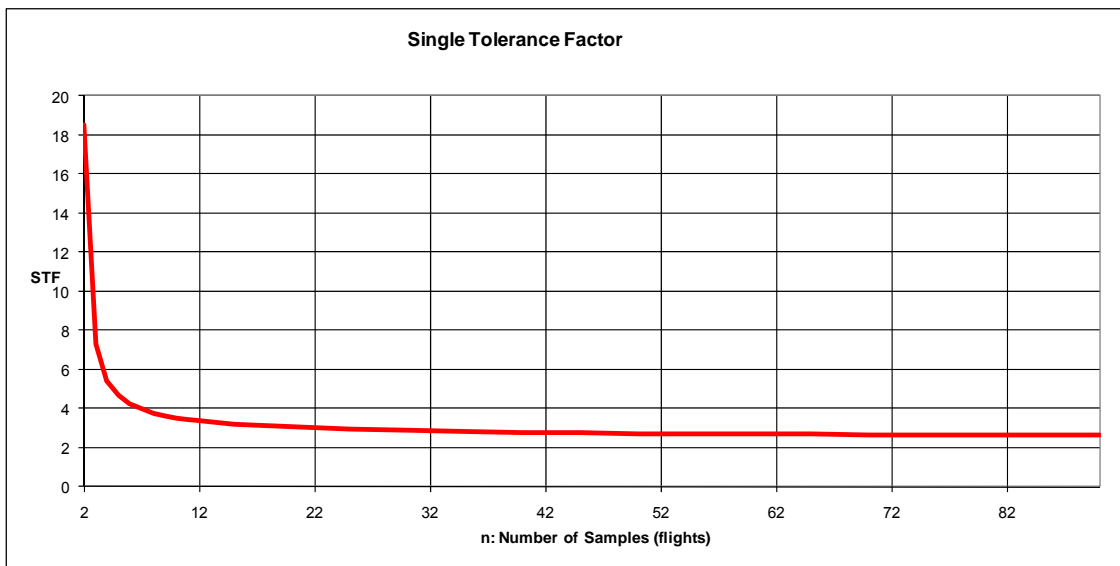


Figure 7.3-5. Tolerance Factor

The NESC team used the thrust axis force (dynamic portion), overturning moment M_y , and torsional moment M_z . The results are summarized in Table 7.3-2.

	NASA Engineering and Safety Center Technical Assessment Report	Document #:	Version:
		NESC- RP-06-071	1.0
Title: Flight Force Measurements of the Gamma-Ray Large Area Space Telescope / Delta II Flight			Page #: 149 of 226

Table 7.3-2. VCLA Liftoff Results Compared with SFM Forces Scaled to P99/90

Liftoff	Fz [lb]	Mz [in lb]	My [in lb]
SFM	5697	22984	67612
CLA	9581	25808	328252
$k_{99/90/90}$	2.80	2.80	2.80
μ (mean)	5697	22984	67612
σ (standard deviation)	1899	7661	22537
P99/90	11014	44436	130717
CLA to P99/90 underprediction	15%	72%	
CLA to P99/90 overprediction			151%

7.3.2 VCLA Airloads Analysis

A similar comparison of VCLA results to measured SFI data that was performed for the Liftoff was completed for the Airloads. For the Delta II launch vehicle in the heavy configuration, the Airloads analysis was performed for three independent flight times consisting of Transonic Mach 0.86 (T+26 seconds), Transonic Mach 1.0 (T+30 seconds), and Max-Q (T+40 seconds). Within each of these flight times, the analysis was performed to cover response due to buffet, gusts, and static-elastic loading (STEL). The results of these analyses are combined statistically to determine the overall response for the specific flight time. The gust analysis was performed in the time domain as a transient analysis in which the gust forcing functions were tuned to specific vehicle bending modes. The buffet analysis was performed as a random dynamic response analysis in the frequency domain. The peak 3-sigma responses from the random buffet analysis were combined with the maximum and minimum gust results in each of the lateral axes resulting in four load cases per event.

Since the Airloads analysis results were the product of a combination of time domain and frequency domain results, it is not possible to extract a time history corresponding to the maximum loading cases for the VCLA Airloads analysis for the GLAST mission. Table 7.3-3 shows the comparison between the absolute maximum accelerations and forces predicted by the VCLA analysis as compared to the comparable quantities measured during GLAST mission by the SFI instrumentation. The table shows the VCLA results over-predict the measured data as expected, but that unlike Liftoff, the percentage over-prediction is comparable between accelerations and forces. This would indicate that if the VLCA analysis was scaled to match the measured accelerations, then the predicted forces would show a reasonable agreement with the measured forces during flight.

	NASA Engineering and Safety Center Technical Assessment Report	Document #:	Version:
		NESC- RP-06-071	1.0
Title: Flight Force Measurements of the Gamma-Ray Large Area Space Telescope / Delta II Flight		Page #: 150 of 226	

Table 7.3-3. Comparison of VCLA Predictions Versus Measured SFI Data for Airloads

	X (g)	Y (g)	Z (g)	Rx (rad/sec ²)	Ry (rad/sec ²)	Rz (rad/sec ²)
VCLA	1.532	1.588	2.691	4.205	4.277	2.136
SFI	0.600	0.706	2.518	2.854	3.412	8.833
	155%	125%	7%	47%	25%	-76%
	Fx (lbs)	Fy (lbs)	Fz (lbs)	Mx (in-lbs)	My (in-lbs)	Mz (in-lbs)
VCLA	12078	12017	26060	766193	765807	46662
SFI	4597	4695	24582	288019	358479	247629
	163%	156%	6%	166%	114%	-81%

As with Liftoff, the VCLA over-predicts the lateral shears and moments (e.g., Fx, Fy, Mx, and My) by more than 100 percent although there is better agreement between the over-prediction seen in both the forces and accelerations. As with Liftoff, the thrust axis force (Fz) shows agreement with the VCLA predictions. The torsional moment (Mz) however is under-predicted by 81 percent. Based on the Delta II Payload Planner's Guide (PPG) [ref. 12], the 3-sigma payload center of gravity limit load factor is ± 2 g for the GLAST spacecraft payload weight. The payload maximum allowed offset from the vehicle centerline is 0.8 inches. The GLAST spacecraft offset (lateral RSS) was 0.36 inches. For a 9,643 pound payload plus PAF the predicted torsional moment for GLAST and for the maximum allowable case are:

$$\begin{aligned} Mz \text{ GLAST} &= 6,866 \text{ in lb at } 0.36 \text{ inches} \\ Mz \text{ maximum} &= 15,414 \text{ in lb at } 0.8 \text{ inches} \end{aligned}$$

The above calculation indicates that estimates of the expected torsional moment using the load factors provided in the PPG significantly under-predicts what was actually measured on the GLAST flight. As is typically with most launch vehicles, the design load factors specified for payload design do not include rotational accelerations.

By performing the same calculations for lateral moments:

$$\begin{aligned} \text{GLAST CGz} &= 53 \text{ inches} \\ Mx \text{ or } My \text{ maximum} &= 1.02 \text{ E6 in lb} \end{aligned}$$

The maximum bending moment for GLAST calculated from the PPG limit loads does indeed envelope what was measured during flight. Note that these lateral moments from the PPG are applied one axis at a time and combined with the PPG axial loads to size the primary structure.

	NASA Engineering and Safety Center Technical Assessment Report	Document #:	Version:
		NESC- RP-06-071	1.0
Title: Flight Force Measurements of the Gamma-Ray Large Area Space Telescope / Delta II Flight		Page #: 151 of 226	

The same exercise as for Liftoff was performed to evaluate the measured flight data against the VCLA results for Airloads. In this case the ULA Post-Flight Report [ref. 9] places the Airloads on the GLAST flight as a P95/50 event (See Figure 6.5-1). Table 7.3-4 shows a comparison of the measured torsional moment (M_z) and the overturning moment (M_y) scaled to a P99/90 level as compared with the VCLA results. As can be seen from the table, the VCLA results under-predicts the torsional moment by a significant margin, but over-predicts the corresponding lateral moment.

Table 7.3-4. VCLA Airloads Results Compared with SFM Forces Scaled to P99/90

Airloads	M_z [in lb]	M_y [in lb]
SFM	247629	358479
CLA	46662	765807
$k_{95/50/39}$	1.66	1.66
$k_{99/90/39}$	2.80	2.80
μ (mean)	159418	230780
σ (standard deviation)	53139	76927
P99/90	308208	446176
CLA to P99/90 underprediction	561%	
CLA to P99/90 overprediction		72%

The significant under-prediction of the torsional moment by the VCLA and the magnitude of the moment measured during flight were not expected. Therefore, time was spent to review the flight data and the calculation methodology to verify that what was being measured for the torsional moment during Airloads was accurate. The conclusion was that the measured torsional moment for the GLAST flight during Airloads appears to be correct and significantly exceeded the VCLA predictions. This conclusion is based on the following:

- Ability of the SFM approach to accurately measure torsional moments was evaluated as part of the static loads testing (Tables 6.3-5 and 6.3-6). There were no issues identified and the prediction accuracy was comparable to that of the bending moments (Table 6.3-7).
- The SFM approach was accurate to 5 percent when the torsional moment exceeds 25,000 in-lbs (Table 6.3-7). This was below the 247,000 in-lbs measured during Airloads.
- Peak rotational acceleration about the thrust axis, which is independently calculated based on the SFI accelerometers, also significantly exceeds the VCLA

	NASA Engineering and Safety Center Technical Assessment Report	Document #:	Version:
		NESC- RP-06-071	1.0
Title: Flight Force Measurements of the Gamma-Ray Large Area Space Telescope / Delta II Flight		Page #: 152 of 226	

prediction and shows the same magnitude of over-prediction as the torsional moment (Table 7.3-3).

- Results from the basedrive analysis using the independently measured SFI accelerations show peak torsional moments which match the measured SFM data within 10 percent (Table 7.5-2).
- The peak torsional moment and rotational acceleration during Airloads achieve their maxima at the same flight time (Table 7.2-3 and 7.2-4).
- SRS of the torsional moment and rotational acceleration about the thrust axis both peak at 10 Hz, which corresponds to the launch vehicle torsional mode (Figures 7.2-24 and 7.2-29).

It appeared from the data that the torsional moment during Airloads was directly related to an excitation of the launch vehicle torsional mode, which was not accurately represented in the GLAST VCLA.

7.3.3 VCLA Summary

- For Liftoff, both accelerations and forces predicted by the VCLA envelope the acceleration and forces measured during flight.
- VCLA forces show a larger percentage of over-prediction as compared with flight data than do the accelerations for Liftoff especially for Fx and My.
- For Liftoff, the interface lateral forces (Fx and Fy) and overturning moments (Mx and My) from the VCLA over-predict the measured flight forces when scaled to a P99/90 level assuming Liftoff on the GLAST flight was a mean event as compared with measured acceleration data from comparable Delta II flights as shown in the ULA Post-Flight Report.
- For Liftoff, the thrust axis force (Fz) and the torsional moment (Mz) from the VCLA under-predict the measured flight forces scaled to a P99/90 level assuming Liftoff on the GLAST flight was a mean event.
- For Airloads, the VCLA results envelope the accelerations and forces measured during flight with the exception of the torsional acceleration and corresponding torsional moment. The VCLA results significantly under-predicted the measured torsion acceleration and moment measured during the GLAST flight.
- The percentage of over-prediction between the Airloads VCLA results and the measured SFI data is comparable between lateral accelerations and lateral loads as well as between lateral accelerations and overturning moments.
- The torsional moment measured in flight during Airloads has been significantly under-predicted by the VCLA results (46,600 in lb < 24,7600 in lb) and is not covered by the Delta II Planners Guide limit load factors (worst case 15,414 in lb << 24,7600 in lb).

	NASA Engineering and Safety Center Technical Assessment Report	Document #:	Version:
		NESC- RP-06-071	1.0
Title: Flight Force Measurements of the Gamma-Ray Large Area Space Telescope / Delta II Flight		Page #: 153 of 226	

- The GLAST VCLA Airloads results for lateral moments had an equivalent $k_{99/90}$ of 6.95, which may have been a valid number for the first three flights only.
- For Airloads, there has been a simultaneous over-prediction of the lateral forces and moments and an under-prediction of the torsional moment by the VCLA results when the measured flight forces are scaled to a P99/90 level assuming that Airloads on the GLAST flight was a P95/50 event as shown in the ULA Post-Flight Report.

7.4 Liftoff Reconstruction and Reconciliation

7.4.1 Full Liftoff Reconstruction

Results of the VCLA liftoff analysis, as described previously, were found to be conservative in regards to predicting the PAF accelerations. The reconstruction was formulated by modifying the Liftoff analysis to take advantage of forces measured during the GLAST spacecraft flight with the goal of matching the measured PAF accelerations. Forces measured in flight include main engine and GEM thrust profiles, and wind direction and magnitude. This left the lateral ignition induced overpressure forces as the only unknown. For the initial run, the analytical overpressure forces were arbitrarily reduced by 50 percent and analyzed with the measured thrust and wind quantities. The pad reaction forces were calculated and PAF accelerations were recovered. The resulting accelerations from this initial case produced mixed results (i.e., exceeding measured data in one lateral direction, but under-predicting in the other). The axial direction, which was not significantly affected by overpressure forces matched. To improve the agreement between the reconstruction and flight data, a trial and error approach was necessary in regards to modifying the overpressure forces. In the end, the modifications were both direction and frequency specific.

The final reconstruction can be summarized as:

- Same models as VLC (system modes to 60 Hz).
- Four sources of vehicle excitation
 - Ignition thrust transients taken from flight data
 - RS-27A engine
 - 6 GEMs
 - Lateral ignition induced overpressure forces
 - Filtered the higher frequency content (>33 Hz)
 - Scaled forces in specific frequency ranges
 - Bidirectional scaling
 - Lateral ground wind forces used measured direction and magnitude
 - Launch vehicle to pad interaction during liftoff (calculated based on previously listed excitations)
- Diagonal system damping

	NASA Engineering and Safety Center Technical Assessment Report	Document #:	Version:
		NESC- RP-06-071	1.0
Title: Flight Force Measurements of the Gamma-Ray Large Area Space Telescope / Delta II Flight			Page #: 154 of 226

- 10 percent damping for spacecraft modes between 22 and 24 Hz, and 5 percent for all others
- 5 percent damping for vehicle modes (1.5 percent for VLC)
- Higher damping for Second Stage and engine modes (same as VLC)
- Specific damping for first (1.8 percent) and second (0.7 percent) axial system modes (same as VLC)

The final reconstruction provided agreement in the area of peak response, 20 to 30 Hz. A peak response at 3 Hz in the SC-y direction was under-predicted in the reconstruction. This response, outside the frequency range of concern, occurred because of the reduction in overpressure.

Figures 7.4-1 through 7.4-3 present interface acceleration results from the full reconstruction CLA and compares them with the flight measured and VLC accelerations at each of the four PAF interface locations.

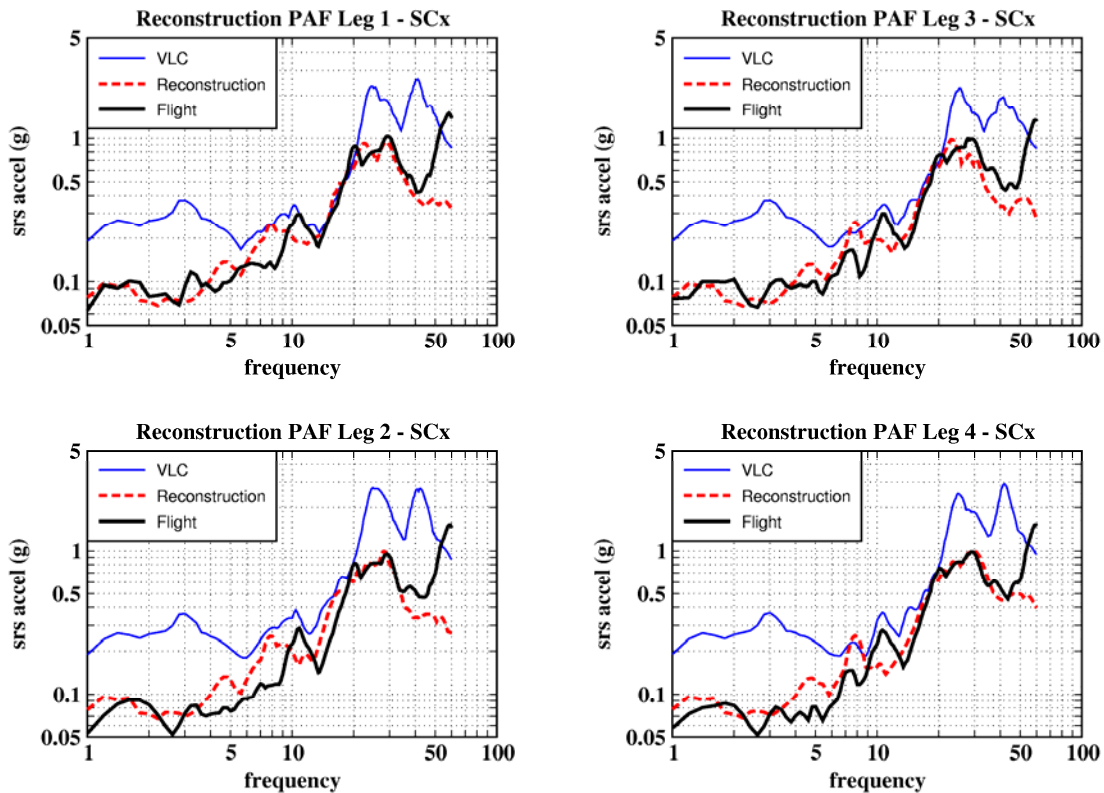


Figure 7.4-1. Reconstructed CLA X axis SRSs



NASA Engineering and Safety Center Technical Assessment Report

Document #:
**NESC-RP-
06-071**

Version:
1.0

Title:

Flight Force Measurements of the Gamma-Ray Large Area Space Telescope / Delta II Flight

Page #:
155 of 226

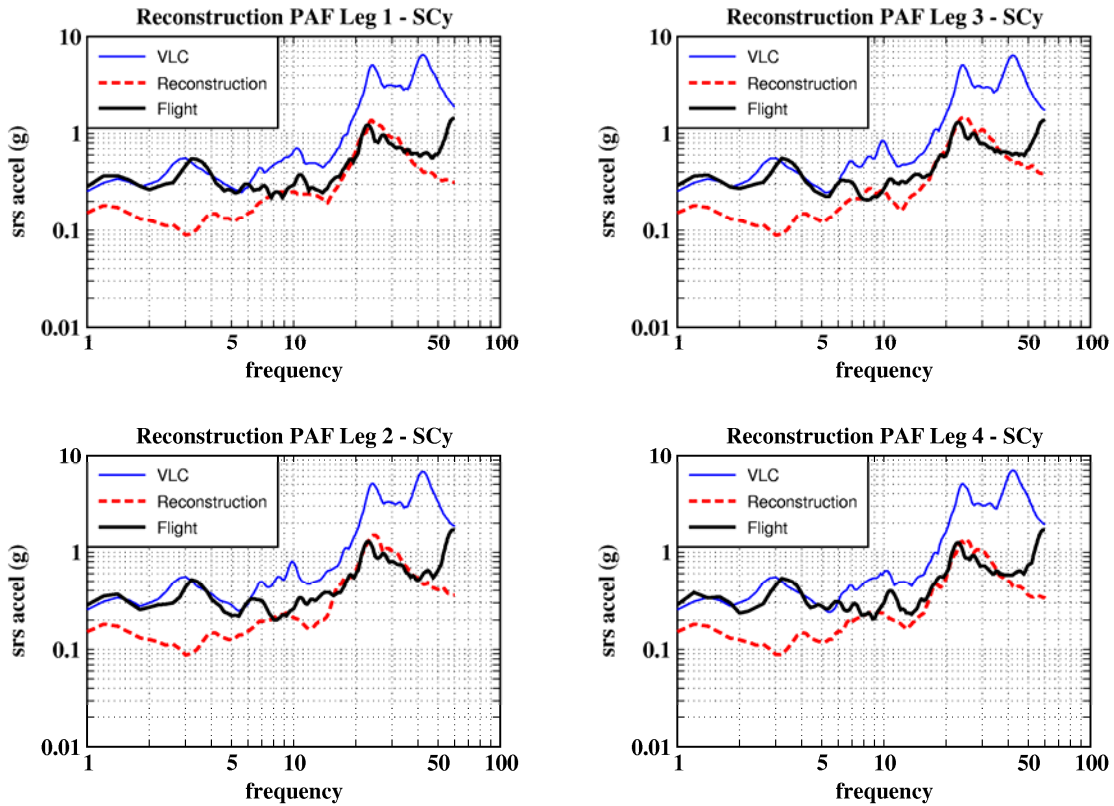


Figure 7.4-2. Reconstructed CLA Y axis SRSs



Title:

Flight Force Measurements of the Gamma-Ray Large Area Space Telescope / Delta II Flight

Page #:
156 of 226

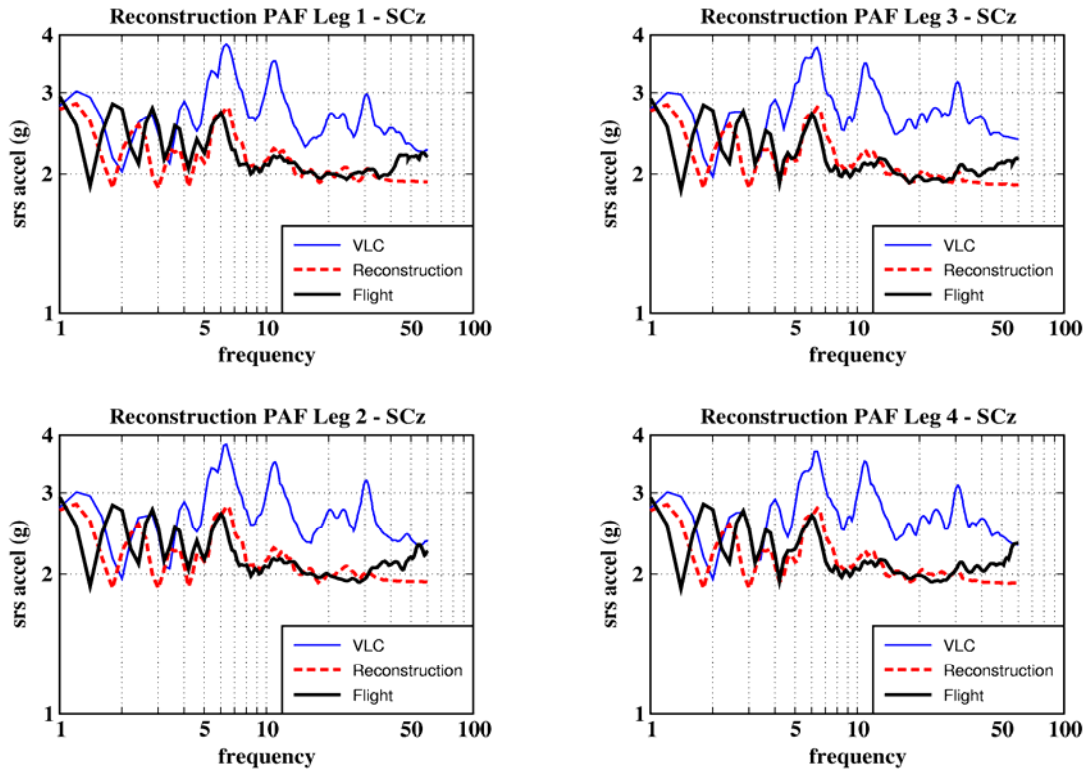


Figure 7.4-3. Reconstructed CLA Z axis SRSs

Figures 7.4-4 through 7.4-7 show the Full Liftoff reconstruction forces and corresponding SRSs.



NASA Engineering and Safety Center Technical Assessment Report

Document #:
**NESC-RP-
06-071**

Version:
1.0

Title:

Flight Force Measurements of the Gamma-Ray Large Area Space Telescope / Delta II Flight

Page #:
157 of 226

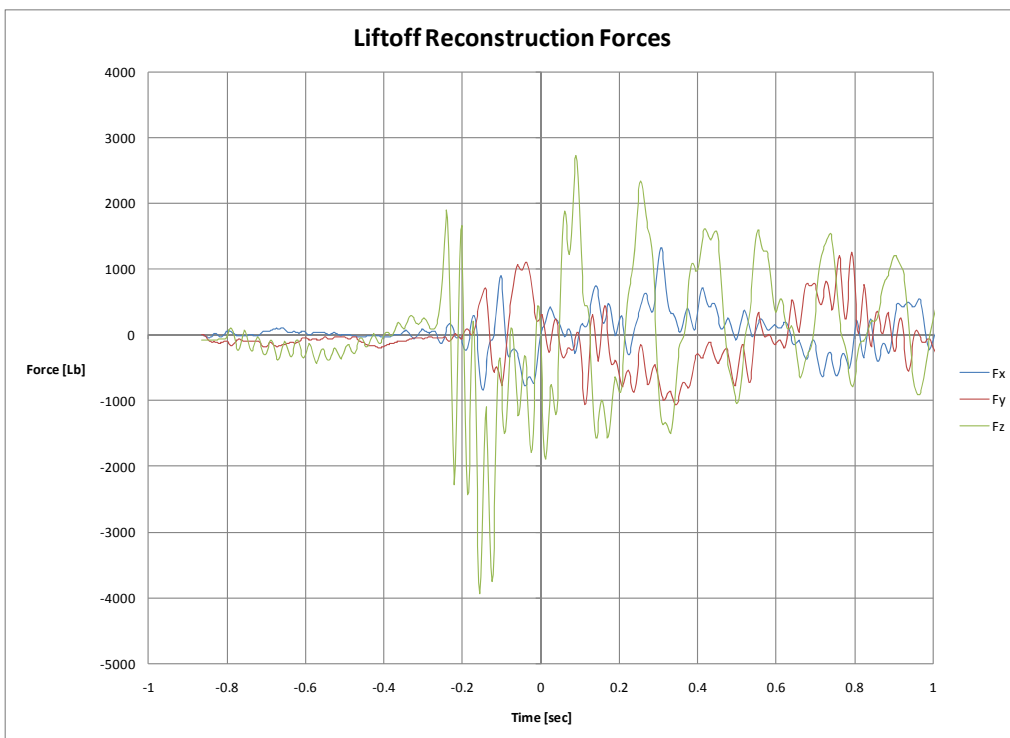


Figure 7.4-4. Liftoff Full Reconstruction Forces



NASA Engineering and Safety Center Technical Assessment Report

Document #:
**NESC-RP-
06-071**

Version:
1.0

Title:

Flight Force Measurements of the Gamma-Ray Large Area Space Telescope / Delta II Flight

Page #:
158 of 226

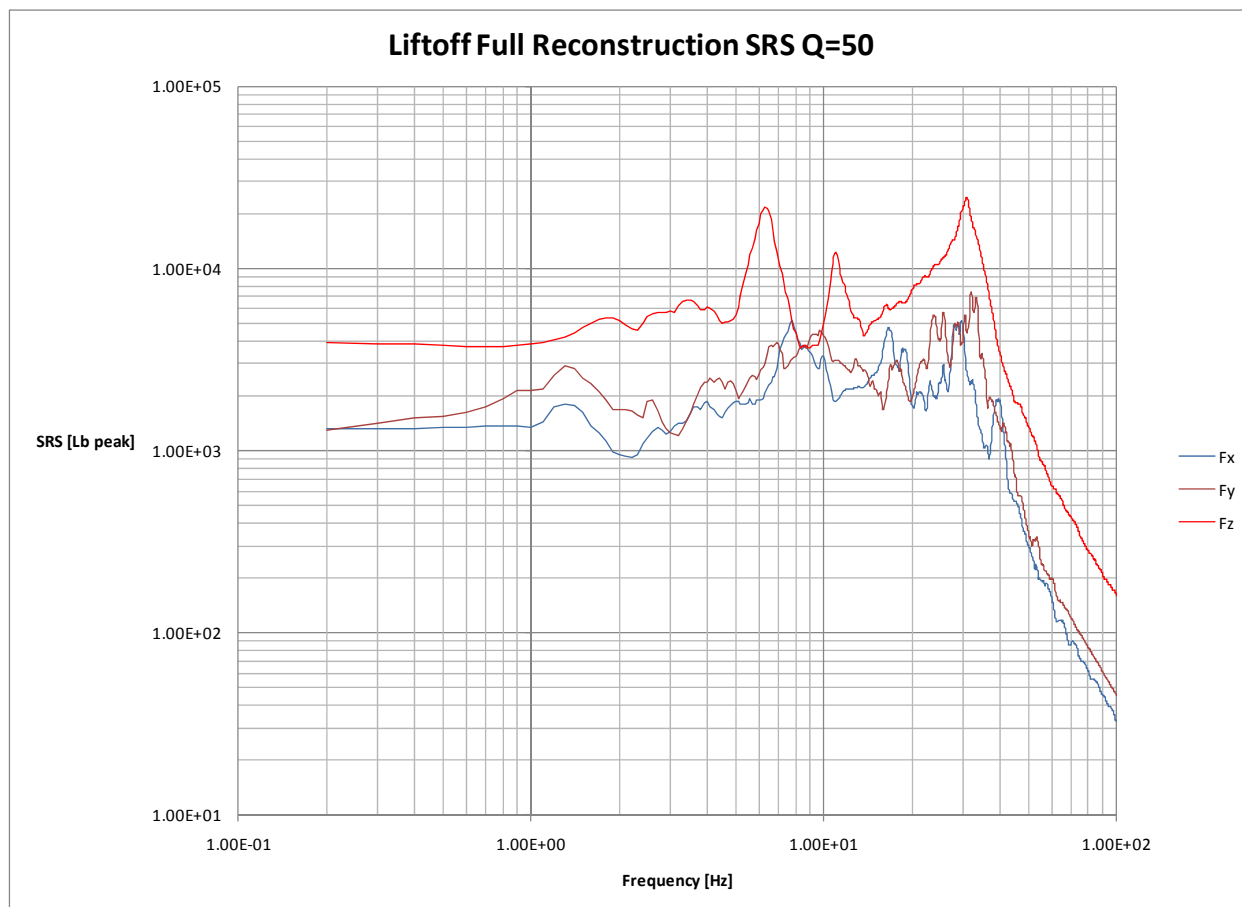


Figure 7.4-5. Liftoff Full Reconstruction Force SRSs



NASA Engineering and Safety Center Technical Assessment Report

Document #:
**NESC-RP-
06-071**

Version:
1.0

Title:

Flight Force Measurements of the Gamma-Ray Large Area Space Telescope / Delta II Flight

Page #:
159 of 226

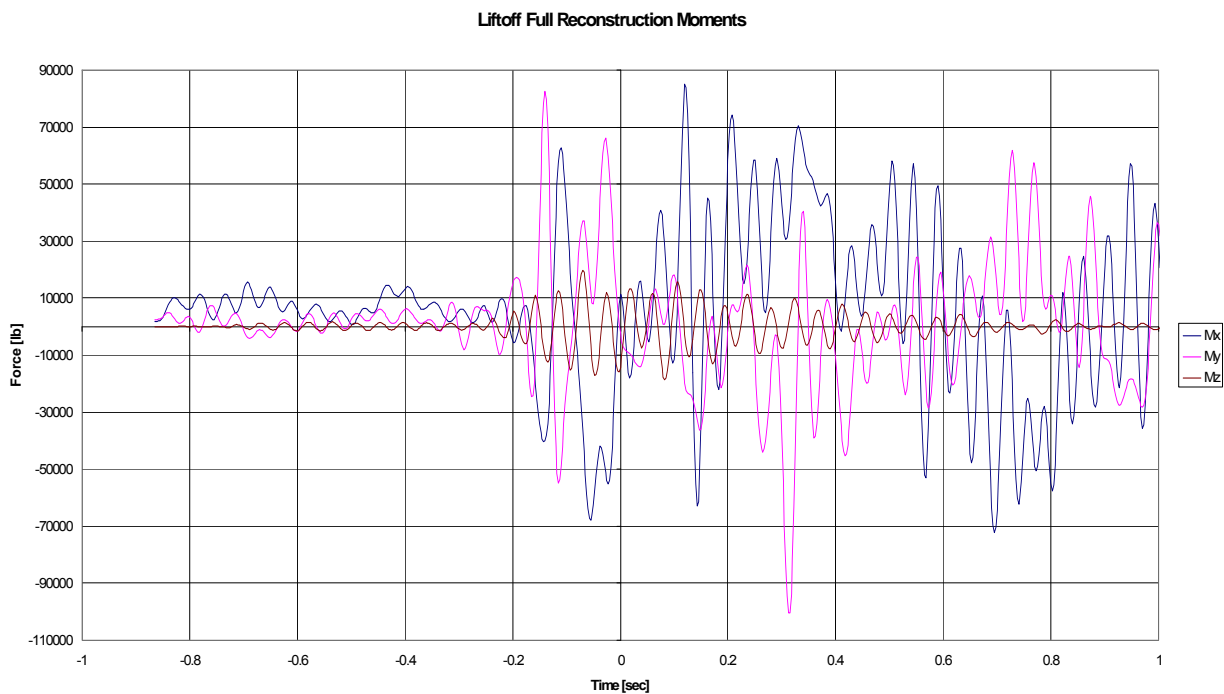


Figure 7.4-6. Liftoff Full Reconstruction Moments



Title:

**Flight Force Measurements of the Gamma-Ray Large
Area Space Telescope / Delta II Flight**

Page #:
160 of 226

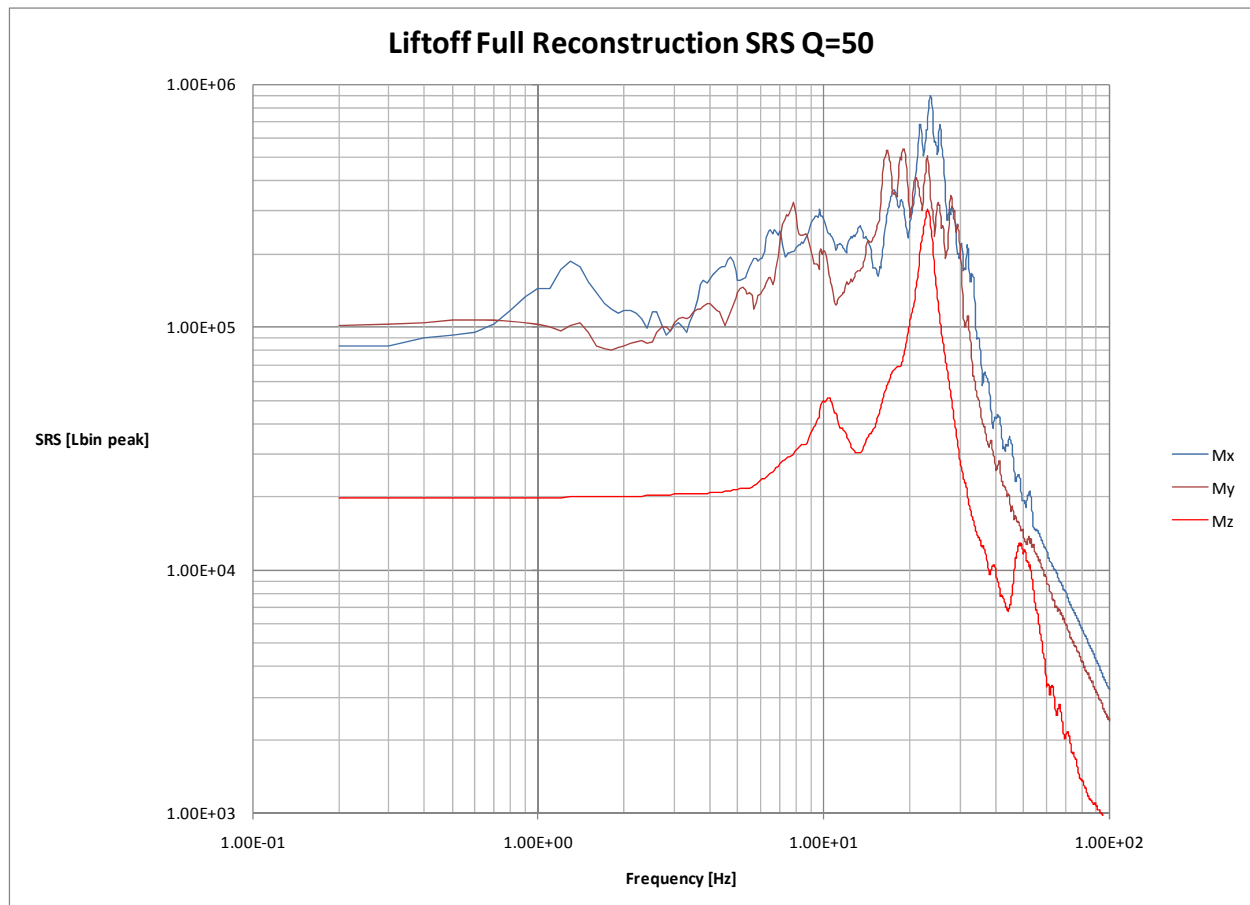


Figure 7.4-7. Liftoff Full Reconstruction Moment SRSs

Useful observations include:

- Lateral forces do not show content at the coupled system first bending mode around 3 Hz, the axial force had content at the coupled system axial mode around 6 Hz, and at the spacecraft mode of 32 Hz. Content above 60 Hz was flat.
- As expected (similar to the forces), the moments do not include content at the first coupled system bending of the coupled system.
- The torsional moment shows dominant content around 24 Hz, close to the spacecraft main torsional mode of 27 Hz.



Title:

**Flight Force Measurements of the Gamma-Ray Large
Area Space Telescope / Delta II Flight**

Page #:
161 of 226

7.4.2 Liftoff Basedrive Analysis - VCLA Model, 2 Percent Damping

Forces and moments at Liftoff are presented with their respective SRS in Figures 7.4-8 through 7.4-11.

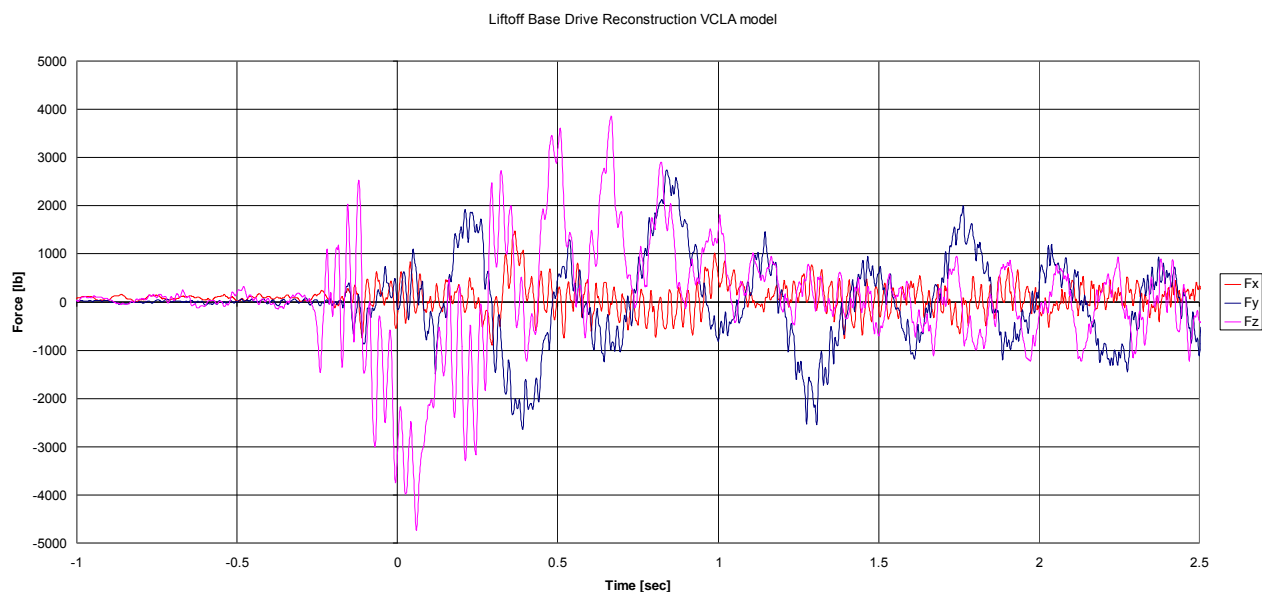


Figure 7.4-8. Liftoff Reconstruction VCLA Model Forces



Title:

**Flight Force Measurements of the Gamma-Ray Large
Area Space Telescope / Delta II Flight**

Page #:
162 of 226

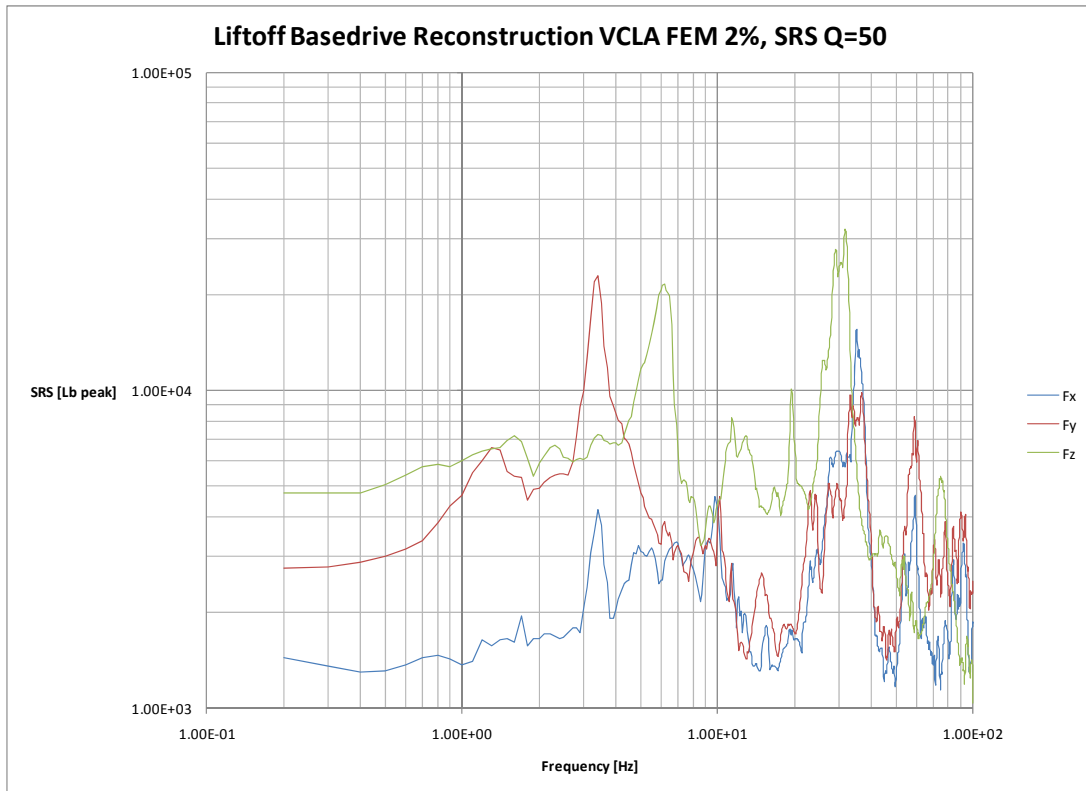


Figure 7.4-9. Liftoff Reconstruction VCLA Model Force SRSs

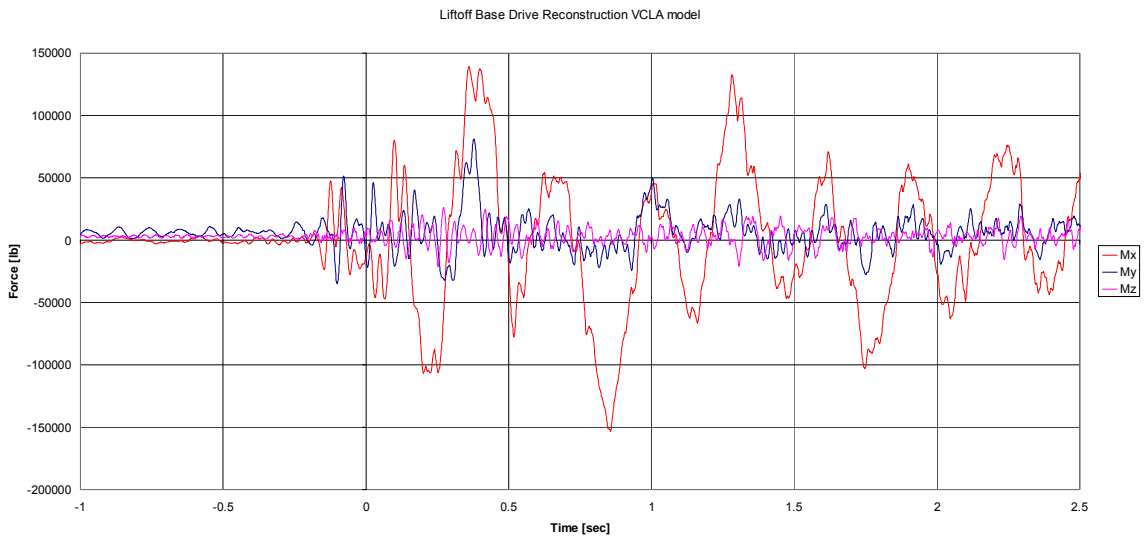


Figure 7.4-10. Liftoff Reconstruction VCLA Model Moments



Title:

**Flight Force Measurements of the Gamma-Ray Large
Area Space Telescope / Delta II Flight**

Page #:
163 of 226

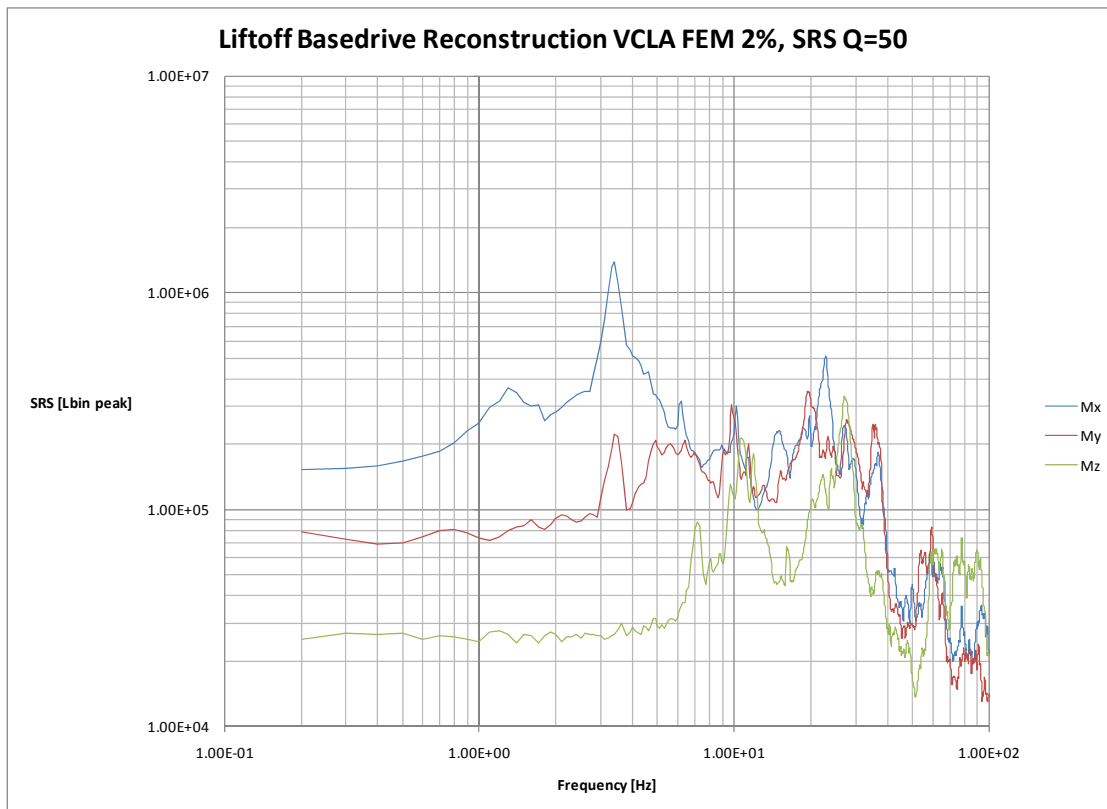


Figure 7.4-11. Liftoff Reconstruction VCLA Model Moment SRSs

The frequency content of forces and moments in the basedrive reconstruction coincide with the basedrive acceleration content presented in Section 7.1.1.4.

7.4.3 Liftoff Basedrive Analysis - Impedance Correlated Model

Similar to the previous section, but for the Impedance Correlated Model, forces and moments at Liftoff are presented with their respective SRS are shown in Figures 7.4-12 through 7.4-15.



NASA Engineering and Safety Center Technical Assessment Report

Document #:
**NESC-RP-
06-071**

Version:
1.0

Title:

Flight Force Measurements of the Gamma-Ray Large Area Space Telescope / Delta II Flight

Page #:
164 of 226

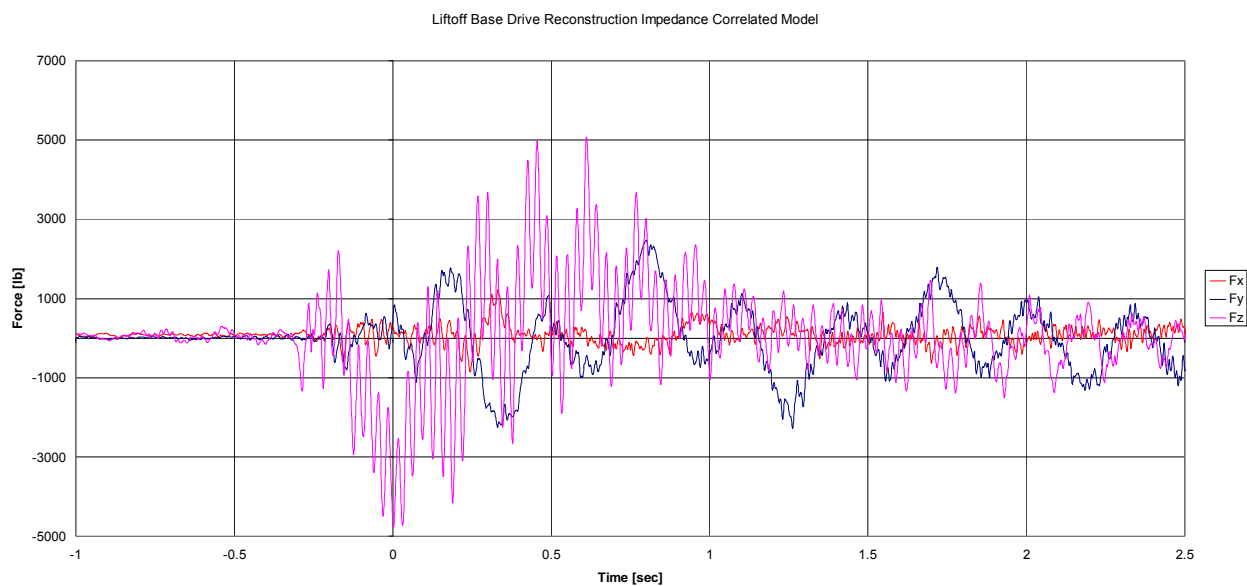


Figure 7.4-12. Liftoff Reconstruction Impedance Correlated Model Forces



Title:

**Flight Force Measurements of the Gamma-Ray Large
Area Space Telescope / Delta II Flight**

Page #:
165 of 226

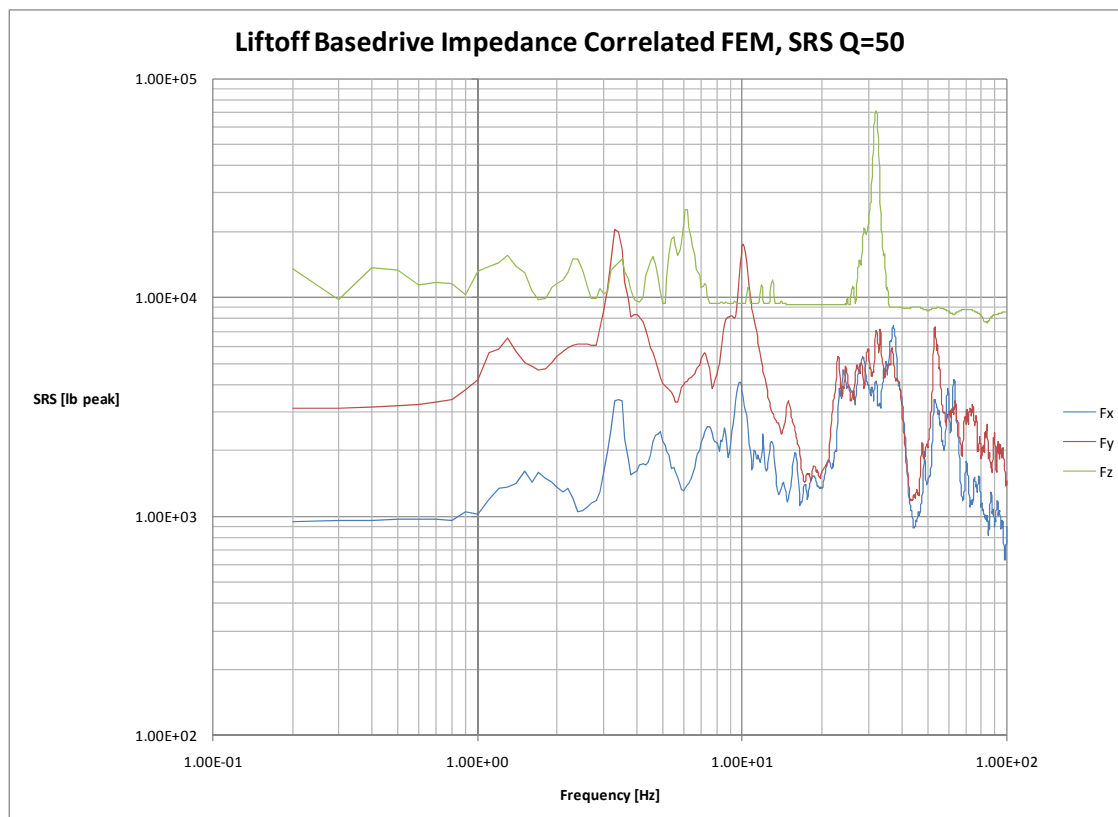


Figure 7.4-13. Liftoff Reconstruction Impedance Correlated Model Force SRSs

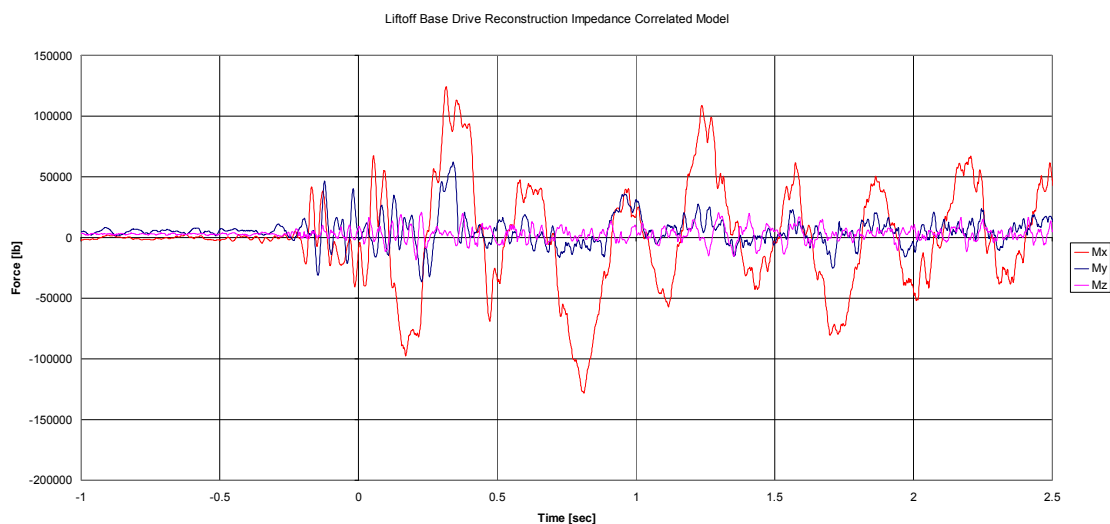


Figure 7.4-14. Liftoff Reconstruction Impedance Correlated Model Moments



NASA Engineering and Safety Center Technical Assessment Report

Document #:
**NESC-RP-
06-071**

Version:
1.0

Title:

Flight Force Measurements of the Gamma-Ray Large Area Space Telescope / Delta II Flight

Page #:
166 of 226

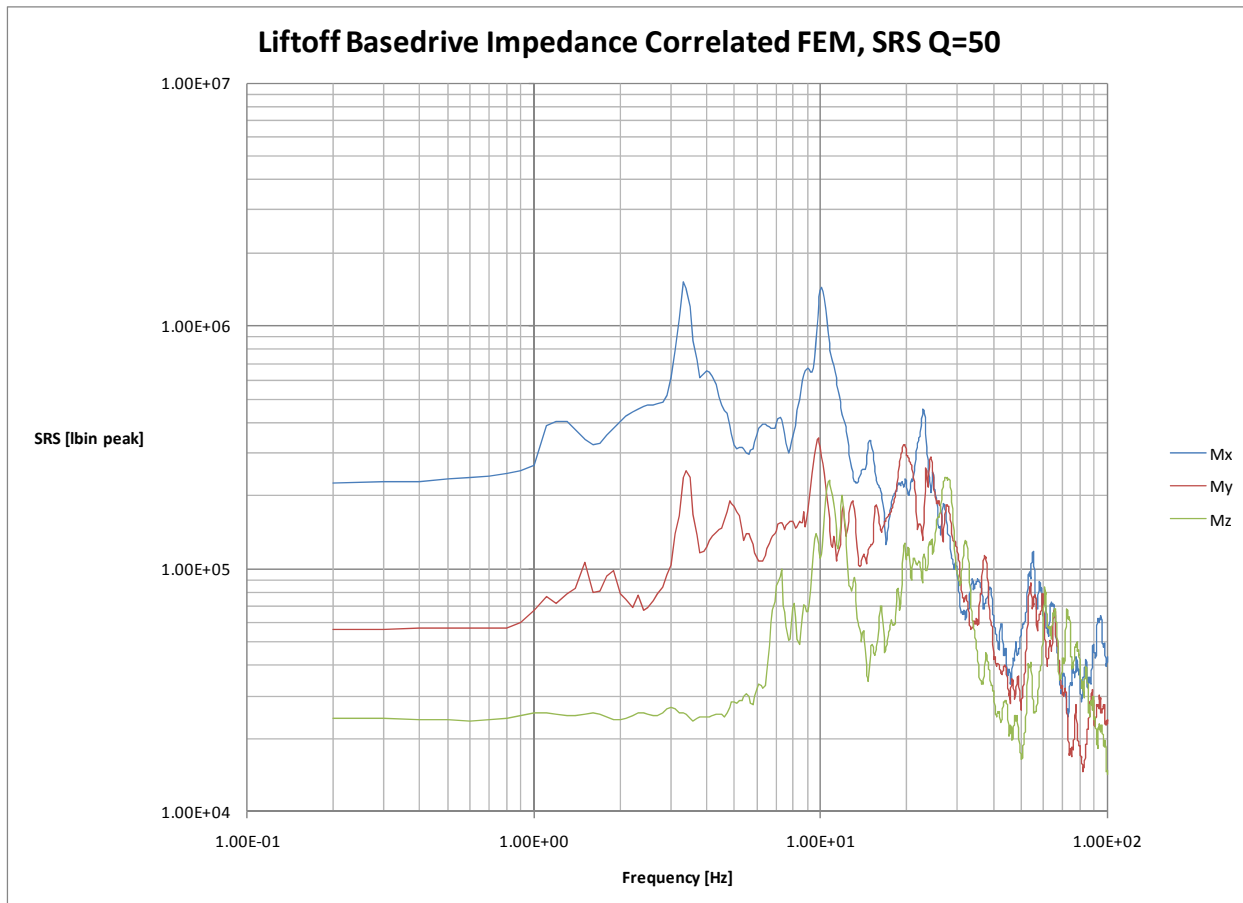


Figure 7.4-15. Liftoff Reconstruction Impedance Correlated Model Moment SRSs



Title:

**Flight Force Measurements of the Gamma-Ray Large
Area Space Telescope / Delta II Flight**

Page #:
167 of 226

7.4.4 Liftoff Analysis - Impedance Method

Figures 7.4-16 through 7.4-19 present the force predictions using the Impedance Method. Note that the thrust axis force magnitude produced from the inverse fourier transform was reversed in sign. This was corrected by multiplying for -1. It was an effect to check and consider when adding or subtracting the steady state.

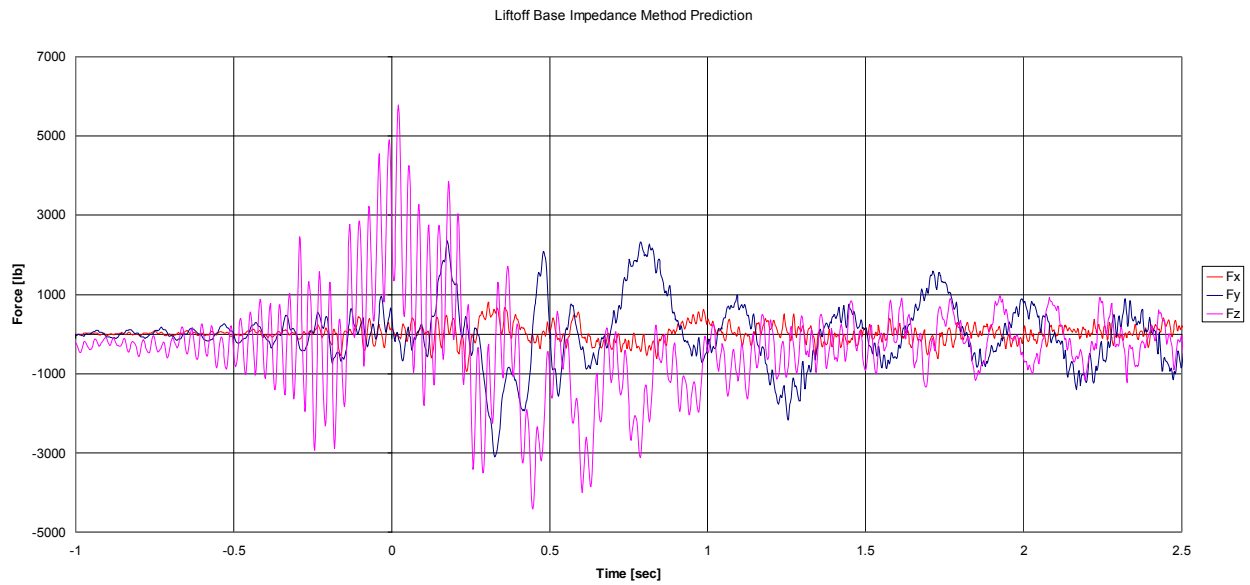


Figure 7.4-16. Liftoff Reconstruction Impedance Method Forces



NASA Engineering and Safety Center Technical Assessment Report

Document #:
**NESC-RP-
06-071**

Version:
1.0

Title:

Flight Force Measurements of the Gamma-Ray Large Area Space Telescope / Delta II Flight

Page #:
168 of 226

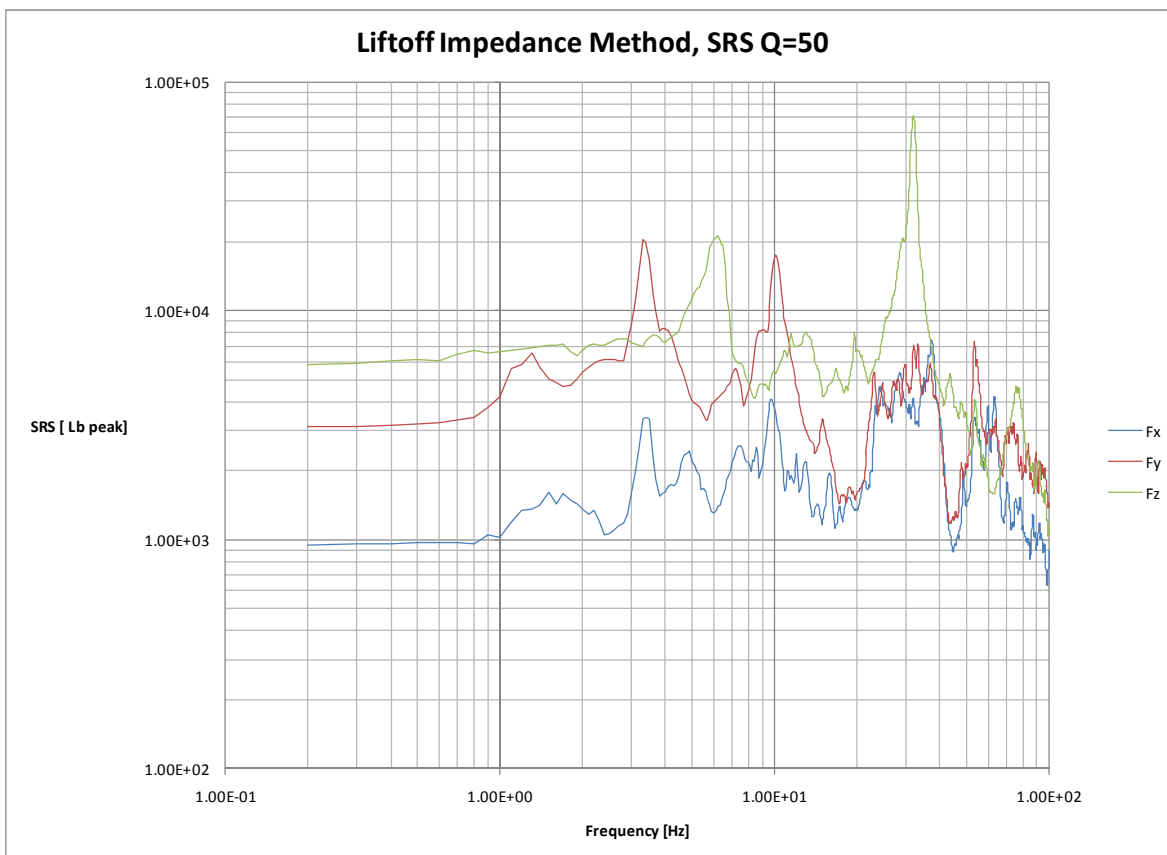


Figure 7.4-17. Liftoff Reconstruction Impedance Method Force SRSs



NASA Engineering and Safety Center Technical Assessment Report

Document #:
**NESC-RP-
06-071**

Version:
1.0

Title:

Flight Force Measurements of the Gamma-Ray Large Area Space Telescope / Delta II Flight

Page #:
169 of 226

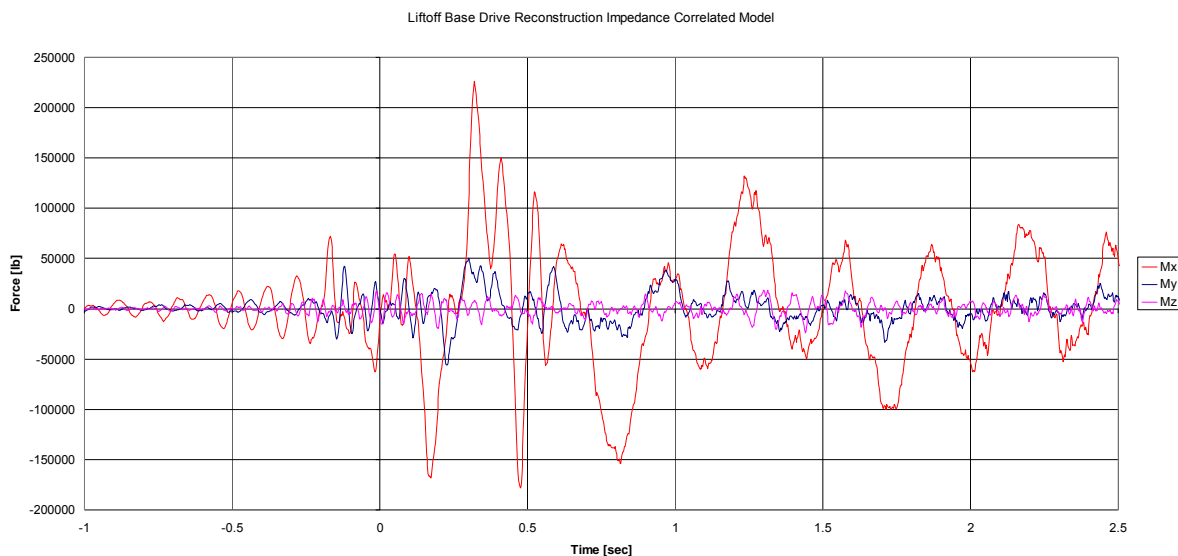


Figure 7.4-18. Liftoff Reconstruction Impedance Method Moment



Title:

**Flight Force Measurements of the Gamma-Ray Large
Area Space Telescope / Delta II Flight**

Page #:
170 of 226

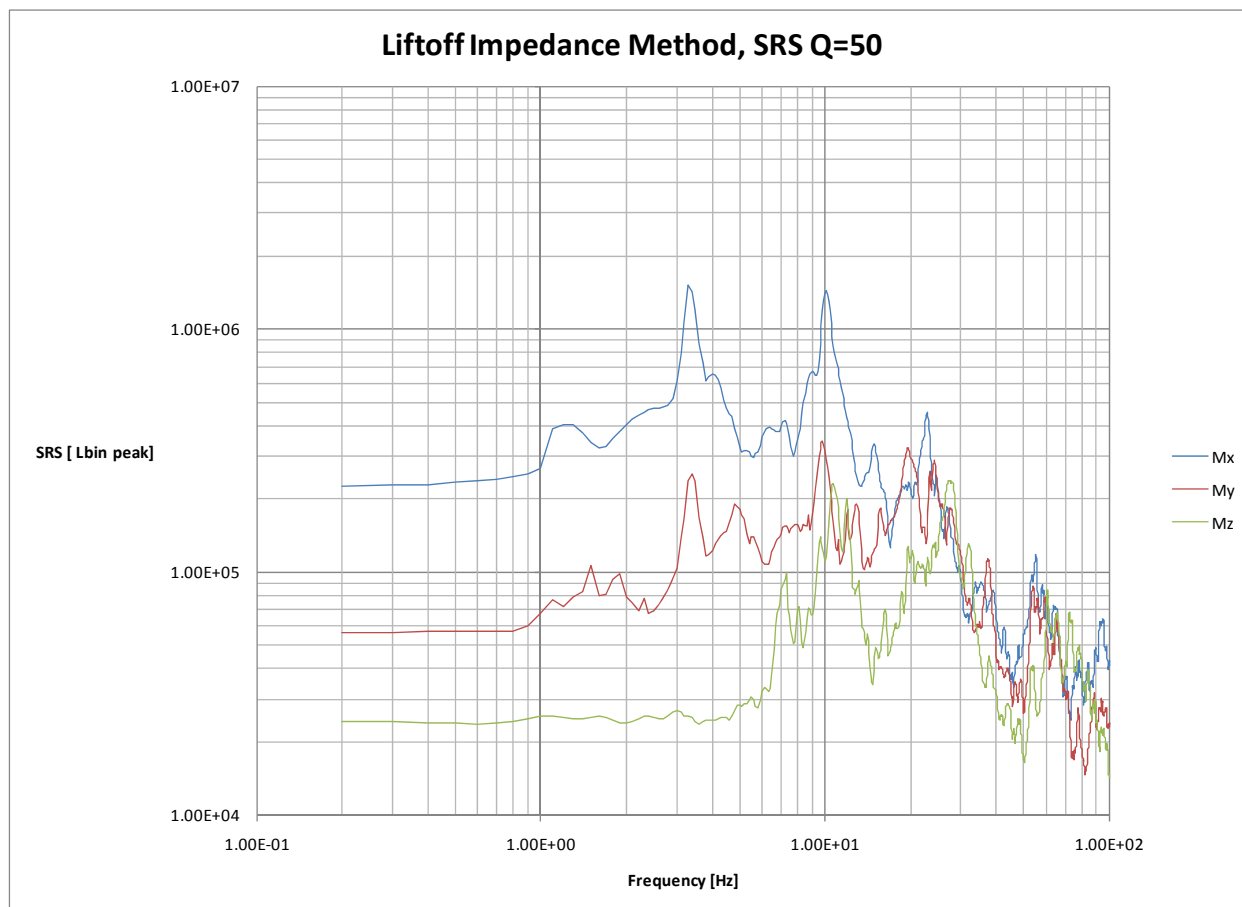


Figure 7.4-19. Liftoff Reconstruction Impedance Method Moment SRSs



Title:

**Flight Force Measurements of the Gamma-Ray Large
Area Space Telescope / Delta II Flight**

Page #:
171 of 226

7.4.5 Liftoff Reconciliation (All Methods) and Summary

In each of the subsequent plots, there is an overlay of accelerations that were used as “inputs” in the basedrive reconstructions and Impedance Method compared with the acceleration “recovered” in the full Liftoff reconstruction. The thrust axis accelerations are shown in Figure 7.4-20.

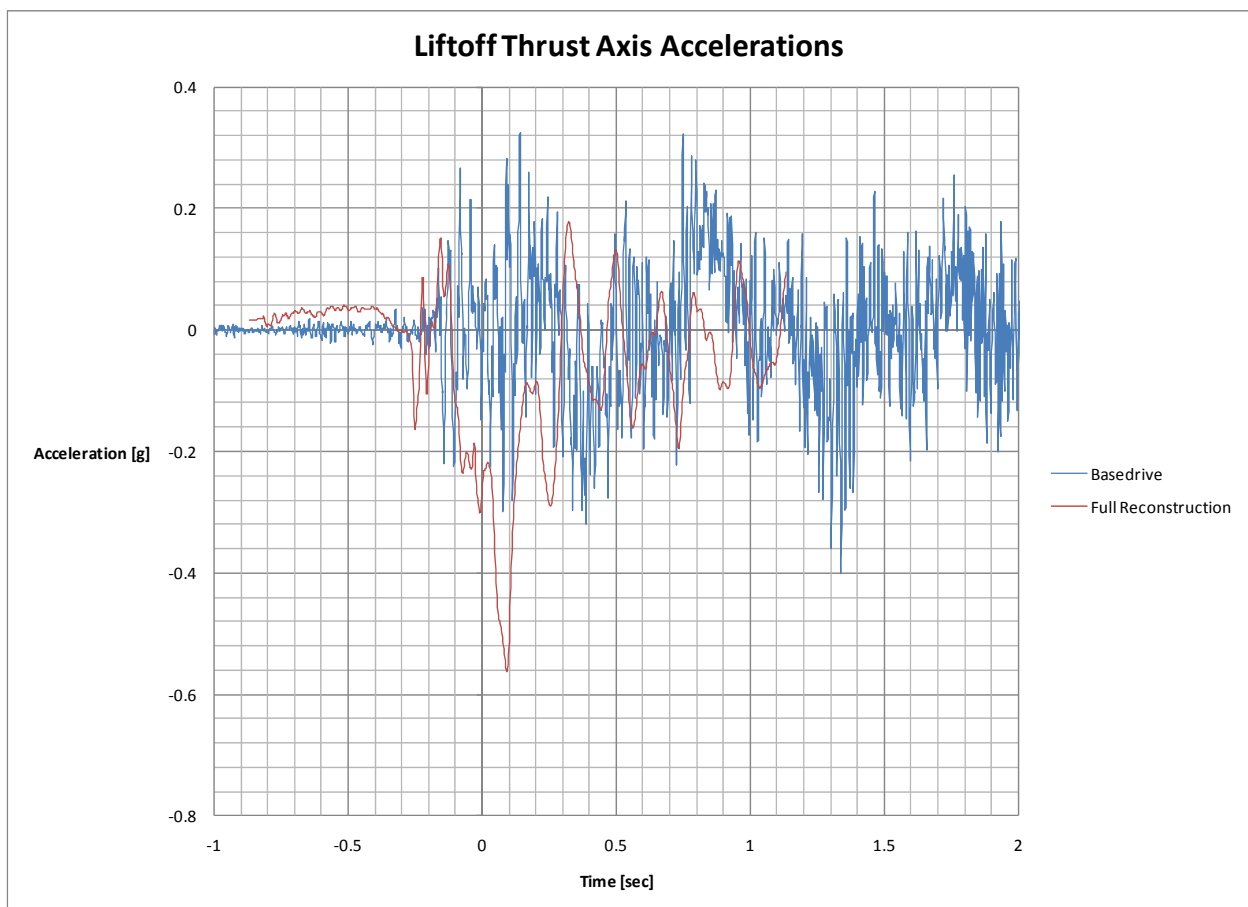


Figure 7.4-20. Liftoff Thrust Axis Accelerations

The acceleration data shown in Figure 7.4-20 includes an offset which is an artifact of the 0.5 Hz HP filter built into the SFI data acquisition system and the effect of the impulsive steady liftoff kick. This effect is discussed in more detail in Section 7.2. A SRS of these accelerations is shown in Figure 7.4-21.

Also a time offset of 0.24 seconds with respect to the real time is observed, this being a telemetry offset between the SFI and the standard Delta 2 flight systems. The full reconstruction



NASA Engineering and Safety Center Technical Assessment Report

Document #:
**NESC-RP-
06-071**

Version:
1.0

Title:

Flight Force Measurements of the Gamma-Ray Large Area Space Telescope / Delta II Flight

Page #:
172 of 226

acceleration shows a roll-off beyond 60 Hz, which is the upper frequency of the modes included in the models. This means that there is content that the full reconstruction does not include.

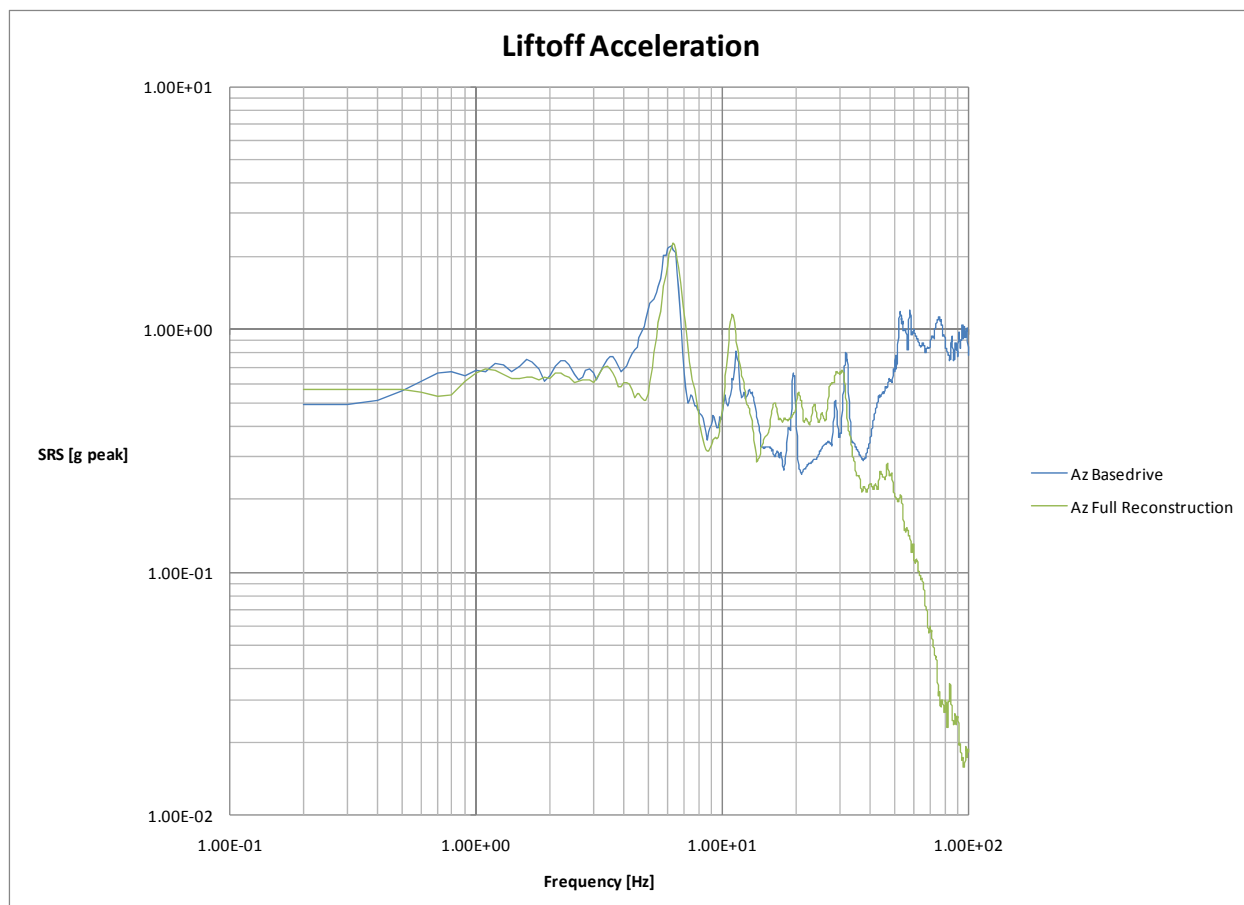


Figure 7.4-21. Liftoff Thrust Axis Acceleration SRSs

The lateral accelerations and corresponding response spectra can be seen in Figures 7.4-22 through 7.4-25.



Title:

**Flight Force Measurements of the Gamma-Ray Large
Area Space Telescope / Delta II Flight**

Page #:
173 of 226

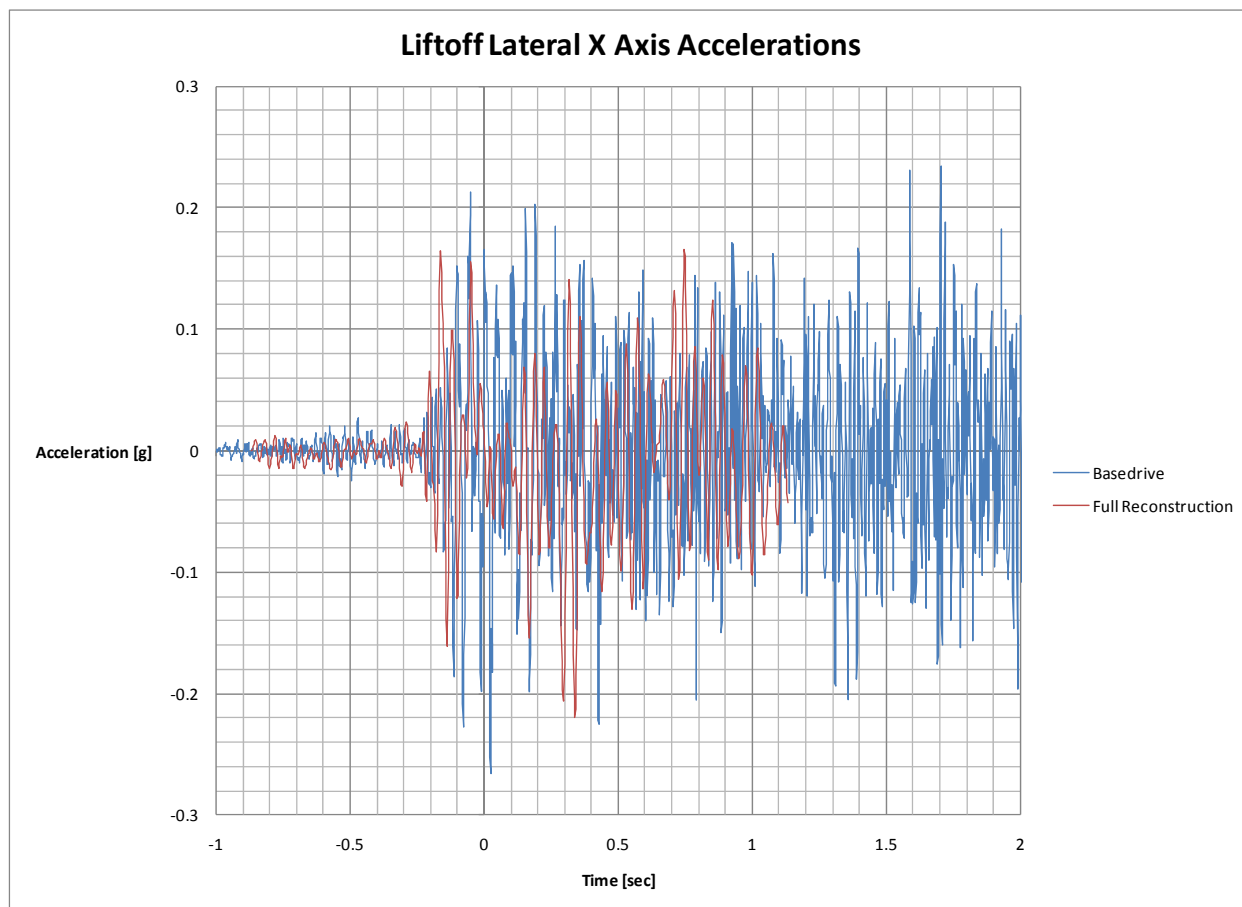


Figure 7.4-22. Liftoff Lateral X Axis Accelerations



Title:

**Flight Force Measurements of the Gamma-Ray Large
Area Space Telescope / Delta II Flight**

Page #:
174 of 226

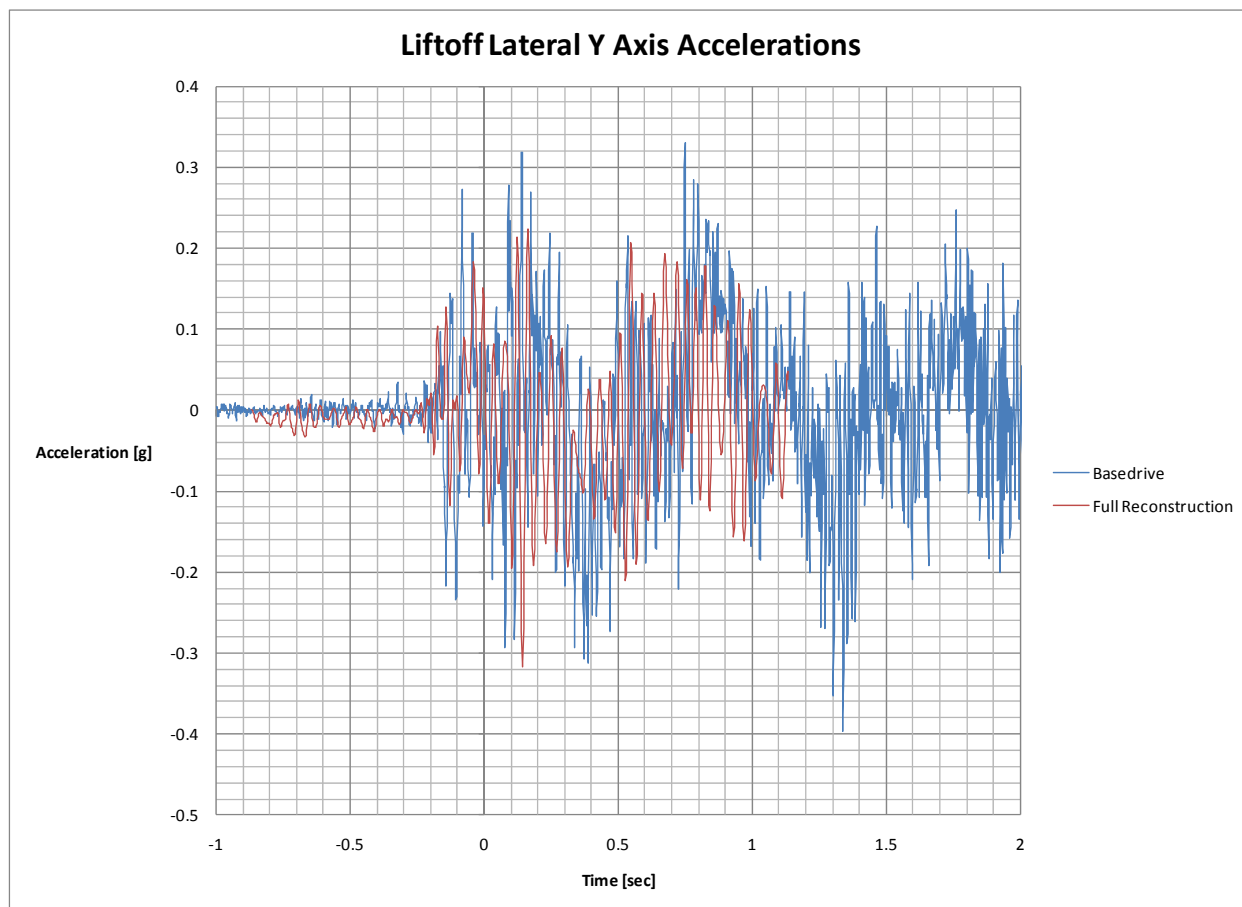


Figure 7.4-23. Liftoff Lateral Y Axis Accelerations



Title:

**Flight Force Measurements of the Gamma-Ray Large
Area Space Telescope / Delta II Flight**

Page #:
175 of 226

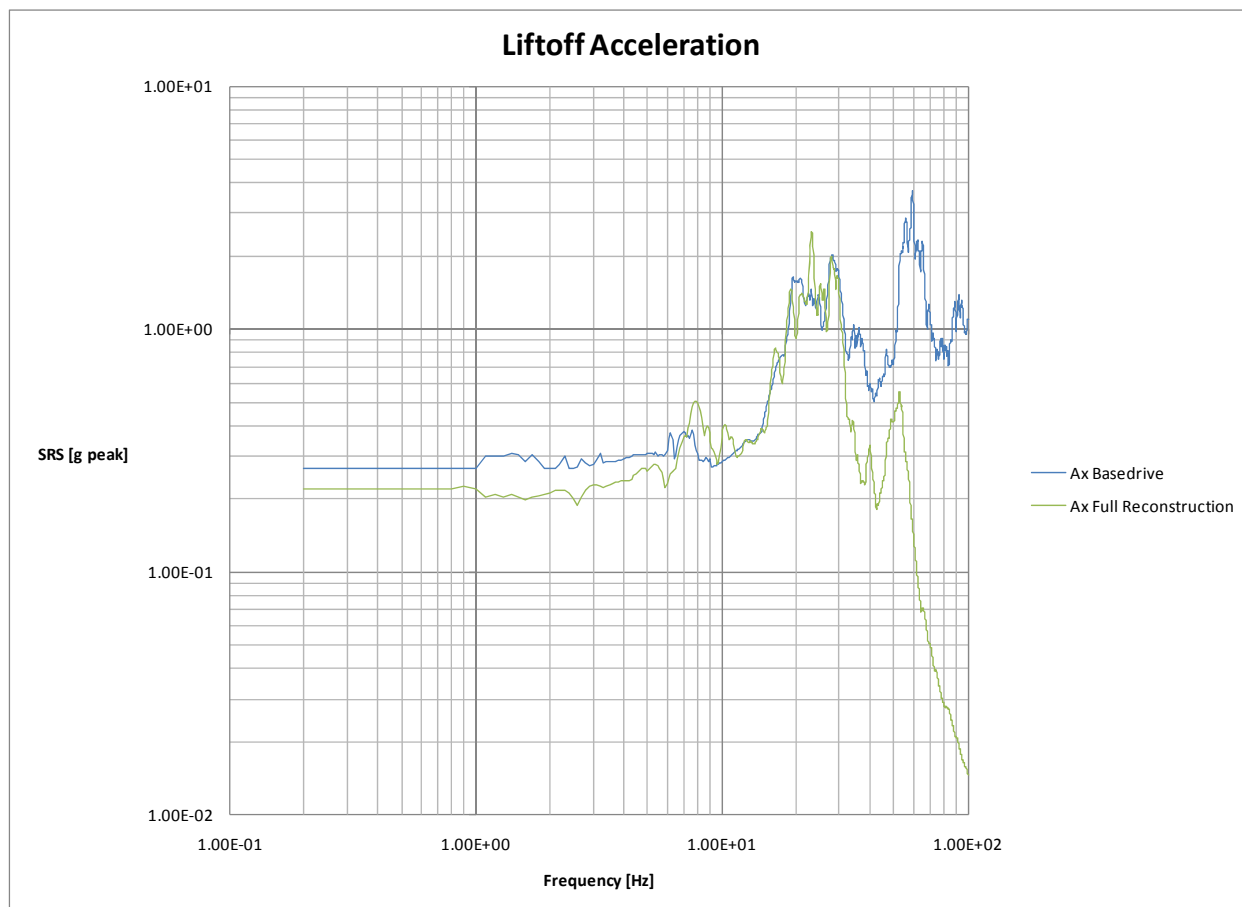


Figure 7.4-24. Liftoff lateral X Axis Acceleration SRSs



Title:

**Flight Force Measurements of the Gamma-Ray Large
Area Space Telescope / Delta II Flight**

Page #:
176 of 226

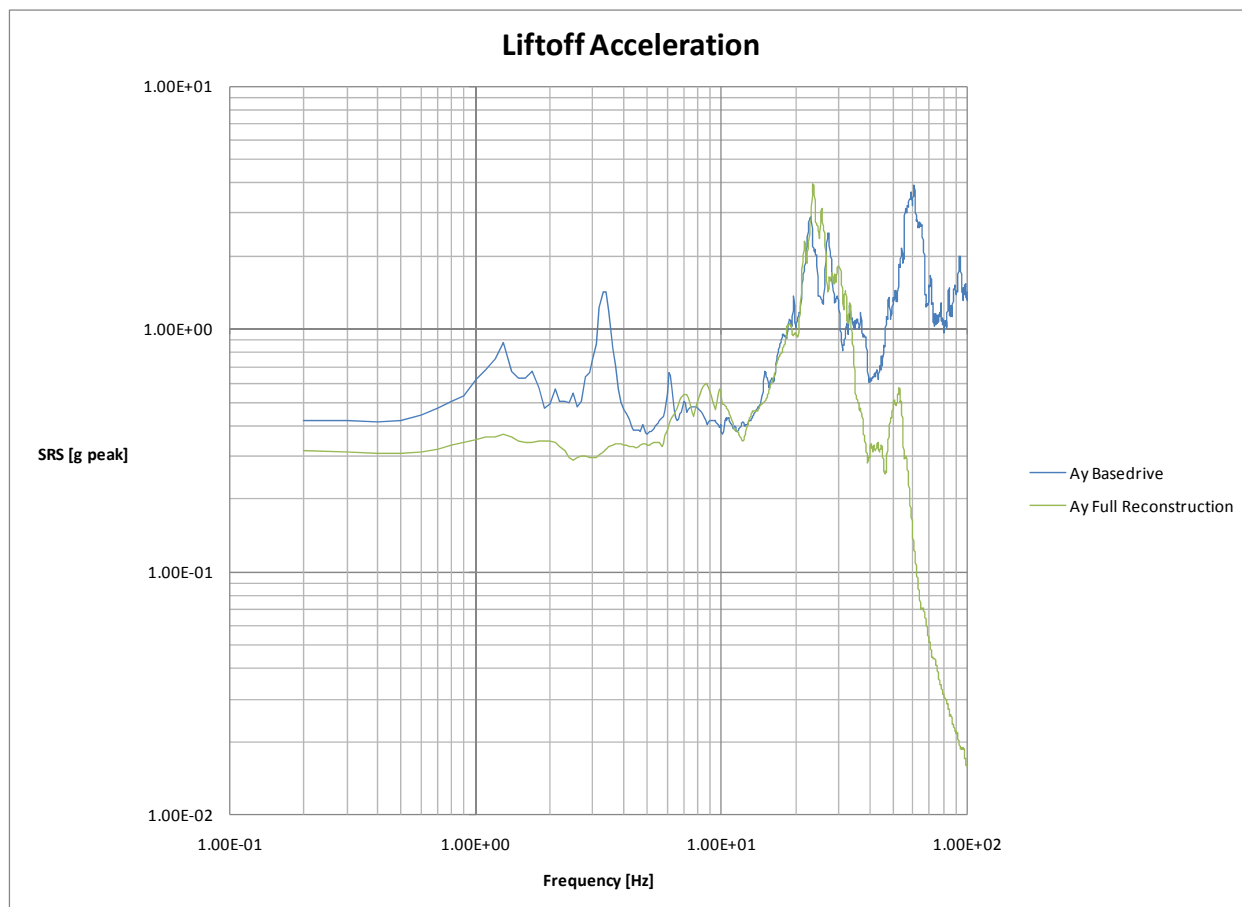


Figure 7.4-25. Liftoff lateral Y Axis Acceleration SRSs



Title:

Flight Force Measurements of the Gamma-Ray Large Area Space Telescope / Delta II Flight

Page #:
177 of 226

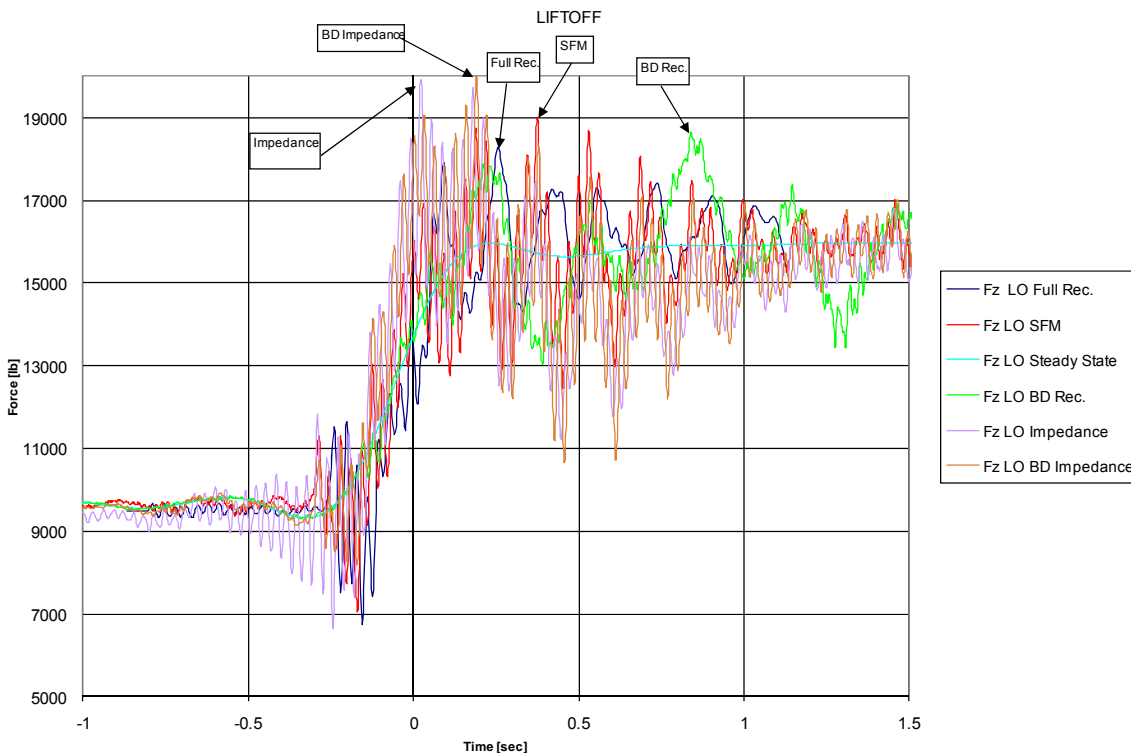


Figure 7.4-26. Liftoff Thrust Axis Forces (Steady+Dynamic)

Figure 7.4-26 shows a comparison between the measured SFM thrust forces and the results from the full Liftoff reconstruction, basedrive analysis, and Impedance Method. In general there was agreement in the thrust axis between the SFM data and the forces predicted using the various analytical techniques. In order to make the comparison between the thrust forces calculated analytically from measured flight accelerations and the SFM results, additional processing of the data was required to account for the steady-state forces. The accelerometers flown as part of the SFI system were AC coupled and did not measure the effect of gravity or the steady-state acceleration as thrust was developed by the vehicle. The SFM results based on strain were DC coupled in that they captured both static and dynamic effects. Therefore, the thrust forces due to the steady-state acceleration of the vehicle needed to be added to the forces calculated using the acceleration based methods.

The steady-state thrust force was calculated either by LP filtering acceleration data from a DC accelerometer flown as part of the standard instrumentation package and then multiplying it by the weight of the spacecraft and PAF, or by LP filtering the SFM thrust force. In either case, once the steady-state thrust force was calculated, it was added to the dynamic force calculated analytically. Care had to be taken when using the DC accelerometer data as the standard data



Title:

**Flight Force Measurements of the Gamma-Ray Large
Area Space Telescope / Delta II Flight**

Page #:
178 of 226

system was not time-synched with the SFI package. In addition, the measured flight acceleration in the thrust axis included an artifact related to the HP filtering built into the SFI accelerometers which affected the accuracy of the flight data in the thrust axis for during flight times in which there was a large change of the steady-state state accelerations levels such as during Liftoff or MECO. Additional filtering was required to account for the presence of this artifact. Details of the filtering artifact and its effect on the measured thrust axis accelerations are discussed in Section 7.2. Future efforts to measure flight forces and to characterize interface acceleration levels may want to evaluate the use of one or more DC accelerometers as part of the SFI package to address some of the above issues.

Figure 7.4-27 shows the forces at liftoff with the steady-state portion removed. The corresponding SRS of the Liftoff dynamic forces is shown in Figure 7.4-28. The measured SFM forces in the thrust axis show agreement with the thrust forces predicted using acceleration-based methods in both the time and frequency domains.

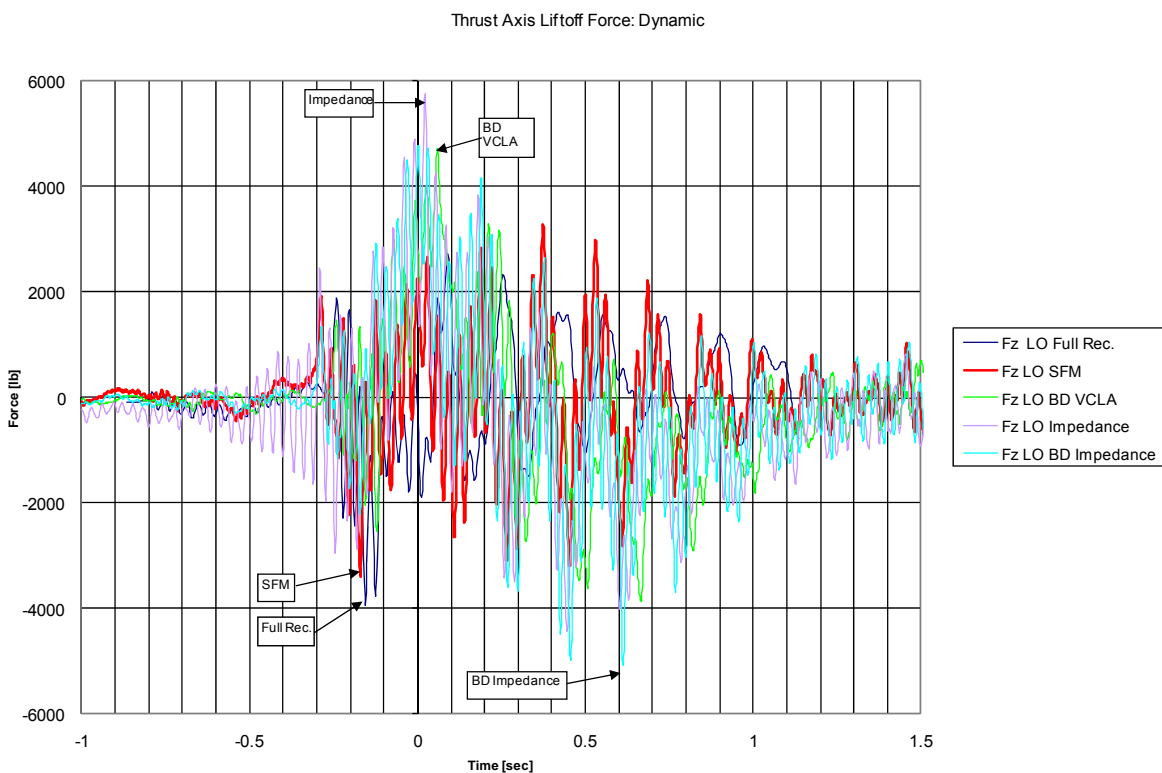


Figure 7.4-27. Liftoff Thrust Axis Dynamic Forces



Title:

**Flight Force Measurements of the Gamma-Ray Large
Area Space Telescope / Delta II Flight**

Page #:
179 of 226

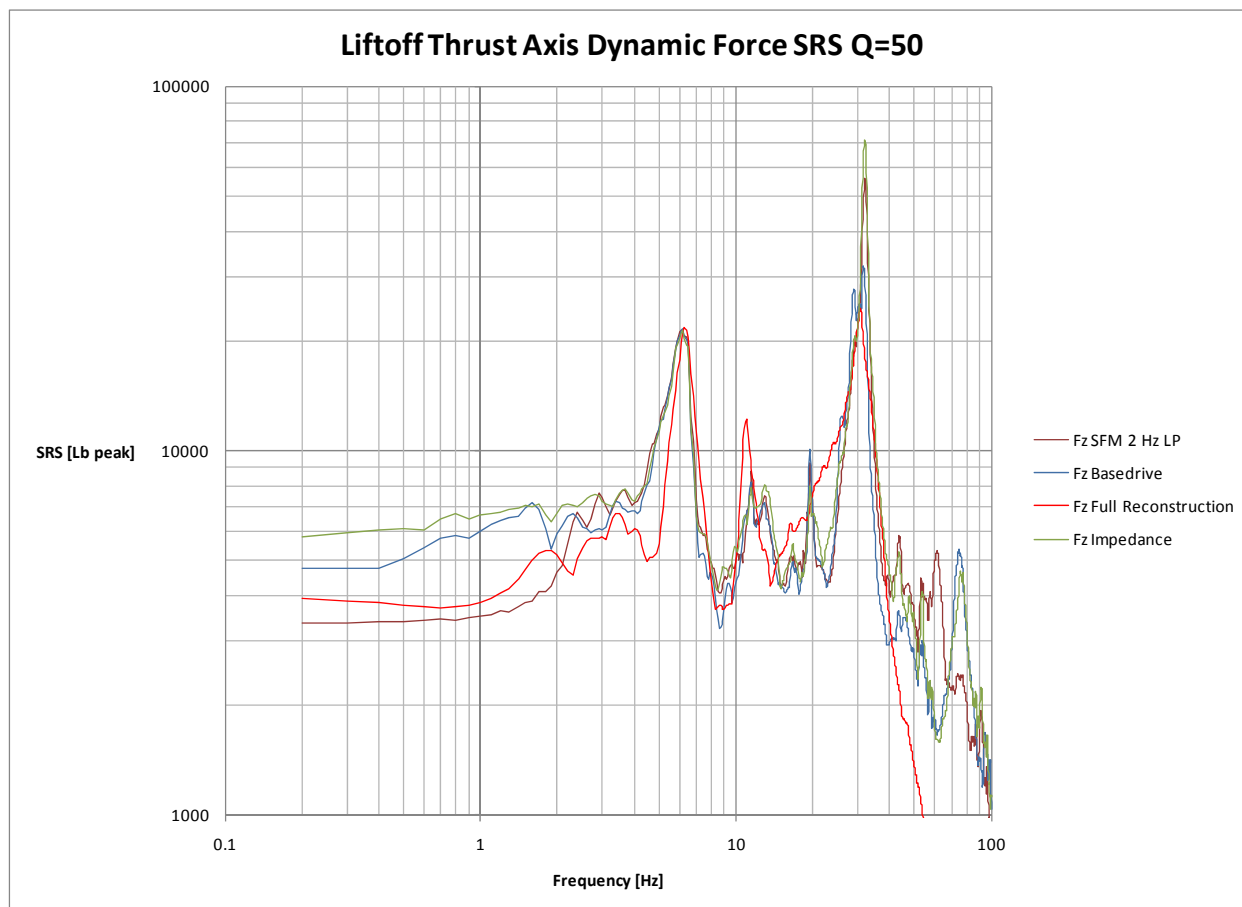


Figure 7.4-28. Liftoff Thrust Axis Force SRSs

The NESC team continued with the lateral forces and moments, in order to ease the plot examination, the basedrive impedance is not shown. The time histories and corresponding SRS results for the remaining forces and moments are shown in Figures 7.4-29 through 7.4-38.



NASA Engineering and Safety Center Technical Assessment Report

Document #:
**NESC-RP-
06-071**

Version:
1.0

Title:

Flight Force Measurements of the Gamma-Ray Large Area Space Telescope / Delta II Flight

Page #:
180 of 226

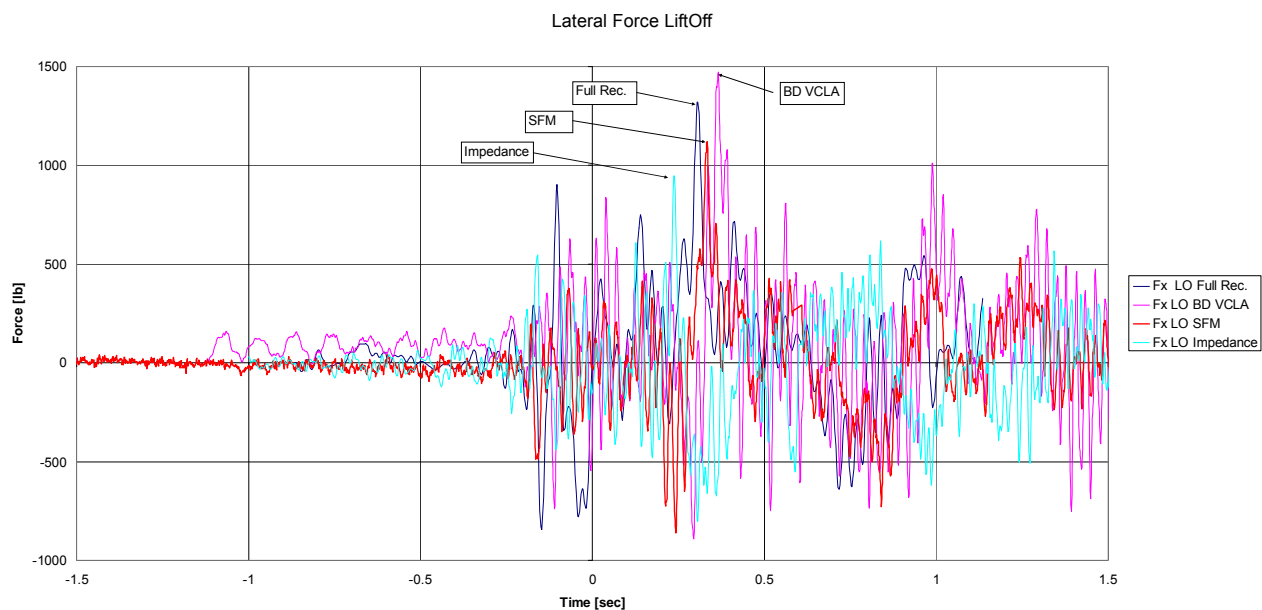


Figure 7.4-29. Liftoff Lateral X Forces



NASA Engineering and Safety Center Technical Assessment Report

Document #:
**NESC-RP-
06-071**

Version:
1.0

Title:

Flight Force Measurements of the Gamma-Ray Large Area Space Telescope / Delta II Flight

Page #:
181 of 226

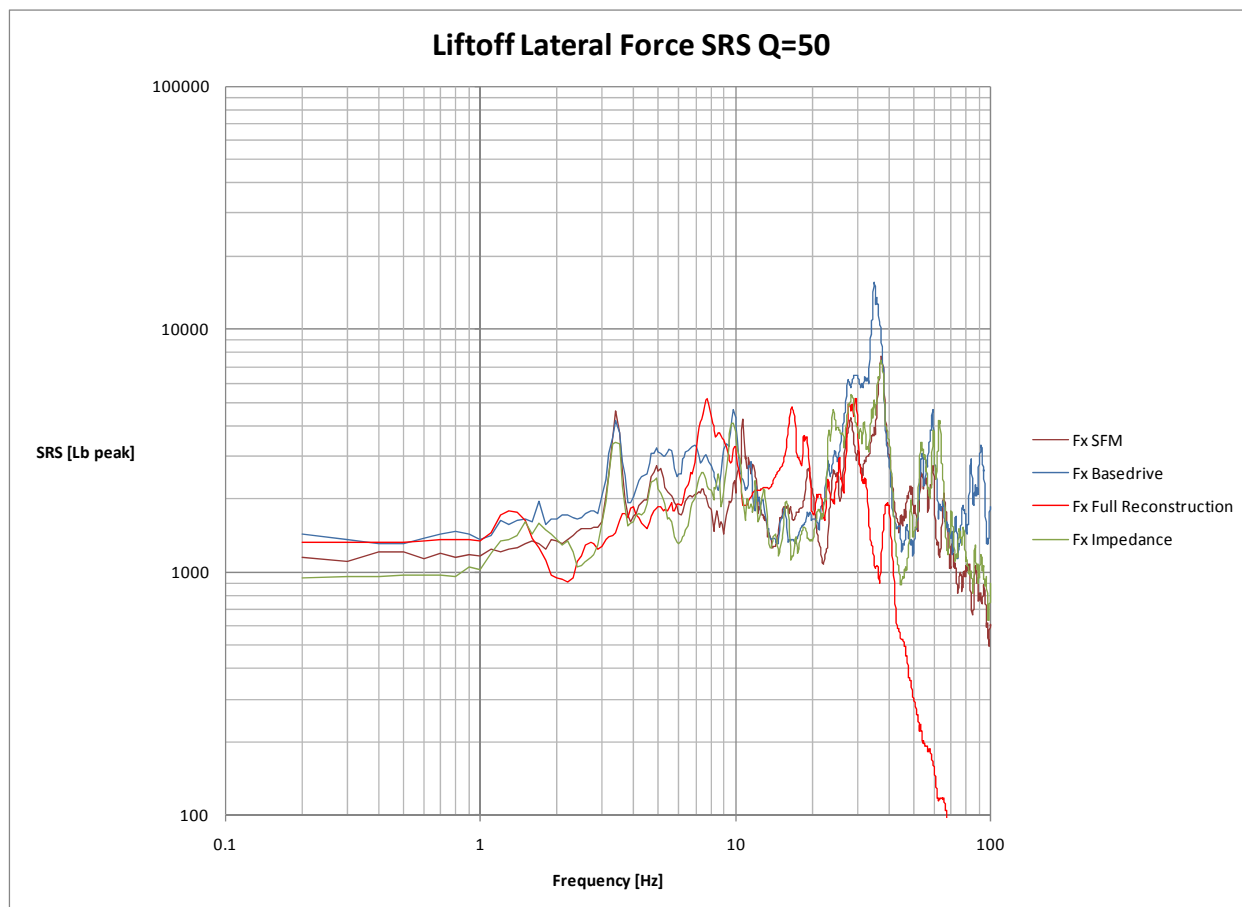


Figure 7.4-30. Liftoff Lateral X Force SRSs



NASA Engineering and Safety Center Technical Assessment Report

Document #:
**NESC-RP-
06-071**

Version:
1.0

Title:

Flight Force Measurements of the Gamma-Ray Large Area Space Telescope / Delta II Flight

Page #:
182 of 226

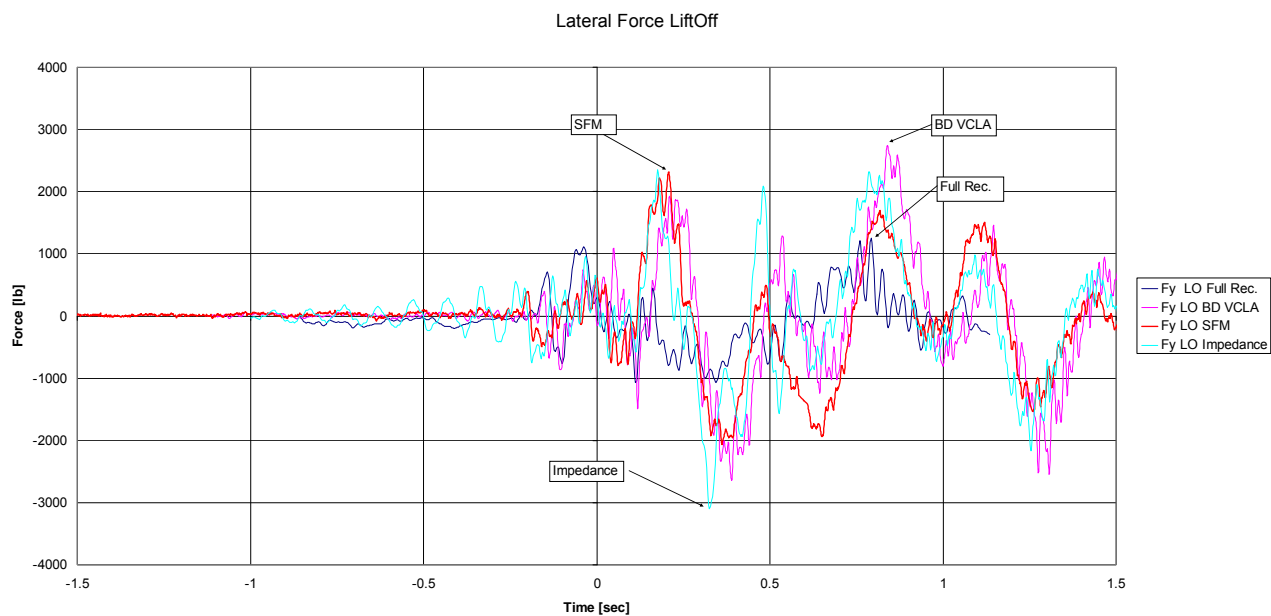


Figure 7.4-31. Liftoff Lateral Y Forces



NASA Engineering and Safety Center Technical Assessment Report

Document #:
**NESC-RP-
06-071**

Version:
1.0

Title:

Flight Force Measurements of the Gamma-Ray Large Area Space Telescope / Delta II Flight

Page #:
183 of 226

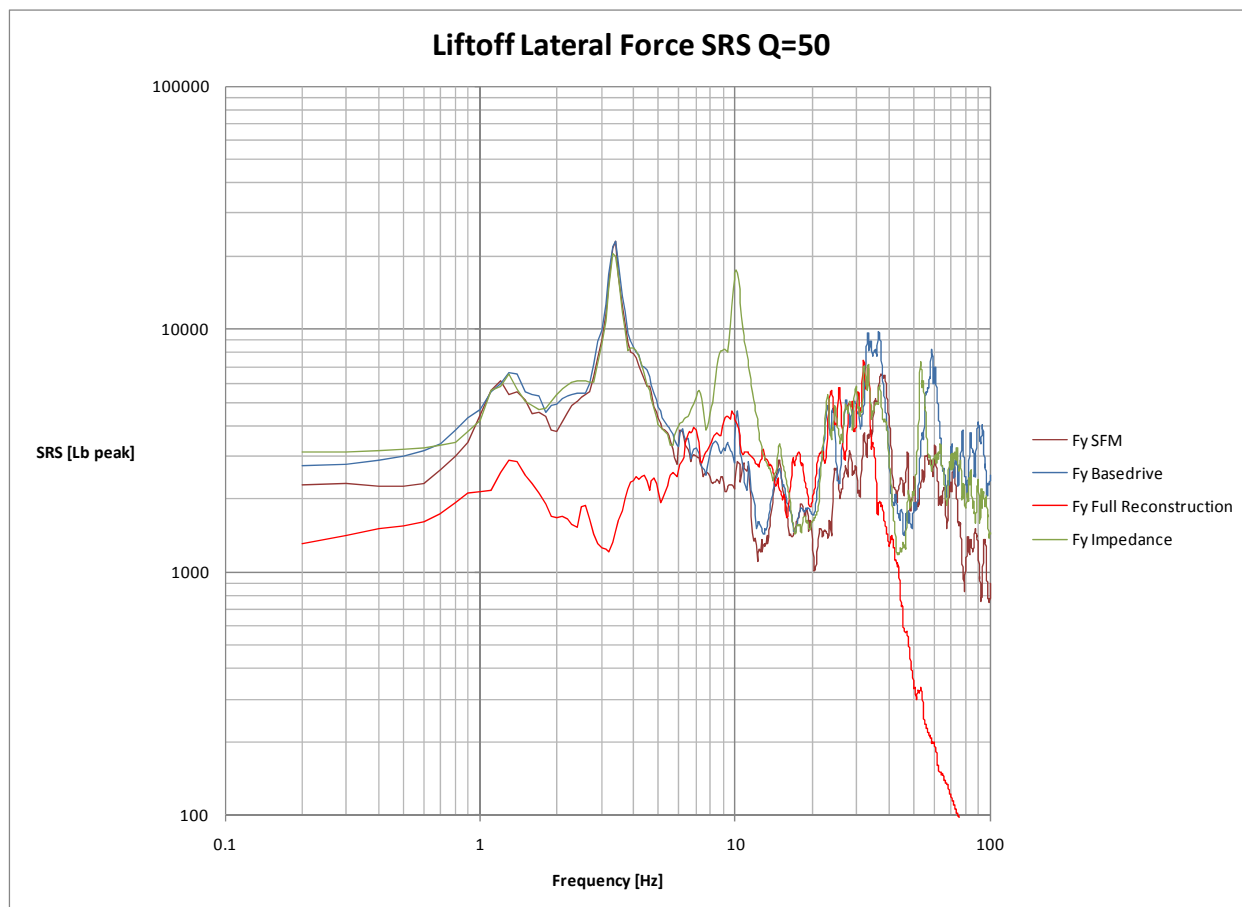


Figure 7.4-32. Liftoff Lateral Y Force SRSs



NASA Engineering and Safety Center Technical Assessment Report

Document #:
**NESC-RP-
06-071**

Version:
1.0

Title:

Flight Force Measurements of the Gamma-Ray Large Area Space Telescope / Delta II Flight

Page #:
184 of 226

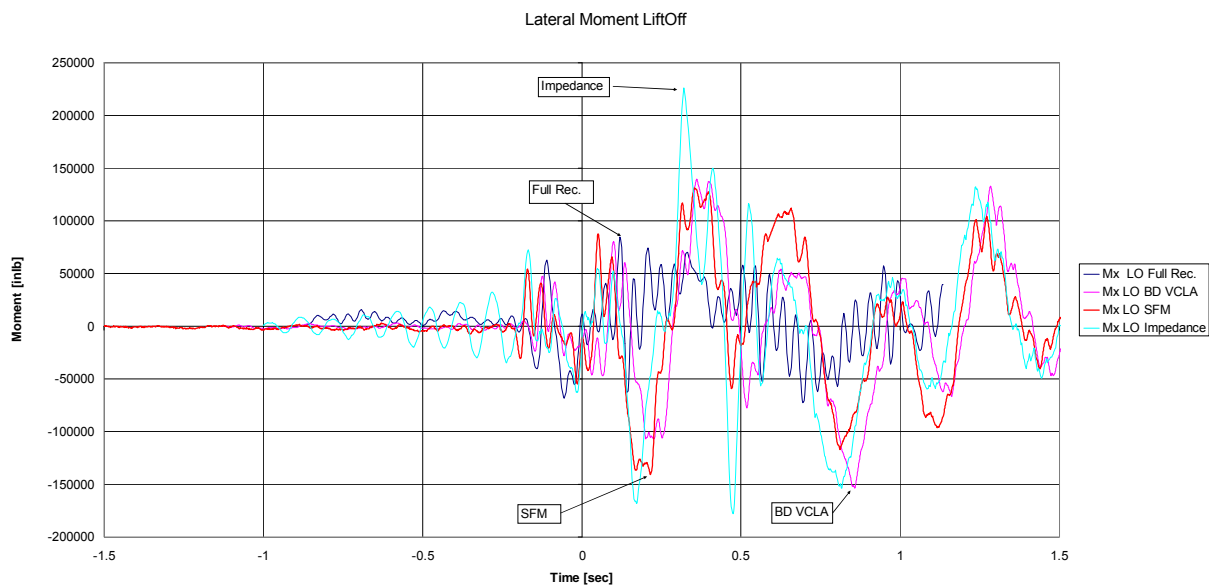


Figure 7.4-33. Liftoff Lateral X Moments



Title:

**Flight Force Measurements of the Gamma-Ray Large
Area Space Telescope / Delta II Flight**

Page #:
185 of 226

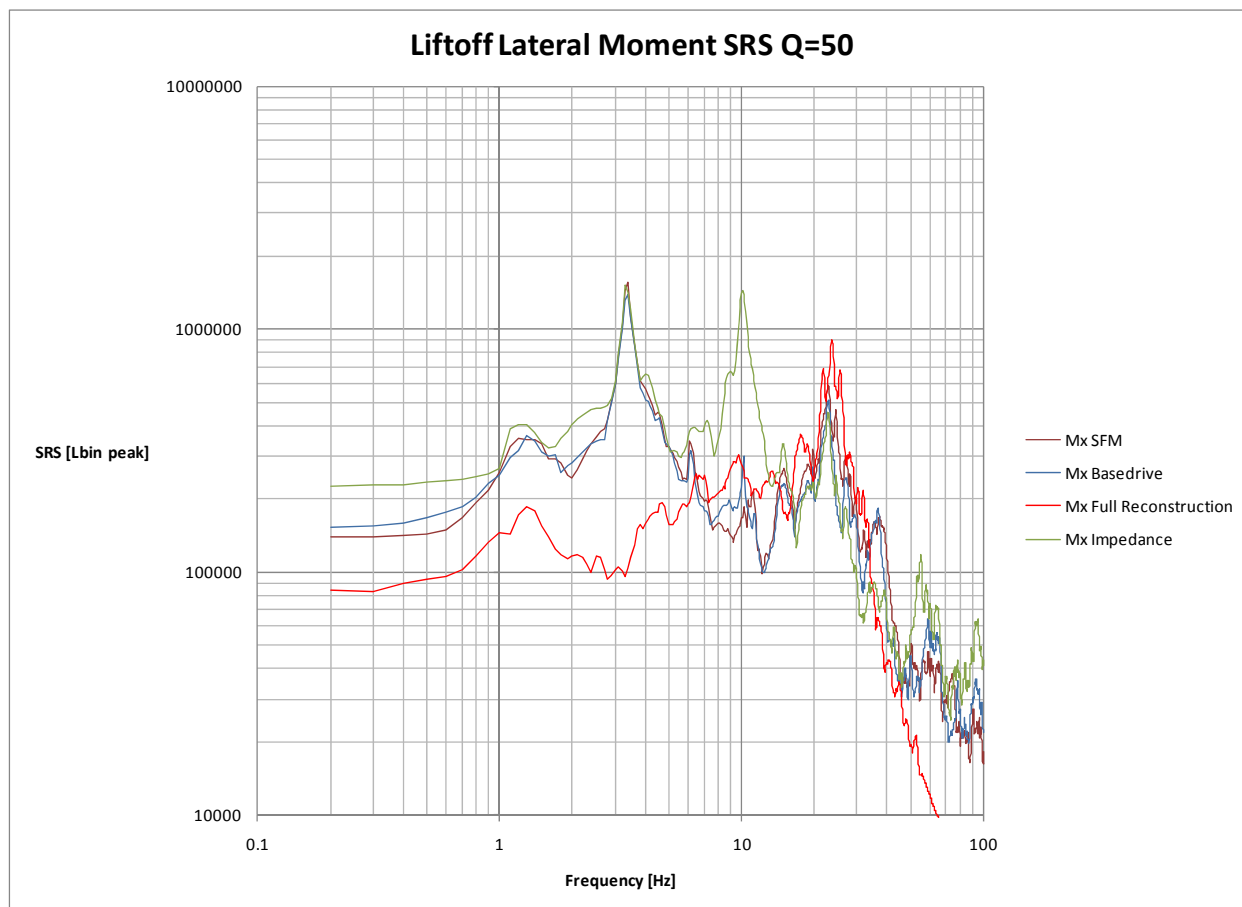


Figure 7.4-34. Liftoff Lateral X Moment SRSs



NASA Engineering and Safety Center Technical Assessment Report

Document #:
**NESC-RP-
06-071**

Version:
1.0

Title:

Flight Force Measurements of the Gamma-Ray Large Area Space Telescope / Delta II Flight

Page #:
186 of 226

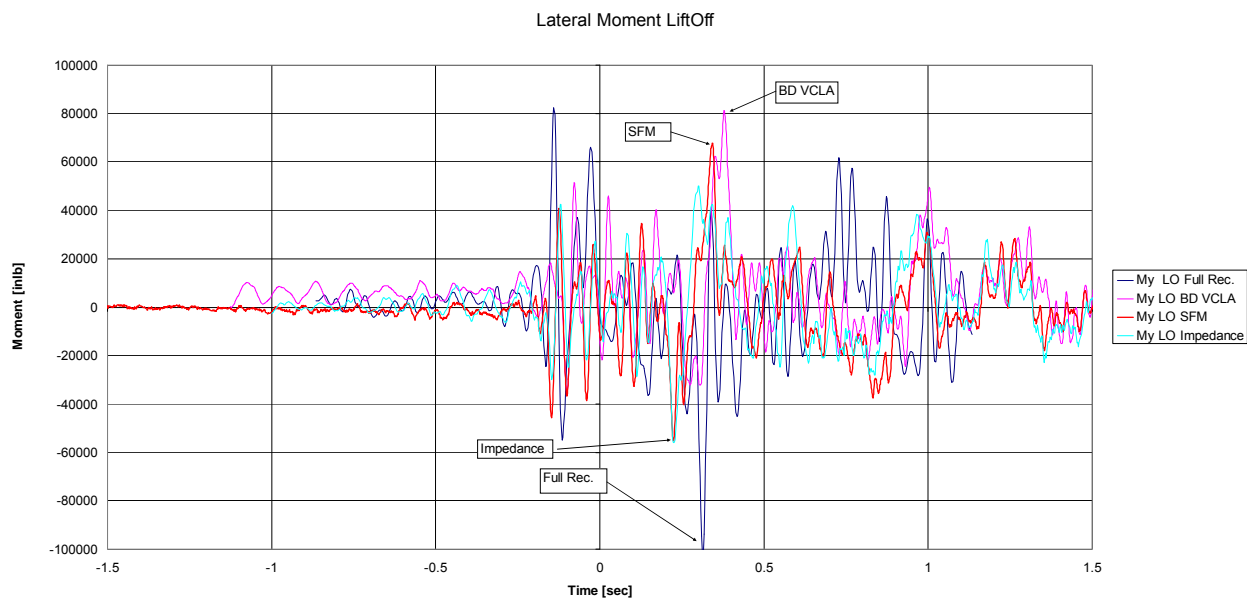


Figure 7.4-35. Liftoff Lateral Y Moments



Title:

**Flight Force Measurements of the Gamma-Ray Large
Area Space Telescope / Delta II Flight**

Page #:
187 of 226

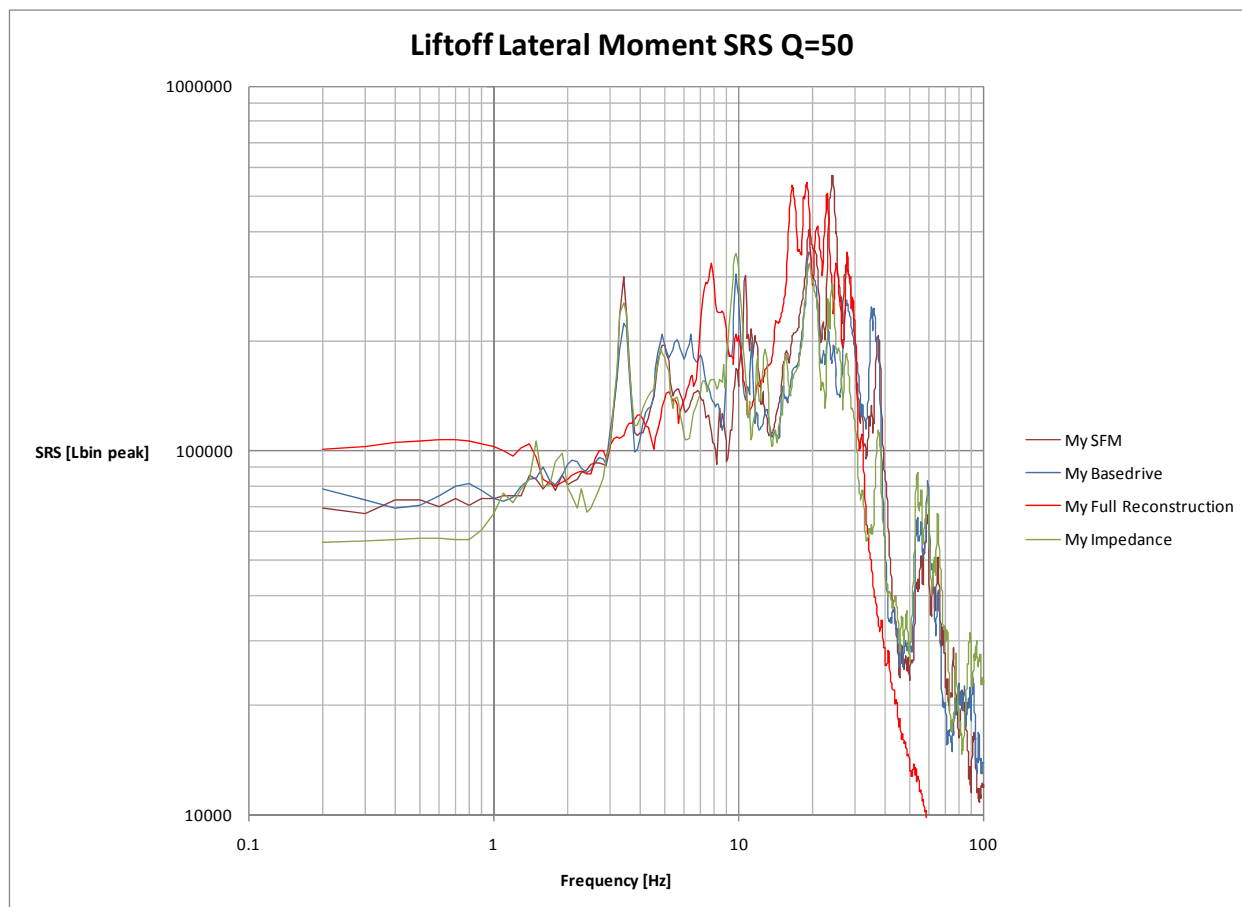


Figure 7.4-36. Liftoff Lateral Y Moment SRSs



NASA Engineering and Safety Center Technical Assessment Report

Document #:
**NESC-RP-
06-071**

Version:
1.0

Title:

Flight Force Measurements of the Gamma-Ray Large Area Space Telescope / Delta II Flight

Page #:
188 of 226

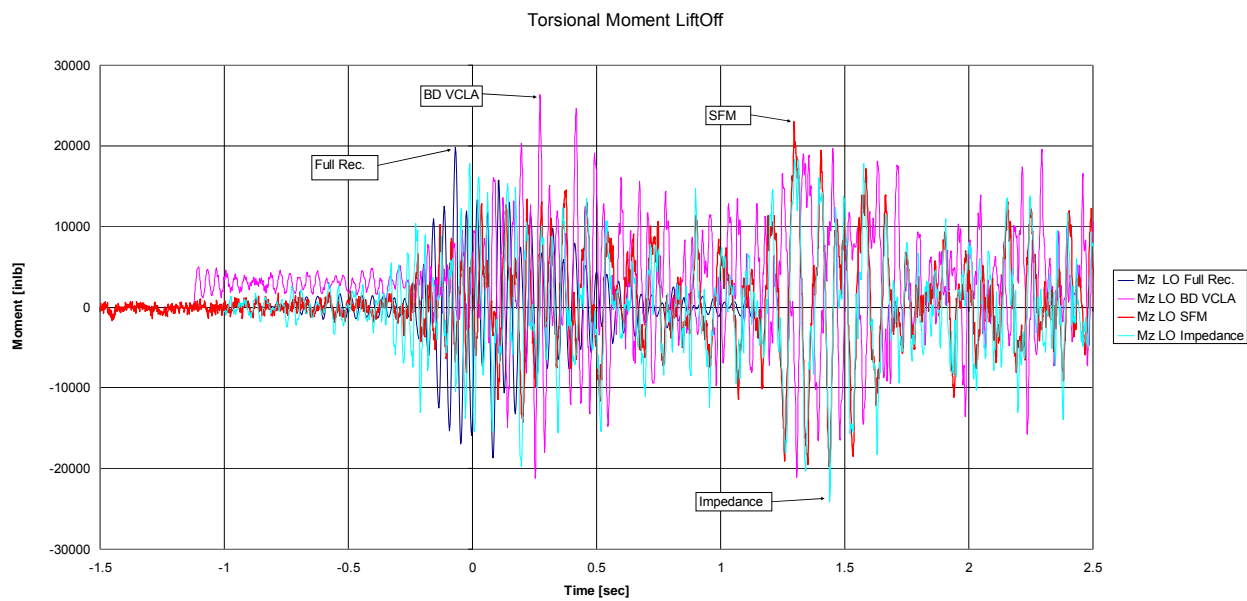


Figure 7.4-37. Liftoff Torsional Moments



Title:

**Flight Force Measurements of the Gamma-Ray Large
Area Space Telescope / Delta II Flight**

Page #:
189 of 226

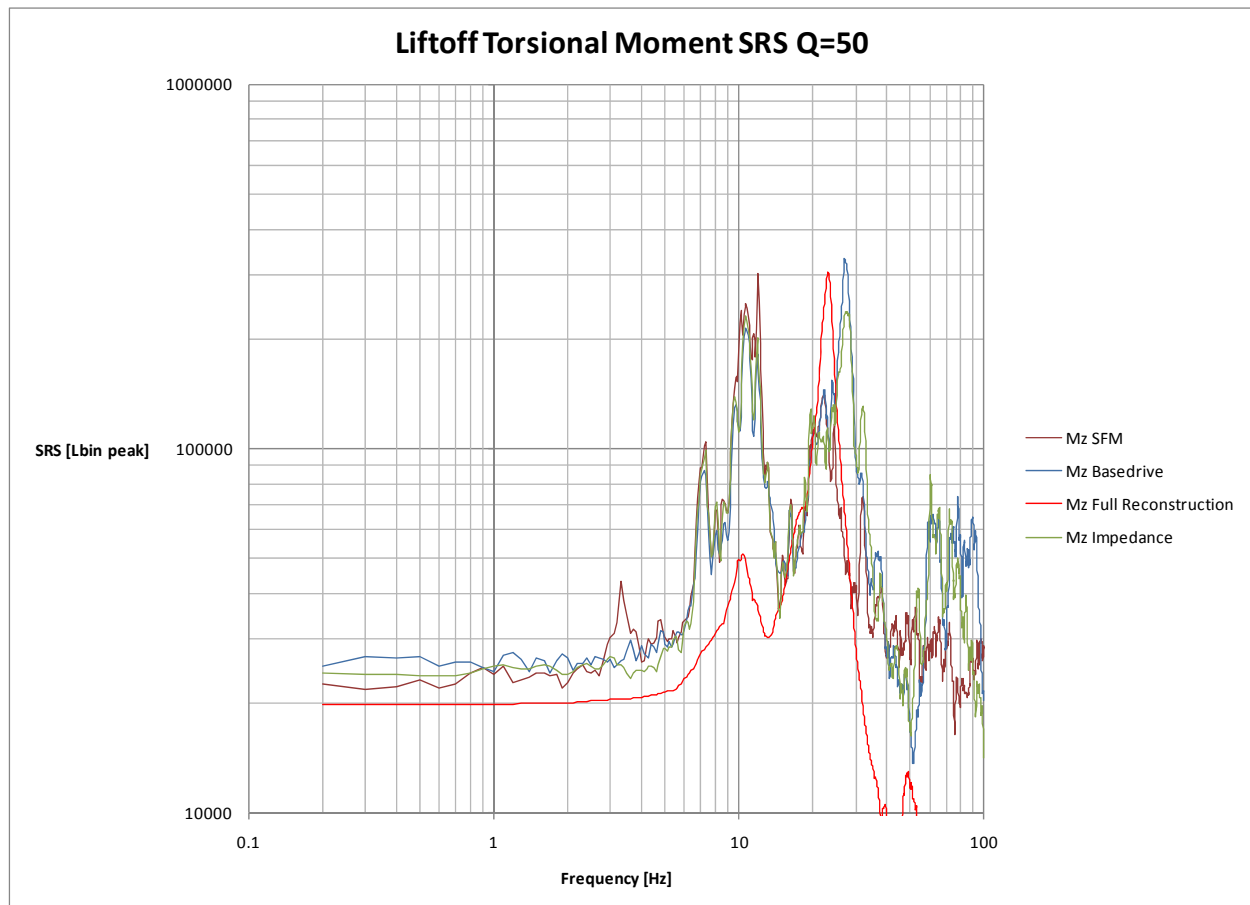


Figure 7.4-38. Liftoff Torsional Moment SRSs

The lateral force and moments lack the coupled system first bending mode content.

A summary table (Table 7.4-1) with all methods is presented showing the maximum absolute force values and VCLA results. The thrust axis included the total (steady + dynamic) and only the dynamic forces. The FEM Method results are not shown and are comparable to the SFM results for Liftoff.

- In the SFM, the maxima for the F_x / M_y (0.333 / 0.343) and F_y / M_x (0.208 / 0.216) occurs around the same time. The same pattern is shown in the other methods.
- In the SFM, the maximum torsional moment occurs after T+1 second and after the thrust and lateral maxima which occur in the first 20 to 40 msec.
- The thrust axis forces show the best agreement with the full reconstruction (1 percent for the dynamic portion). The Impedance Method showed the same 1 percent. Maxima



NASA Engineering and Safety Center Technical Assessment Report

Document #:
**NESC-RP-
06-071**

Version:
1.0

Title:

Flight Force Measurements of the Gamma-Ray Large Area Space Telescope / Delta II Flight

Page #:
190 of 226

occurs around the same time (within the first 90 msec of the flight for the dynamic portion and 180 to 380 msec for the total).

- Both basedrive and Impedance Methods show agreement with the SFM in terms of $F_y > F_x$ and consequently $M_x > M_y$.
- The full reconstruction method showed F_x higher than F_y and consequently $M_y > M_x$. However, M_x is under-predicted and M_y is over-predicted.
- Torsional moment's maxima are predicted within 15 percent of the SFM.
- The lateral forces / moments show the same maxima over-prediction pattern in the basedrive and the SFM. F_x / M_y (31 and 20 percent) and F_y / M_x (18 and 9 percent). The other methods can either over- or under-predict.
- The maximum over-prediction is for the Impedance Method and amounts to 61 percent on M_x . The maximum under-prediction occurs on the full reconstruction in the amount of -46 percent on F_y .
- The VCLA maximum interface forces showed important over dimensioning numbers in the lateral forces and overturning moments. The thrust axis force and torsional moments are comparable with the SFM predictions.

Table 7.4-1. Liftoff Summary Table

Method	Maximum Fx [lb]	Time [sec]	Maximum Fy [lb]	Time [sec]	Maximum Fz [lb]	Time [sec]	Maximum Mx [inlb]	Time [sec]	Maximum My [inlb]	Time [sec]	Maximum Mz [inlb]	Time [sec]
SFM: total	1121	0.333	2321	0.208	19004	0.374	140658	0.216	67612	0.343	22984	1.296
dynamic					3374	-0.170						
	10%		5%		5%		5%		5%		5%	
Predicted High	1233		2437		19954		147691		70993		24133	
					3543							
Predicted Low	-10%		-5%		-5%		-5%		-5%		-5%	
	1019		2210		18099		133960		64392		21890	
					3213							
Full Reconstruction	1321	0.308	1251	0.793	18293	0.255	85022	0.120	100327	0.313	19821	0.083
					3928	-0.155						
			18%		-46%		-40%		48%		-14%	
					16%							
Base Drive Reconstruction VCLA model 2 % damping	1473	0.366	2746	0.839	18641	0.839	153374	0.857	81253	0.378	26377	0.272
					4739	0.059						
	31%		18%		-2%		9%		20%		15%	
					40%							
Base Drive Imp. Corr. Model	1220	0.331	2481	0.802	20074	0.190	128095	0.812	61996	0.341	20721	0.227
					5067	0.612						
	9%		7%		6%		-9%		-8%		-10%	
					50%							
Impedance	947	0.238	3095	0.326	19928	0.022	226139	0.320	55962	0.226	24141	1.440
					5777	0.022						
	-16%		33%		5%		61%		-17%		5%	
					71%							
Method	Maximum Fx [lb]		Maximum Fy [lb]		Maximum Fz [lb]		Maximum Mx [inlb]		Maximum My [inlb]		Maximum Mz [inlb]	
VCLA	5477		9455		22888		385609		328252		25808	
	389%		307%		20%		174%		385%		12%	

	NASA Engineering and Safety Center Technical Assessment Report	Document #:	Version:
		NESC-RP-06-071	1.0
Title:		Page #:	
Flight Force Measurements of the Gamma-Ray Large Area Space Telescope / Delta II Flight		191 of 226	

7.5 Airloads Reconstruction and Reconciliation

7.5.1 Airloads Basedrive Reconstruction

The basedrive analysis for the GLAST spacecraft during the Airloads flight time was performed using the 6 centerline accelerations (3 translations and 3 rotations) calculated from the 4 triax accelerometers located around the PAF base that were part of the SFI instrumentation. Two different model configurations were analyzed as part of the basedrive reconstruction for Airloads. One set of basedrive runs was performed using the VCLA model with a constant 2 percent damping for all modes. The other set of basedrive runs was performed using the VCLA model which had been correlated based on data from the GLAST sine vibration testing. The measured damping values from the sine test were used for this basedrive configuration. The correlation process is outlined in Reference 10.

The forces and moments from the basedrive analysis were compared with the measured forces and moments from flight. For the first pass data review, no filtering was performed on the measured flight forces. Table 7.5-1 provides a summary of the basedrive results for the two GLAST model configurations as compared to the measured SFM data. The table shows the percent error associated with the SFM measurement based on the defined prediction accuracy measured during TPAF static testing. The percent difference between the basedrive results and the calculated SFM forces is shown for each model configuration. In cases where the basedrive results were greater than the expected error of the SFM measurement, the values are in bold. For instances where the basedrive results under-predict the SFM measurements, the values are underlined. It should be noted that the force due to the steady-state acceleration has been added to the basedrive results for direct comparison with the SFM measurements.

Table 7.5-1. Unfiltered Airloads Force Comparison - SFM versus Basedrive

Method	Maximum Fx (lb)	Time sec	Maximum Fy (lb)	Time sec	Maximum Fz (lb)	Time sec	Maximum Mx (in-lb)	Time sec	Maximum My (in-lb)	Time sec	Maximum Mz (in-lb)	Time sec
SFM	4596.51	32.444	4694.86	32.115	24581.83	21.19	288019.16	29.015	358478.65	32.443	247628.57	33.214
% Error	±5%		±5%		±5%		±5%		±5%		±5%	
Correlated	5029.94	32.568	4723.49	32.261	24335.43	21.191	262093.31	32.243	268588.37	32.555	237891.58	33.217
% Diff	9.4%		0.6%		<u>-1.0%</u>		<u>-9.0%</u>		-25.1%		<u>-3.9%</u>	
VCLA	5206.22	32.563	5228.49	32.259	24261.18	21.198	322407.42	32.244	324101.88	31.978	264057.74	33.216
% Diff	13.3%		11.4%		<u>-1.3%</u>		11.9%		-9.6%		6.6%	

As a check to ensure that the average centerline accelerations were being calculated correctly, a basedrive analysis was run for Airloads in which the full set of 12 accelerations were applied to the base of the PAF model. The interface force results from this analysis were compared to the force results from the nominal basedrive using the centerline accelerations. Comparison of these results showed no significant differences. All basedrive runs presented in this report were performed using the centerline accelerations derived from the full set of 12 measured accelerations.



NASA Engineering and Safety Center Technical Assessment Report

Document #:
**NESC-RP-
06-071**

Version:
1.0

Title:

Flight Force Measurements of the Gamma-Ray Large Area Space Telescope / Delta II Flight

Page #:
192 of 226

Figures 7.5-1 through 7.5-3 show the time history data comparing the measured SFM forces against the basedrive results for the VCLA and correlated models for the lateral force (F_x), thrust axis force (F_z), and maximum overturning moment (M_y). It can be seen from the time-history data that there is agreement in the overall shape of the response, and the predicted maximums from the basedrive occur closely with the SFM measurement. However, the basedrive results for the X-axis force over-predict the SFM results, while the basedrive results for the Y-axis moment (M_y) under-predict the peak response. In both cases, the force calculated using the basedrive technique is greater than the error associated with the SFM measurement. This would indicate that the basedrive technique is inadequate for predicting the interface forces. The thrust axis prediction for both basedrive configurations shows agreement with the measured flight data and is within the expected SFM measurement error.

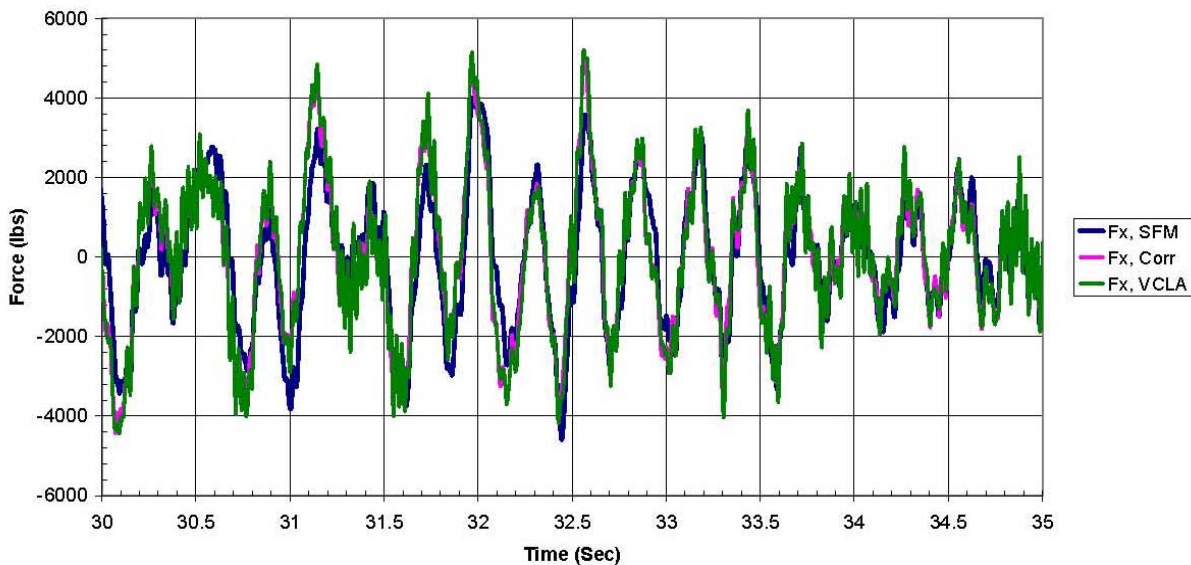


Figure 7.5-1. Airloads X-Axis Force - SFM Versus Basedrive



Title:

Flight Force Measurements of the Gamma-Ray Large Area Space Telescope / Delta II Flight

Page #:
193 of 226

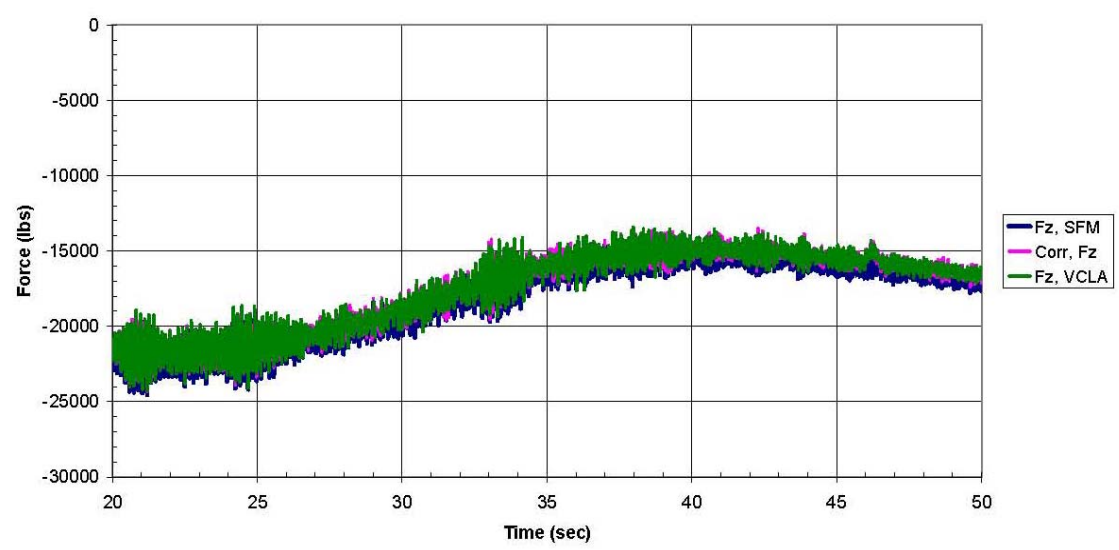


Figure 7.5-2. Airloads Z-Axis Force - SFM Versus Basedrive

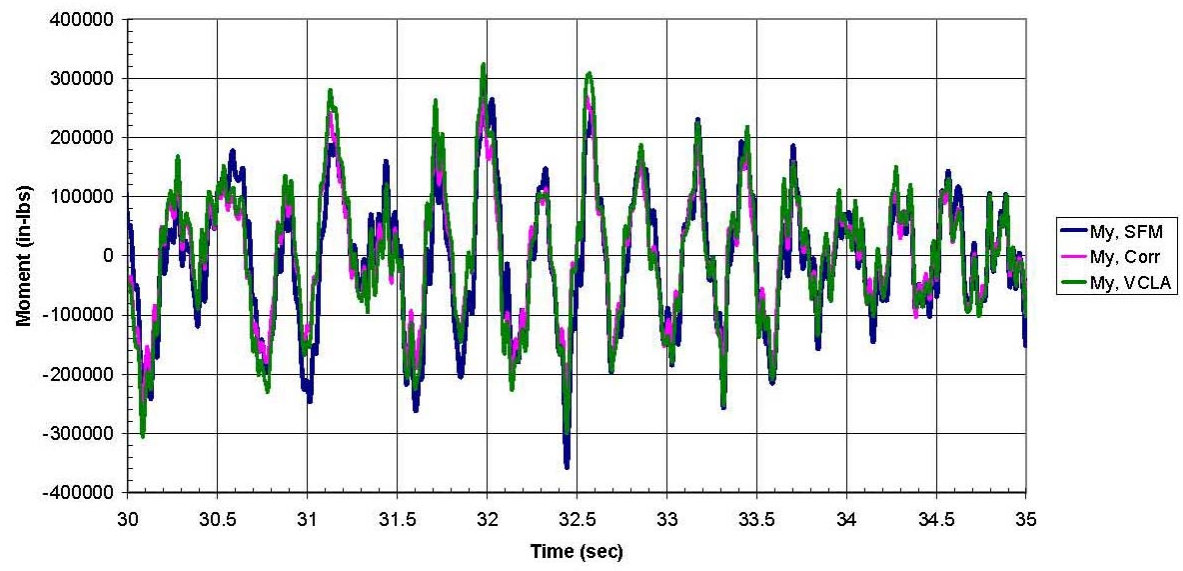


Figure 7.5-3. Airloads Y Moment - SFM Versus Basedrive

Figures 7.5-4 and 7.5-5 show the SRS processing of the Airloads time history data. The SRS plots show that the largest forces and moments occur below 5 Hz at the fundamental modes of



NASA Engineering and Safety Center Technical Assessment Report

Document #:
**NESC-RP-
06-071**

Version:
1.0

Title:

Flight Force Measurements of the Gamma-Ray Large Area Space Telescope / Delta II Flight

Page #:
194 of 226

the coupled launch vehicle/spacecraft system. The SRS plots show the lateral bending modes at 3.5 Hz as the driver for the interface shear and moments. Based on these figures, it can be seen that the basedrive analysis tends to over-predict the lateral forces generated above 10 Hz with significant over-prediction in the 30 to 40 Hz range for the VCLA model using a constant two percent damping.

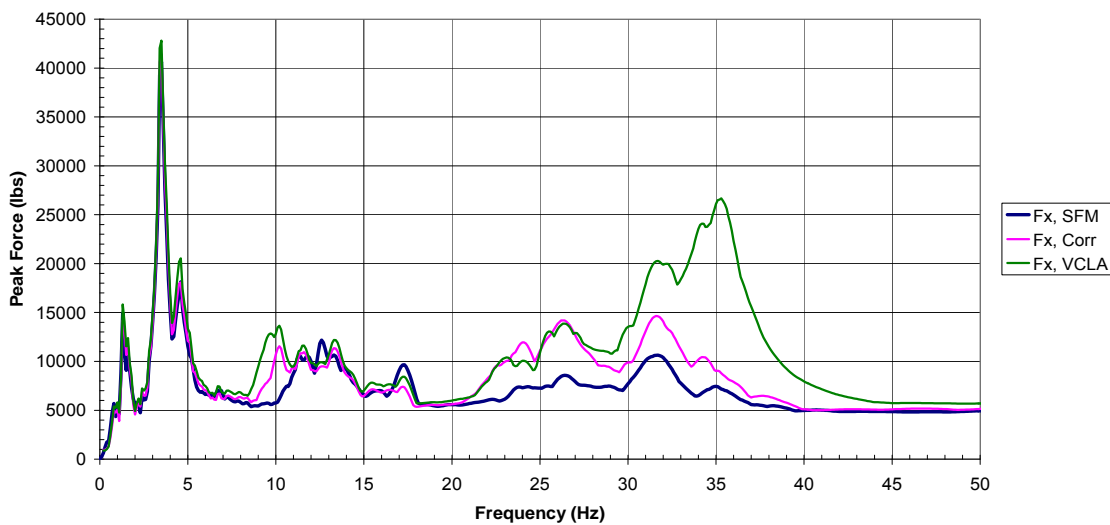


Figure 7.5-4. Airloads X Axis SRS Force (Q=20), SFM Versus Basedrive



Title:

**Flight Force Measurements of the Gamma-Ray Large
Area Space Telescope / Delta II Flight**

Page #:

195 of 226

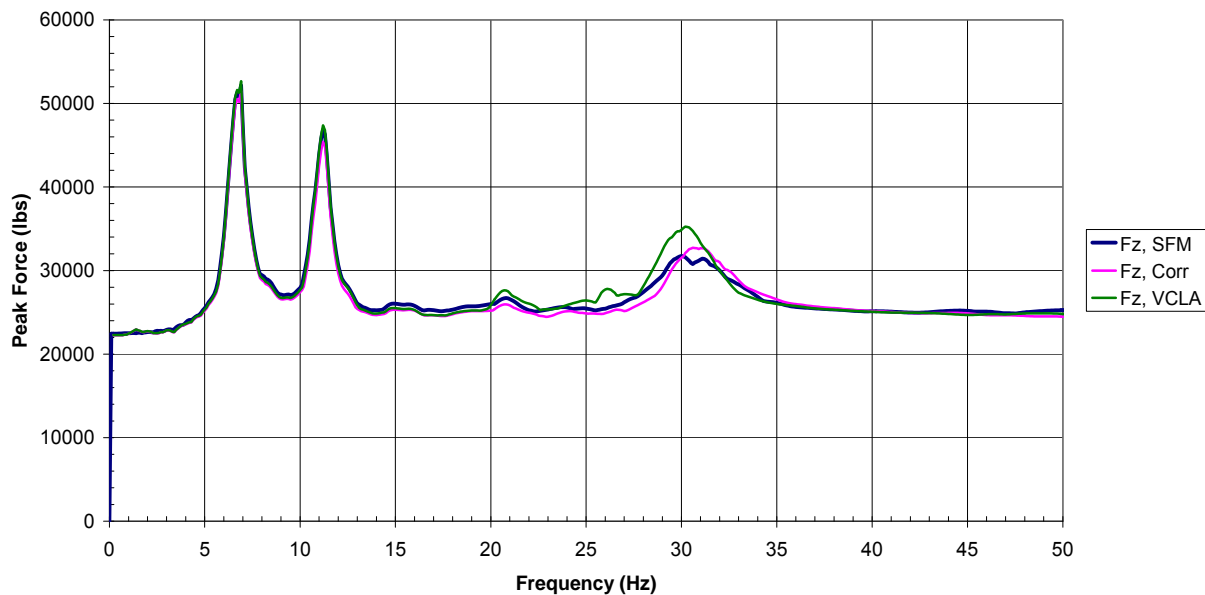


Figure 7.5-5. Airloads Force Z SRS (Q=20) SFM Versus Basedrive

The frequency content of the thrust axis shows agreement between the basedrive predictions and the SFM measurement. The VCLA model using two percent damping over-predicts the forces associated with the spacecraft axial mode at 30 Hz while the correlated model shows better agreement with the measured forces at that frequency. The offset due to the steady state acceleration can be seen in the SRS plot.

The SRS for the Y-axis moment, seen in Figure 7.5-6 shows a different trend from the lateral axis result. In this case, the basedrive results tend to under-predict the SFM measurement across the entire frequency range with the exception of a peak around 10 Hz associated with the fixed-base bending mode of the spacecraft. In general, even with the under-prediction, there is reasonable agreement in the frequency content between the basedrive predictions and the SFM measurement.

In order to better understand the under-prediction of the lateral bending moments, a detailed review of the two modeling configurations was performed. This review showed differences in the mass properties between the VCLA and Correlated models. The Correlated model had less rotational inertia than the VCLA configuration as a result of how the propellant mass was modeled. This accounts for the larger under-prediction by the Correlated model of the lateral bending moments as compared to the flight data. The under-prediction of both models in the higher frequency ranges is most likely due to the inability of either FEM to adequately represent the modal effective rotational inertia about the fundamental bending mode.



NASA Engineering and Safety Center Technical Assessment Report

Document #:
**NESC-RP-
06-071**

Version:
1.0

Title:

Flight Force Measurements of the Gamma-Ray Large Area Space Telescope / Delta II Flight

Page #:
196 of 226

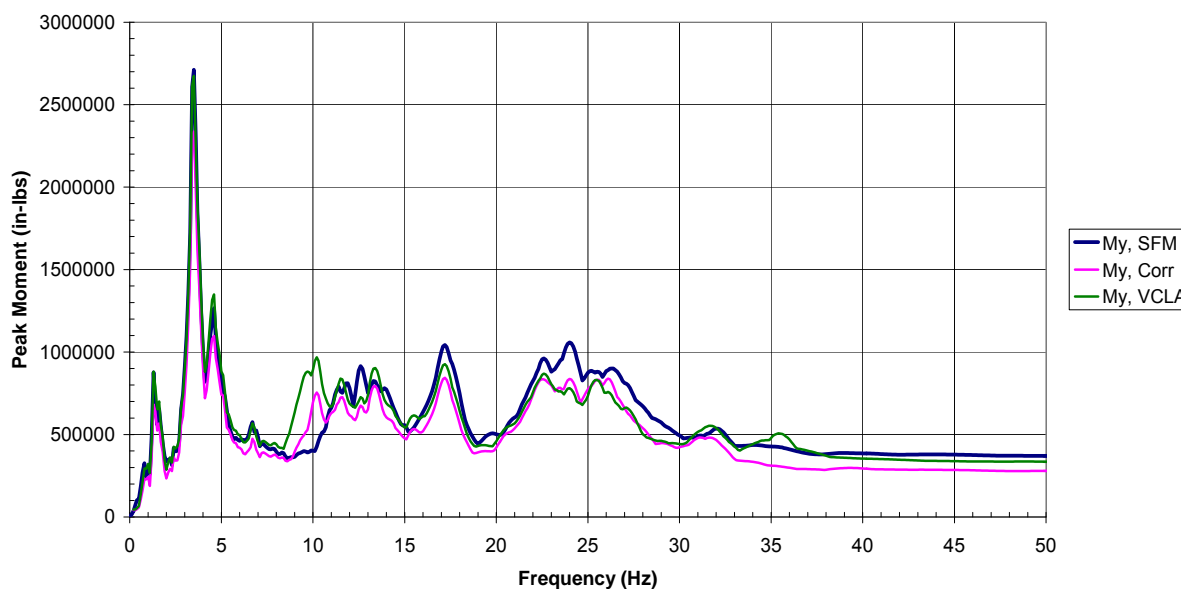


Figure 7.5-6. Airloads Moment Y SRS (Q=20), SFM Versus Basedrive

The SRS plots indicate that the basedrive approach shows significant differences with the SFM measurement above 5 Hz. This is the frequency range which will tend to drive local response on the spacecraft. The time history data was filtered in order to get a better understanding of how the measured interface forces using the SFM approach compare with the forces predicted based on measured accelerations in this frequency range. The basedrive analysis was rerun with the acceleration input filtered using a BP filter to keep frequency content in the 5 to 150 Hz range. The SFM results were filtered using a 5 Hz HP filter to exclude forces with frequency content below 5 Hz. It can be seen from previous SRS plots that the interface loads (forces and moments) generated during the Airloads event have minimal frequency content above 50 Hz so it was not necessary to perform HP filtering of the force data. A summary of the basedrive results after filtering the data is shown in Table 7.5-2.

	NASA Engineering and Safety Center Technical Assessment Report		Document #: NESC-RP- 06-071	Version: 1.0
	Title: Flight Force Measurements of the Gamma-Ray Large Area Space Telescope / Delta II Flight			Page #: 197 of 226

Table 7.5-2. Airloads Filtered Absolute Max Values – SFM versus Basedrive

Method	Maximum Fx (lb)	Time sec	Maximum Fy (lb)	Time sec	Maximum Fz (lb)	Time sec	Maximum Mx (in-lb)	Time sec	Maximum My (in-lb)	Time sec	Maximum Mz (in-lb)	Time sec
SFM	1407.76	35.178	1496.85	39.621	2539.51	21.19	167836.8	37.93	141576.73	35.929	250252.2	33.214
% Error	±10%		±10%		±10%		±5%		±5%		±5%	
Correlated	1916.74	38.89	2050.91	26.258	2650.33	33.027	119096.76	38.765	112120.24	35.929	241083.64	33.217
% Diff	36.2%		37.0%		4.4%		-29.0%		-20.8%		-3.7%	
VCLA	2379.18	41.976	2194.1	37.482	2858.07	24.683	152503.5	37.932	128209.27	33.317	267236.96	33.216
% Diff	69.0%		46.6%		12.5%		-9.1%		-9.4%		6.8%	

The results in Table 7.5-2 show that approximately a third of the lateral force generated at the interface is due to response above 5 Hz and that the over-prediction of the lateral interface loads increases after the data is filtered. The thrust axis force prediction degrades slightly as a result of data filtering with the VCLA results increasing outside of the expected measurement error.

Table 7.5-2 shows that the peak overturning moments (Mx and My) drop by about 50 percent after filtering indicating that a roughly half of the bending moments is driven by modes above 5 Hz. The percent difference between the SFM data and the bending moments predicted by the basedrive are maintained or become slightly worse as a result of data filtering. The most significant effect is on the X-axis moment, which shows a 20 percent increase in the under-prediction between the maximum basedrive results and the SFM measurement. The relative comparison between basedrive results and flight data for the Y-axis and torsional (Mz) moments is relatively unchanged as a result of filtering. The peak magnitude of the torsional moment shows only a small change indicating that the predominant frequency content is above 5 Hz. This is expected given that the launch vehicle fundamental torsional mode occurs at 10 Hz.

Figures 7.5-7 and 7.5-8 show the filtered time histories corresponding to the X-axis force and the Y-axis moment. After data filtering, the X-axis time histories peak at different times indicating that different frequency content is present in each record. The basedrive results show more high frequency content, which contributes to the over-prediction as seen by the differences in the 20 to 40 Hz range on the SRS plot for the X-axis forces.



NASA Engineering and Safety Center Technical Assessment Report

Document #:
**NESC-RP-
06-071**

Version:
1.0

Title:

Flight Force Measurements of the Gamma-Ray Large Area Space Telescope / Delta II Flight

Page #:
198 of 226

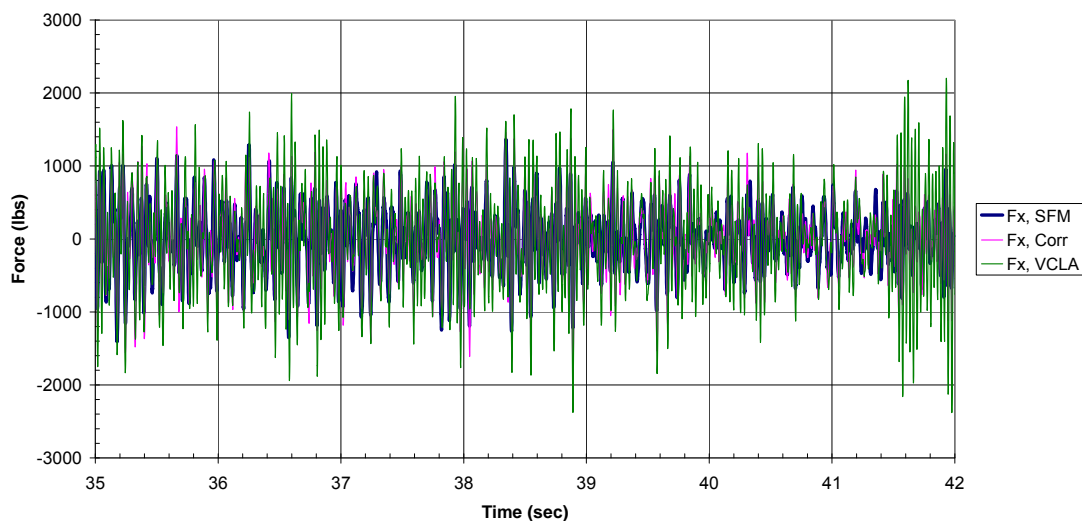


Figure 7.5-7. Airloads X Force, SFM Versus Basedrive (Filtered)

The filtered Y-axis moment data for Airloads shows closer agreement between the basedrive results and the SFM measurement than the filtered X-axis force data. The absolute maximum value still occurs at around the same time and the overall characteristic of the response between the flight measurements and the basedrive predictions is similar.

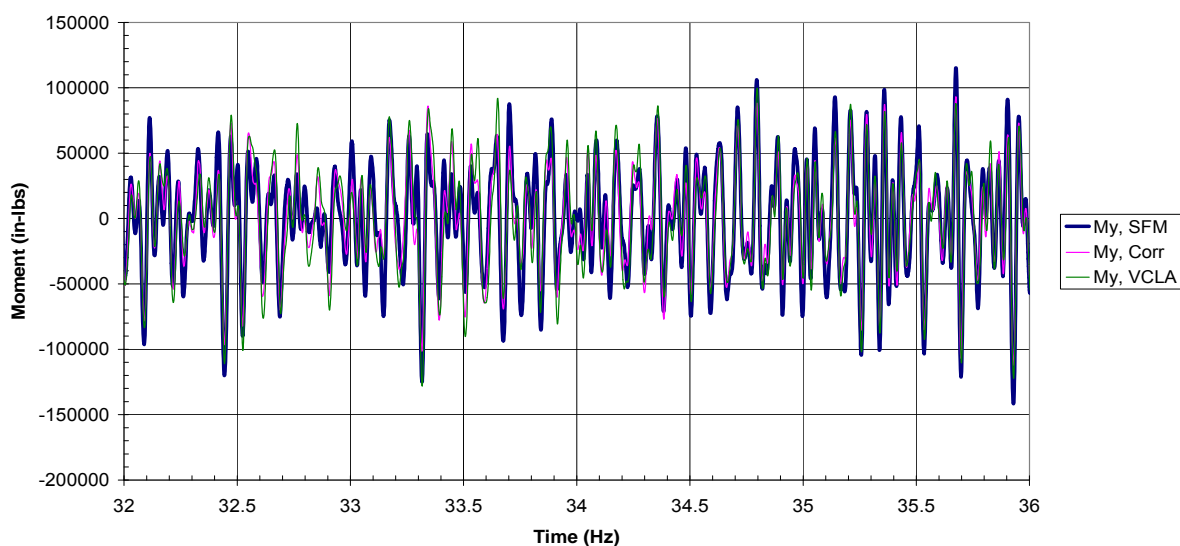


Figure 7.5-8. Airloads Moment Y, SFM Versus Basedrive (Filtered)

	NASA Engineering and Safety Center Technical Assessment Report	Document #: NESC-RP- 06-071	Version: 1.0
Title: Flight Force Measurements of the Gamma-Ray Large Area Space Telescope / Delta II Flight		Page #: 199 of 226	

7.5.2 Airloads Summary

- The basedrive results for the VCLA and correlated models show significant differences in predicting interface forces as compared to measured flight data. These differences can be traced to modeling assumptions of modal frequencies and damping.
- The basedrive results for both models over-predicted the peak lateral forces compared to the flight measurement. In most cases the over-prediction was greater than the measurement error associated with the SFM technique.
- The basedrive results for both models tended to under-predict the peak overturning moments (Mx and My) compared to the flight measurements. In most cases the under-prediction was greater than the measurement error.
- Agreement between basedrive predictions and measured flight forces for the peak thrust axis force and torsional moment was within the measurement error.
- SRS processing of the lateral axis forces shows agreement between basedrive and flight data below 5 Hz corresponding to the 3.5 Hz vehicle bending mode.
- SRS processing of the basedrive results for both models over-predicts the lateral forces above 10 Hz with the VCLA model showing a significant exceedance (due to damping differences) compared to the correlated model in the 30 to 40 Hz range.
- SRS processing of the thrust axis force shows agreement between measured flight data and basedrive predictions for both models. The primary drivers in the thrust axis are the low-frequency vehicle modes at 7 and 12 Hz.
- SRS processing of the thrust axis basedrive results for the VCLA model shows that it over-predicts the force at 30 Hz corresponding to the spacecraft axial mode. This is probably due to differences in damping (2 percent versus measured).
- When the SFM data is HP filtered at 5 Hz, the lateral forces drop to approximately one-third of the unfiltered values indicating that most of the lateral force measured during Airloads is below 5 Hz. The percent over-prediction of lateral forces by the basedrive analysis increases after data filtering.
- The comparison between basedrive results and the measured flight data for the thrust axis force degraded when filtered, but was within (or close to) the expected measurement error.
- The peak lateral bending moments from flight drop by roughly 50 percent when the data is HP filtered at 5 Hz indicating that half of the measured bending moment is driven by modes above that frequency.
- The peak torsional moment is unchanged as a result of HP filtering at 5 Hz as the fundamental vehicle torsional mode occurs at 10 Hz.
- After filtering, the under-prediction of the peak X-axis bending moment by the basedrive results increases by about 20 percent while the under-prediction of the peak Y-axis moment was relatively unchanged.

	NASA Engineering and Safety Center Technical Assessment Report	Document #:	Version:
		NESC-RP-06-071	1.0
Title:		Page #:	
Flight Force Measurements of the Gamma-Ray Large Area Space Telescope / Delta II Flight		200 of 226	

7.6 MECO Reconstruction and Reconciliation

7.6.1 MECO Basedrive Reconstruction

Basedrive analysis studies were performed for the MECO flight time to understand the differences between the interface forces measured directly during flight based on the SFM approach and those calculated from measured flight accelerations. The centerline accelerations shown in Section 7.2 were used as input to GLAST spacecraft/PAF models. Two different GLAST spacecraft models were used in this analysis. One model was the reduced GLAST model that was used for the VCLA described in Section 7.3. A constant 2 percent damping was used for this configuration as this is a typical value used for spacecraft basedrive analysis. The other version was the GLAST spacecraft plus PAF model that was correlated based on the spacecraft sine test data. For the basedrive analysis, both models were coupled to the Delta II 6915 PAF model that was developed for the FFM activity and used to derive the relationship between measured strain and interface loads. In addition, based on the sine test data, a correlated damping schedule for modes to 150 Hz was developed. The correlation process is outlined in Reference 10.

The MECO basedrive analysis for the GLAST spacecraft was performed using the 6 centerline accelerations calculated from the 4 triax accelerometers located around the PAF base. For the first pass data review, no filtering was performed. Table 7.6-1 provides a summary of the basedrive results for the two GLAST spacecraft model configurations as compared to the measured SFM data. The table shows the percent error associated with the SFM measurement based on the defined prediction accuracy. The percent difference between the maximum (absolute) basedrive results and the SFM forces is shown for each model configuration. In cases where the basedrive results are outside the prediction error of the SFM measurement, the values are shown in bold. For instances where the basedrive results under-predict the SFM measurements, the values are shown underlined. It should be noted that the force due to the steady-state acceleration has been added to the basedrive results for direct comparison with the SFM measurements.

Table 7.6-1. MECO Absolute Maximum Forces – SFM versus Basedrive (Unfiltered)

Method	Maximum Fx (lb)	Time sec	Maximum Fy (lb)	Time sec	Maximum Fz (lb)	Time sec	Maximum Mx (in-lb)	Time sec	Maximum My (in-lb)	Time sec	Maximum Mz (in-lb)	Time sec
SFM	494.7	265.24	394.41	265.578	52520.47	264.804	26326.62	265.446	26941.25	265.259	18947.03	265.173
% Error	>±10%		>±10%		±5%		>±10%		>±10%		±10%	
Correlated	544.98	265.39	691.39	265.582	54125.55	264.807	42111.49	265.584	27202	265.396	22642.73	265.177
% Diff	10.2%		75.3%		3.1%		60.0%		1.0%		19.5%	
VCLA	737.33	265.39	958.86	265.312	54352.45	264.807	51953.62	265.585	41739.43	265.4	23233	265.178
% Diff	49.0%		143.1%		3.5%		97.3%		54.9%		22.6%	



NASA Engineering and Safety Center Technical Assessment Report

Document #:
**NESC-RP-
06-071**

Version:
1.0

Title:

Flight Force Measurements of the Gamma-Ray Large Area Space Telescope / Delta II Flight

Page #:
201 of 226

Based on Table 7.6-1, the measured forces and moments with the exception of the maximum thrust force are relatively small. There is a significant over-prediction of the interface loads by the basedrive analysis as compared with the values measured by the SFM. Only the thrust axis forces show agreement. However, this is expected as the thrust axis forces are dominated by the steady-state thrust, which reaches a maximum just before MECO.

The overlays of the time history data comparing the peak measured SFM forces with the basedrive results are shown in Figures 7.6-1 through 7.6-4. Based on the time history plots, the basedrive results have the same overall characteristics as the SFM data, but that the basedrive analysis tends to over-predict the lateral shear and overturning moments at the GLAST spacecraft interface. The thrust axis plot seen in Figure 7.6-3 shows reasonable agreement between the SFM data and the basedrive analysis but the effect of the HP filter built into the SFI accelerometer channels can be seen in the basedrive results. The large X-axis moments from the basedrive analysis seen in Figure 7.6-4 just prior to the start of the MECO Shock Transient event (T+ 264.5 to +265.1 seconds) are a result of the analysis driving the fixed-base bending mode at 10 Hz. This effect is not seen in the SFM data.

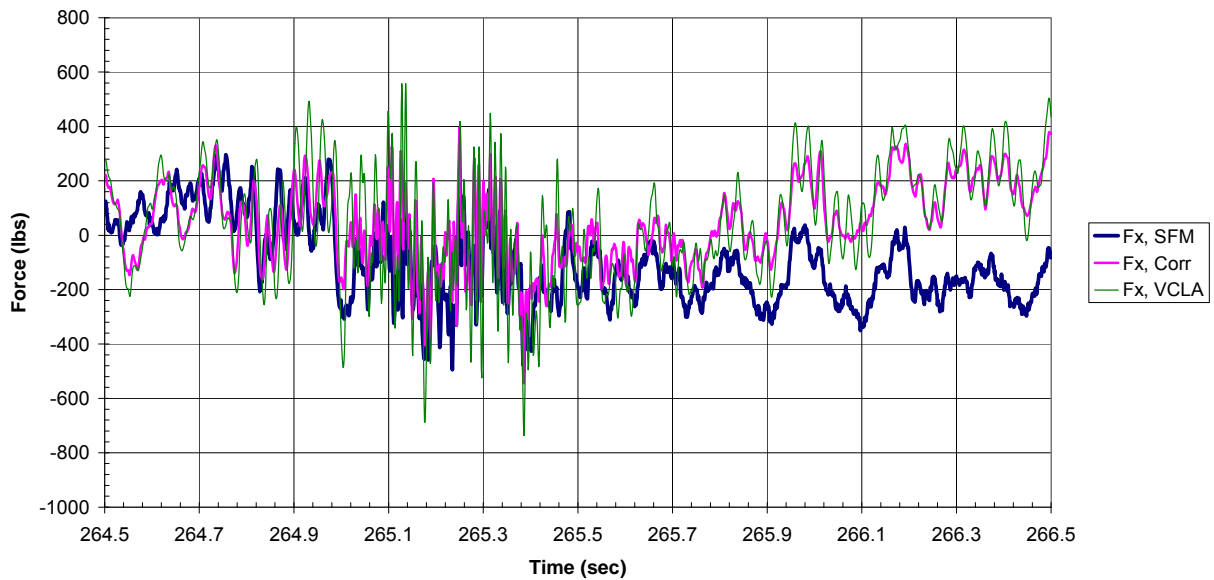


Figure 7.6-1. MECO X-Axis Force – SFM Versus Basedrive



NASA Engineering and Safety Center Technical Assessment Report

Document #:
**NESC-RP-
06-071**

Version:
1.0

Title:

Flight Force Measurements of the Gamma-Ray Large Area Space Telescope / Delta II Flight

Page #:
202 of 226

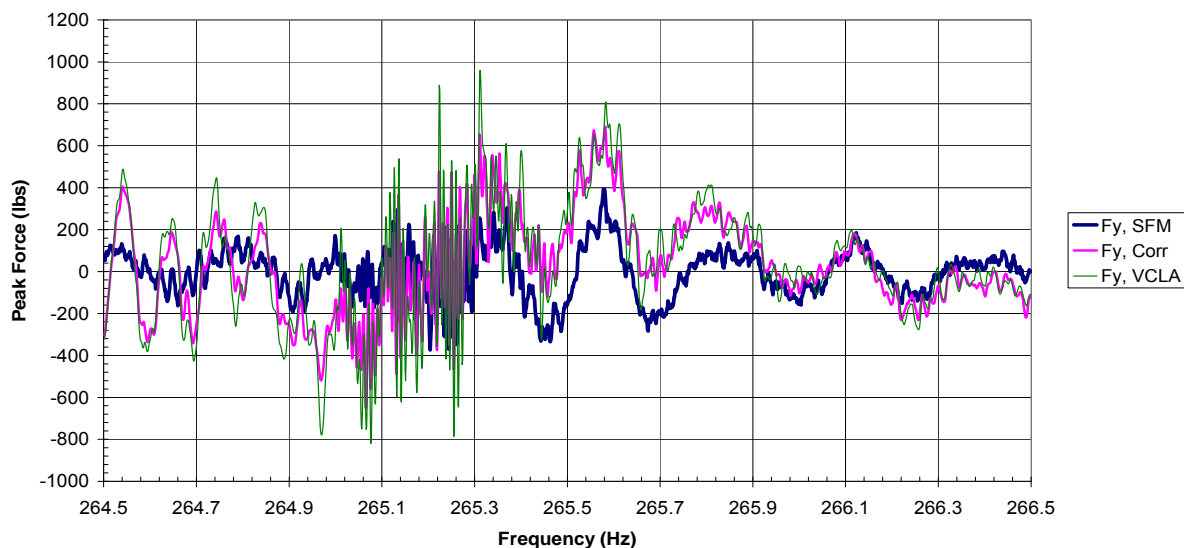


Figure 7.6-2. MEKO Y-Axis Force - SFM Versus Basedrive

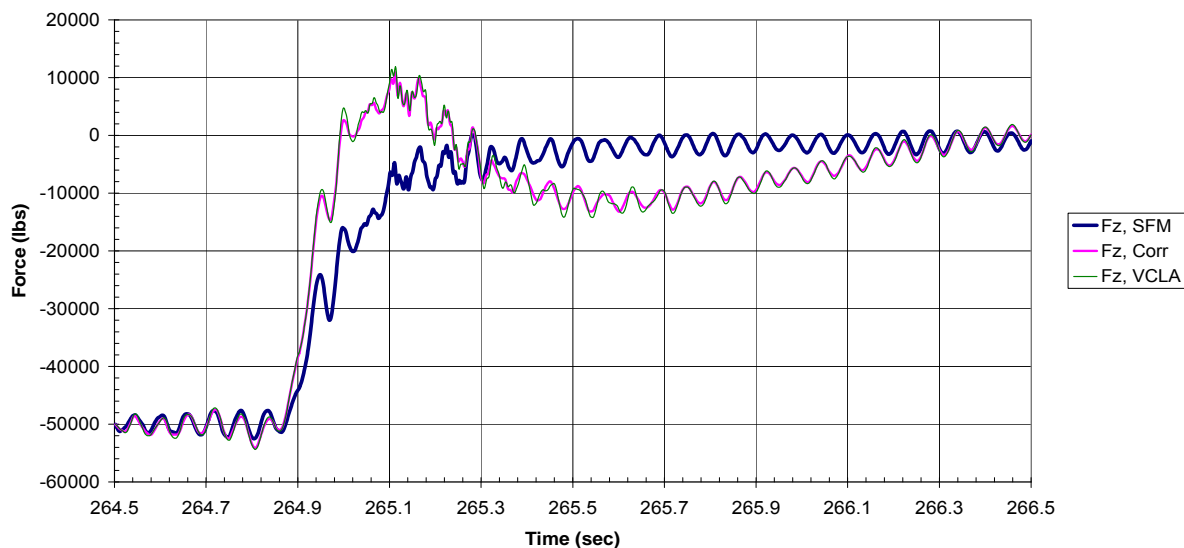


Figure 7.6-3. MEKO Thrust (Z-Axis) - SFM Versus Basedrive



NASA Engineering and Safety Center Technical Assessment Report

Document #:
**NESC-RP-
06-071**

Version:
1.0

Title:

Flight Force Measurements of the Gamma-Ray Large Area Space Telescope / Delta II Flight

Page #:
203 of 226

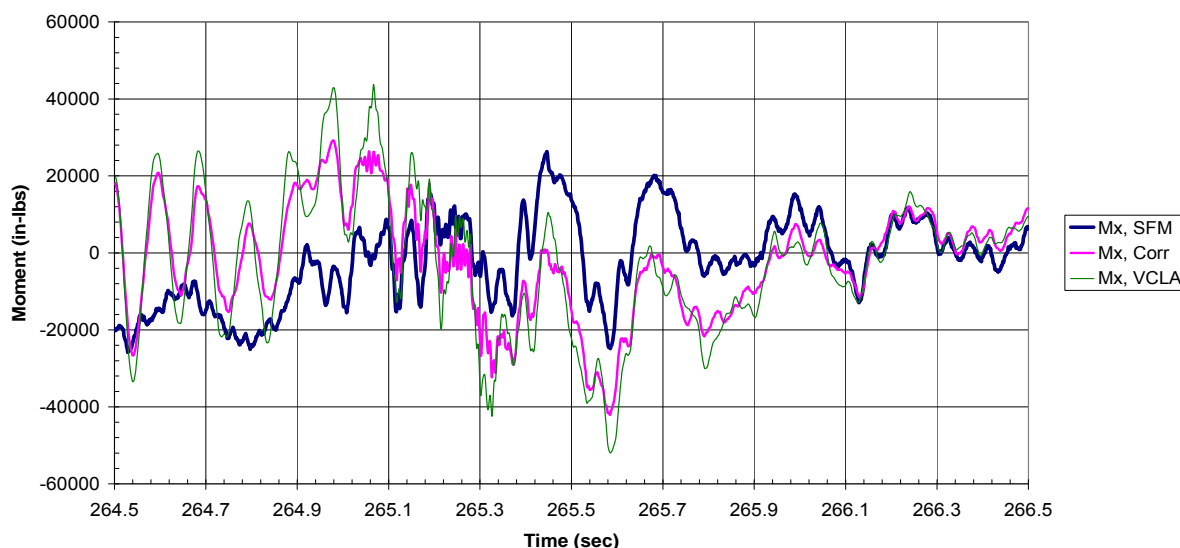


Figure 7.6-4. MECO X-Axis Moment - SFM Versus Basedrive

Figures 7.6-5 and 7.6-6 show the SRS processing of the time history data comparing the frequency content of the measured SFM forces with the basedrive results for the two models. The lateral Y-axis shows significant over-prediction across the entire frequency range. In the MECO Shock Transient event frequency range, which typically occurs from 90 to 140 Hz, both basedrive configurations show larger lateral axis forces than measured during flight. Of particular interest is the 10 Hz GLAST spacecraft lateral mode, which is visible in the basedrive results, but not in the SFM data. This effect can also be seen in the time history data for the X-axis moment shown in Figure 7.6-4. The basedrive results prior to T+265.1 seconds show large peaks due to excitation of the spacecraft lateral mode. The VCLA model tends to show a greater over-prediction as compared with the SFM data than the correlated model which can most likely be attributed to using a constant 2 percent damping in the basedrive analysis. However, even with a damping schedule based on data from the sine test, the correlated model still over-predicts relative to the measured flight data across the frequency range of interest.



NASA Engineering and Safety Center Technical Assessment Report

Document #:
**NESC-RP-
06-071**

Version:
1.0

Title:

Flight Force Measurements of the Gamma-Ray Large Area Space Telescope / Delta II Flight

Page #:
204 of 226

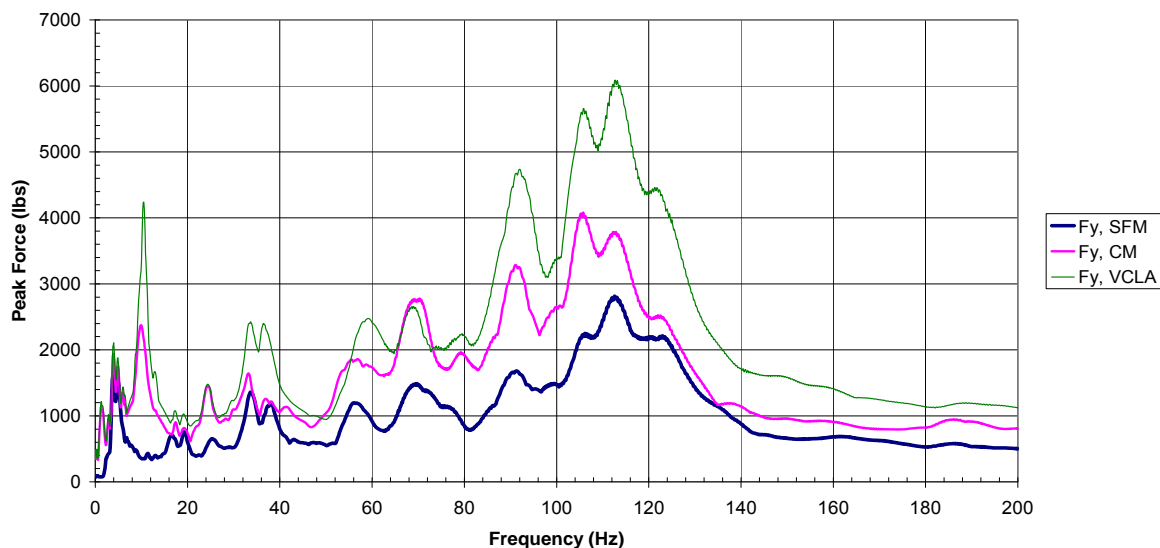


Figure 7.6-5. MECO Y-Axis Force SRS (Q=20) - SFM Versus Basedrive

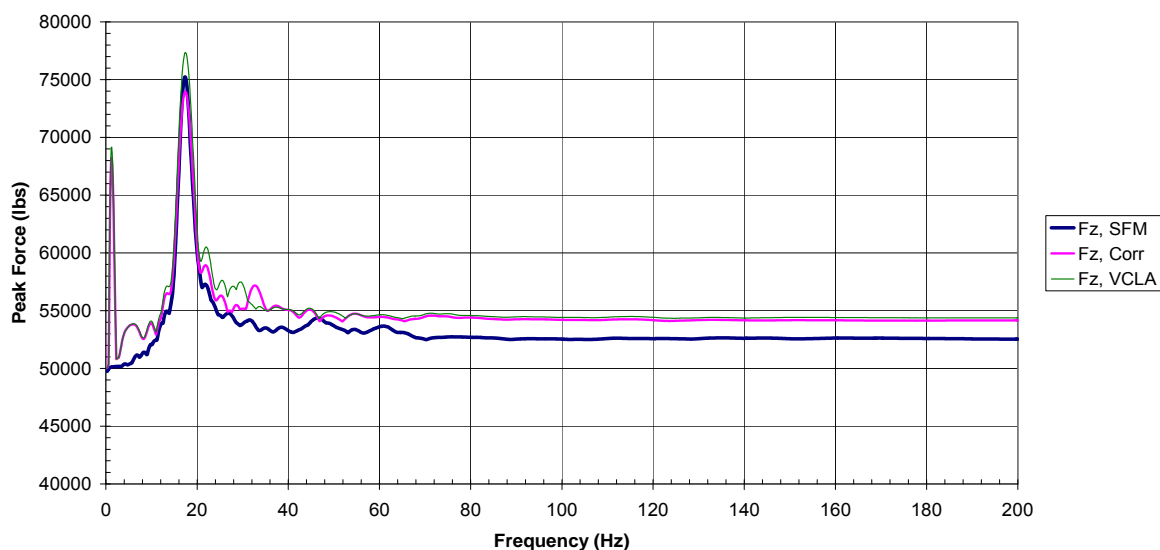


Figure 7.6-6. MECO Thrust (Z) Axis SRS (Q=20) - SFM Versus Basedrive

The SRS of the thrust axis forces from MECO show the primary axial mode of the launch vehicle at 18 Hz. None of the plots show frequency content associated with the 120 Hz MECO Shock Transient event, but this is due to the fact that it the forces associated with the MECO Shock Transient as small compared to the steady-state MECO forces. Also seen on the SRS plot



NASA Engineering and Safety Center Technical Assessment Report

Document #:
**NESC-RP-
06-071**

Version:
1.0

Title:

Flight Force Measurements of the Gamma-Ray Large Area Space Telescope / Delta II Flight

Page #:
205 of 226

is the low-frequency peak at approximately 1 Hz which is an artifact associated with the HP filter built into the accelerometer channels of the SFI system.

When the thrust forces are filtered from 30 to 150 Hz to remove the steady state-acceleration and the large input from the prior-to-MECO event, the forces due to the MECO Shock Transient event can be resolved. The SRS plots corresponding to filtering the thrust axis forces using a BP filter from 30 to 150 Hz can be seen in Figure 7.6-7. The dominant frequency content can be seen in the 70 to 125 Hz range. Both of the basedrive configurations show a significant over-prediction around 80 Hz compared to the measured interface forces corresponding to axial modes of the GLAST spacecraft. The fundamental axial mode of the spacecraft can also be seen on the plot around 30 Hz.

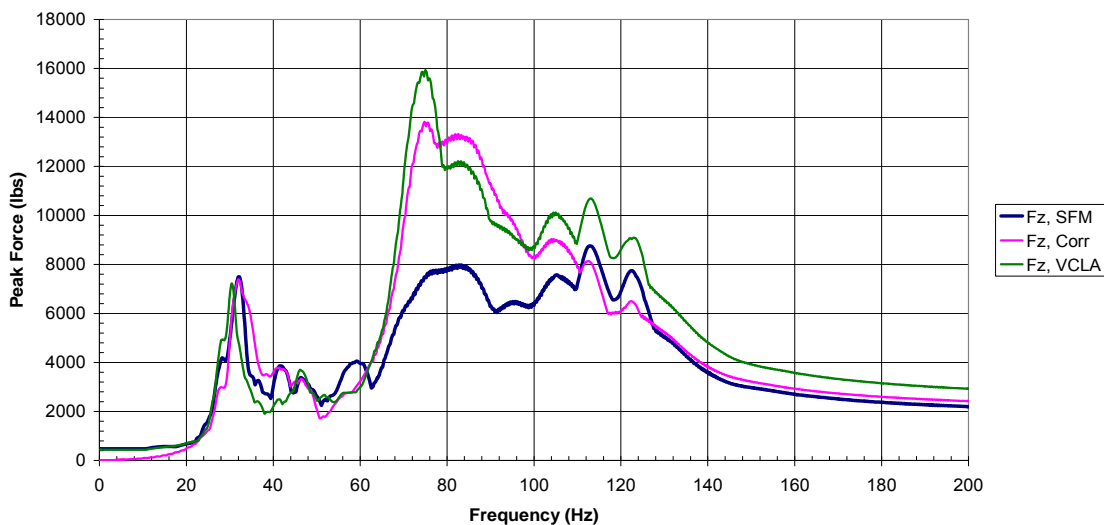


Figure 7.6-7. MECO Thrust SRS ($Q=50$) Filtered 30 to 150 Hz



Title:

Flight Force Measurements of the Gamma-Ray Large Area Space Telescope / Delta II Flight

Page #:
206 of 226

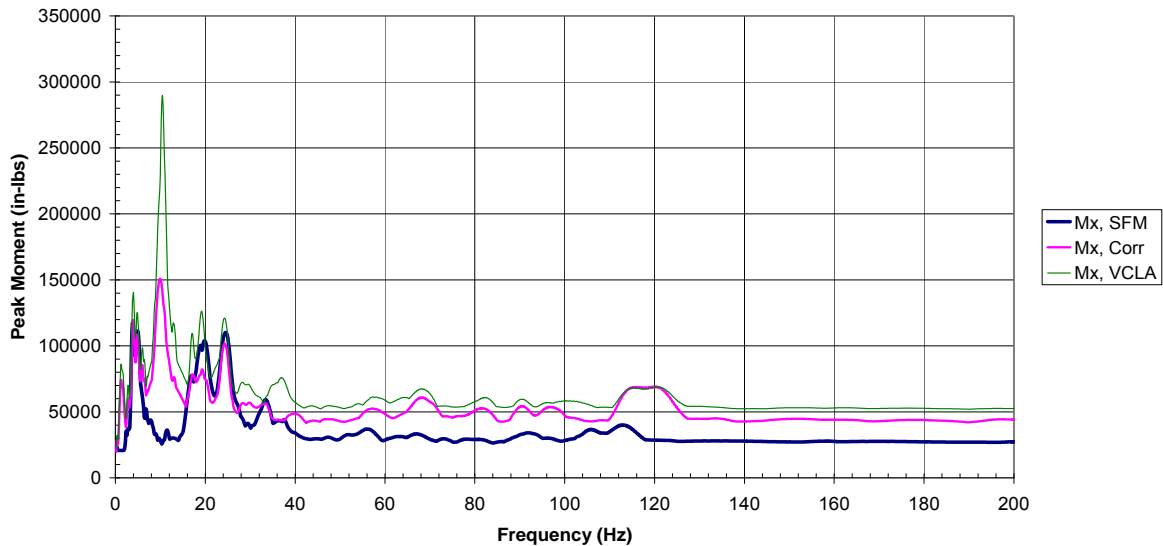


Figure 7.6-8. MECO X-Axis Moment SRS ($Q=20$) - SFM Versus Basedrive

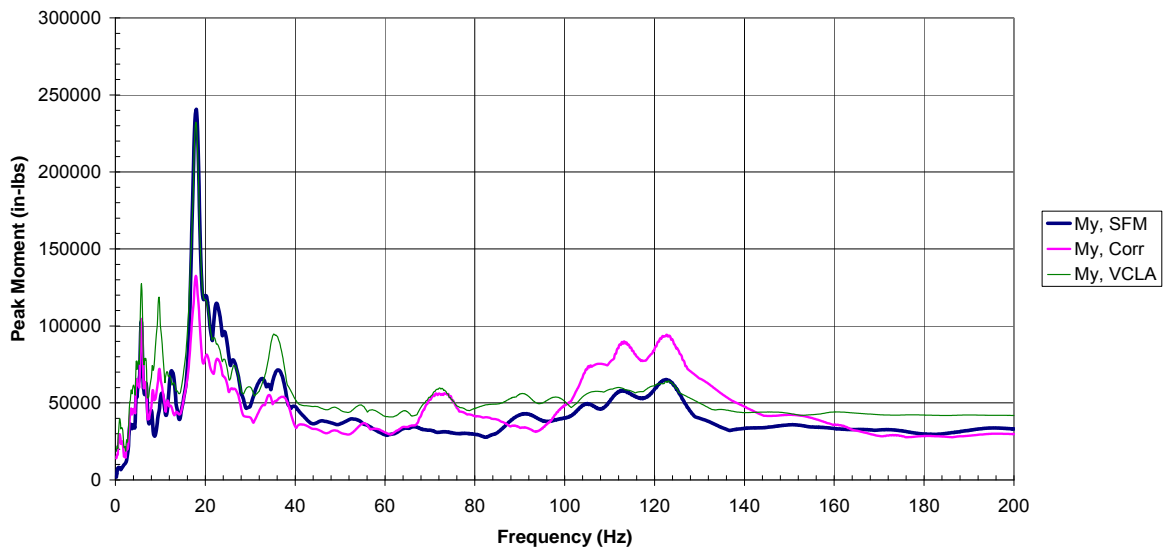


Figure 7.6-9. MECO Y-Axis Moment SRS ($Q=20$) - SFM Versus Basedrive

The SRS results for the lateral moments indicate different behaviors depending on the axis. The SRS processing of the X-axis moment (Figure 7.6-8) shows that both models over-predict the bending moment at 10 Hz corresponding to the fixed-base mode of the spacecraft (although it is



NASA Engineering and Safety Center Technical Assessment Report

Document #:
**NESC-RP-
06-071**

Version:
1.0

Title:

Flight Force Measurements of the Gamma-Ray Large Area Space Telescope / Delta II Flight

Page #:
207 of 226

stronger in the VCLA model) but that the 10 Hz mode does not appear in the SFM data. The VCLA model also tends to over-predict the X-axis moment in the low-frequency range below 40 Hz while the correlated model tends to under-predict the flight data in that same frequency range due to poor modeling of the rotational inertia associated with the mass of propellant. Both models over-predict the X-axis bending moment in the MECO Shock Transient frequency range around 120 Hz.

The SRS processing of the Y-axis moment (Figure 7.6-9) shows agreement for the VCLA model at 18 Hz which results from coupling with the launch vehicle axial mode. However, the VCLA model over-predicts the bending moment at frequencies above and below the 18 Hz axial mode, especially at frequencies corresponding to fixed-base modes of the spacecraft. The correlated model tends to under-predict the Y-axis moment in the low-frequency range, but over-predicts the moment across much of the frequency range above 70 Hz including the MECO Shock Transient range around 120 Hz. Once again, the response differences between the VCLA and correlated models in the prediction of overturning moments at the interface can be traced to poor modeling of the rotational inertia associated with the propellant mass in the correlated model.

SRS processing of the torsional moment (M_z) shown in Figure 7.6-10 indicates that both models over-predict the measured flight moment over much of the frequency range with significant exceedances at 27 and 75 Hz, which are probably the cause of the 20 percent over-prediction seen in the peak torsional moment when comparing absolute maximum results from Table 7.6-1.

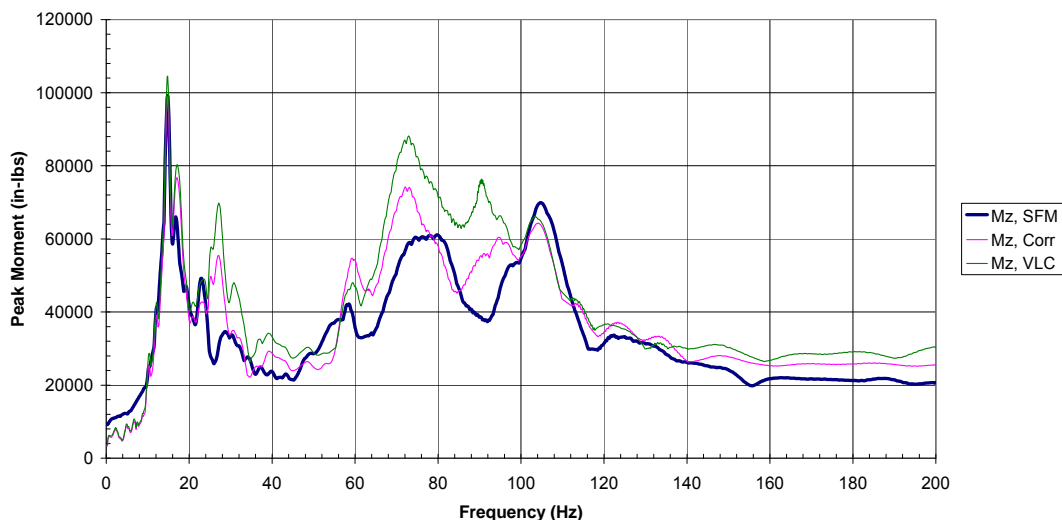


Figure 7.6-10. MECO Torsional (M_z) Moment SRS ($Q=20$) - SFM Versus Basedrive

	NASA Engineering and Safety Center Technical Assessment Report	Document #:	Version:
		NESC-RP-06-071	1.0
Title: Flight Force Measurements of the Gamma-Ray Large Area Space Telescope / Delta II Flight		Page #: 208 of 226	

The SRS plots indicate that the basedrive approach shows significant differences with the SFM measurement above 5 Hz. This is the frequency range which will tend to drive the GLAST spacecraft local response. Data filtering provides a better understanding of how the measured interface forces using the SFM compare with the forces predicted based on measured accelerations. The basedrive analysis was rerun with the acceleration input filtered using a BP filter to keep frequency content in the 5 to 150 Hz range. The SFM results were filtered using a 5 Hz HP filter to only include force content above 5 Hz. The filtered MECO absolute maximum forces are shown in Table 7.6-2.

Table 7.6-2. MECO Absolute Maximum Forces - SFM versus Basedrive (5 to 150 Hz)

Method	Maximum Fx (lb)	Time sec	Maximum Fy (lb)	Time sec	Maximum Fz (lb)	Time sec	Maximum Mx (in-lb)	Time sec	Maximum My (in-lb)	Time sec	Maximum Mz (in-lb)	Time sec
SFM	307.48	265.24	314	265.239	7243.55	264.97	14614.53	265.17	22616.35	265.259	16276.27	265.173
% Error	>±10%		>±10%		±5%		>±10%		>±10%		±10%	
Correlated	436.03	265.25	589.62	265.255	6753.2	264.946	19444.48	265.00	19101.85	265.137	19175.63	265.177
% Diff	41.8%		87.8%		-6.8%		33.0%		-15.5%		17.8%	
VCLA	611.17	265.00	907.61	265.255	7262.66	264.946	26953.43	265.003	30650.67	265.014	19646.71	265.178
% Diff	98.8%		189.0%		0.3%		84.4%		35.5%		20.7%	

The results in Table 7.6-2 show that most of the lateral load measured during MECO is caused by frequencies above 5 Hz as the maximum values show little reduction as a result of the filtering process. The amount of over-prediction in the lateral forces from the basedrive analysis for both configurations increased as a result of filtering the data. This would indicate that the basedrive using the acceleration data consistently over-predicts the lateral interface forces as compared to the measured SFM force data. The thrust axis force shows a significant reduction in magnitude as the effect of the filtering is to remove the steady-state thrust, which is the largest portion of the force measured during this flight time. However, after filtering the thrust axis forces show agreement and within the measurement error.



Title:

**Flight Force Measurements of the Gamma-Ray Large
Area Space Telescope / Delta II Flight**

Page #:
209 of 226

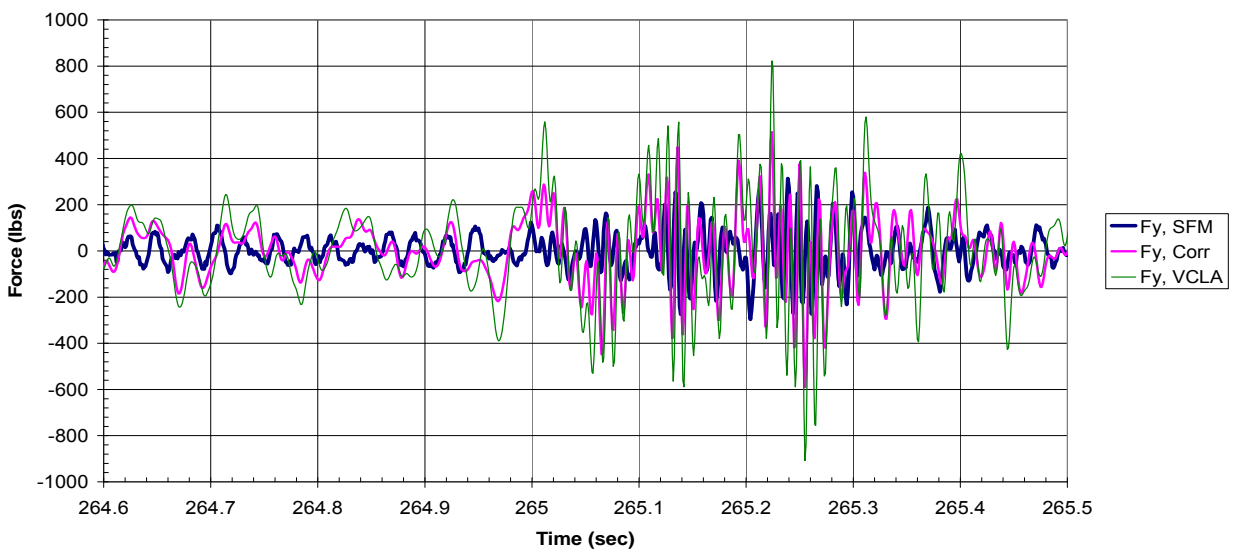


Figure 7.6-11. MECO Y-Axis Force (Filtered)

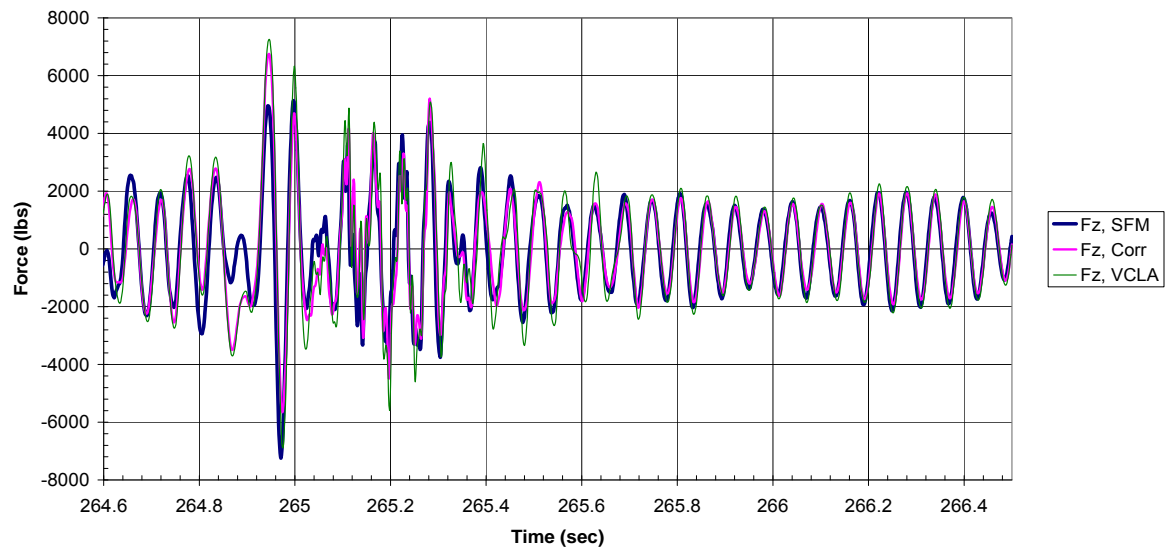


Figure 7.6-12. MECO Thrust (Z) Axis (Filtered)

The peak X-axis moment showed an approximately 50 percent reduction due to data filtering. The reduction was greater for the SFM measurement than for the basedrive results, but the resulting comparisons were showing over-predictions that were greater than the error associated with the SFM measurement. This is primarily because the basedrive peak was occurring at the



NASA Engineering and Safety Center Technical Assessment Report

Document #:
**NESC-RP-
06-071**

Version:
1.0

Title:

Flight Force Measurements of the Gamma-Ray Large Area Space Telescope / Delta II Flight

Page #:
210 of 226

spacecraft 10 Hz fixed-base mode. For the Y-axis moment, the VCLA model was showing significant over-prediction relative to the flight data after filtering, but the amount of the over-prediction had been reduced. The correlated model was showing under-prediction after filtering the Y-axis moment as a result of removing the contribution of the low-frequency launch vehicle modes. The differences seen in the basedrive results for lateral bending moments between the two models is primarily due to differences in the model's mass properties. A comparison of the rigid body mass properties between the two models showed that the rotational inertia terms for the correlated GLAST spacecraft model were approximately 15 percent lower than the VCLA configuration. This difference has been traced to the development of the correlated model in which the translational mass was increased to account for the differences between the test and flight configurations. However a similar increase was not made for the rotational inertia terms. The effects of this inertia difference can be seen in the under-prediction of the 18 Hz response by the correlated model in Figure 7.6-9.

The filtered time histories are shown in Figures 7.6-11 through 7.6-13. It should be noted that the force and acceleration data filtering had relatively little impact on the time at which the absolute maximum force or moment occurred (i.e., the maximums all occurred within ± 0.2 seconds of the MECO Shock Transient event start).

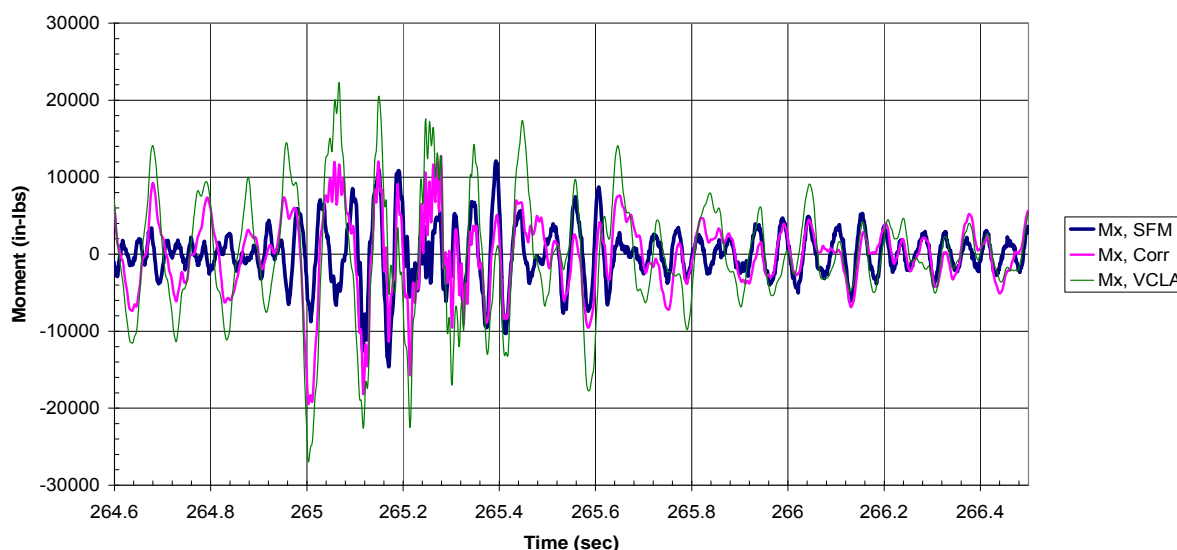


Figure 7.6-13. MECO X-Axis Moment (Filtered)

In the case of the Delta II MECO Shock Transient event, payloads are designed to withstand the event using a frequency domain basedrive analysis in the 80 to 140 Hz range. The input is an envelope of measured acceleration levels from previous flights. Basedrive analysis is used

	NASA Engineering and Safety Center Technical Assessment Report	Document #:	Version:
		NESC-RP-06-071	1.0
Title: Flight Force Measurements of the Gamma-Ray Large Area Space Telescope / Delta II Flight			Page #: 211 of 226

because it has not been possible to develop a coupled loads simulation which can accurately match measured flight accelerations. However, the basedrive analysis has in many cases resulted in high responses predicted on the spacecraft requiring the use of standard force limiting methods (e.g., Semi-empirical, Blocked Force, Norton-Thevenin), which have resulted in significant reduction in predicted response. However, the MECO transient base-drive analysis and the force-limited results have never been validated with measured flight forces.

Analysis for the MECO Shock Transient event is typically performed using thrust and lateral forcing functions derived as equivalent sinusoidal input over the 80 to 140 Hz frequency range. To get a better understanding of how the measured forces compare with the basedrive analysis in that frequency range, the SFM and basedrive results were filtered in the 80 to 150 Hz range. The absolute maximum values for this data are shown in Table 7.6-3.

It can be seen from this table that a basedrive performed in the 80 to 150 Hz range to calculate the forces generated by the MECO Shock Transient event using measured accelerations as input over-predicts the interface forces measured during flight. The differences tend to be more significant for the lateral forces and overturning moments. The VCLA model tended to show the largest over-prediction in the lateral axis forces with the calculated Fy force almost 150 percent larger than the comparable force measured during flight. The correlated model tended to show the largest over-prediction with the SFM results for the lateral bending moments showing a similar over-prediction of around 150 percent. The basedrive results did not entirely over-predict the measured forces. The correlated model under-predicted the torsional moment (Mz) by around 20 percent, while the VCLA model over-predicted Mz by around 30 percent. In the case of the torsional moment, the measurement accuracy was greater than 10 percent and the results were not inconsistent with the expected measurement error.

Table 7.6-3. MECO Absolute Maximum Forces – SFM Versus Basedrive (80 to 150 Hz)

Method	Maximum Fx (lb)	Time sec	Maximum Fy (lb)	Time sec	Maximum Fz (lb)	Time sec	Maximum Mx (in-lb)	Time sec	Maximum My (in-lb)	Time sec	Maximum Mz (in-lb)	Time sec
SFM	174.32	265.13	263.09	265.248	1082.18	265.11	3045.54	265.116	3558.2	265.245	5277.29	265.167
% Error	>±10%		>±10%		±10%		>±10%		>±10%		>±10%	
Correlated	263.55	265.29	398.48	265.255	1347.56	265.113	4908.82	265.25	8849.75	265.132	4142.84	265.254
% Diff	51.2%		51.5%		24.5%		61.2%		148.7%		-21.5%	
VCLA	343.99	265.29	645.11	265.26	1501.71	265.114	3394.42	265.246	5391.35	265.261	6998.31	265.219
% Diff	97.3%		145.2%		38.8%		11.5%		51.5%		32.6%	

7.6.2 Main Engine Cutoff Reconstruction and Reconciliation Summary

- Measured forces and moments for MECO were small compared to other flight events but the basedrive results show the largest over-prediction for both forces and moments.

	NASA Engineering and Safety Center Technical Assessment Report	Document #: NESC-RP- 06-071	Version: 1.0
Title: Flight Force Measurements of the Gamma-Ray Large Area Space Telescope / Delta II Flight			Page #: 212 of 226

- Thrust axis force predictions for both basedrive configurations show agreement with measured flight forces and were within the measurement error.
- SRS processing of the Y-axis force data shows that the basedrive results over-predict the measured flight forces across the frequency range from 5 to 200 Hz including the MECO transient frequency range from 90 to 140 Hz. The VCLA model shows the largest over-prediction due to the use of 2 percent constant damping for all modes.
- SRS processing of the Y-axis force data shows a strong 10 Hz mode in the basedrive results corresponding to the first lateral mode of the fixed-base spacecraft on the PAF, which does not appear in the measured flight data.
- SRS processing of the unfiltered thrust axis time history data shows the 18 Hz vehicle axial mode in the SFM and the basedrive data, but show little frequency content above 40 Hz. This is due to the forces associated with the MECO Shock Transient event were small compared with the steady-state forces at MECO.
- SRS processing of the thrust time history data filtered from 30 to 150 Hz shows the dominant frequency content to be in the 70 to 125 Hz range associated with the MECO Shock Transient event.
- SRS processing of the lateral moment about the X-axis (M_x) shows that both basedrive configurations over-predict the peak basedrive moment at 10 Hz corresponding to the fixed-base bending mode of the spacecraft. The 10 Hz mode does not appear in the M_x force data measured during flight.
- Both basedrive configurations over-predict the M_x bending moment in the MECO Shock Transient frequency range between 100 to 140 Hz.
- SRS processing of the lateral moment about the Y-axis (M_y) indicate that the dominant frequency content occurs at 18 Hz due to axial/bending coupling with the launch vehicle fundamental axial mode. The VCLA model shows agreement with the measured flight data at 18 Hz. The under-prediction of the correlated model can be traced to poor modeling of the rigid body rotational inertia associated with the propellant mass.
- SRS processing of the basedrive results for the torsional moments (M_z) shows significant over-prediction around 27 and 75 Hz, which accounts for the 20 percent difference seen in peak response.
- Filtering the lateral MECO forces using a 5 Hz HP filter results in minimal reduction in the peak values as the most of the lateral force during MECO is above this frequency. However, the amount of over-prediction increased after filtering.
- The thrust axis force data shows significant reduction due to filtering of the large steady-state force, but the basedrive predictions continue to show agreement with the measured flight forces.
- After filtering the data, M_x was reduced by about 50 percent as it was more dependent on the coupled system bending mode at 3 Hz. M_y showed less of a reduction because it was

	NASA Engineering and Safety Center Technical Assessment Report	Document #: NESC-RP- 06-071	Version: 1.0
Title: Flight Force Measurements of the Gamma-Ray Large Area Space Telescope / Delta II Flight		Page #: 213 of 226	

more dependent on coupling with the 18 Hz axial mode. The amount of over-prediction by the basedrive analysis for the lateral bending moments was reduced by filtering.

- When the MECO force data was BP filtered from 80 to 140 Hz, the basedrive techniques over-predicted all forces except for the torsional moment. The basedrive results from the VCLA model showed the largest over-prediction of the lateral and thrust axis forces while the correlated model showed the largest over-prediction of the lateral bending moments. The correlated model under-predicted the torsional moment after BP filtering.

7.7 Summary of Flight Reconstruction and Reconciliation Efforts

A full flight reconstruction analysis of the GLAST mission proved to be more difficult and complex than originally anticipated. In the end, it was only possible to perform a full coupled reconstruction analysis for the Liftoff flight event. The initial attempt at Liftoff reconstruction over-predicted both the measured flight accelerations and forces. A significant amount of work was required to create a Liftoff flight reconstruction that showed reasonable agreement with the measured acceleration and this analysis did not show agreement with the measured flight forces. The full reconstruction analysis under-predicted the peak lateral force and overturning moment. It is not clear whether a full reconstruction analysis offers additional benefit over the simpler basedrive analysis.

The basedrive analysis technique using measured accelerations as input to calculate interface forces was sensitive to model predictions of mode shapes and modal frequencies, and to damping assumptions. Slight differences between models were shown to produce different interface forces predictions. The basedrive results were sensitive to how the input acceleration data was processed including data filtering and dropout correction.

The acceleration based methods did a poorer job predicting lateral forces and overturning moments as compared with the axial force predictions. In most cases, the axial force predictions were within the measurement error of the strain-to-force recovery methods, while the lateral load and bending moments showed a larger variation with respect to the measured forces. In many cases, this was due to the quasi-static thrust load which was a significant portion of the measured force in the thrust axis. However, even after filtering to remove the steady-state effects, the trend was that the thrust axis force predictions were within 20 percent, while the prediction of shear forces and moments showed a significantly wider variation. It is not clear how to improve the predictions using acceleration based methods without the availability of future FFMs and /or the improvement of force prediction techniques (force limits based on acceleration and impedance methods).

The basedrive analysis over-predicted the lateral interface forces for all major flight events (Liftoff, Airloads, and MECO). This is most likely due to differences between the fixed-base modes of the GLAST spacecraft predicted by the math model and the actual physical behavior of the GLAST spacecraft when coupled with the launch vehicle. Therefore, the frequency content

	NASA Engineering and Safety Center Technical Assessment Report	Document #: NESC-RP- 06-071	Version: 1.0
Title: Flight Force Measurements of the Gamma-Ray Large Area Space Telescope / Delta II Flight			Page #: 214 of 226

of the peaks and valleys of the measured accelerations during flight at the spacecraft interface do not exactly correspond to the frequencies analytically predicted for the spacecraft assuming a fixed-base interface. These differences would tend to over-predict the forces especially for modes that have significant modal effective mass.

The basedrive analysis tended to under-predict the measured peak lateral bending moments. This effect was more pronounced for the analysis using the correlated model as compared with the basedrive results for the VCLA model. Comparison of the mass matrices for both models showed that the correlated model has less rotational inertia than the VCLA model, which would account for the under-prediction results. The lower rotational inertia of the correlated model was an artifact of the process use to create the correlated model. Both the VCLA and correlated models, however, tended to under-predict the lateral moments above the fundamental bending modes of the spacecraft. This was most likely due to fact that neither model accurately characterizes the distribution of rotational inertia for the GLAST spacecraft fixed-base modes above the fundamental lateral bending modes.

Filtering of the time history data was necessary to fully understand the relationship between measured flight forces and the forces predicted by the basedrive approach. The thrust axis forces measured during flight were DC coupled and reflected loads due to both launch vehicle steady-state thrust acceleration and vibration input. Since the magnitude of the steady state thrust was significantly greater than the vibration input, in many cases the forces due to the steady-state condition saturated the dynamic behavior in the SRS comparisons. A HP filter was used to remove the effect of the steady-state thrust acceleration from the measured data. In addition, the accelerometers used to derive the input for the basedrive analysis were HP filtered to remove a data acquisition system artifact, which showed a low-frequency (approximately 1 Hz) oscillation after being exposed to a significant change in steady-state thrust levels such as at Liftoff and MECO. Finally, BP filters were necessary to understand how the measured flight data and predicted forces compared over different frequency ranges of interest. It should be noted that the magnitude of the SRS results did not have a clear physical meaning when applied to force time histories as the technique was derived to evaluate the damage potential of an acceleration signal. However, the SRS technique was used strictly as a means to compare the frequency content and relative magnitudes of the time history data between the measured flight forces and the basedrive results.

The assessment of the percentile associated with a particular flight event as compared against a statistical database of previous flights using only a single measured d-o-f may not hold true for other response d-o-f. To perform a complete post-flight characterization, it may be necessary to perform this assessment for multiple payload d-o-f for a given flight event. For example, the ULA Post-Flight Report [ref. 9] for the GLAST mission showed that the acceleration level during Airloads was equal to the P95/50 level for 31 previous flights based on a single lateral acceleration measurement made by a SSGS tangential accelerometer. However, when the

	NASA Engineering and Safety Center Technical Assessment Report	Document #: NESC-RP- 06-071	Version: 1.0
Title: Flight Force Measurements of the Gamma-Ray Large Area Space Telescope / Delta II Flight		Page #: 215 of 226	

measured flight forces and accelerations were compared with CLA predictions, not all response directions showed a consistent amount of over-prediction corresponding to the same flight level. The lateral acceleration may be at a 95/50 level. However, the system torsional response may only reflect the mean value for the same number of flights. Therefore, care should be taken when using a single measurement to characterize the statistical flight level on a particular flight and a given flight event.

7.8 Closing Arguments

This section will attempt to answer the questions the NESC team proposed at the beginning of this assessment.

7.8.1 Method(s) to Measure Flight Forces

The initial preference to measure forces would be to place force gages in the load path. However, in absence of such possibility, the NESC team developed and demonstrated the viability of several methods to predict ground and/or flight forces. Two strain-based methods (SFM and FEM Method) and one acceleration-based method (Impedance Method) were examined. There is a preference for the SFM, based on its independence of launch vehicle boundary conditions and smaller predicted errors. However, the other methods were complementary and would have proven useful in case of loosing critical data channels for the SFM. It is worth noting that prediction errors for the Impedance Method have not been estimated.

Developing a methodology to accurately calculate interface forces at the separation plane using strain based measurements on a launch vehicle PAF is a complex process. The NESC team found the strain based methods even on a relatively simple truss structure like the 6915 Delta II PAF required a lengthy and complex development effort. The development process for the 6915 PAF was complicated by the fact that the strut cross-section was not rectangular and twisted as it transitioned from the upper to lower interface ring. This combined with the relatively short legs and the generous leg to ring fillet radii added to the complexity of deriving the calculation methodology and determining strain gage placement.

The decision to pursue a strain based approach was driven by the impracticality of obtaining force gages directly in the system load path. The use of force gages would be the first option to measure interface forces for a number of flights over a wide range of payloads and adapter types. In the future, if the use of forces gages is not feasible, then the development cost associated with strain based approach may payoff if several flights are planned with the same payload adapter.

It is not clear that the use of strain gages as a force measurement approach is feasible for shell-like payload adapters. This was based on the fact that the load path in a shell structure is much less determinate than in a truss structure and it may not be feasible to develop an accurate transformation between strain and load with a realistic number of strain gages. No attempt was

	NASA Engineering and Safety Center Technical Assessment Report	Document #: NESC-RP- 06-071	Version: 1.0
Title: Flight Force Measurements of the Gamma-Ray Large Area Space Telescope / Delta II Flight			Page #: 216 of 226

made during the FFM study to examine the feasibility of applying the strain gage force measurement technique to other PAF geometry.

7.8.2 Benefits of Acquiring Interface Force Measurements during Flight

Question #1: “Is flight correlation and reconstruction with acceleration measurements sufficient?”

Acceleration-based techniques are inherently limited by the fact that while it is relatively easy to measure acceleration response, the quantity of interest is the load which is generated by the acceleration field acting on the hardware. In order to predict how much load is associated with a given acceleration level, it is necessary to derive a mathematical model which requires assumptions about the modal parameters of the physical systems (e.g., frequency and mode shape) and estimations of damping which can be difficult to quantify for a specific configuration and event. While the NESC team had the tools necessary to improve the model fidelity used to predict flight loads such as modal survey and ground vibration testing, the team was limited based modeling assumptions and modeling accuracy. The measurement of flight forces is the most direct path to determining the quantity of interest (e.g., forces and stresses), and provides a means for grounding any analysis used to simulate how launch vehicle payloads respond to flight environments.

The conclusions based on the data gathered during this activity were that basedrive techniques using measured flight accelerations tend to over-predict the interface loads driven by the payload resonant behavior as compared to measured flight forces. This primarily seems to be caused by the frequency content of the measured accelerations used as input to the basedrive is a function of coupled system behavior. Therefore, the input will have peaks at the coupled system frequencies and have dips or notches corresponding to the payload fixed-base modes. If the payload model used in the basedrive analysis does not exactly match the payload modal behavior under the boundary conditions which reflect the payload to booster interface, then the basedrive analysis will tend to over-predict the interface loads. This is because the payload modes are not exactly aligned with the corresponding input notches. This situation is made worse when acceleration data from multiple flights is used to derive an input spectrum in the frequency domain. In this case, the enveloping process smoothes over the valleys and the input levels are based on peak acceleration values. The only means by which to mitigate the over-prediction resulting from a basedrive analysis is to have measured flight forces which allow the interface loads to be limited to realistic levels within a given frequency range.

Based on the results of this assessment, the CLA accuracy is not as straightforward to assess against measured flight forces as was the basedrive analysis technique. From the measured flight data, the VCLA shows a significant over-prediction of the interface forces. However, the VCLA results cannot be directly compared with the measured flight data as the VCLA is designed to cover a 3-sigma worst case scenario such that it is difficult to draw definitive conclusions from a

	NASA Engineering and Safety Center Technical Assessment Report	Document #: NESC-RP- 06-071	Version: 1.0
Title: Flight Force Measurements of the Gamma-Ray Large Area Space Telescope / Delta II Flight			Page #: 217 of 226

single flight of measured data. The NESC team found that the ability to perform flight reconstruction analysis using measured parameters from a particular flight, and therefore remove the statistical uncertainty from the analysis, is severely limited. Therefore, the team cannot draw definitive conclusions other than to state that it appears that the forces predicted by the VCLA are significantly higher than would be expected given the statistical derivation of the forcing functions and the comparison between the measured accelerations for the GLAST mission as compared with previous Delta II flights. This comparison would seem to indicate that by measuring interface forces on additional flights, it may be possible to demonstrate the conservatism in the CLA process and to improve the accuracy of the prediction technique. However, force measurements from additional flights would be required to make this determination. A sample exercise case was presented in the VCLA section to show quantitatively the amount of over-prediction on the laterals forces based on the acceleration evaluation of 39 flights.

Question #2: “How much can the loads and therefore design/qualification requirements be reduced by having force measurements?”

The NESC team identified two distinct hardware groups where the design / qualification requirements could be improved. Group 1 consisted of payload primary structure, larger subsystems, and their associated support structure. Group 2 consisted of smaller subsystems, instruments, components, and the secondary support structure, which attaches these items to the spacecraft. The different hardware groups were distinguished by the dimensioning loads and processes that are used to design and analyze each type of structure.

The structures which belong to Group 1 were typically sized based on the load factors published in the PPG. This was done early in the design cycle prior to having a CLA performed. The primary structure design loads as specified in the PPG define the maximum expected payload net center of gravity responses as long as the minimum frequency requirements specified are met. The design limit loads for primary structure were derived based on an envelope of CLA results over a range of payload parameters such as mass, center of gravity location, and stiffness.

Early in the design cycle, structures in Group 2 were typically designed based on loads derived from two sources:

- a. Mass Acceleration Curve (MAC) - These curves define limit loads as a function of the mass of the item. MACs are derived based on enveloping results from previous coupled loads and may account for mechanically transmitted vibroacoustic loading. Usually a MAC is derived for a vehicle or family of vehicles with similar launch characteristics.

	NASA Engineering and Safety Center Technical Assessment Report	Document #: NESC-RP- 06-071	Version: 1.0
Title: Flight Force Measurements of the Gamma-Ray Large Area Space Telescope / Delta II Flight			Page #: 218 of 226

- b. Acceleration Basedrive Analysis – Typically performed in the frequency domain by applying the prescribed swept sine acceleration spectrum from the PPG at the spacecraft/launch vehicle interface. The analysis is typically limited such that the interface loads do not exceed the design load factors for primary structure. Acceleration responses for locations of interest are recovered from this analysis to derive the necessary design limit loads for instruments, subsystems, components, and associated support structure.

Therefore, if the NESC team wanted to affect the primary structure design, first they would have to reduce the conservatism in the CLA used to derive the design limit loads specified in the PPG. In the GLAST spacecraft case, the torsional moment has been under-predicted by both the CLA and the PPG design load factors. Setting aside the PPG load factors under-predict the torsional moment measured on the GLAST flight, the data acquired seems to indicate that the lateral forces and moments have been in general over-predicted by CLA and the PPG factors based on the statistical derivation of the CLA methodology as discussed in Section 7.3. For example, if it was assumed that Airloads were equivalent to a P95/50 level based on the measured interface accelerations, then the bending moment (which is a significant factor in the design of the primary structure) was over-predicted by 72 percent compared to what would be expected from an analysis intended to represent a 3-sigma (99/90) type response. In order to understand the implications of the forces measured during the GLAST mission, the NESC team would need to have force measurements from additional Delta II flights to evaluate specifically why the CLA results over-predicted lateral loads and bending moments while at the same time significantly under-predicted the torsional moment. While the data from this investigation seems to indicate that there are improvements that could be made in the CLA process to reduce conservatism in the loads predictions, it is not possible to conclusively determine specific areas to address without measured force data from additional flights to confirm the findings from the GLAST mission.

While the design of hardware in the Group 2 would benefit from improvements in the CLA process as this would eventually lead to reduced MAC limit loads, hardware in this group could more immediately benefit by the development of force limits which could be used along with basedrive analysis to develop design limit loads. As noted previously, the typical approach used in the design cycle for these items was to progressively reduce the loads from the MAC values through a basedrive analyses using the input sine spectrum defined in the PPG. Typically, the basedrive analysis has used the Net Center of Gravity (CG) design limit loads from the PPG as the means to more accurately replicate the behavior of the coupled system and to reduce the severity of the input, which represents an envelope of levels over a number of flights. The force limit based on the design loads has typically been specified as a single maximum value over the entire frequency range of the analysis. This approach usually results in a notch associated with

	NASA Engineering and Safety Center Technical Assessment Report	Document #: NESC-RP- 06-071	Version: 1.0
Title: Flight Force Measurements of the Gamma-Ray Large Area Space Telescope / Delta II Flight		Page #: 219 of 226	

the major spacecraft mass modes at the lower end of the analysis frequency range, but provides little relief for other system modes that occur at frequencies different from the fundamental modes. Providing a force limit as a spectrum over the entire frequency range of the basedrive analysis would allow for a more accurate prediction of design loads for Group 2 hardware.

Measurements of forces over a number of flights could be used to derive the force spectra necessary to improve the derivation of design limits loads for Group 2 hardware using basedrive analysis. Two possible approaches could be used to address the derivation of these force spectrums:

- a) Use FFMs to generate a statistically meaningful force spectrum based on flight data.
- b) Use FFMs to improve force limiting techniques by correlating flight results with analytically derived force spectrums for specific flight configurations.

It was not possible for the NESC team to evaluate how the predicted response of items on-board the GLAST spacecraft would be affected by the use of force spectra as part of performing a basedrive analysis to simulate the flight event.

One of the original motivations behind this assessment was to provide an additional understanding of the severity of the MECO Shock Transient event. Because this event has frequency content above 100 Hz, it was difficult to develop a CLA technique which adequately replicates the acceleration responses measured in flight. Therefore, the event was simulated as a frequency response basedrive analysis using an envelope of measured flight accelerations. One of the significant conclusions of this activity is that the basedrive methods using measured flight acceleration data tends to be overly conservative in predicting interface loads especially when driven by the payload resonant response. This was particularly evident for the case of the MECO Shock Transient event in which the basedrive analysis using the measured acceleration data as input consistently over-predicted the measured flight forces at the GLAST/PAF interface.

Therefore, the MECO Shock Transient event is one for which the design and test requirements could be reduced by developing an appropriate force spectrum to be used along with the input acceleration levels when performing a basedrive simulation. This approach was used analytically in the past for the EOS-Aqua and Aura missions to reduce the severity of the basedrive analysis for the MECO Transient event as the simulation was exciting a spacecraft thrust mode with significant modal mass at 85 Hz causing the prediction of high responses for certain on-board components. The analytically derived force-limits allowed for a 30 to 50 percent reduction in response, which was sufficient to demonstrate compliance of the hardware for the flight event, but there was never any measurement of flight forces to directly validate the results. It should be noted that the force data from the GLAST mission showed that the basedrive analysis for the MECO Transient event over-predicted the measured thrust-axis forces

	NASA Engineering and Safety Center Technical Assessment Report	Document #: NESC-RP- 06-071	Version: 1.0
Title: Flight Force Measurements of the Gamma-Ray Large Area Space Telescope / Delta II Flight		Page #: 220 of 226	

in the 80 to 150 Hz range by around 25 percent (basedrive = 1,347 pounds versus SFM = 1,082 pounds). The trends seen in this investigation appear to be consistent with the analytical results from the EOS missions, where force limiting prediction techniques were used to reduce the conservatism in the basedrive analysis, but flight force data from additional missions would be needed to develop the appropriate force limits for the MECO Transient event.

7.9 Proposed Future Work

An area of proposed future work that could be performed using the force and acceleration data measured during the GLAST mission would be to investigate the development of force spectra to improve the accuracy of basedrive analysis as a design tool.

As the Agency waits for additional FFMs, an investigation team could establish an approach for developing force spectra that would be used along with the standard basedrive analysis to improve the early design process. The most promising point in the design flow to impact the primary/secondary structure and component design is around the payload PDR time-frame. This is typically when basedrive analysis is performed using sine specifications from the PPG to evaluate design loads. The focus of this proposed future study could be to investigate how force spectra could be derived from measured flight data and how the spectra derived from this effort would compare with the results of standard force limiting techniques. This study could also examine how the derived force spectra might be used to improve the accuracy of payload testing. This work would be performed using the flight data measured on the GLAST mission during Liftoff and Airloads (CLA events) and for the MECO Shock Transient event. Force and acceleration data from the GLAST spacecraft sine test would also be used. The proposed study could encompass the following areas:

- a) Development of the methodology for deriving force-limit spectrums based on measured flight data. Several different techniques could be evaluated including BP filtering, SRS processing, and Fourier based methods to determine the most accurate method for deriving the force spectrum.
- b) Comparison of force spectrums derived using existing force-limiting techniques with the force data from the GLAST spacecraft flight to evaluate the how effective these techniques are for replicating the measured flight environment.
- c) Quantitative assessment of how spacecraft responses are affected by the application of the derived force spectrums. Basedrive responses using the GLAST spacecraft VCLA and associated output transformation matrices (OTMs) could be compared with and without force-limiting.

	NASA Engineering and Safety Center Technical Assessment Report	Document #: NESC-RP- 06-071	Version: 1.0
Title: Flight Force Measurements of the Gamma-Ray Large Area Space Telescope / Delta II Flight		Page #: 221 of 226	

- d) Parametric analysis using the GLAST spacecraft FEM to determine how effective the application of the derived force spectrums will be given the types of modeling uncertainties in mass and stiffness that may exist in the preliminary design phase.
- e) Evaluation of the methods for implementing force limiting during spacecraft shaker sine and/or random testing.
- f) Assessment of Fourier based methods for deriving equivalent sine spectrum for payload design and testing as compared with traditional SRS/Q approach.

8.0 Findings and Recommendations

8.1 Findings

The following NESC team findings were identified:

- F-1.** The results from the GLAST VCLA grossly under-predicted the maximum torsional moment (Mz) during flight. (Section 7.3.2)
- F-2.** The results from the GLAST VCLA showed a greater than expected over-prediction of lateral forces and bending moments at the interface compared to the measured SFM results. (Sections 7.3.1 and 7.3.2)
- F-3.** The basedrive analysis using measured flight accelerations over-predicted the lateral interface forces for all major flight events (Liftoff, Airloads and MECO). (Sections 7.4.2, 7.4.3, 7.5.1, and 7.6.1)
- F-4.** The basedrive analysis using measured flight accelerations did not consistently over or under-predict the lateral bending moments for liftoff and Airloads. The prediction accuracy was dependent on model configuration and assumed damping. (Sections 7.4.2, 7.4.3, and 7.5.1)
- F-5.** In general, the basedrive analysis did a poorer job predicting lateral forces and overturning moments as compared to predicting axial forces. (Sections 7.4.2, 7.4.3, 7.5.1, and 7.6.1)
- F-6.** A full flight reconstruction analysis of the GLAST flight proved to be more difficult and complex than originally anticipated. (Section 7.4.1)
- F-7.** Comparison of the Liftoff SRS data for the torsional moment between the full reconstruction analysis and the measured flight data showed that the reconstruction analysis under-predicted the forces at the 10 Hz torsional mode of the launch vehicle. (Figure 7.4-38)
- F-8.** The interface forces calculated by the full liftoff reconstruction did not show frequency content at 3.5 Hz corresponding to the launch vehicle fundamental bending mode which

	NASA Engineering and Safety Center Technical Assessment Report	Document #: NESC-RP- 06-071	Version: 1.0
Title: Flight Force Measurements of the Gamma-Ray Large Area Space Telescope / Delta II Flight		Page #: 222 of 226	

is present in the lateral forces and bending moments measured during flight. (Sections 7.4.1 and 7.4.5)

- F-9.** The accuracy of the strain-based force measurements is dependent on the load level due to non-linearity's in the boundary conditions, sensitivity of the gages, and noise in the system at low levels of loading. (Sections 6.3.8 and 6.3.9)
- F-10.** The strain gage size had negligible effect on the calculation of interface forces using the SFM and FEM Methods. (Section 6.3.7)
- F-11.** Geometry based methods for transforming measured strain to force is more robust than methods which rely on the stiffness matrix from a finite-element model. (Sections 6.1.5, 6.1.6, and 6.3.9)

8.2 NESC Recommendations

The following NESC recommendations are directed to the NESC, the NASA Launch Services Program, the GSFC Chief of the Mechanical Division, and the JPL Spacecraft Mechanical Engineering Section and Supervisor of the Dynamic Environments Group:

- R-1.** Evaluate the ability of launch vehicle design limit loads and CLA techniques to adequately simulate the torsional loading during launch. Current methods may not be conservative for structures which are sensitive to torsional loading. (*F-1*)
- R-2.** Obtain additional force measurements over a number of flights for a given launch vehicle in order to: (*All Findings*)
 - a. Improve the accuracy of CLA by reconciling against a database of both force and acceleration measurements. (*F-1, F-2*)
 - b. Develop statistically meaningful force spectra that could be used in conjunction with basedrive analysis to provide a more accurate tool for preliminary spacecraft design. (*F-3, F-4, F-5*)

9.0 Alternate Viewpoints

There were no alternate viewpoints expressed during this assessment.

10.0 Other Deliverables

- 10.1 Referenced ATK Space Division Reports
- 10.2 SFI Data from ULA
- 10.2 Processed Flight Data (Centerline Accelerations and Interface Forces)
- 10.3 FFM Matrices
- 10.4 FFM Models (GLAST Spacecraft and PAF)

	NASA Engineering and Safety Center Technical Assessment Report	Document #: NESC-RP- 06-071	Version: 1.0
Title: Flight Force Measurements of the Gamma-Ray Large Area Space Telescope / Delta II Flight		Page #: 223 of 226	

10.5 GLAST Test Data (Static and Dynamic)

The following data will be available on CD-ROM by request. Please contact Scott Gordon (scott.a.gordon@nasa.gov) to process your request.

11.0 Lessons Learned

There were no lessons learned.

12.0 Definitions of Terms

Corrective Actions	Changes to design processes, work instructions, workmanship practices, training, inspections, tests, procedures, specifications, drawings, tools, equipment, facilities, resources, or material that result in preventing, minimizing, or limiting the potential for recurrence of a problem.
Finding	A conclusion based on facts established by the investigating authority.
Lessons Learned	Knowledge or understanding gained by experience. The experience may be positive, as in a successful test or mission, or negative, as in a mishap or failure. A lesson must be significant in that it has real or assumed impact on operations; valid in that it is factually and technically correct; and applicable in that it identifies a specific design, process, or decision that reduces or limits the potential for failures and mishaps, or reinforces a positive result.
Observation	A factor, event, or circumstance identified during the assessment that did not contribute to the problem, but if left uncorrected has the potential to cause a mishap, injury, or increase the severity should a mishap occur. Alternatively, an observation could be a positive acknowledgement of a Center/Program/Project/Organization's operational structure, tools, and/or support provided.
Problem	The subject of the independent technical assessment/inspection.
Proximate Cause	The event(s) that occurred, including any condition(s) that existed immediately before the undesired outcome, directly resulted in its occurrence and, if eliminated or modified, would have prevented the undesired outcome.
Recommendation	An action identified by the assessment team to correct a root cause or deficiency identified during the investigation. The recommendations may

	NASA Engineering and Safety Center Technical Assessment Report	Document #: NESC-RP- 06-071	Version: 1.0
Title: Flight Force Measurements of the Gamma-Ray Large Area Space Telescope / Delta II Flight		Page #: 224 of 226	

be used by the responsible Center/Program/Project/Organization in the preparation of a corrective action plan.

Root Cause One of multiple factors (events, conditions, or organizational factors) that contributed to or created the proximate cause and subsequent undesired outcome and, if eliminated or modified, would have prevented the undesired outcome. Typically, multiple root causes contribute to an undesired outcome.

13.0 Acronyms List

AC	Alternating Current
ATK	Alliant Techsystems
ATP	Authority to Proceed
BD	Basedrive
BP	Band-Pass
CAD	Computer Aided Design
CDR	Critical Design Review
CLA	Coupled Loads Analysis
COLA	Constant Output Level Amplitude
COV	Coefficient of Variation
DC	Direct Current
D-O-F	Degree of Freedom
DUF	Dynamic Uncertainty Factor
ELV	Expendable Launch Vehicle
ERB	Engineering Review Board
FEM	Finite Element Model
FFMsDT	Flight Forces Discipline Teamflight force measurements
GD	General Dynamics
GEM	Graphite Epoxy Motors
GLAST	Gamma-ray Ray Large Angle Space Telescope
GSFC	Goddard Space Flight Center
HP	High-Pass
JPL	Jet Propulsion Lab
JSC	Johnson Space Center
LaRC	Langley Research Center
LOX	liquid oxygen
LP	Low-Pass
LVDT	Linear Variable Differential Transformers
MAC	Mass Acceleration Curve

	NASA Engineering and Safety Center Technical Assessment Report	Document #: NESC-RP- 06-071	Version: 1.0
Title: Flight Force Measurements of the Gamma-Ray Large Area Space Telescope / Delta II Flight		Page #: 225 of 226	

MECO	Main Engine Cutoff
MOV	Main Oxidizer Valve
NESC	NASA Engineering and Safety Center
NRB	NESC Review Board
OFE	Other Flight Events
OTM	Output Transformation Matrix
PAF	Payload Adapter Fitting
PDR	Preliminary Design Review
PPG	Payload Planners Guide
SECO	Second Engine Cut-Off
SFI	Special Flight Instrumentation
SFM	Summed Force Method
SMTU	Sub Master Telemetry Unit
SOW	Scope of Work
SRS	Shock Response Spectra
SSGS	Second Stage Guidance Section
STEL	Static-Elastic Loading
STF	Single-tailed Tolerance Factor
TPAF	Test Payload Adaptor Fitting
ULA	United Launch Alliance
USS	Upper Stage Simulator
VCLA	Verification Coupled Loads Analysis
VLC	Verification Loads Cycle
XTE	X-Ray Timing Experiment

14.0 References

1. SAI-TM-3150, Rev. A, "Methodology for PAF Flight Force Measurement" from William Haile, Swales Aerospace, to Daniel Kaufman, GSFC 542, 20 Aug. 2007.
2. "Independent Verification and Analysis of Flight Force Measurement Methodology", Dan Takahashi and Siamak Ghofranian, 8 August 2007.
3. ATK-RPT-823 Rev B, "TPAF Static Test Plan for the NESC", William Haile and Michael Fendya, 2 July 2008.
4. ATK-RPT-0890, "Test Report of the TPAF Static Test for the NESC", by Michael Fendya and William Haile, 28 July 2008.
5. ATK-RPT-834, "Test Plan for the NESC Measurements during the GLAST Vibration Test", William Haile, 5 July 2007.

	NASA Engineering and Safety Center Technical Assessment Report	Document #: NESC-RP- 06-071	Version: 1.0
Title: Flight Force Measurements of the Gamma-Ray Large Area Space Telescope / Delta II Flight		Page #: 226 of 226	

6. ATK-RPT-0851, "Test Report for the NESC Measurements from the GLAST Vibration Test", by William Haile, 1 Nov 2007.
7. A-3-Delta-StrDyn-2007-034R1, "GLAST-Delta 7920H-10 Verification Loads Cycle (VLC) Dynamic Response Analysis (Revision 1), ULA Document, 15 October 2007.
8. ERB-1690, "GLAST Special Flight Instrumentation System Critical Design Review", by United Launch Alliance, 30 Jan 2008.
9. 08H0049, "GLAST Launch Vehicle Post-Flight Analysis Report", ULA Document, August 2008.
10. ATK-TM-3282, "Impedance of the GLAST Spacecraft", William Haile, 31 July 2008.
11. ATK-RPT-0888, "FFM Reconstruction of the GLAST Flight Loads", William Haile, 19 Sep 2008.
12. 06H0214, "Delta II Payload Planners Guide", ULA Document, December 2006.
13. "Delta II Upper Stage Flexibility, Rev A", William Haile and Michael Fendya, ATK Presentation, 8 August 2007.